



Terms and Conditions of Use of Digitised Theses from Trinity College Library Dublin

Copyright statement

All material supplied by Trinity College Library is protected by copyright (under the Copyright and Related Rights Act, 2000 as amended) and other relevant Intellectual Property Rights. By accessing and using a Digitised Thesis from Trinity College Library you acknowledge that all Intellectual Property Rights in any Works supplied are the sole and exclusive property of the copyright and/or other IPR holder. Specific copyright holders may not be explicitly identified. Use of materials from other sources within a thesis should not be construed as a claim over them.

A non-exclusive, non-transferable licence is hereby granted to those using or reproducing, in whole or in part, the material for valid purposes, providing the copyright owners are acknowledged using the normal conventions. Where specific permission to use material is required, this is identified and such permission must be sought from the copyright holder or agency cited.

Liability statement

By using a Digitised Thesis, I accept that Trinity College Dublin bears no legal responsibility for the accuracy, legality or comprehensiveness of materials contained within the thesis, and that Trinity College Dublin accepts no liability for indirect, consequential, or incidental, damages or losses arising from use of the thesis for whatever reason. Information located in a thesis may be subject to specific use constraints, details of which may not be explicitly described. It is the responsibility of potential and actual users to be aware of such constraints and to abide by them. By making use of material from a digitised thesis, you accept these copyright and disclaimer provisions. Where it is brought to the attention of Trinity College Library that there may be a breach of copyright or other restraint, it is the policy to withdraw or take down access to a thesis while the issue is being resolved.

Access Agreement

By using a Digitised Thesis from Trinity College Library you are bound by the following Terms & Conditions. Please read them carefully.

I have read and I understand the following statement: All material supplied via a Digitised Thesis from Trinity College Library is protected by copyright and other intellectual property rights, and duplication or sale of all or part of any of a thesis is not permitted, except that material may be duplicated by you for your research use or for educational purposes in electronic or print form providing the copyright owners are acknowledged using the normal conventions. You must obtain permission for any other use. Electronic or print copies may not be offered, whether for sale or otherwise to anyone. This copy has been supplied on the understanding that it is copyright material and that no quotation from the thesis may be published without proper acknowledgement.

**OPTICAL AND ELECTRICAL CHARACTERISATION OF
HEXABENZOCORONENE DERIVATIVE MOLECULAR
SELF-ASSEMBLIES**

ALEXANDER FLEMING

PhD. Thesis

Supervisor Prof. Blau
School of Physics, Trinity College Dublin

2006

TRINITY COLLEGE
10 NOV 2006
LIBRARY DUBLIN

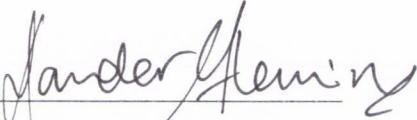
THESIS
7998

DECLARATION

I declare that the work in this dissertation has not been previously submitted as an exercise for a degree to this or any other university.

The work described herein is entirely my own work, except for the assistance mentioned in the acknowledgements and the collaborative work mentioned in the list of publications.

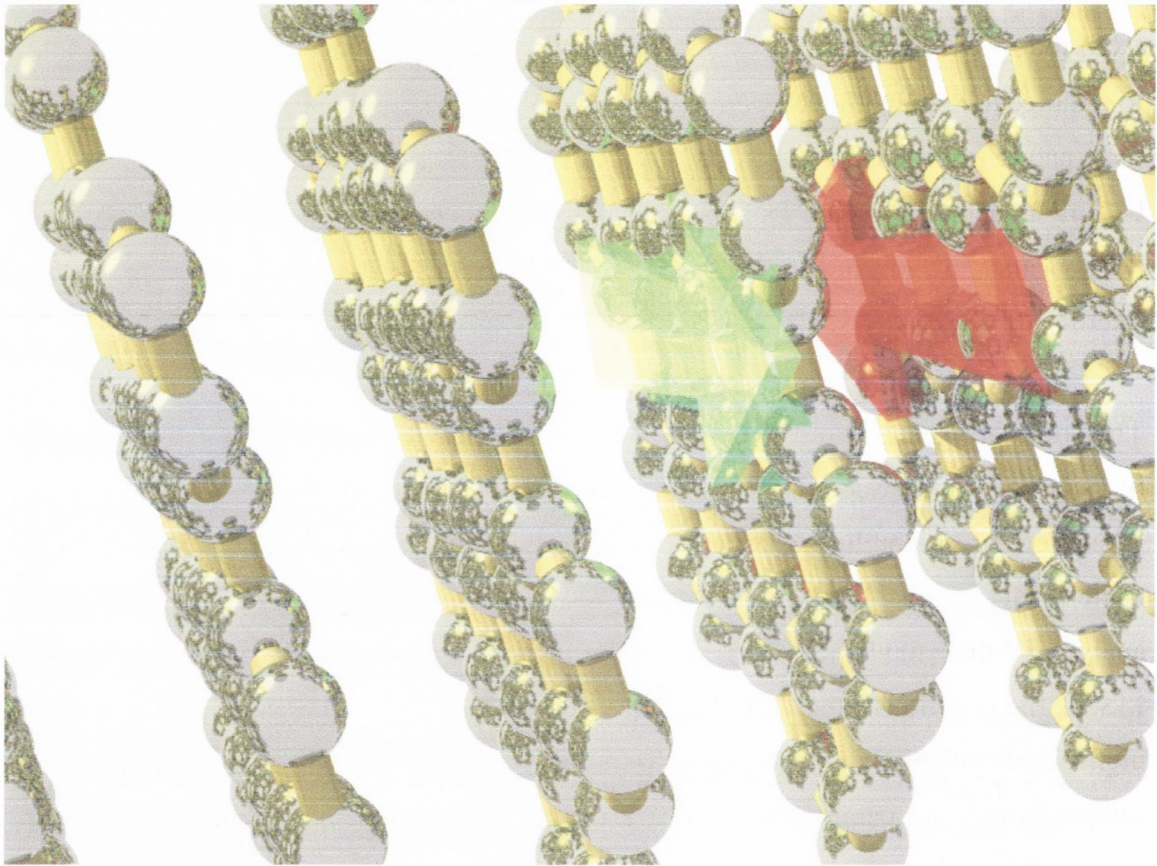
I agree that Trinity College Dublin Library may lend or copy this dissertation upon request.


Alexander Fleming

SUMMARY

In this thesis the optical properties of molecular aggregates of Hexa-peri-benzocoronene derivatives are investigated for evidence of Frenkel Exciton Resonance (FER). Using photo-luminescence and optical absorption measurement techniques the HBC derivatives are observed, in the optical spectra, to aggregate in solution to form ordered Molecular Self-Assemblies (MSAs). The change from isolated to aggregated form gives rise to spectroscopic signatures that are best explained by FER. The determination that the low concentration species is the isolated molecule allows the photo-physics of isolated and aggregated molecules to be compared. From this it appears that HBC spectra published previously, are of aggregates and not isolated molecules as has been previously thought. From the appearance of distinctive FER transitions of H-aggregates the molecular stacking in the MSA can be elucidated. This is confirmed by comparing the photo-luminescence and photo-luminescence-excitation spectra of the symmetrically and asymmetrically substituted HBC derivatives investigated. The observation of H-aggregate emission is explained by the construction of a photo-absorption-luminescence cycle that is relevant to FER excitons in van der Waals aggregates. The FER model that is constructed, also indicates why long localisation range FER systems appear to have no vibrational-electronic structure in the optical spectra. From the model, the method of measuring the Stokes shift is found to be different for spectra of isolated and FER aggregates. The structure of the HBC MSAs formed, are also determined from the percolation threshold of excimer emission, or charge carrier conduction, of a network of HBC MSAs in an inert polymer matrix. The aspect ratio ~ 1000 calculated for the inclusions is found to agree with atomic-force-microscope and scanning-electron-microscope images. The overall aim is to investigate how the optical spectra of molecular aggregates are affected by the structure and super-structure of the aggregate.

Foreword.....	1
Ch. 1 Introduction.....	5
1.1 <i>Electronic Properties of Organic Materials</i>	7
1.2 <i>Molecular Interactions</i>	10
1.3 <i>Isolated Molecule Energy States</i>	13
1.4 <i>Aggregate Molecular Energy States</i>	18
Ch.2 Experimental Setups.....	31
2.1 <i>Spectroscopic Measurements of Solution and Solid State samples</i>	32
2.2 <i>Excimer Percolation and Solubility Measurements</i>	35
2.3 <i>Electrical Measurements</i>	36
2.4 <i>AFM measurements</i>	37
Ch.3 Absorption and PLE Spectra.....	39
3.1 <i>Introduction</i>	40
3.2 <i>Isolated Molecule</i>	42
3.3 <i>Aggregates</i>	49
3.4 <i>Experimental Results</i>	55
3.5 <i>Discussion</i>	69
3.6 <i>Conclusions</i>	90
Ch.4 PL and PLE spectra.....	93
4.1 <i>Introduction</i>	93
4.2 <i>Results</i>	94
4.3 <i>Discussion</i>	113
4.4 <i>Conclusions</i>	130
Ch. 5 Excimer and Solubility measurements.....	133
5.1 <i>Introduction</i>	133
5.2 <i>Results</i>	134
5.3 <i>Discussion</i>	151
5.4 <i>Conclusions</i>	158
Ch.6 New Spectroscopic Insights into the Resonance of Frenkel Excitons in MSAs....	161
6.1 <i>Introductions</i>	162
6.2 <i>Gedankenexperiment</i>	164
6.3 <i>Resonance in Real Aggregate Systems</i>	169
6.4 <i>Comparisons to Experiment</i>	175
6.5 <i>Conclusions</i>	183
Ch.7 Electrical Properties and Microscopy.....	189
7.1 <i>Introduction</i>	189
7.2 <i>Results</i>	190
7.4 <i>Discussion</i>	210
7.5 <i>Conclusions</i>	213
Ch.8 Conclusions.....	215
Appendix A: Effective Conjugation Area of HBC Molecules.....	219
Appendix B: Spectra and FER Decoherence.....	224



Graphic illustration of the induction of a transition dipole moment by the transition dipole moment of a neighbouring molecule in an H-aggregate molecular self-assembled nanowire of HBC (alkyl chains are not shown). It is this asymmetric induced dipole alignment that makes an H-aggregate much more likely to facilitate exciton hopping (along the nanowire) rather than photo-luminescence. Note: colour scheme of arrows is not relevant.

Foreword

On a molecular scale, the accurate and controlled application of intermolecular forces can lead to new, previously unachievable, nanostructures. This is why Molecular Self-Assembly (MSA) is a highly topical and promising field of research in Nanotechnology (NT) today. MSA encompasses all structures formed by molecules selectively binding to a molecular site without external influence. With many complex examples all around us in nature (ourselves included), MSA is a widely observed phenomenon that has yet to be fully understood. Being more a physical principle than a single quantifiable property, it appears in physics, chemistry and biochemistry, and is therefore truly interdisciplinary¹.

The problem to date with researching the fundamental physics behind MSAs has tended to be that prime examples of MSAs are mainly found in the biological sciences. Biomolecular assemblies, such as light-harvesting antenna complexes found in some bacteria, are sophisticated and often hard to isolate, making systematic and progressive analyses of their fundamental physics very difficult. What in fact are needed are simpler MSAs, the constituent molecules of which can be readily synthesised by chemists to a high degree of purity – high quality sample preparation, chemical purity and known sample history are paramount in MSA research. These molecules should self-assemble into simpler constructs that can be easily assessed with current experimental techniques.

Weak intermolecular bonds, such as van der Waals bonds, that selectively bind molecules to a site in an assembly, are what make MSAs so varied. It would be almost impossible to mimic MSA complexity using synthetic, aggressive chemistry to join molecules together via covalent bonding. Although a covalent bond is much stronger, precursors, acidic/basic conditions and high temperatures are required for chemical synthesis. For MSAs, synthetic chemistry is only used to construct the basic building blocks (i.e. the molecules) and weaker intermolecular bonds are involved in arranging and binding the blocks together into a structure. This weak bonding makes solution, and hence reversible, processing of MSAs possible.

The current top-down approach to NT, whereby nano-structures are created, manipulated and modified by machine, is incapable of offering the complexity and economy-of-scale that MSA demonstrates in nature. Thus, solution processing and manufacturing of MSAs offer the enviable goal of mass production with the possibility of error-correction at any stage of assembly. It is well recognised that this method could prove to be the most cost-effective way to produce functional nanodevices such as nanowires, nanotransistors and nanosensors in large numbers (hundreds of billions at a time) for the semiconductor electronics industry. Although these nanodevices will be the first to become available with MSA research, they are, in fact, the simpler cousins to the complex integrated nano-structures to come, in which many *different* molecules assemble².

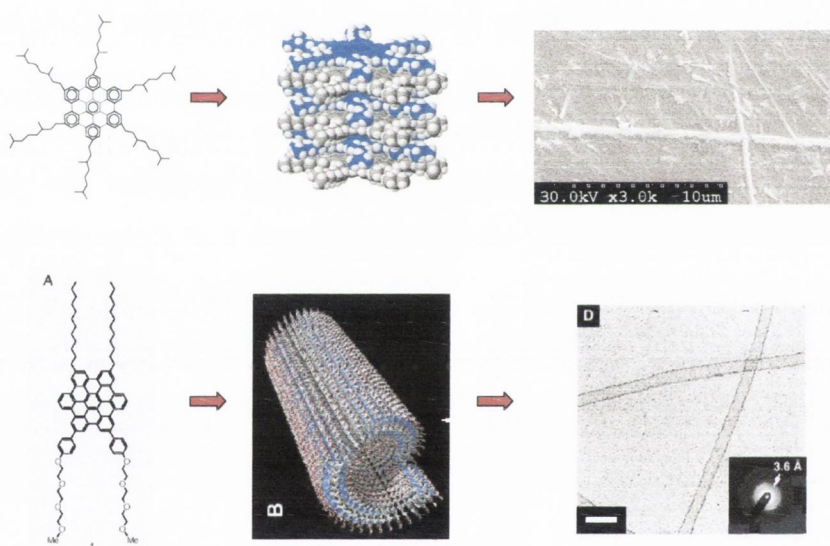


Figure 1: Examples of MSAs formed in solution by Hexabenzocoronene derivative molecules, symmetrically substituted HBC-C8,2 and asymmetrically substituted J-HBC⁵. Left: molecular structure, Centre: MSA simulation and Right: Scanning and Transmission Electron Microscope images of the respective MSAs.

Our ultimate goal is to understand how to form ordered functionality-tailored nanostructures via self-assembly in solution. These nano-sized novel structures, with novel properties, will form by ordered assembly of different molecules. However, at present, the physics of a single molecule and its bulk molecular crystal is much better

understood compared to the intermediate size range of small molecular assemblies. Therefore, research has focused on ordered assemblies of *identical* molecules that self-assemble in solution. The strategy is to use conventional investigation techniques to determine the physical structure, electronic properties and other interesting physical phenomena of simple MSAs, which will then pave the way for an understanding of more complex MSAs. In this respect, hexa-*peri*-hexabenzocoronene (HBC) derivative molecules offer a good molecular template from which to advance to complex MSAs³.

HBCs are beautiful examples of molecular plate like structures. As shown in the figure, symmetrically substituted HBC-C_{8,2} molecules self-assemble in solution into nanowires of several hundred nanometers length and 3 nm diameter. At high concentrations, these molecular nanowires assemble further into entropically favourable nanowire bundles of several tens of micrometers length and typically tens of nanometers diameter (as shown in the inset SEM image). The ordered alignment of the molecules in the assembly ensures a homogeneous electronic coupling along the length of the nanowire. This in turn leads to the extended delocalisation of the exciton eigenstates, which is confirmed by sharp peaks in their optical spectra.

For instance the asymmetrically substituted amphiphilic J-HBC molecule have been shown to self-assemble into remarkably defect-free large nanotubular objects⁵, more than 14 nanometers wide and up to 10 μm long, with a clearly defined helicity, each involving around 50,000 HBC molecules.

At present, there is a huge global research effort targeted at Carbon Nanotubes (CNTs). They are being investigated for applications ranging from actuators to reinforcement agents, nanoelectronic devices to controlled drug release agents – each application requiring a different, precisely defined physical and/or electronic structure⁴. A major drawback of CNTs, however, is our apparent lack of structural control due to the fact that CNTs are formed by either a gas-phase or a plasma process⁶. The route taken by Hill et al. demonstrates that precise control of intermolecular and environmental forces can lead to graphitic nanotubes with defined dimensions, helicity and electronic properties – exactly as one frequently needs in molecular electronics and most other applications of CNTs.

Demonstrating that synthetic molecules can form ordered MSAs is a key step. However, attaining a small degree of functionality with simple MSAs, will be very significant, as it may indeed open up new avenues for investigating complex MSAs and other nano-systems. Known and functional MSAs will be very useful as local probes to investigate more complex MSAs. In other words, MSAs could become the nano-tools of the future.

Extract from:

“**Designer Nanotubes by Molecular Self-Assembly**”, W. J Blau, A. J. Fleming, *Science*, **304**, 2004

¹ George M. Whitesides and Bartosz Grzybowski, *Self-Assembly at All Scales*, Science 29 March 2002; 295: 2418-2421

² F. Cacialli, P. Samori and C. Silva, *Supramolecular Architectures (Review)*, Materials Today April 2004, 24-32.

³ J. H. Wu, MD Watson; K Mullen, *The versatile synthesis and self-assembly of star-type hexabenzocoronenes*, *Angewandte Chemie-International Edition* 2003, 42, 5329

⁴ Ray H. Baughman, Anvar A. Zakhidov, and Walt A. de Heer, *Carbon Nanotubes--the Route Toward Applications*, Science 2 August 2002; 297: 787-792

⁵ J.P. Hill, W. Jin, A. Kosaka, T. Fukushima, H. Ichihara, T. Shimomura, K. Ito, T. Hashizume, N. Ishii, T Aida, *Self-Assembled Hexa-peri-hexabenzocoronene Graphitic Nanotube*, Science **304**, 2004.

⁶ Private communication with Prof. W. J. Blau.

Chapter 1: INTRODUCTION

Highly integrated, nano-scale electronic circuitry could be constructed, in the future, from self-assembling molecules. For the assembly processes to be efficient, molecular nanowires, molecular transistors and other nano-scale components will be required to self-arrange passively with little external assistance. In general, processes of energy minimisation through molecular interaction, will induce a tendency for molecules to aggregate. These processes can include permanent dipole - permanent dipole interactions (Coulombic), permanent dipole - induced dipole interactions (induction) and flickering dipole - induced dipole interactions (dispersion or van der Waals). A discotic material such as hexa-*peri*-hexabenzocoronene (HBC) with a small permanent dipole moment and a large polarisability, offers a well defined, self-arranging system that can be studied and modified to help develop our understanding of aggregation processes.

Presented here are five very similar compounds: alkyl- substituted HBC (HBC-C_{8,2})¹ and hexa(4-*n*-dodecylphenyl) substituted HBC (HBC-PhC₁₂)², Fluorinated alkyl-substituted HBC (F-HBC), an amphiphilic substituted HBC (J-HBC) and a nitrogen heteroatoms substituted N-HBC . The chemical structures of the five derivatives are given in Figure 1.1 and Chapter 3. The slight modification of the side chains may seem trivial but in fact give rise to significant differences in the electronic and physical properties of the assembled materials.

Due to the strong π - π interactions, substituted HBC molecules self-assemble into highly ordered columnar stacks³ (see schematic in Figure 1.1(c)) which are further arranged in various 2D arrays in the solid state. Figure 1.1(c) shows an idealised situation where the disks are parallel and *perfectly rotationally staggered*. X-ray diffraction measurements¹ have demonstrated that the cores of HBC-C_{8,2} and other alkyl substituted HBCs are tilted and crystallised (no rotation or translation) relative to the columnar axis at room temperature. Upon heating above a given thermotropic phase transition, the disks become perpendicular to the columnar axis and gain mobility to spin about the axis. Due to the *exo*-phenyl groups of HBC-PhC₁₂ which suppress crystallisation, these latter features are observed already at room-temperature. Some of these physical properties,

as will be shown later, are strongly correlated to the optical spectroscopy results presented here.

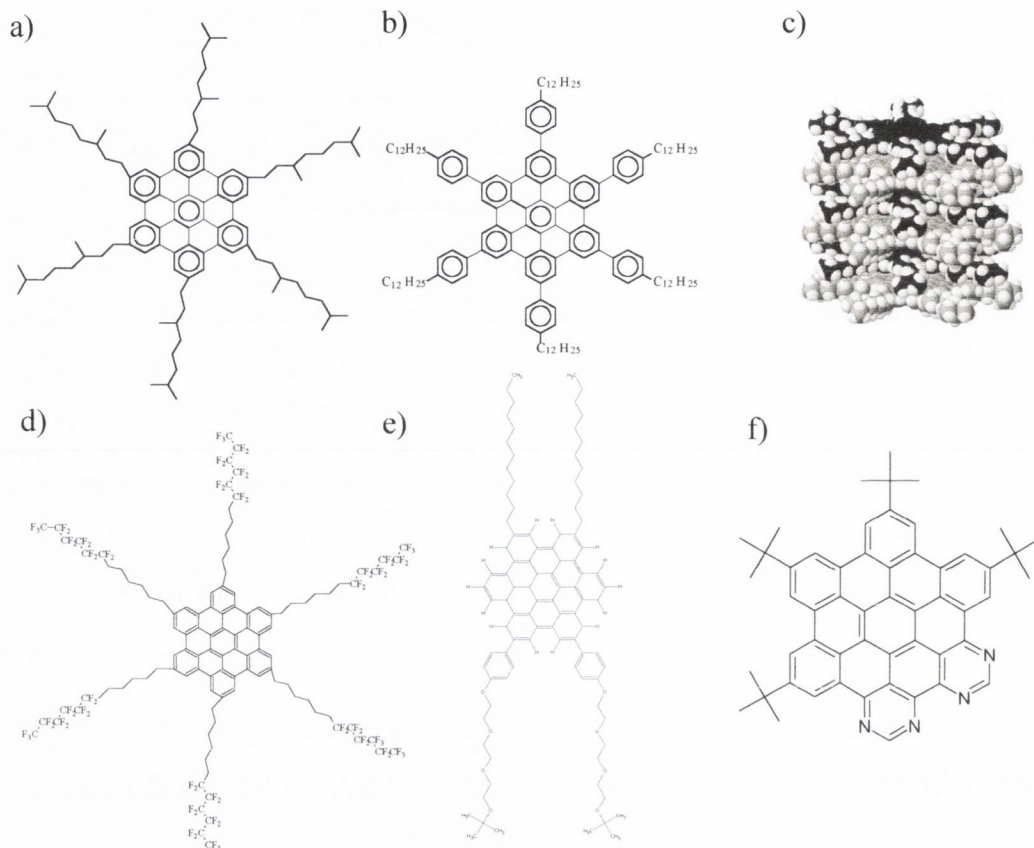


Figure 1.1: The HBC derivative molecules studied in this thesis are a) alkyl substituted HBC (HBC-C_{8,2}, Mr = 1364.21); b) hexa(*para-n*-dodecylphenyl) substituted HBC (HBC-PhC₁₂, Mr = 1989.12); c) Schematic showing an example of HBC-C_{8,2} stacking (in this possible arrangement each successive molecule in the stack is rotated by 30°); d) Fluorinated alkyl substituted HBC (F-HBC, Mr = 2935); e) Amphiphilic HBC (J-HBC Mr = 1335); f) Nitrogen heteroatoms substituted HBC (N-HBC Mr = 754).

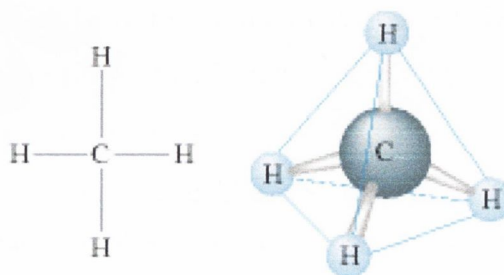
The large aromatic core of the HBC derivatives ensures an extensive π - π overlap of neighbouring molecules in the columnar aggregate stacks. This is demonstrated by the high charge carrier mobilities of alkyl substituted HBC and HBC-PhC₁₂ films, studied by van der Craats⁴ *et al.* In the solid crystalline phase, a charge carrier mobility in excess of $0.1 \text{ cm}^2 \text{ V}^{-1} \text{ s}^{-1}$ has been reported, falling to half this value in the liquid-crystalline hexagonal columnar phase. HBC derivatives also display the largest microwave frequency charge mobility observed for a discotic liquid crystal⁵ and have successfully been used in highly efficient organic solar cells⁶.

The high solubility of these alkyl- and alkyl-phenyl- and other substituted HBCs has made it possible to measure the optical properties of the materials at low concentrations, yielding information on the isolated, non-aggregated molecules. In this study the luminescence and luminescence-excitation spectra of the materials' isolated molecules are recorded at very low concentration (10^{-15} - 10^{-9} M), where the high photoluminescence quantum efficiency of the single molecules makes it possible to measure the spectrum with a standard luminescence spectro-photometer.

It will be shown that such low concentrations are required to observe the spectroscopic signature of the un-aggregated molecules, and that the effects of aggregation may be seen at concentrations as low as 10^{-9} M. It should be noted that the average optical response of a large number of isolated molecules and/or aggregates is recorded and *not* the optical response of a single molecular entity or single molecular aggregate. This differentiates these measurements from the field of single molecule spectroscopy.

1.1 ELECTRONIC PROPERTIES OF ORGANIC MATERIALS

When a carbon atom is isolated its electronic structure is governed by the population of its outer 2p electronic level (two unpaired electrons with parallel spins in different orbitals). However this situation is energetically unfavourable when the carbon atom is covalently bound in a molecule. A preferred situation is a linear combination of the 2s and 2p orbitals. For instance methane (CH_4) is bound together by carbon sp^3 hybridized orbitals (the chemical term for linear combination of two or more orbitals). The fact that the three 2p orbitals and one 2s orbital combine to form four energetically equal electronic levels leads to a tetrahedral geometry. The four orbitals now lie at the corners of a regular tetrahedron. The bonds formed by the overlap of sp^3 bonds and s orbitals (in this case from the hydrogen atoms) are called “ σ -bonds”.



They can be bonding (σ) or anti-bonding (σ^*) molecular orbitals depending on the symmetry of the wavefunction. The anti-bonding state is also known as the electronic excited state.

Carbon has a valence of four¹, but because of the linear combination it can be bound to fewer than four singly covalent atoms and yet maintain structural and electronic stability. In the case of ethene (C_2H_2) the most stable electronic configuration results from a linear combination of the 2s and two of the three available 2p orbitals. This leads to sp^2 hybridized orbitals. The interesting result from this is that there is still one singly occupied 2p orbital left (call this $2p_z$). This electron combines with the identical $2p_z$ electron in the neighbouring carbon atom to form a covalent bond called a “ π -bond”. This molecular bond is of vital importance in conjugated systems. As in the case of methane, a σ -bond is also formed between the two carbon sp^2 bonds. This bond essentially provides mechanical stability and is the restoring force between the two carbon atoms. So in effect there exists a double bond between the two carbons: one π -bond and one σ -bond. The energy of the π electrons is closer to vacuum than σ electrons, so the π -bond excited state, π^* , is encountered at lower transition energies under optical and electrical excitations (i.e. less energy is required for promotion to the excited state).

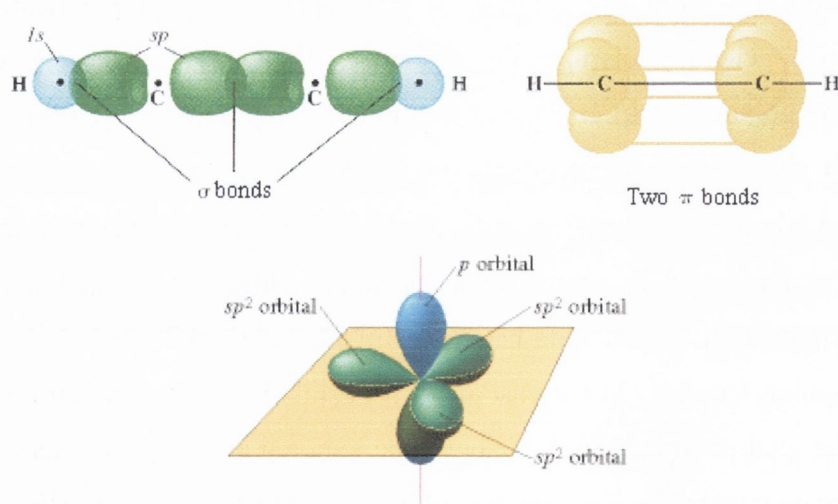


Figure 1.2: The molecular structure of ethene with sigma and pi bonds indicated as are the sp^2 hybridised orbitals.

¹ Heteroatoms like sulphur and nitrogen can be treated similarly.

Conjugation is used to describe the alternation of single (only one σ -bonds) and double bonds (one σ and one π bond) along the carbon main-chain of molecule or polymer (an extended molecule). The advantage of conjugated materials is that the π -bond electrons are essentially “free” as they don’t significantly affect the physical bonding of the carbon atoms. They do, however, limit the available rotations in a molecular system. Rotation about a double bond is not possible, although torsion to a certain extent is. The reason is that the π -bond wavefunction extends “above and below” the σ -bond. As these π electrons are not strongly bound to a particular site on the carbon main-chain they are free for conduction under the influence of an external electric field.

The conduction of conjugated molecules is however not metallic, rather it is semiconducting - the synonym “synthetic metal” has been adopted for materials such as doped poly-acetylene (PA). This polymer when suitably doped has a conductivity similar to copper (up to 1000 S cm^{-1}), but is unfortunately unstable under ambient conditions⁷.

The extent of the π bonding along a polymer chain is known as the “conjugation length”. It can be thought of as a measure of the distance for which an uninterrupted sequence of alternating single and double bonds extends along the carbon main chain. However, impurities from the catalyst or elsewhere during polymerisation of the monomer units, generally disrupts the sequence. They can interfere by chemically bonding to the polymer main chain (substitutional) or by an additive reaction on side chains which can disrupt the geometry of the polymer. Anything that reduces the overlap of the π -bond wavefunctions will reduce the conjugation length. In this way the greater the torsion angle in aromatic (i.e. benzene rings) conjugated polymers the shorter the conjugation length. In a batch of polymers there will be a statistical spread of the conjugation lengths². In the case of mLPPP this is about fourteen repeat units⁸, even when the total polymer length is about one hundred and fifty. Shorter conjugation lengths can be guaranteed by limiting the polymer length as is the case with hexaphenyl. Typically, however, in the long range limit, the energy gap doesn’t decrease below 1.5 eV.

² This is responsible in part for the lowering in energy of the photoluminescence (leaving aside Stokes’ shift), as excitons migrate to chains with longer conjugation lengths.

Since the conjugated system is one-dimensional and can be treated as a 1-D quantum well, with L equal to the conjugation length, we can see how the longer the conjugation length the smaller the energy gap between the ground and first excited state. If this energy is given in units of $h\nu$ this corresponds to the resonance frequency and hence the frequency of light emitted or absorbed. For example the visual pigment β -carotene is a polyene oligomer with ten repeat units. It absorbs in the blue spectral range and hence appears yellow when viewed in daylight. For identical reasons mLPPP, a blue emitting polymer, has a yellow hue.

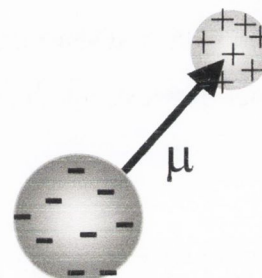
1.2 MOLECULAR INTERACTIONS

When two or more molecules are brought into close proximity, they can combine chemically or physically. A chemical interaction of two identical, or dissimilar, molecules will form a new molecular compound whereby the electrons of both starter molecules are exchanged or partially shared. This reaction forms a “chemical bond”. The energy associated with this exchange is of the order of > 4 eV and consequently will lower the total energy of the system by a similar amount leading to a stable new molecule.

Physical interactions of molecules on the other hand are far more common and their effects need to be studied. Whereas a chemical union leads to new bonds being formed that did not exist in either original molecule, a physical union will leave the starter molecules largely unchanged. The interaction described is a physical bonding between molecules (often referred to as monomers) brought close together to form an aggregate (a dimer being the simplest case). The situation however is not so simple: the molecules in an aggregate may now be dipole coupled and will therefore behave, in an analogous way, as coupled oscillators. The resonance interaction between the individual molecules in the aggregate will lead to changes in their electronic (and vibrational-electronic) behaviour. This can then be measured and used to determine the extent of the coupling between the molecules.

The kind of interaction of molecules that will be discussed is governed by three main properties of molecules: the permanent dipole moment, the polarisability and the transition dipole moment. The interplay of these factors will affect the degree of physical and electronic coupling of the individual molecules as part of an aggregate.

The permanent dipole moment (μ) of a molecule is an electrostatic dipole that arises from the difference in electronegativity of the atoms that constitute a molecule. Convention dictates that the dipole moment points from the (diagram right) more electronegative region of a molecule (i.e. the region with the largest electron density) to the region of least electronegativity (lowest electron density).



If a molecule has mobile electrons (as is the case with an extensive π -bond system), then the ease with which these electrons can be redistributed throughout the molecule by a static electric field will determine the polarisability of the molecule. The more easily the charge is redistributed the more polarisable the molecule is.

The transition dipole moment (M) is the dipole moment that arises from the shift in charge around the molecule as electrons move from one orbital to another during electronic excitation (absorption) or radiative de-excitation (luminescence). The interaction between transition dipole moments of molecules is crucial in understanding the collective behaviour of aggregates (in the point-dipole approximation).

PERMANENT – PERMANENT DIPOLE

Also known as the Coulombic interaction between molecules, it arises from the interplay of two dipole moments. Classic electrostatics determines that the potential for this attractive interaction decreases by r^{-3} , where r is the distance between the centres of both dipoles.

PERMANENT – INDUCED DIPOLE

When a permanent dipole moment is brought close to a polarisable molecule a dipole moment is set up in the polarisable molecule. This leads to an Induction force that will

attract the molecules closer together. The attractive potential for this interaction varies as r^{-6} , where r is the intermolecular distance.

FLICKERING – INDUCED DIPOLE

Also known as Dispersion or London interaction, the slight quantum fluctuations in the distribution of the electron density cloud around the molecule sets up a flickering dipole. This flickering dipole can then, by the same Induction process as described above, induce a dipole moment that will lead to a weak attractive potential. This potential will therefore also vary as r^{-6} .

PAULI REPULSION

All atoms repel each other strongly if they get too close. This is because core electrons cannot overlap without infringing the Pauli exclusion principle (electrons are *fermions* and thus can't occupy the exact same state). The interaction energy goes as $\sim r^{-12}$.

LENNARD-JONES POTENTIAL

The combination of the Dispersion and Pauli repulsion interactions leads to an overall, and simplified, potential. This summation leads to the Lennard-Jones potential that describes how molecules can be physically brought together and maintained in position i.e. aggregate.

SELF-ASSEMBLY OF MOLECULES

The molecular interactions described above are the driving force of self-assembly of molecular structures. In nature, many organic systems are the product of self-assembly processes (for instance DNA). Processes of energy minimisation through molecular interaction will induce a tendency for molecules to aggregate. If, as in the case of alkyl substituted HBC, the single molecule structure lends itself to an ordered arrangement then a 'superstructure', such as a molecular nanowire will self-assemble.

1.3 ISOLATED MOLECULE ENERGY STATES

The total energy of a molecule is a sum of its electronic, vibrational and rotational energies. When a molecule absorbs light in the visible and near UV regime the result is an electronic transition accompanied by vibrational and rotational transitions. Electronic transition energies are typically of the order of eV, whereas vibrational (~ 0.1 eV) and rotational (~ 0.01 eV) transition energies are much lower.

GROUND STATE

Finding the molecular electronic energies requires solving the time-independent Schrödinger eigenvalue problem of a many-particle system containing all nuclei and electrons of the molecule. Due to the extensive number of parameters that have to be included in order to obtain the eigenfunctions of the molecule, many approximations, of varying simplicity, have been used to determine the energy states of molecules. Only for hydrogen, or hydrogen analogs, is the Schrödinger equation,

$$H\Psi = E\Psi$$

exactly solvable. In the Hartree-Fock model of electronic states the spin-orbit coupling is neglected (non-relativistic case) and the Born-Oppenheimer (B-O) adiabatic approximation, whereby the nuclei are assumed to be static with respect to the electrons, is built upon (i.e. the electrons of a molecule move in a field of fixed nuclei). This is a reasonable assumption as the mass of nucleus is $\sim 10^3$ times heavier than that of the electron. The electronic wavefunction is therefore calculated using the instantaneous nuclear positions, while the motion of the nuclei is treated as moving in a potential given by the electronic energy, which is a function of nuclear configuration. The vibronic wavefunctions for the molecule (neglecting spin) are thus composed of

$$\Psi_{total} = \phi_{electronic} \chi_{nuclear}$$

where $\phi_{electronic}$ is the electronic wavefunction satisfying the eigenvalue equation

$$[H_E + H_{NE}] \phi_{electronic} = E \phi_{electronic}$$

and

$$[E + H_N] \chi_{nuclear} = E \chi_{nuclear}$$

where H_E and H_{NE} are the Hamiltonians of the electronic and electronic-nuclear interactions. However $\phi_{electronic}$ and $\chi_{nuclear}$ are still not eigenfunctions of the total Hamiltonian for the system $H_{total} = H_E + H_{NE} + H_N$ since the effects of H_N on $\phi_{electronic}$ are neglected in the B-O approximation. Within this approximation, the total energy of a molecular vibronic state is a simple sum of electronic and vibrational energy. In the Hartree-Fock Model the following *electronic* Hamiltonian is used:

$$H = -\sum_{i=1}^N \frac{\hbar^2}{2m_e} \Delta_i - \sum_{i=1}^N \sum_{A=1}^M \frac{1}{4\pi\epsilon_0} \frac{Z_A e^2}{|\vec{R} - \vec{r}_i|} + \sum_{i=1}^N \sum_{j>1}^N \frac{1}{4\pi\epsilon_0} \frac{e^2}{|\vec{r}_i - \vec{r}_j|}$$

This Hamiltonian incorporates H_E as the first sum, the second sum corresponds to the Coulomb attraction between N electrons and M nuclei (H_{NE}) and the third sum includes electron-electron (e-e) repulsion. Since electrons are Fermions, which are particles with half-integer spin ($s = 1/2$), the many-electron wavefunction must be anti-symmetric with respect to the interchange of space and spin coordinates of any two electrons. Pauli's exclusion principle is thus incorporated into the Hartree-Fock model by constructing the many-electron wavefunction as follows (here simplified for the exchange of only two electrons):

$$\Psi(x_1, x_2) = \frac{1}{\sqrt{2}} [\chi_a(x_1)\chi_b(x_2) - \chi_b(x_1)\chi_a(x_2)]$$

where χ_a and χ_b are the spin orbitals (if both Fermions occupy the same spin orbital ($a = b$) then the two-particle wavefunction would vanish). Extending this to a N -electron system can be done by writing the above wavefunction as a Slater determinant

$$\Psi(x_1, x_2, \dots, x_N) = \frac{1}{\sqrt{N!}} \begin{vmatrix} \chi_i(x_1) & \chi_j(x_1) & \dots & \chi_k(x_1) \\ \chi_i(x_2) & \chi_j(x_2) & \dots & \chi_k(x_2) \\ \vdots & \vdots & & \vdots \\ \chi_i(x_N) & \chi_j(x_N) & \dots & \chi_k(x_N) \end{vmatrix}$$

Such anti-symmetric many-particle wavefunctions incorporate the exchange correlation which means that the motion of two electrons with parallel spin is correlated and therefore can not be described by the same wavefunction.

The electronic Hamiltonian is impossible to solve analytically, but approximations can be made. In the Hartree-Fock approximation, the ground state is of a molecule is described by a single Slater determinant of the above form. The variational principle states that the best wavefunction of this form is the one with the lowest possible energy (i.e. $E_0 = \langle \Psi_0 | H | \Psi_0 \rangle = \min$). By minimising E_0 with respect to the spin orbitals chosen one ends up with the Hartree-Fock equations:

$$F_i \chi_i = E_i \chi_i$$

where F_i is an effective one-electron operator (Fock operator) of the form

$$F_i = -\frac{\hbar^2}{2m_e} \Delta_i - \sum_{A=1}^M \frac{1}{4\pi\epsilon_0} \frac{Z_A}{|\vec{R}_A - \vec{r}_i|} + v_i^{HF}$$

and v_i^{HF} is the average potential experienced by the i^{th} electron due to the presence of other electrons. The Hartree-Fock model thus includes the Coulomb and exchange integrals which come into play because of the asymmetry of the total wavefunction. In this way the coupled Schrödinger equation is separated into one-electron problems. Since v_i^{HF} is gained from integrals over all other single-electron wavefunctions, the Hartree-Fock equations must be solved iteratively. After an initial guess of the spin orbitals, iterations are made until v_i^{HF} doesn't change and the spin orbitals used to construct the Fock operator are the same as its eigenfunctions. This is a self-consistent method and forms the basis for the Linear Combination of Atomic Orbitals method (LCAO) for molecular orbital theory. The N spin orbitals with the lowest energy are the called the occupied or hole spin orbitals. The Slater determinant formed from these orbitals is the Hartree-Fock *ground state* wave function. A further simplification can be made by dividing the electrons into two sets, those constituting the σ -bonds and those that are mobile and form the π -bonds. The total molecular electronic wavefunction is given as $\psi = \psi_\sigma \psi_\pi$. Most optical transitions correspond to transitions of the π -electrons, therefore only ψ_π changes and the σ -bonds, along with the nuclei, can be thought of forming a fixed potential in which the π -electrons move. The LCAO method of approximating molecular orbitals (MOs) is motivated by the expectation that when a given electron is in the vicinity of a particular nucleus, its wavefunction will be similar to what it would be in the valence orbital of that atom.

The wavefunction of a π -MO in the LCAO approximation can be written as

$$\psi_{\pi} = \sum_{l=1}^N a_l \phi_l$$

where the ϕ_l terms are atomic orbitals, and the a_l terms are coefficients determined by minimising the whole system. The sum is over all N carbon atoms of the molecule, therefore N molecular wavefunctions are obtained, each with a different a_l coefficient and accommodating to electrons of opposite spin. Filling the lowest $N/2$ levels gives the ground state wavefunction of the system:

$$\psi_{\pi}(\text{ground}) = \psi_1 \alpha_1 \psi_1 \beta_1 \dots \psi_{N/2} \alpha_{N/2} \psi_{N/2} \beta_{N/2}$$

α_l and β_l denote electron spin functions for up and down respectively.

Molecular orbitals are called *bonding* when the linear combination of atomic orbitals is energetically lower than the separated atomic orbitals (the filled levels). MOs higher in energy are called *antibonding* orbitals (unfilled levels). A singly excited wavefunction is gained when using the lowest $N-1$ spin orbitals and one excited spin orbital in the Slater determinant (i.e. promoting an electron from a bonding to an antibonding orbital).

OPTICAL EXCITED STATE

In the elementary Hückel MO theory only the diagonal terms and terms contributed to by the nearest-neighbour bonding atoms r and s of the molecular Hamiltonian (the Slater determinant above) are assumed non-zero. For arbitrary site energies on a molecule in terms of $H_{r,r} = a$ for all diagonal elements and $H_{r,s} = b$ for σ -bonded atoms r and s , the molecular levels are

$$E_l = a + m_l b$$

where m_l terms are the roots of the classic polynomial associated with the molecular Hamiltonian. The individual MO energies E_l can thus be represented as a series of energy levels above and below an energy of zero taken as a itself. The lowest optical transition has an energy equal to the difference in energy between the lowest antibonding orbital, E_f , and the highest bonding orbital, E_g ; thus

$$\Delta E = E_f - E_g = b(m_f - m_g)$$

where the subscript g stands for ground and f the final orbital and m_f and m_g the roots for the characteristic polynomial for the lowest antibonding and highest bonding

orbitals, respectively, and b is the nearest neighbour resonance integral and represents the interaction energy of two bonding *atomic* orbitals. The inclusion of the nearest-neighbour atomic bond overlap causes a spreading in the antibonding levels and thus lifts the degeneracy in bonding (π) to antibonding (π^*) transitions. This treatment, whereby a molecule is thought of as a many one-electron system (atomic valence electrons) brought closer together causing an interaction, with a resonance interaction energy b , that lifts the degeneracy of the system is in some manners similar to the approach adopted for the treatment of dimers and larger aggregates which will be discussed later on.

A molecular system subjected to an external electromagnetic field will respond by changing its state. These changes may be linear in the intensities of the external beam of light, but also non-linear. The most familiar linear optical observable is the absorption spectrum, which describes how much energy is taken out of the external beam due to the excitation of the molecular system to a higher quantum state. This spectrum can be calculated by using Fermi's Golden Rule, which follows from first-order time-dependent perturbation theory in the molecule-field interaction. This interaction is given by $V = -\hat{\mu} \cdot \vec{E}$ where $\hat{\mu}$ denotes the total dipole operator of the molecule and \vec{E} is the electric field. Excluding non-interesting constants the absorption spectrum is given by:

$$A(\omega) = \sum_f \left| \langle f | \hat{\mu} \cdot \mathbf{e} | g \rangle \right|^2 \delta(E_f - E_g - \hbar\omega)$$

where \mathbf{e} is the polarisation vector of the light. Furthermore $|g\rangle$ denotes the state of the molecule before the light was turned on (the collective ground state), while $|f\rangle$ is summed over all molecular excited states. The quantities E_g and E_f denote the energies of these states, while ω is the frequency of the incident light wave. The Krönecker delta function reflects the conservation of energy: absorption will only take place when the photon energy is resonant with one of the molecular transitions. Thus, the absorption spectrum will show a series of delta peaks. In practice, this does not occur due to lifetime broadening of the excited states. In condensed phases (solutions, glasses and crystals), this lifetime is dominated by the dephasing times imposed by interactions with dynamic degrees of freedom in the environment. The area under each absorption peak gives the so-called (oscillator) strength of the transition. The strength is given by the

absolute square value of the transition dipole moment projected along the direction of the polarisation of the light wave (the matrix element of the dipole moment between the ground state and final state). The width of the peak, on the other hand, reflects the lifetime or dephasing time of the final state, with a short lifetime leading to a broader absorption peak. For dipole-forbidden transitions, this dipole vanishes and no absorption peak is associated with the transition. Spontaneous emission, i.e. the decay of an excited state to the ground state by emission of a photon of the appropriate energy, being the inverse of absorption, also occurs at a rate (probability per unit time) that is proportional to the oscillator strength of the transition.

1.4 AGGREGATE MOLECULAR ENERGY STATES

In 1936, Jelley and Scheibe independently discovered that upon increasing the concentration of pseudo-isocyanine (PIC) solutions the broad absorption of PIC monomers at 525nm was replaced by a much narrower absorption band around 570nm. This narrow band is now known as the *J* (Jelley) band and is associated with extended electronic excitations of large groups of PIC molecules, much like the Frenkel excitons in molecular bulk crystals. This class of molecular aggregates with a red-shifted narrow absorption band are called *J*-aggregates. The optical response of aggregates is fundamentally different from the addition of the optical response of individual molecules that make up the aggregate. This results from the collective Frenkel excitons that describe the excited states and optical response of the aggregate system. The narrowness observed is ascribed to the exchange (or motional) narrowing of disorder by the delocalised exciton states and the ultrafast cooperative spontaneous emission (exciton superradiance) is due to the giant oscillator strength found in aggregates.

GROUND STATE

Considering first the case of an ordered dimer, the physical-dimer Hamiltonian operator can be written as the sum of the operators for the isolated molecules H_1 and H_2 plus an intermolecular interaction energy term V_{12} :

$$H = H_1 + H_2 + V_{12}$$

Suppressing the vibrational and spin parts of the overall wavefunction, the ground state wavefunction of the dimer can be approximated as

$$\psi_g = \psi_1 \psi_2$$

where ψ_1 and ψ_2 are the ground state wavefunctions of molecules 1 and 2 respectively. However ψ_g is not an eigenfunction of the total Hamiltonian. For this, the mixing of the excited states of molecules 1 and 2 with ψ_g by V_{12} would have to be included in what is known as a “configuration interaction”. This will be neglected in the following discussion, although it does provide a major contribution to the stability of the dimer, namely the van der Waals energy. With these approximations the ground state energy of the physical dimer is

$$E_g = E_1 + E_2 + \langle \psi_1 \psi_2 | V_{12} | \psi_1 \psi_2 \rangle$$

where E_1 and E_2 are the energies corresponding to the monomer states ψ_1 and ψ_2 . The last term

$$W = \langle \psi_1 \psi_2 | V_{12} | \psi_1 \psi_2 \rangle$$

denotes the Coulombic binding energy W of the dimer and is negative for dimers and positive for excimers. Excimers are physical dimers composed of one electronically excited molecule paired with a ground state of the same kind of molecule. The above expression for the binding energy of the dimer gives values in poor agreement with experiment due to the lack of inclusion of the van der Waals interaction stabilising the dimer.

OPTICAL EXCITED STATE

Having established the ground state of the ordered dimer, the excited state can now be considered. Let ψ_1^* and ψ_2^* denote equivalent excited electronic states of two identical molecules, then both $\psi_1^* \psi_2$ and $\psi_1 \psi_2^*$ have the same energy when the interaction V_{12} is neglected. Without this interaction energy the excitation would also remain on only one molecule. For $V \neq 0$, however, this degeneracy is lifted and the energy of one of the configurations will be different to the other. It must be stressed, that in this model the interaction of the molecules is assumed not to change the basis electronic states of the individual molecules (in a coupled pendulum model, the length of each pendulum

remains unaltered). The interaction only lifts the degeneracy by coupling the two molecules. A result of this interaction is that the excitation energy will oscillate coherently between the two molecules.

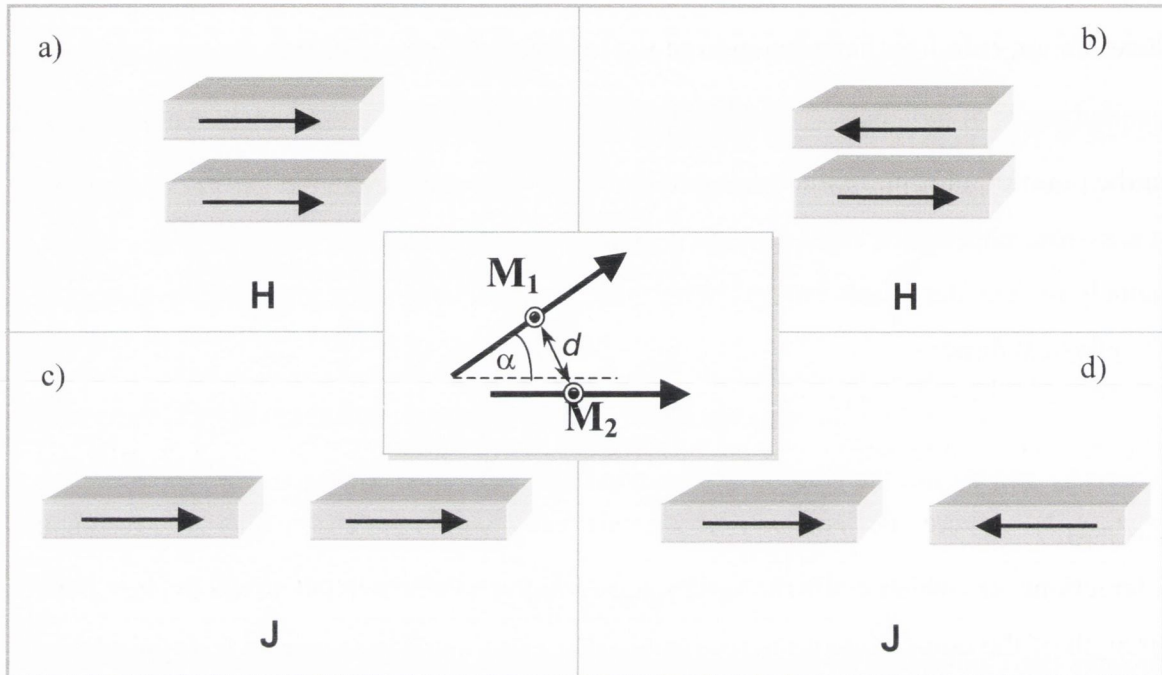


Figure 1.3: Possible FER states for the different molecular aggregate structures, a) Symmetric H-aggregate, b) Anti-symmetric H-aggregate, c) Symmetric J-aggregate and d) Anti-symmetric J-aggregate. Inset: The generalised description of the dipole-dipole interaction between the transition dipole moments of molecules M , where α is the angle between dipoles and d the distance between dipoles in the point-dipole approximation (the latter is taken as the distance between the centres-of-mass of each molecule).

The energy difference between the $\psi_1^*\psi_2$ and the $\psi_1\psi_2^*$ state is determined by the interaction energy and thus the relative orientation of the molecules, in particular the transition dipole moments (see Figure 1.3). The sharing of the excitation energy (from an optical transition) is described by wavefunctions that are linear combinations of the unperturbed (parent) states

$$\psi_E = c_1\psi_1^*\psi_2 + c_2\psi_1\psi_2^*$$

In the special case of identical molecules, $|c_1| = |c_2| = 1/\sqrt{2}$ in order to satisfy the normalisation conditions and the monomer excitation energies $E_1^* = E_2^*$ and the now non-degenerate state energies are given by

$$E(\pm) = E_1^* + E_2 + W' \pm \beta$$

where β is the resonance interaction energy term and determines the splitting between the two energy states (+) and (-) i.e.

$$\beta = \langle \psi_1^* \psi_2 | V_{12} | \psi_1 \psi_2^* \rangle$$

and W' is the Coulombic energy of interaction of the charge distribution of the excited state of molecule 1 with the ground state of molecule 2 (or vice versa):

$$W' = \langle \psi_1^* \psi_2 | V_{12} | \psi_1 \psi_2 \rangle$$

In the point-dipole approximation, used here, the resonance interaction term is given by

$$\beta = \frac{(\overline{M}_1 \cdot \overline{M}_2) |\overline{r}_{12}|^2 - 3(\overline{M}_1 \cdot \overline{r}_{12})(\overline{M}_2 \cdot \overline{r}_{12})}{|\overline{r}_{12}|^5}$$

where r_{12} is the relative position vector of the two molecules (see Figures 1.3 and 1.4). The resonance interaction mixes the degenerate singly-excited states $\psi_1^* \psi_2 = |1\rangle$ and $\psi_1 \psi_2^* = |2\rangle$. There is, however a second class of interaction: the *non-resonant* interactions, in which both molecules are simultaneously excited or de-excited. The strength of the non-resonant interactions is also given by β , however as β is typically of the order of (1000cm^{-1} or 0.12 eV), which is smaller than the energy difference (typically 20000cm^{-1} or 2.47 eV) between $|12\rangle = |\psi_1^* \psi_2^*\rangle$ and $|g\rangle = |\psi_1 \psi_2\rangle$ that are mixed by it, the effect is small and usually ignored. This is known as the Heitler-London approximation, where the dimer ground state is the state with both molecules in their ground state.

The corresponding singly-excited stationary states (eigenstates) arising from the resonant interaction are thus

$$\psi_{E(+)} = \frac{1}{\sqrt{2}} (\psi_1^* \psi_2 + \psi_1 \psi_2^*)$$

$$\psi_{E(-)} = \frac{1}{\sqrt{2}} (\psi_1^* \psi_2 - \psi_1 \psi_2^*)$$

with energies $E_{\pm} = \omega_0 \pm \beta$. This reflects the well-known linear splitting of two degenerate states upon coupling them. These two orthogonal stationary solutions can be thought of as the quantum mechanical equivalent of the two normal modes of a pendulum. For these stationary states the excitation is shared between the two molecules at all times. Having neglected the antisymmetrisation of the electronic wavefunctions,

required by the Pauli exclusion principle, has simplified matters - in fact for singlet excited states, the Coulombic interactions dominate over the electron exchange interactions (however this is not the case for triplet states).

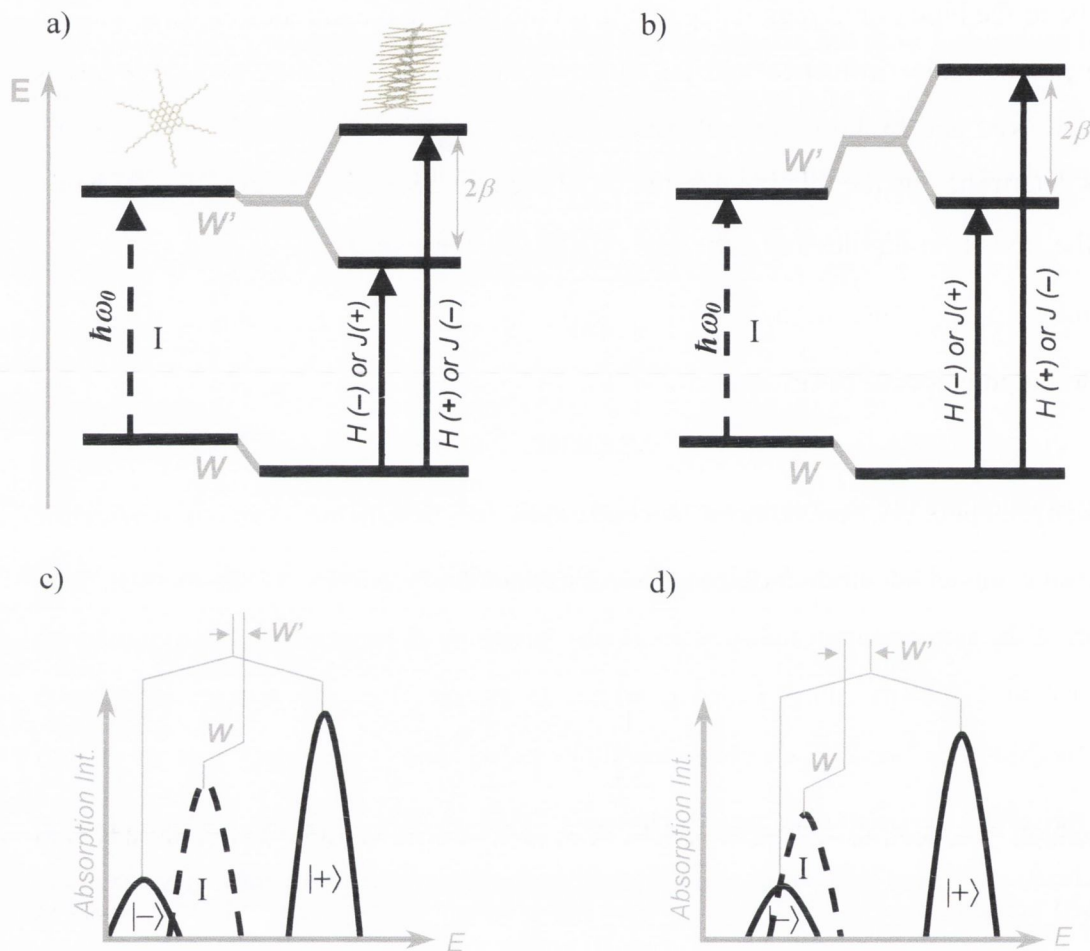


Figure 1.4: Energy level diagram for FER systems a) where $W' \sim 0$ and b) where $W' > 0$. The H-aggregate optical absorption spectrum for each case is given in c) and d) respectively. Since most of the HBC derivatives studied are non-polar, W can be estimated to be approximately zero - this will allow W' to be calculated from the absorption spectrum in Chapters 3 and 4. Note that I represents the isolated molecule transition energy $\hbar\omega_0$. In Chapter 3, aggregate species with $W' \sim 0$ and $W' > 0$ are labelled L and C species respectively. Note that for non-polar molecules $W \sim 0$.

In the language of molecular aggregates, the two states $\psi_{E(+)}$ and $\psi_{E(-)}$ (also labelled $|+\rangle$ and $|-\rangle$) are referred to as one-exciton states (or Frenkel exciton states) as they describe states in which the molecules share one excitation quantum. The one-exciton states of a homogenous dimer are both delocalised: the probability of excitation is

spread evenly over both molecules. The states differ only in the relative phase of the excitation amplitude on both molecules.

As illustrated in Figure 1.4, the observed spectral shift of the dimer absorption can either be to the blue or red region depending on the relative magnitudes of W , W' and of course β . The major influence will be which of the dimer stationary excited states is dipole allowed and by how much these are shifted from the monomer's excited state. This is determined by the relative orientation of the transition dipole moments. To begin with, the transition dipoles from the ground state to the two singly excited states $|+\rangle$, $|-\rangle$, and from the ground to the doubly excited state $|12\rangle$ must be determined. The total transition dipole operator is given by

$$\mathbf{M} = \overline{M}_1 + \overline{M}_2.$$

One must calculate the matrix elements of this operator:

$$\langle \pm | \mathbf{M} | g \rangle = \frac{1}{\sqrt{2}} (\overline{M}_1 + \overline{M}_2)$$

or

$$M_{(\pm)} = \frac{1}{\sqrt{2}} (\overline{M}_1 \pm \overline{M}_2)$$

from which we see, using $|\overline{M}_1| = |\overline{M}_2|$, that the two transitions $M_{(+)}$ and $M_{(-)}$ are polarised perpendicular to each other. Thus, one-exciton states give rise to two peaks in the absorption spectrum, separated by an energy difference of $2|\beta|$ and which have an intensity ratio

$$\frac{I_+}{I_-} = \frac{(1 + \cos \alpha)}{(1 - \cos \alpha)}$$

where α is the angle between the two transition dipole moments \overline{M}_1 and \overline{M}_2 (see Figure 1.3). Considering the case where both dipoles lie parallel, then only one of the states is dipole allowed. For J-aggregates, where the dipoles lie head to toe (and $\alpha = 180^\circ$), only the symmetric state $M_{(+)}$ (also labelled $|+\rangle$) is dipole-allowed and contains an oscillator strength of $2\mu^2$. This state is the lowest lying of the two transition states with an energy $E_{(+)} = \omega_0 - \beta$. Qualitatively speaking, the most stabilising alignment (i.e. minimum interaction of dipoles) is one where both dipoles point in the same direction in

the head to toe configuration. On the other hand, when both dipoles point towards each other, the configuration is more unstable, resulting in a higher interaction energy ($E_{(-)} = \omega_0 + \beta$). For H-aggregates with the transition dipole aligned parallel, the most stabilising arrangement is the non-symmetric anti-parallel alignment with an energy $E_{(-)} = \omega_0 - \beta$. The dipole-allowed, symmetric state, where both transition dipoles point in the same direction lies at higher energy ($E_{(+)} = \omega_0 + \beta$) as it is more unstable.

INHOMOGENEOUS DIMER

In practice, a completely homogenous dimer will not occur in solution. Inhomogeneities, caused by the solvent interacting with the molecules in solution, will result in the molecules in the dimer experiencing different shifts of their transition frequencies. Accordingly, and from now on, the transition frequencies of molecule 1 and molecule 2 will be ω_1 and ω_2 , respectively. Keeping the Heitler-London approximation, so that the dimer's ground state is still the state with both molecules in their ground state, which is not mixed by the two-exciton state $|12\rangle$, the effect of the inhomogeneity on the singly-excited states can be studied. The Hamiltonian of the dimer coupled by the resonance interaction is now

$$H = \begin{pmatrix} \omega_1 & \beta \\ \beta & \omega_2 \end{pmatrix} = \frac{\omega_1 + \omega_2}{2} + \begin{pmatrix} \frac{\omega_1 - \omega_2}{2} & \beta \\ \beta & -\frac{\omega_1 - \omega_2}{2} \end{pmatrix}$$

The resulting eigenstates are thus determined by relative weighting of the energy difference $(\omega_1 - \omega_2)/2$ and the resonance interaction β . In the limit of large inhomogeneity, where $|(\omega_1 - \omega_2)/2| \gg |\beta|$, the interaction is not strong enough to yield appreciable mixing of the states $|1\rangle$ and $|2\rangle$. The resulting excited states of the individual molecules are the proper one-exciton eigenstates. These states, localized on just one of the molecules, have the single molecule oscillator strength given by μ^2 . The absorption spectrum of the dimer would have two peaks, at ω_1 and ω_2 , with equal intensity. In the strong inhomogeneity limit, the molecules can be considered to be totally decoupled and there is no collective optical response from the dimer.

On the other hand, in the weak inhomogeneity limit, where $|(\omega_1 - \omega_2)/2| \ll |\beta|$, the eigenstates are identical to the completely delocalised collective dimer states $|+\rangle$ and $|-\rangle$ defined previously:

$$\Omega_{\pm} = \frac{\omega_1 + \omega_2}{2} \pm |\beta|$$

So the absorption spectrum of a dimer in the weak inhomogeneity limit will have two peaks with average position $(\omega_1 + \omega_2)/2$ and separated by $2|\beta|$, with the angle α , between the two transition dipoles, determining the relative oscillator strengths. For the case of parallel transition dipole moments (as in an H-aggregate), the $+$ state is super radiant and the $-$ state is dark.

Generally, an ensemble of dimers, as opposed to an individual dimer, is measured. In the strong disorder limit ($\sigma \gg \beta$), most of the dimers (say in solution) will be in the strong-inhomogeneity limit and the ensemble spectrum will be identical to that obtained from an ensemble of non-interacting molecules, exhibiting one Gaussian absorption peak of FWHM = 2.35σ .

In the case of weak disorder, where $\sigma \ll \beta$, the vast majority of the dimers will be in the weak inhomogeneity limit, carrying delocalised one-exciton states. The position of these states is given by Ω_{\pm} , which contains the average $(\omega_1 + \omega_2)/2$. As both ω_1 and ω_2 are random variables, their average is also a random variable. The average of two uncorrelated Gaussian random variables is another Gaussian variable with its mean value and variance, respectively, given by the averages of the mean values and the variances of the two underlying variables. Applying this, the absorption spectrum of the ensemble contains two Gaussian peaks which are centred at frequencies $\omega_0 \pm |\beta|$, respectively, and both peaks have a FWHM of $2.35\sigma/\sqrt{2}$. The narrowing of the absorption peaks relative to the single-molecule spectrum by a factor $\sqrt{2}$ is called *exchange narrowing*. Generalised to N molecules the narrowing is of the order \sqrt{N} . The narrowing originates from the fact that in the weak-disorder limit, the eigenstates are delocalised and thus average over the individual inhomogeneous offsets

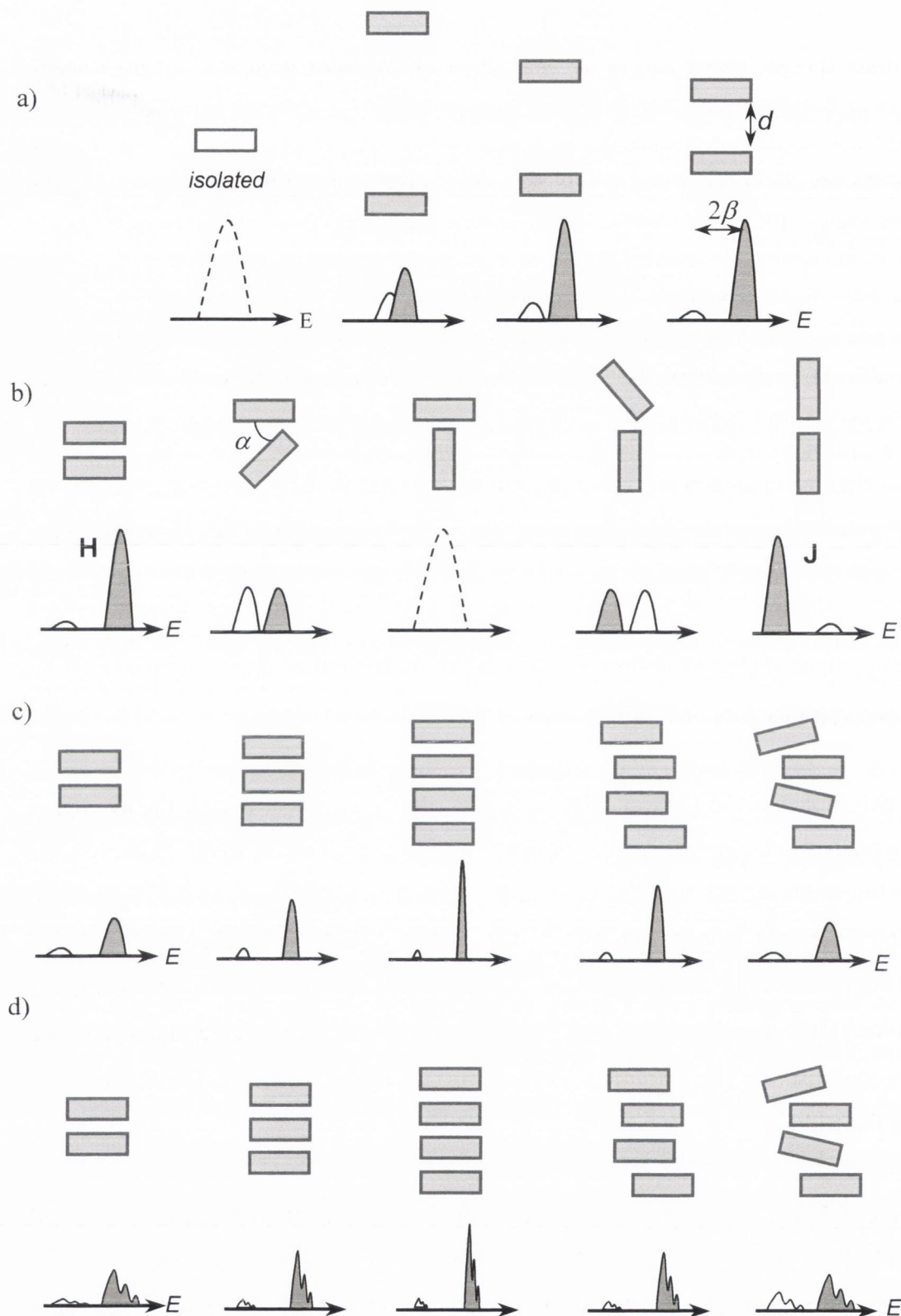


Figure 1.5: Illustration of the correspondence between the physical geometry and order of a molecular aggregate system to the optical absorption properties. a) Strength of resonance interaction β as a function of the intermolecular distance d illustrated here for an H-aggregate. Notice how the peak splitting increases as the intermolecular distance decreases. b) Transformation of an H-aggregate to a J-aggregate by increasing the angle α between the molecules. In an H-aggregate the highest energy FER state has all

the oscillator strength. Notice how in the point-dipole approximation when $\alpha \sim 60^\circ$ the non-zero intensities of the higher and lower FER states are equal. When $\alpha \sim 90^\circ$ the transition dipoles are decoupled therefore the isolated molecular absorption spectrum is observed and the FER states have an identical zero intensity. Upon further rotation, the molecules adopt a J-aggregate configuration whereby the lowest energy FER excited state has all the oscillator strength. c) Optical absorption spectrum as a function of the number of molecules N in resonance. Upon increasing the number of molecules, the oscillator strength of the optical transition increases as a function of N whereas the FWHM is observed to decrease (see text). The FER interaction is limited to nearest neighbour dipole-dipole coupling therefore 2β is not a function of the number of molecules in resonance. Upon decreasing the order of the system 2β may decrease, but more significantly the FWHM will increase and the oscillator strength will decrease as FER is disorder limited. However in real systems disorder will tend to limit FER to approximately a dimer even though the physical size of the aggregate may be much larger. d) The effect of FER on the vibrational-electronic (v-e) properties of the absorption spectrum as a function of the order of the system. It is typically observed that the v-e features of the spectrum tend to disappear as the number of molecules in resonance increases. This is the extensive topic of Chapter 6. Hollow rectangles represent isolated molecules, shaded rectangles represent molecules as part of an aggregate. In the spectra, dashed lines correspond to the isolated molecule, shaded peaks indicate the symmetric FER transition, non-shaded peaks represent the anti-symmetric FER transition.

of the two molecules in the dimer. If these two offsets are uncorrelated, the averaging process tends to eliminate large deviations from the overall mean value. However, the narrow linewidth should only be expected for the lower energy state, as the higher state will tend to rapidly relax to the lower one, leading to lifetime broadening. Exchange narrowing becomes more pronounced when increasing the number of interacting molecules. Only the diagonal disorder has been discussed but for larger aggregates the off-diagonal disorder (i.e. variations in β) is also exchange narrowed, leading to much smaller linewidths.

In Figure 1.5, the main spectroscopic characteristics of FER systems are described schematically. There are two main contributions to the spectrum: the aggregate geometry and the degree of order of the aggregate system (orientation order translates into energetic order and plays the major role if chemical purity is not considered). The orientation of the molecules in an aggregate can affect the level of resonance interaction and decide which FER state will have the highest oscillator strength. The degree of order of the aggregate system will determine the number of molecules in resonance since FER is disorder limited. In Figure 1.5 d), the effect of the resonance range on the

vibrational-electronic properties of the absorption spectrum are illustrated. This will be further discussed in Chapter 6.

MOLECULAR CRYSTAL EXCITATIONS

The excited state splitting described above arises when two single molecules are brought into close proximity. The degenerate energy levels ($\omega_1 = \omega_2$) when coupled split into two components. Further splitting, however, can arise when the molecules comprising the aggregate are arranged in a periodic manner, such as in a crystal. First described by Davydov, a given molecular energy level may be split into as many components as there are inequivalent molecules per unit cell. This splitting is *in addition to* the level splitting produced by the interaction energy between two adjacent identical molecules. The splitting W_D between the crystal components at $k = 0$ is known as the Davydov splitting and depends upon the interactions between molecules that are translationally inequivalent, whereas the mean energy displacement downward depends on interactions between equivalent molecules. The Davydov component bandwidth is 4β . Typically this extra splitting will only be observed in single crystal systems. The aggregates described in this thesis tend to form an ensemble of nanocrystals and therefore this additional Davydov splitting is not observed.

¹ Fechtenkötter, A.; Tchegotareva, N.; Watson, M.; Müllen, K.; *Tetrahedron* **2001**, *57*, 3769.

² Fechtenkötter, A.; Saalwächter, K.; Harbison, M. A.; Müllen, K.; Spiess, H. W.; *Angew. Chem. Int. Ed.* **1999**, *20*, 3039.

³ Schmitz-Hübsch, T.; Sellam, F.; Staub, R.; Törker, M.; Fritz, T.; Kübel, Ch.; Müllen, K.; Leo, K.; *Surface Science* **2000**, *445*, 358-367.

⁴ "Charge Transport in Self-Assembling Discotic Liquid Crystalline Materials", PhD. Thesis by Anick van der Craats, Radiation Chemistry Department of the Interfaculty Reactor Institute, Delft Institute of Technology, The Netherlands, June 2000.

⁵ van der Craats, A. M.; Warman, J. M.; Fechtenkötter, A.; Brand, J. D.; Harbison, M. A.; Müllen, K.; *Advanced Materials* **1999**, *11*, 1469.

⁶ Schmidt-Mende, L.; Fechtenkötter, A.; Müllen, K.; Moons, E.; Friend, R. H.; MacKenzie, J. D.; *Science* **2001**, 293, 1119.

⁷ H.Meyer, D.Haarer, H.Naarman, H.H.Hörhold, *Phys. Rev. B* **52**, 2587 (1995)

⁸ For a good description of the synthesis of mLPPP see “Conjugated Ladder-Type Structures”, U. Scherf, *Handbook of Conjugated polymers* (1997)

1.1

Chapter 2: EXPERIMENTAL SET-UP

In this Chapter the experimental sample preparation procedures and experimental set-ups will be discussed. The experimental optical measurement techniques employed here are conventional techniques and were carried out in standard instruments with no additional modifications required. The materials used were provided by:

HBC-C8,2 and HBC-PhC12

Max-Planck-Institute fuer Polymer Forschung, Mainz, Germany. (Figure 2.1)

N-HBC

Chemistry Department, Trinity College Dublin, Ireland. (Figure 2.2)

J-HBC

Aida Nanospace Project, Exploratory Research for Advanced Technology, Japan. (Figure 2.2)

F-HBC

Department of Chemistry, Freiburg University Switzerland (courtesy of FOCAS, Dublin Institute of Technology, Ireland). (Figure 2.2)

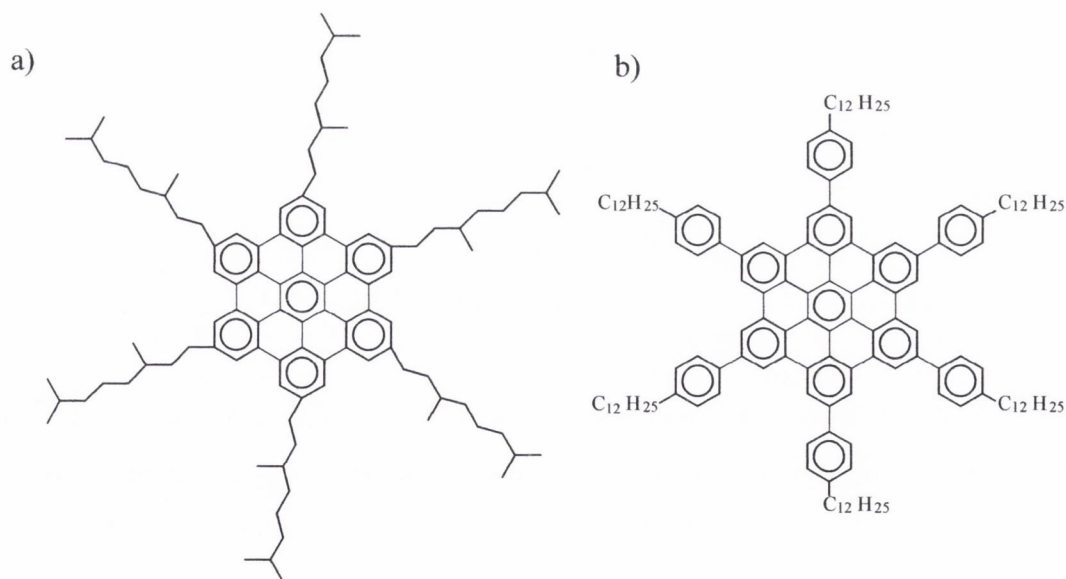


Figure 2.1: Chemical drawings of the molecular structure of a) HBC-C8,2 and b) HBC-PhC12.

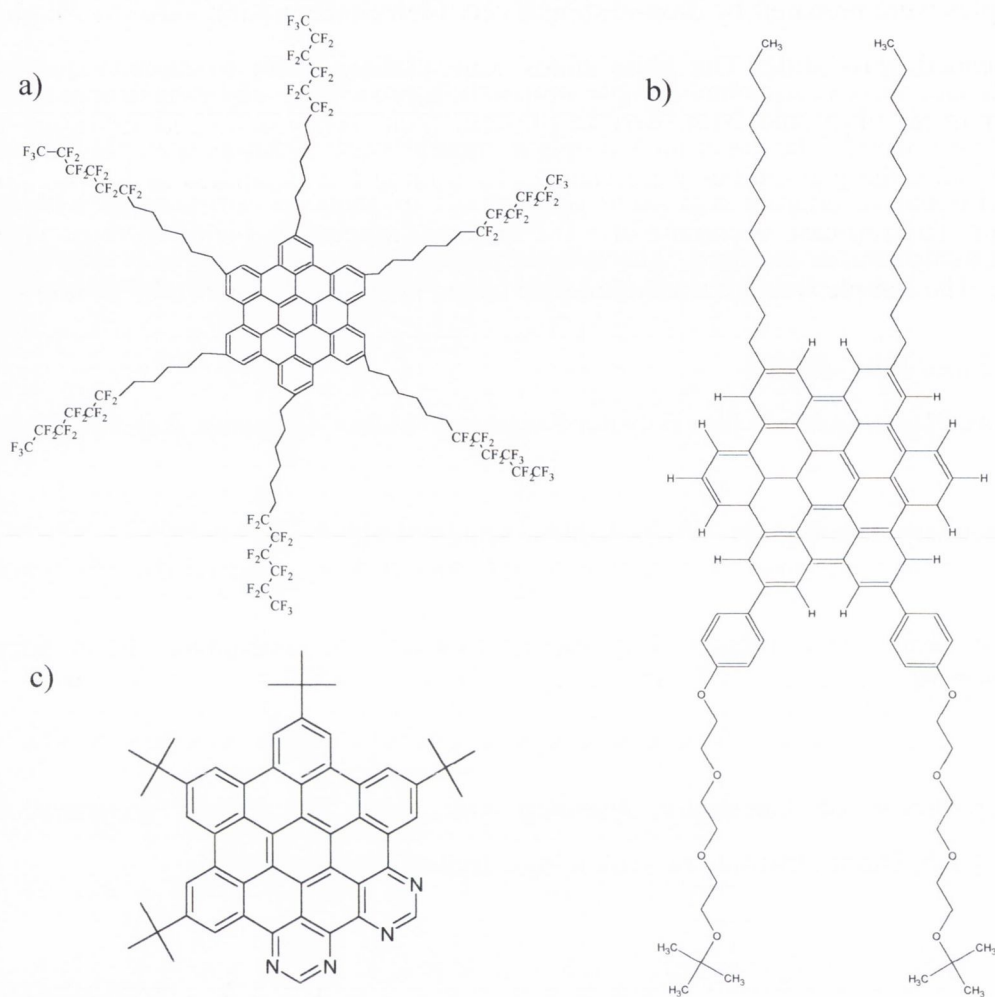


Figure 2.2: Chemical drawings of the molecular structure of a) F-HBC, b) J-HBC and c) N-HBC.

2.1 SPECTROSCOPY IN SOLUTION AND SOLID-STATE

The HBC materials in powder form, as synthesised, were weighed and dissolved, into approximately 10^{-3} Molar solutions in spectroscopic grade organic solvent such as toluene or chloroform. Each solution was then sonicated using a sonic tip to break up the large aggregates (20% of 600 Watts). An example of a dilution series used is: 1.66ml volume was taken and diluted by one-third by adding 3.32ml of toluene. This sample was then sonicated and the procedure repeated using the diluted sample as the starter until 24 solutions of progressively lower concentrations were made up for each material. The sample concentrations thus spanned a range from 10^{-3} M to

approximately 10^{-15} M as illustrated schematically in the top row of Figure 2.3. Solid state samples were prepared by drop-casting a very high concentration $\sim 10^{-3}$ M solution onto a cleaned glass slide. The glass slides were cleaned, prior to drop-casting, by sonication in an ultrasonic bath, first in toluene, then isopropanol and followed by acetone. Finally the glass slides were cleaned by boiling for 2 minutes in acetone and dried in air. To drop-cast, a volume of ~ 0.2 ml was dropped on a slide for each HBC derivative. The sample was left to dry and then baked in an oven at 50 °C for 24 hours.

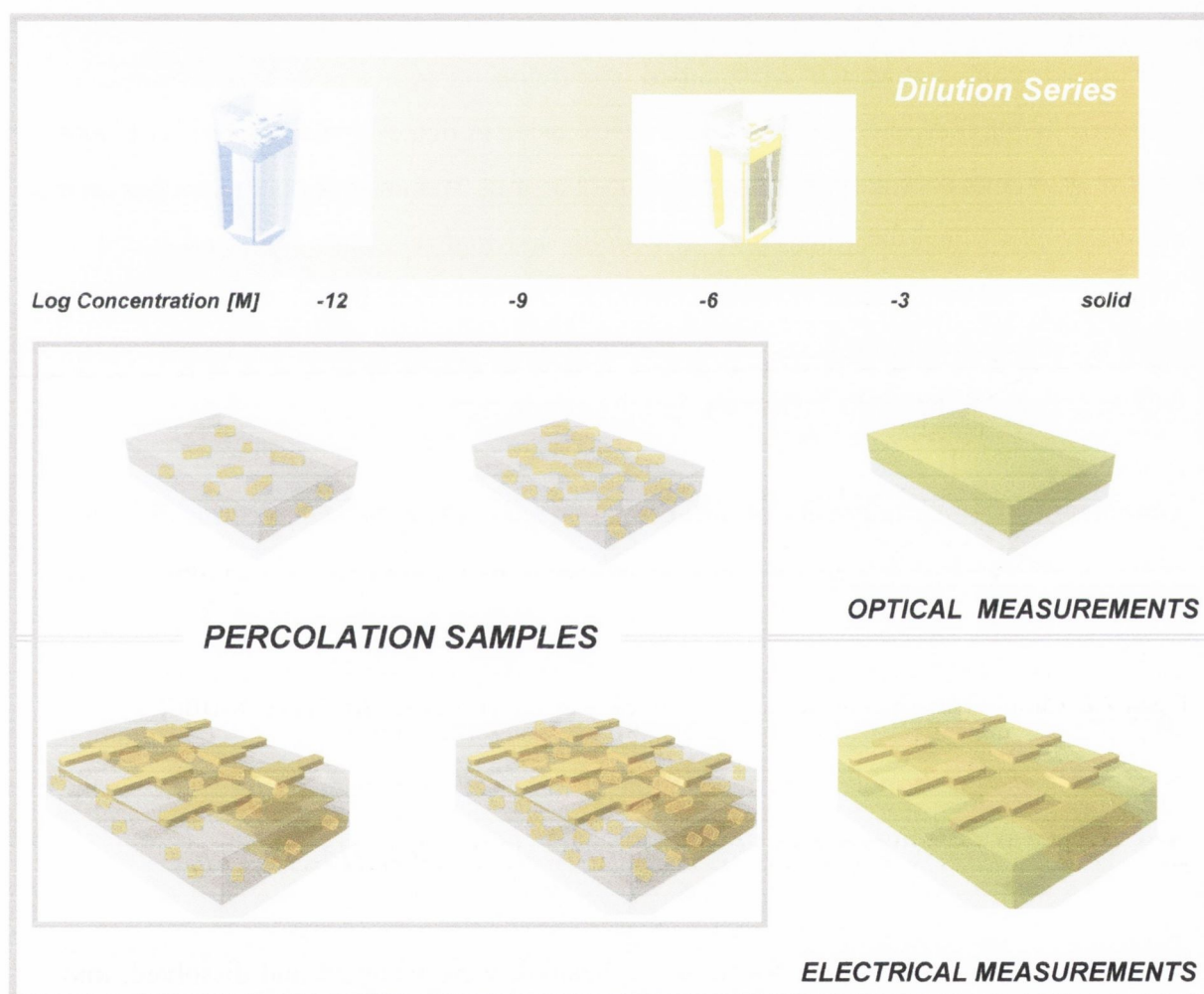


Figure 2.3: Illustration of the most important samples, for each HBC derivative, discussed in this thesis: Optical measurements of a dilution series of a given HBC molecule, optical measurements of a percolation series of increasing MSA loading (up to and including pristine solid films) and electrical measurements of the same percolation networks (and pristine solid films). The solution samples were prepared by careful dilution and sonication in a series. The percolation networks were prepared by mixing a solution of an inert polymer with a solution of HBC and spinning onto a glass slide. For electrical measurements bottom and top metal electrodes were applied.

The absorption properties were measured using a sample and reference (quartz cuvette and solvent) using ultra-violet and visible (UV-vis) wavelengths transmission comparison technique. The fluorescence properties of the samples were measured using photo-luminescence (PL) and photo-luminescence-excitation (PLE) techniques. All UV-vis absorption, PL and PLE spectra measured were carried out in solution in 1cm path-length quartz sample cuvettes. UV-vis measurements were performed using a Shimadzu UV-1601PC UV-vis Spectrometer, and PL and PLE spectra were performed using a Perkin-Elmer LS 50 B (and LS 55) Luminescence Spectrometer.

At concentrations below 10^{-7} M standard absorption photometers are not as optically sensitive as luminescence spectrometers (it is easier to detect a small amount of light than it is to detect a small decrease in light intensity). The absorption spectra for each derivative were therefore measured at medium and high concentration, and found to match the excitation spectra of each peak in the luminescence spectra, thus proving that there is only one chromophore per molecule present. In most cases excitation spectra will be presented due to their superior signal-to-noise ratios.

Throughout the measurements of the excitation and luminescence spectra, there are some instances when two species (or two chromophores) are observed in solution. This is at high concentration when isolated molecules of F-HBC or HBC-PhC₁₂, in addition to aggregates, were found to be in solution. In general, and unless otherwise indicated, all luminescence spectra are obtained from exciting the molecules at the excitation maximum, and all luminescence-excitation spectra were measured by detecting the fluorescence at the luminescence maximum.

To calculate the absorption/extinction coefficient, the log base 10 absorbance acquired by the machine was corrected for by multiplying by 2.3 (to change to ln base e). Now the usual Lambert-Beer law was applied, and the corrected absorbance was divided by the path length (1cm) and the concentration (C) to give the following equation:

$$\begin{aligned}
 I &= I_0 \exp(-\alpha LC) \\
 \ln\left(\frac{I}{I_0}\right) &= -\alpha LC \\
 \ln(10) \log\left(\frac{I}{I_0}\right) &= -\alpha LC \quad (2.1) \\
 \therefore \alpha &= \frac{2.3 \log\left(\frac{I}{I_0}\right)}{LC} \quad [Lmol^{-1}cm^{-1}]
 \end{aligned}$$

2.2 EXCIMER PERCOLATION / MOLECULE SOLUBILITY

For MSA dopants in inert polymer matrices, 0.2 mL of a given HBC derivative solution of known concentration $\sim 10^{-5}$ M (prepared as above) was added to each sample bottle of a dilution series of a polymer solution. Three polymers were tested for suitability namely polystyrene, polycarbonate and PMMA. These polymers have characteristically high band-gap and are therefore transparent at visible wavelengths probed during the measurements. The glass substrates to be used were cleaned by sonication in toluene, then isopropanol followed by acetone. The glass slides were finally boiled in acetone for 2 minutes and dried in air.

For each excimer percolation network sample made, the dopant loading of the MSA is determined from the ratio of the mass of the HBC derivative to the total mass of polymer and dopant in the composite solution. Since the density of the polymer and HBC derivatives are comparable, the mass loading ratio is roughly similar to that of the volume loading ratio. To prepare the solid state films ~ 0.1 ml of a given composite solution was dropped onto a cleaned glass slide. After drying in air the samples were heated in an oven at 50° C for 24 hours. In this manner solid state composite samples, on glass, with dopant loadings, given by $M_A/(M_A + M_B)$ - where M_A and M_B are the masses of the dopant and matrix polymer respectively, ranging from 5×10^{-6} (0.0005 %) to 0.71 (71%) were prepared for each HBC derivative (see middle row of Figure 2.3). The PL and PLE spectra of the composite solutions were measured using Perkin-Elmer LS 55 Luminescence Spectrometer. To determine the ratio of the PL to red-shifted

(excimer) emission, the ratio of the PL maximum intensity to red-shifted emission maximum was determined. These values were then plotted against their respective MSA loadings and plotted.

For Hildebrand solubility parameter measurements, acetonitrile and hexane were titrated into solutions of MSA derivatives in chloroform or toluene of known concentration (from the solution dilution series prepared as described above). For the measurement of the Hildebrand solubility parameter of isolated molecules and aggregates, a solution concentration of $\sim 10^{-13}$ M and $\sim 10^{-5}$ M was used respectively. The latter concentration was chosen to be below the threshold of self-absorption effects altering the PL spectra. The Hildebrand solubility parameter for the solvent mixture is calculated, for example, as follows $\delta_{\text{mix}} = \delta_{\text{chloroform}} \times (V_{\text{chloroform}} / V_{\text{tot}}) + \delta_{\text{hexane}} \times (V_{\text{hexane}} / V_{\text{tot}})$. If a molecule is soluble in a solvent mixture of a given δ_{mix} then the Hildebrand solubility parameter of the molecule $\delta_{\text{mol}} \sim \delta_{\text{mix}}$. The natural miscibility of solvents (driven by entropy) will give rise to a range of allowed values of δ .

2.3 ELECTRICAL MEASUREMENTS

Composite and pristine films of HBC derivatives were prepared for electrical measurements by the construction of planar sandwich devices. Glass slides (12 × 12 mm) were cleaned in a sonic bath by sonication in toluene, then isopropanol, followed by acetone. Finally the glass slides were further cleaned by boiling in acetone for 2 minutes. The glass slides were then left to dry in air. Gold bottom electrodes were prepared by sputtering gold, by Ar ion bombardment, onto the glass slides at high vacuum $\sim 10^{-6}$ mbar. The deposition of the metal was controlled by a quartz crystal thickness monitor and sputtering terminated after typically ~ 500 Å was deposited. See last row in Figure 2.3 for illustration of electrical samples.

Pure or composite solutions were then deposited by spin-coating techniques at rotational speeds of 1000 – 2000 r.p.m. in air. The samples were then allowed to dry and baked at 50° C for 24 hours. The samples were then introduced into the top electrode evaporation machine and kept at high vacuum $\sim 10^{-6}$ M for 8 -12 hrs. The top electrode metal, either

gold or aluminium, was evaporated, by thermal indirect heating of a tungsten boat, through a six pad shadow mask. The top electrode thickness was controlled, via a quartz crystal monitor, to be typically $\sim 400 \text{ \AA}$ thick (using a slow initial deposition rate of $\sim 0.5 - 1 \text{ \AA/s}$).

2.4 ATOMIC FORCE MICROSCOPY MEASUREMENTS

Atomic Force Microscopy Non-Contact measurements were conducted on the samples used for the pristine electrical samples described above using a Frequency Modulation technique of an etched silicon cantilever on a NanoScope III Atomic Force microscope. Other Non-Contact AFM images acquired are described where necessary in Chapter 7. Scanning Electron Microscope measurement were carried out by depositing the HBC MSAs from solution onto a silicon wafer ($5 \times 5 \text{ mm}$), cleaned by boiling in a 1:1:5 NH_4 (aqueous): H_2O_2 : H_2O solution for 15 minutes. A 10 \AA surface of gold was evaporated on the substrates to make them conductive. SEM measurements were then performed using a Hitachi S 3500N scanning electron microscope.

Chapter 3: ABSORPTION AND PLE SPECTRA

The aim of this chapter is to demonstrate that the optical properties of solutions of molecules are heavily dependent on whether the solution is composed of an ensemble of isolated molecules or an ensemble of aggregated molecules. Usually it is assumed that species in solution are isolated, despite the fact that generally the photo-physical properties of solutions of conjugated molecules are not the same as is expected for the photo-physical properties of an ensemble of isolated molecules¹. The discrepancy between theory and experiment is especially obvious for non-polar molecules^{2, 3}. For instance, for solutions of non-polar molecules at high concentration 10^{-6} M: a) there is often a negligible optical absorption transition energy shift upon a change in solvent polarity (even though the PL transition energy may decrease) b) there is a negligible difference between the optical transition energies of a solution of supposedly isolated molecules and a solid state film of the same molecules c) there are significant changes to the oscillator strength of the absorption band upon changes in solvent d) there is a negligible Stokes shift for supposedly isolated molecules (self-absorption at high concentration may give rise to what seems like a large Stokes shift), e) the FWHM of a large ensemble of supposedly isolated molecules is too small for an uncorrelated ensemble, and finally the optical spectra of similar size and shape molecules are vastly different in structure but not in energy. All these discrepancies, we will show, can be explained if the solution of conjugated molecules is considered as an ensemble of aggregates.

Various solutions of derivatives of HBC are investigated in this chapter. The absorption and PLE spectra obtained at various concentration ranges (High $\sim 10^{-6}$ M, Medium $\sim 10^{-8}$ M and Low $\sim 10^{-13}$ M) are compared and the suitability of an isolated molecule description is assessed. Failing an isolated molecule photo-physical description, the spectra are then assessed in terms of an aggregated FER description.

The absorption spectra of all the molecules are compared and examined for evidence of FER. As described in the Introduction Chapter, FER is a good indicator of molecular aggregation. By comparing the varying degrees of FER observed in the absorption spectra (and PLE spectra) of closely related aggregate systems, several structural

parameters can be elucidated. These include the general aggregate structure and superstructure, the ground state – ground state interaction and the excited state – ground state interactions between neighbouring molecules in an assembly. From the optical spectra, the species at low concentration, and some species at high concentration, are found to be best described as isolated molecules. Higher concentration solutions, with some exceptions, are found to be suitably described in terms of aggregates. The optical spectra of several HBC derivative solutions are found to be best described by two morphologically different aggregate species in solution. The exception are some solutions, of liquid crystalline derivatives of HBC, that are composed of aggregated and isolated species at high concentration.

3.1 INTRODUCTION

From the nano-scale to the macro-scale, all natural and man-made constructions can be described in terms of different structural hierarchical levels⁴. At the nano-scale, each change in structural hierarchy involves a new set of dominant interactions. These interactions are essentially different manifestations of the electrostatic force. The Coulombic interaction force magnitude and direction, as well as the range of each interaction, are determined by the electronic charge distributions and physical dimensions of a structure. From quantum mechanics the relationship between the energy and the physical dimensions of a system is established and accordingly, different structural hierarchical levels tend to give rise to different interaction energies.

In optical spectroscopy, the electronic properties of nano-scale structures are probed by using photons to determine the energy of optically allowed electronic transitions between the electronic energy levels of a system^{5,6}. From this, a correlation between the physical dimensions and energetic structure can be determined. In molecular optical spectroscopy, the tendency has been to interpret absorption and photo-luminescence spectra solely in terms of the molecular structure. This ignores all but one structural hierarchical level, namely the molecular structure. Although usually this is a valid first-order approximation, we will show that much more can be gleaned from optical spectra

if higher structural levels, such as the aggregate structure and aggregate super-structure, are considered.

Beyond the molecular structure, there exist two major structural levels that can influence the optical spectra⁷: the molecular aggregate structure and the supra-organisation of molecular aggregates. As shown in Figure 3.1, for HBC derivative molecules, these structural levels describe the nanowire and nanowire bundles respectively (for some HBC derivatives studied the superstructure of the MSA is a nano-tubule). The impact these large dimension super-structures can have on the optical spectra^{8,9} is best highlighted by the fact that on average the wavelength of the light probing the system is approximately 3 orders of magnitude greater than the smallest component (a single molecule $\sim 1\text{nm}$). Note that for HBC molecules in solution the terms aggregate and MSA are interchangeable. The former implies disordered aggregation where as the latter implies some order in the aggregate formed.

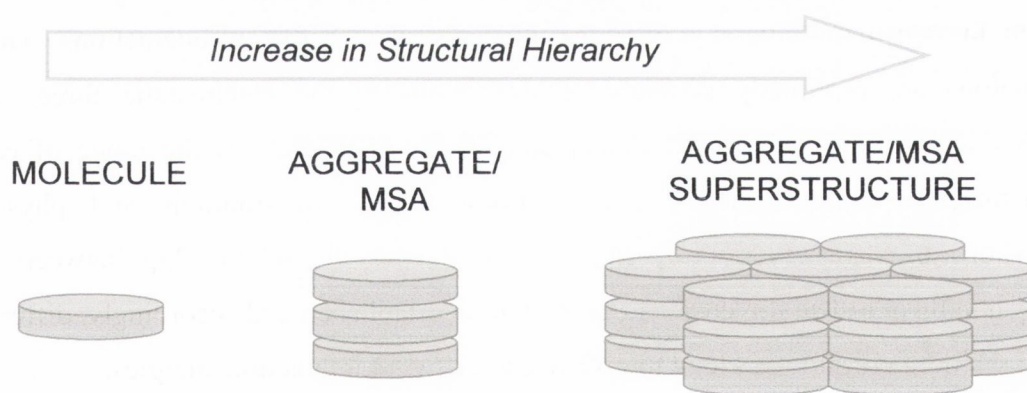


Figure 3.1: Illustration of the successive structural hierarchies from isolated molecule, to aggregate to aggregate superstructure. For the HBC derivatives studied, the aggregates are nanowires and the aggregate superstructures are nanowire bundles and/or nano-tubules.

3.2 ISOLATED MOLECULE

2D QUANTUM BOX

The dimensionality and physical size of a quantum box system will determine the energy levels accessible to an electron located in the well. Molecules can therefore be viewed as quantum wells where electrons populate several molecular orbitals (MOs) of different energies. For sp hybridised molecular systems, bonding electrons can be subdivided into two groups: σ -bonds and π -bonds. These two classes of bonds differ not only in geometry but also in energy. It is the difference in energy that is of interest here. In this regard the low energy π electrons are confined to regions of π -bonding and the high energy σ electrons are confined to regions of σ -bonding. Taking HBC as an example molecule, the aromatic core of the molecule has both π and σ electrons and whereas the aliphatic side-chains exclusively have σ electrons. In terms of the photo-physics of HBC, a photon of energy equal to that of a π - π^* electronic transition will only be probing the aromatic core of the molecule and not the side-chains (see Figure 3.2).

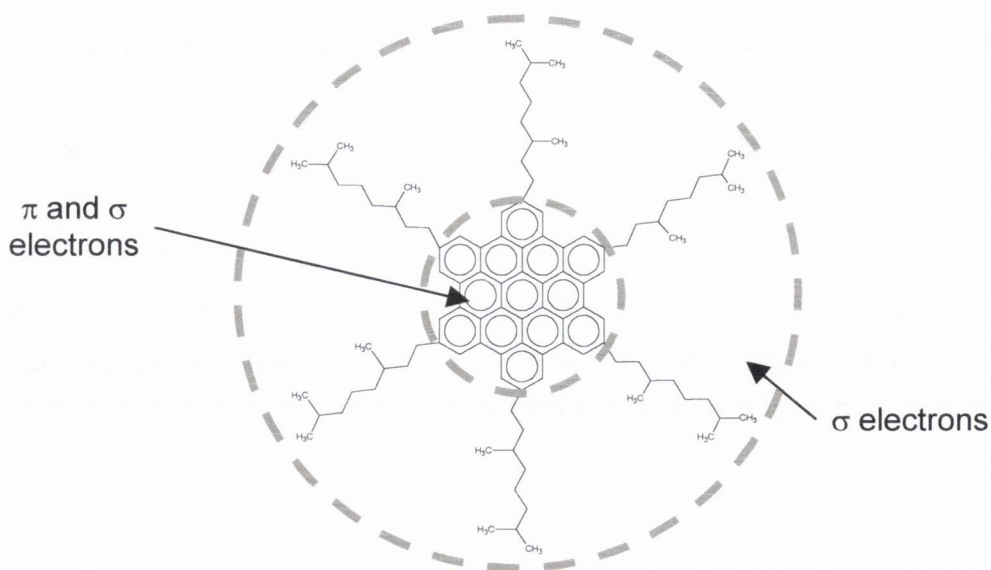


Figure 3.2: The molecular structure of HBC-C8,2. The aromatic core of the molecule has both σ and π bond electrons whereas the aliphatic chains have only σ -bond electrons.

HBC molecules are approximately 2D planar molecules. Applying Schrödinger's equation, for a particle in a 2D box, to the HBC molecule, allows a rough determination of the energy levels and transition energy of the molecular system (see Eqn. 3.1). This will be useful when interpreting the optical absorption spectrum. Approximating the HBC molecular core as a 1 nm \times 1 nm quantum well, gives the eigenvalues of the respective 2D quantum well eigenstates (see Table 3.1). To determine the lowest energy optical transition, the electronic levels are filled up with the 42 π electrons of a HBC molecule. Therefore the highest occupied energy level E_0 for HBC corresponds to the degenerate energy levels (3,5) and (5,3) at 12.78 eV using the convention (n_x, n_y) . The next unoccupied energy level E_1 (degenerate (6,1) and (1,6)) is at a higher energy 13.91 eV. Therefore, the lowest energy optical transition S_1 is given by $E_1 - E_0 = 1.13$ eV (1097 nm). The next highest unoccupied energy level E_2 is also degenerate (2,6) and (6,2) and is at 15.04 eV. The S_2 optical transition energy between the ground state and the second excited state is given by $E_2 - E_0 = 2.26$ eV (548 nm). Similarly calculated, the S_3 transition energy is 2.63 eV. Note the large energy difference ~ 1.13 eV between the S_1 and S_2 optical transitions.

$$E_{(x,y)} = \frac{\hbar^2}{2m_e} \left(\frac{\pi}{L} \right)^2 (n_x^2 + n_y^2) \quad (3.1)$$

As a useful comparison the energy levels of coronene were also calculated. The dimensions of coronene are 7.4 Å \times 7.4 Å., therefore theoretically, the energy of an electron confined in coronene will be at higher energy than an electron in HBC. Following the same procedure as for HBC, the energies of the eigenstates and electronic transitions of coronene are listed in Table 3.2. The energies of the S_1 , S_2 and S_3 transition states are 3.43 eV, 4.12 eV and 6.17 eV respectively.

		n_x						
		1	2	3	4	5	6	7
n_y	1	0.752	1.88	3.76	6.392	9.776	<i>13.912</i>	18.8
	2	1.88	3.008	4.888	7.52	10.904	<u>15.04</u>	19.928
	3	3.76	4.888	6.768	9.4	12.784	16.92	21.808
	4	6.392	7.52	9.4	12.032	15.416	19.552	24.44
	5	9.776	10.904	12.784	15.416	18.8	22.936	27.824
	6	<i>13.912</i>	<u>15.04</u>	16.92	19.552	22.936	27.072	31.96
	7	18.8	19.928	21.808	24.44	27.824	31.96	36.848

Table 3.1: Eigenvalues for 2D – QB of the dimensions of HBC. The values in **bold**, *italics* and underlined correspond to the HOMO, LUMO and LUMO +1 energy levels respectively.

		n_x						
		1	2	3	4	5	6	7
n_y	1	1.372	3.43	6.86	11.662	<u>17.836</u>	25.382	34.3
	2	3.43	5.488	8.918	13.72	19.894	27.44	36.358
	3	6.86	8.918	12.348	<i>17.15</i>	23.324	30.87	39.788
	4	11.662	13.72	<i>17.15</i>	21.952	28.126	35.672	44.59
	5	<u>17.836</u>	19.894	23.324	28.126	34.3	41.846	50.764
	6	25.382	27.44	30.87	35.672	41.846	49.392	58.31
	7	34.3	36.358	39.788	44.59	50.764	58.31	67.228

Table 3.2: Eigenvalues for 2D – QB of the dimensions of coronene. The values in **bold**, *italics* and underlined correspond to the HOMO, LUMO and LUMO +1 energy levels respectively.

PERIMETER FREE ELECTRON ORBITAL THEORY

In PFEO theory molecular orbitals are only a function of the electronic coordinates. The advantage of this method is that all the electronic energy is kinetic and any potential energy terms are assumed constant. It therefore represents a level of simplification similar to that employed in the 2D quantum box. In PFEO theory a Poly-Aromatic-Hydrocarbon (PAH) molecule is treated as a ring of atoms around which π -electrons can move freely¹⁰. This method is reasonably successful at determining the singlet excited states of catacondensed PAH molecules such as benzene, naphthalene and anthracene¹¹. Applying the same method to coronene and HBC reveals some interesting results when compared to the optical spectra. Although, chemically speaking coronene is described as having 7 fused benzene rings, in terms of PFEO theory it can be

described as a molecule composed of 6 catacondensed aromatic rings arranged in a circle such that the first aromatic ring is fused to the 6th and last ring (see Figure 3.3).

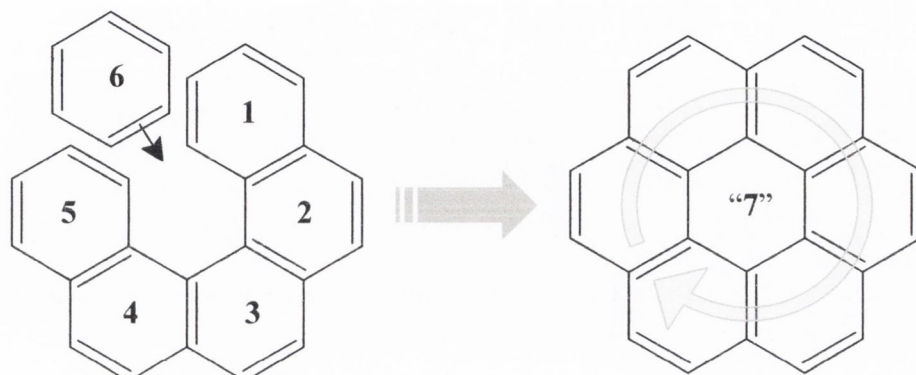


Figure 3.3: Illustration of how coronene can be described as a chemical construct derived from the fusion of 6 benzene rings. The “7th” benzene ring is essentially formed in the centre by sharing carbon atoms with the 6 benzene rings in the periphery of the molecule. Sextet ring current of coronene is indicated by arrow.

In PFEO theory the energy of an electron is given by the electrons’ angular momentum in the plane around the perimeter formed by the fused benzene rings. The angular momentum is constrained to integral multiples $h/2\pi$. From the relationship $E = p^2/2m$, where p and m are the momentum and mass of an electron respectively, the energy levels are given by:

$$E_q = \frac{\hbar^2}{2m_e} \left(\frac{1}{r} \right)^2 q^2 \quad (3.2)$$

where q is the orbital angular momentum quantum number. The radius r is given by $c_0 a = 2\pi r$ where c_0 is the number of aromatic C = C bonds around the perimeter and the bond length a is 1.38 Å. In general the number of π -electrons in a linear catacondensed PAH system is given by $2(2n+1)$ where n is the number of cyclic rings. For a circular catacondensed PAH system the fusion of the first and the last rings results from the sharing of π -electrons between these rings, therefore the total number of π -electrons is given by $4n$. Coronene, with $n = 6$ rings, has 24 π electrons that fill the available energy levels as shown in Figure 3.4.

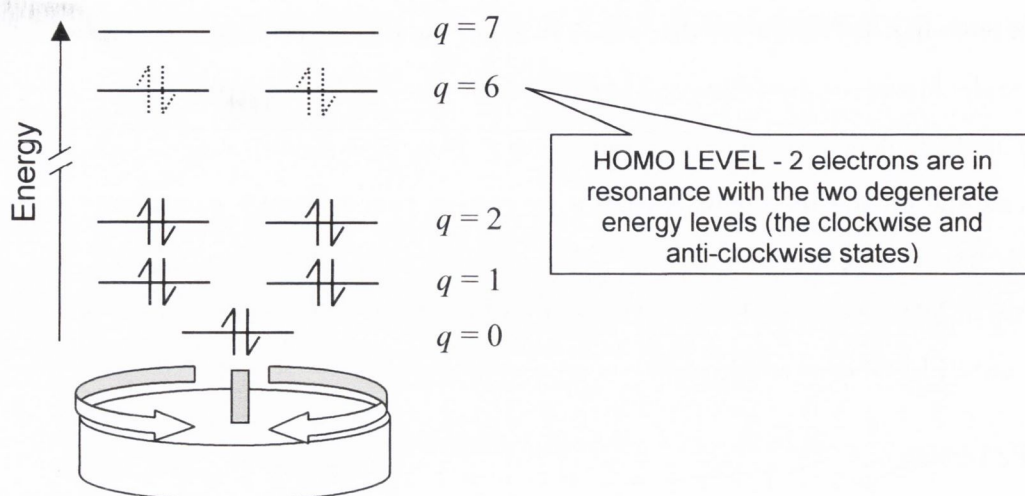


Figure 3.4: The PFEO description of the eigenstates of a coronene molecule. For coronene, all the levels ($q = 0, 1, 2, 3, 4$ and 5) are filled with the exception of the HOMO level ($q = 6$), which is partially filled. In the molecular ground state, the 24 π -electrons fill the lowest available states. Note that the HOMO level of coronene in the PFEO theory has only 2 electrons (compared to the 4 that are required to fill the level). Therefore, in order to conserve angular momentum, in this framework of PFEO theory, the 2 electrons must be in resonance with the clockwise and anti-clockwise states. Otherwise the molecule would have a net angular momentum in the molecular electronic ground state. The lowest state $q = 0$ has no net angular momentum and is therefore not degenerate. The LUMO level is given by $q = 7$.

This allows the determination of the highest occupied level and is assigned the subscript f . The next highest level, by convention, is assigned the subscript g . The transition energy of the first singlet excited state is thus the energy difference between the g and f levels, and can be calculated from Eqn 3.2. Inserting the correct values gives an energy of the first excited singlet state S_1 of coronene is ~ 3.16 eV (or $\sim 25,556$ cm^{-1}). This is remarkably close to the energy of the lowest transition of coronene¹² between 2.85 eV – 3.34 eV ($23,000$ cm^{-1} – $27,000$ cm^{-1}).

PFEO theory can also be applied to HBC molecules although it is less straightforward than for coronene. The reason is that the extra 6 peri-benzene rings are arranged in such a way that on their own they cannot form a larger perimeter ring current to that of coronene (see Figure 3.5). However, the perimeter of the HBC molecule is fully aromatic, therefore it is possible for π -electrons to migrate freely around the perimeter if the π -electrons are readily exchanged between the inner sextet rings and the outer rings. In this case $c_0 = 30$ and the radius of the system $r = 6.59\text{\AA}$. The biggest difficulty with

applying PFEO theory to HBC is determining the number of π -electrons in the perimeter ring. It is unlikely that all 42 π -electrons reside on the outer perimeter of the molecule. However, by filling the electronic levels calculated for the outer ring of HBC with all 42 π -electrons, an upper limit to the S_1 transition can be obtained (in general the larger q the greater the energy of the S_1 transition to $q + 1$). With $q_f = 10$ and $q_g = 11$, the S_1 transition energy is 1.84 eV. This value is reasonably close to the S_1 transition energy of HBC calculated for a 2D quantum box. In the discussion section the quantum box and PFEO theory results will be compared to optical spectra of HBC derivatives.

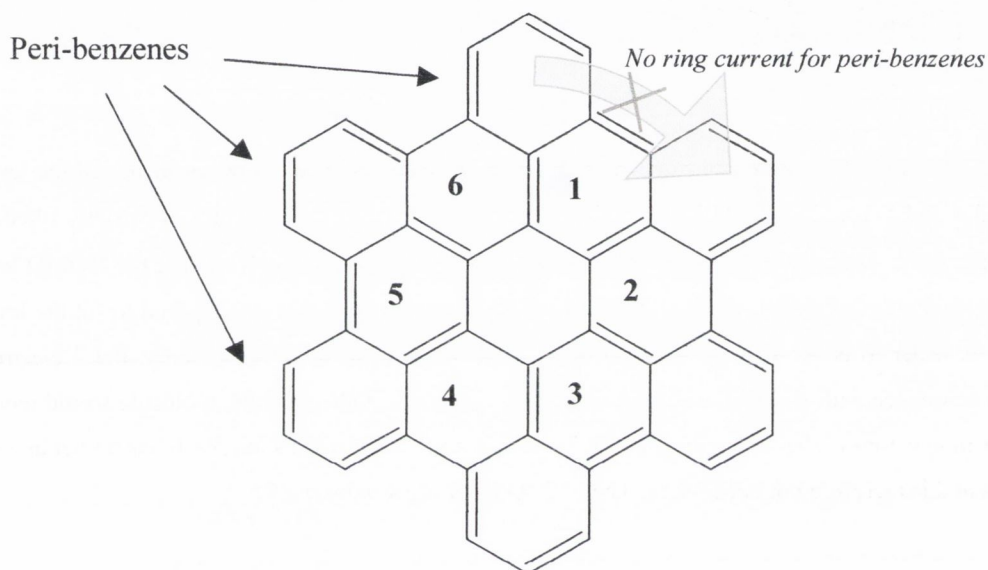


Figure 3.5: The molecular structure of HBC. The ring numbers of coronene given in Figure 3.3 are given for comparison. Note how extra six peri-benzenes of HBC cannot form another ring current.

MOLECULAR GEOMETRY OPTIMISATIONS

In order to understand the aggregate structure – optical spectra relationship, the molecular structure must be investigated first. The geometry optimised molecular structures of each molecule were determined by applying a Molecular Mechanics optimisation (MM+) followed by an Austin Model 1 (AM1) geometry optimisation using the HyperChem software package. The convergence conditions were in general set to a gradient of 0.02. This convergence limit was found to be the most suitable for the n-alkyl and other substituted HBC molecules. The optimised molecular structures are given in Figure 3.6. The most significant detail is the rotation of the exo-phenyl

groups of HBC-PhC12 by 20° with respect to the HBC aromatic plane. In reality the six exo-phenyl rings will rotate out of phase with each other.

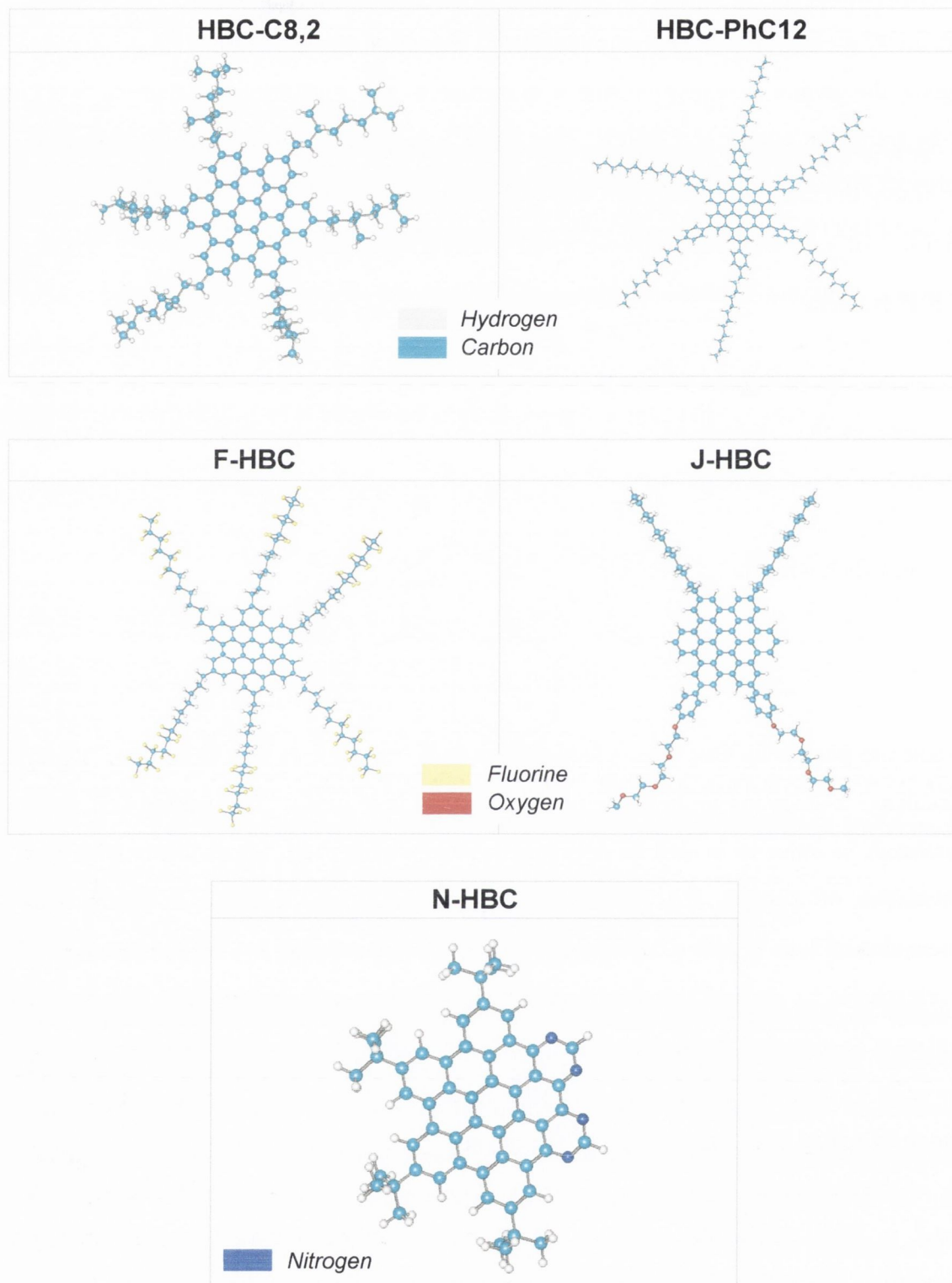


Figure 3.6: The MM+ followed by AM1 geometry optimised structures of the HBC derivatives. Light Blue represents Carbon atoms, Grey represents Hydrogen, Yellow represents Fluorine, Red represents Oxygen and Dark Blue represents Nitrogen. Chemical drawings are given in Figure 1.1.

3.3 AGGREGATES

3D QUANTUM BOX

As illustrated above, an isolated molecule can be viewed as a 2D quantum box. But can this interpretation be extended to molecular aggregates? If upon aggregation, the π electrons of one molecule can be readily exchanged with π electrons of another molecule, then the molecular aggregate system becomes a 3D quantum box. The eigenstates of an electron in this case are determined not only by the physical dimensions of the molecule in the x - and y -direction but also by the size of the aggregate in the z -direction. The *confinement* of an electron is therefore no longer aggregate size independent, but will decrease with increasing aggregate size. However, as with any delocalised electron system, there will be a certain coherence length of the electron which will limit the effective delocalisation length.

To test the possibility that the optical transitions in the spectra may arise from highly delocalised π -electrons in an aggregate, the energy levels of a 3D quantum box were calculated. In order to model the aggregate, 2 sizes were used: first a dimer with box dimensions of $1\text{nm} \times 1\text{nm} \times 0.7\text{nm}$ (asymmetrical) and second, a trimer with dimensions of $1\text{nm} \times 1\text{nm} \times 1\text{nm}$ (symmetrical). Given in Table 3.4, are the energies of the electronic levels and transitions obtained by filling each system with the correct number of π -electrons available, 84 and 126 for a dimer and trimer respectively. It is important to note that for both systems the electron density of the π -electrons per unit volume is nearly constant at ~ 120 (electrons. nm^{-3}). Table 3.4 demonstrates how, in the case of the dimer, the asymmetry of the box dimensions disrupts the z degeneracy with x and y . This results in much smaller transition energies than for a completely symmetric system like the trimer. In this example the trimer (given by a cube $1\text{nm} \times 1\text{nm} \times 1\text{nm}$) is a special case. In practice, it is likely that any variability in the z dimension will lift the z degeneracy. The resultant increase in the number of non-degenerate energy levels will thus give rise to smaller transition energies between

successive energy levels. With this in mind, the 1.12 eV S_2 aggregate transition energy of the trimer is unlikely to be observed. However, it is conceivable that an absorption band in the 1 – 2 eV range could be due to an aggregate S_n transition where n is very large. The large number of S_n transitions of a 3D aggregate quantum box will inevitably (even with selection rules) give rise to a very broad absorption spectrum spanning over a very large range of wavelengths. However, in the experimental results section we will demonstrate that in fact a total charge delocalisation throughout an aggregate is unlikely in a van der Waals system and therefore the possibility that optical spectra of HBC aggregates is due to the formation of 3D quantum boxes is rather small.

	HOMO (eV)	LUMO (eV)	LUMO+1 (eV)	S_1 (eV)	S_2 (eV)
Dimer ($x = y \neq z$)	12.80	12.84	13.02	0.04 (30,995nm)	0.22 (5,635 nm)
Trimer ($x = y = z$)	12.04	12.78	13.16	0.74 (1675nm)	1.12 (1107nm)

Table 3.4: The possible eigenvalues and respective transition energies for a symmetrical and asymmetrical 3D quantum box formed by aggregates of HBC if there is intermolecular charge sharing (see text).

AGGREGATE GEOMETRY OPTIMISATIONS

In Chapter 1 in the FER section, it is suggested that the optical spectrum of a solution of HBC aggregated species will have a different optical spectrum to the isolated species due to the various interactions described previously, namely the β , W and W' interactions. To account for this a geometry optimisation was performed for dimers of all the molecules. Although lacking the completeness of a full geometry optimisation of the aggregates and aggregate bundles, it will allow an extrapolation of likely intermolecular distances, rotations, and tilts.

To determine the aggregate structure, a geometry optimisation of molecular dimers was performed using the same procedure as for the isolated molecules. The structures are given in Figure 3.7. The computationally costly optimisation of large aggregates was

not found to be necessary, as in general molecular interactions are limited to nearest – neighbour interactions. A list of the measured parameters from the geometry optimisations are given in Table 3.5. The physical meaning of the measured parameters is explained in Figure 3.8.

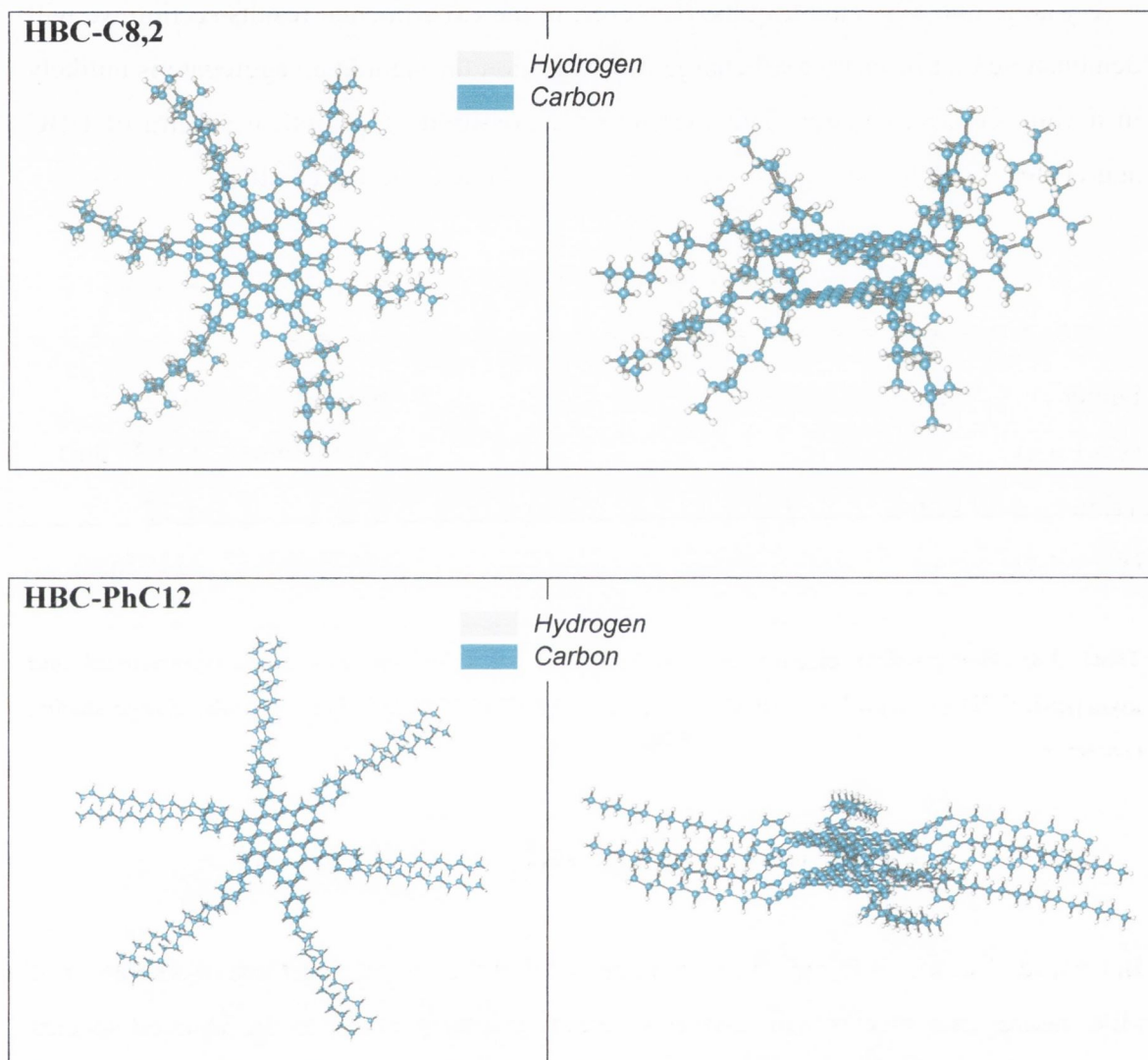


Figure 3.7(a): The geometry optimised dimers of HBC-C8,2 and HBC-PhC12. The left image is a top-view of the dimer, the right image is a side-view of the dimer. See Figure 3.3 and Table 3.5 for calculated structural parameters. Light Blue represents Carbon atoms and Grey represents Hydrogen.

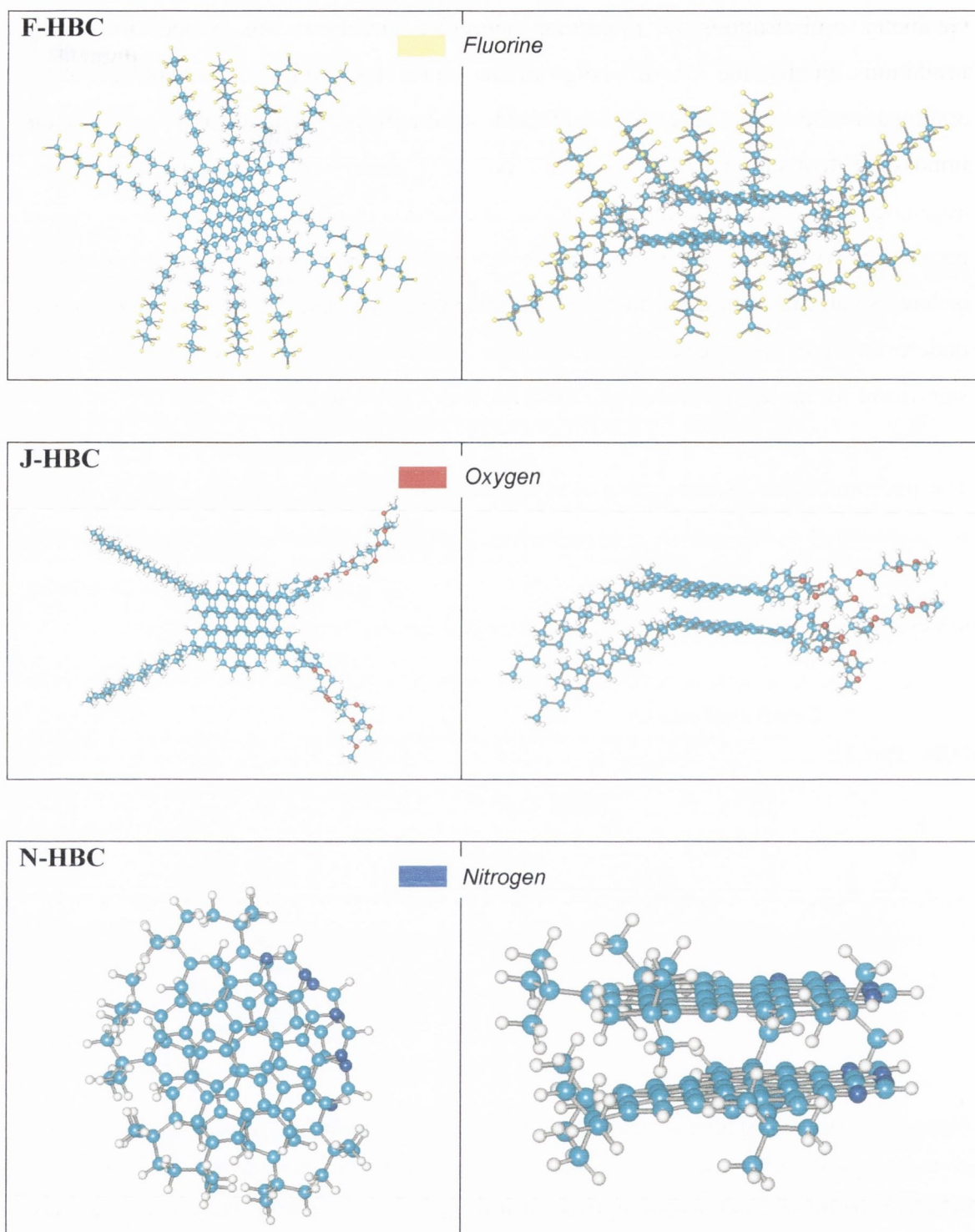


Figure 3.7(b): The geometry optimised dimers of F-HBC, J-HBC and N-HBC. The left image is a top-view of the dimer, the right image is a side-view of the dimer. See Figure 3.3 and Table 3.5 for calculated structural parameters. Light Blue represents Carbon atoms, Grey represents Hydrogen, Red represents Oxygen, Yellow represents Fluorine and Dark Blue represents Nitrogen.

Geometry optimisations of molecular aggregate structures are subject to several limitations. Firstly, the kinetic energy of the molecules and/or parts of a molecule is assumed to be zero. Therefore optimised structures are performed at a physically impossible temperature of 0 K. Only potential energy molecular interactions are accounted for and minimised. Values measured from the optimised aggregate geometries will therefore be significantly less accurate than geometry optimisations of isolated small molecules. For instance, the intermolecular distance measurements are an underestimate of the intermolecular distance at room temperature. This becomes more significant for molecules with small mass but bulky side-groups.

The intermolecular distances measured for all molecules are within the range expected for graphitic systems ~ 3.5 Å. The exception is N-HBC which is described below. The inter(symmetrically-identical)atom distance h , between molecules is a useful parameter to describe a crystal as it describes the wave-vector of the crystal.

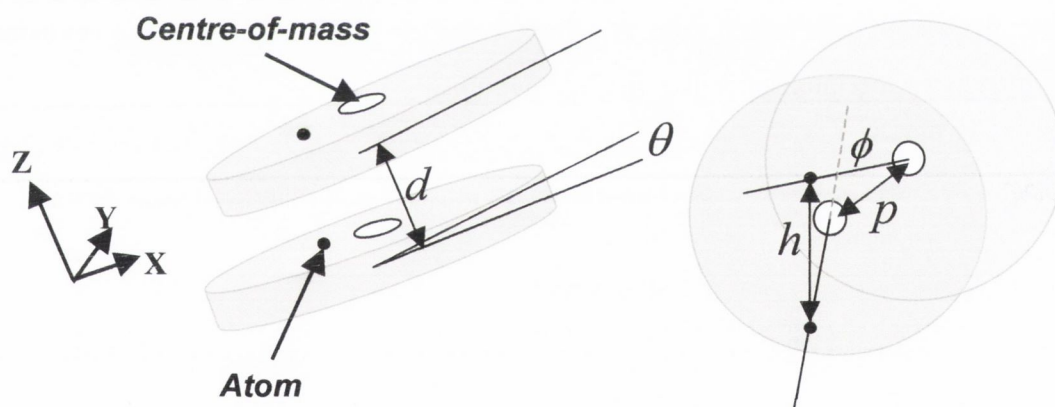


Figure 3.8: Diagram illustrating intermolecular geometrical parameters of an aggregate. The distance d , is given by the distance between the molecular x-y planes. The identical atom distance h is the distance between symmetrically identical atoms. The rotation angle ϕ is the angle of rotation around the z-axis between symmetrically identical atoms. The tilt angle θ is the rotation in the x or y axis between the molecular z axis of each molecule. The displacement p is the sliding distance along the x-y plane of the centre-of-mass of each molecule.

From Table 3.5, the MSAs studied here form crystals that are disordered as a result of the many degrees of freedom of the side chains. This gives rise to large differences in the values of h measured from the geometry optimisations for each HBC derivative

MSA. Large values of h are measured for all derivatives except HBC-PhC12 (HBC-PhC12 has a smaller value in a narrower range). The reason for this is the steric hindrance of the 2 hydrogen atoms covalently bonded to the first carbon of each alkyl chain (closest to the aromatic core). At 0K, an energy minimised geometry optimisation is achieved by rotating the alkyl chains until they are at an angle of ~ 50 degrees to the x-y plane of the molecule (at room temperature the side-chains will flex around). This conformation enables a maximised interaction between the side chains of neighbouring molecules while at the same time reducing the steric hindrance between the hydrogen atoms on the alkyl chains and the aromatic core (even though it gives rise to an intermolecular lateral displacement). This illustrates the difference in the conformational degrees of freedom, and hence the difference in the absolute intermolecular binding energies (including entropic effects), of the alkyl and aromatic HBC cores. The alkyl chains, much more flexible than the rigid aromatic cores, have many conformational states accessible, at room temperature, on the surface of another alkyl chain (from the neighbouring molecule). The decrease in energy that arises from favourable alkyl-chain interactions is weighed against the change in energy associated with increasing the intermolecular displacement, p .

MOLECULE	Distance d (straight) Å	Identical Atom Distance h Å	Rotation ϕ degrees	Tilt θ	Displacement p Å
HBC	3.50 ± 0.01		~ 0	~ 0	0.65 ± 0.01
C8	3.52	3.72	~ 0	~ 0	3.18
C8,2	3.4 – 3.5	3.4 – 4.5	$\sim < 22$	~ 0	3.5 – 4.4
PhC12	3.4 – 3.5	3.4 – 3.5	~ 0	~ 0	~ 0
F-HBC	3.4 – 3.7	5.0 – 5.1	~ 0	~ 0	3.1 – 3.4
J-HBC	3.4 – 3.6	4.4 – 4.5	~ 0	~ 0	2.4 – 2.5
N-HBC	3.4 – 3.9 (along symmetric axis)	~ 3.4 (centre) ~ 4.5 (edge)	$\sim 30 - 45$	5–6	~ 0 (centre) 2.4 – 3.0 (edge)

Table 3.5: Intermolecular parameters of the geometry optimised molecular aggregate structures given in Figure 3.7 (parameters are explained in Figure 3.8)

Since the aromatic cores are a periodic aromatic structure, two molecules can be displaced relative to each other without drastically affecting the change in free energy upon aggregation. From inspection of Table 3.5, the displacement magnitude is of the order of the size of a benzene molecule (2 - 3Å). The resultant aggregate structure formed by the displaced aromatic cores is similar to the herring-bone structure often associated with small linear molecules such as sexithienyl¹³. For most of the MSAs studied the side chains do not give rise to a rotation about the z-axis of the molecules in the aggregate. However from Table 3.5, HBC-C8,2 and N-HBC both have geometry optimised structures that include a rotation. Comparing HBC-C8¹⁴ to HBC-C8,2 reveals why this rotation about the z-axis arises. For HBC-C8,2, the steric hindrance of the methane side groups on the second and seventh carbon atom of the side chain in HBC-C8,2 prevents the alkyl chains from aggregating as close together as with HBC-C8. This small steric interaction is sufficient to ensure that the structural energy minimum is achieved by a rotation in the x-y plane of the HBC-C8,2 molecule. For the N-HBC MSA the steric interaction of the side groups is similar. However, the three methane groups of a t-butyl group are arranged at an angle of 120 degrees with respect to each other. This gives rise to steric interactions in the x- y- and z- direction no matter which way the t-butyl groups rotate. Due to the asymmetric substitution of the t-butyl groups on a N-HBC molecule, the N-HBC MSAs energy minimised geometry optimisation is formed by rotating the molecule in the x-y plane and by tilting the molecule out of the x-y plane (a rotation around the x or y axis).

3.4 EXPERIMENTAL RESULTS

PLE OF LOW CONCENTRATION SPECIES IN SOLUTION

Low concentration solutions of each derivative were prepared and measured using a photo-luminescence-excitation technique. The spectra obtained at $\sim 10^{-13}$ M, given in Figure 3.9 a) and b), are remarkably different to those obtained at $\sim 10^{-5}$ M (see Figure 3.10). At the lowest concentration explored (3×10^{-15} M), any isolated and therefore non-aggregated molecules present have an average intermolecular distance of the order of 80 μm . In a good solvent, this separation is expected to be sufficient to prevent any attractive intermolecular interactions that could lead to an increase in the rate of

aggregation. In practice, the aggregation process is controlled by random molecular collisions, and at these low concentrations, collisions are expected to be rare. This should result in a negligible number of aggregates present compared to the number of isolated molecules present. Of all the low concentration solutions prepared, only some of the derivatives were detected using photo-luminescence-excitation techniques. The reasons for this will be discussed later and in other Chapters. As detailed in the Introduction, the active chromophore of each derivative investigated is essentially the same (with the exception of N-HBC). Therefore the PLE spectra obtained for HBC-C8,2 and HBC-PhC12 in toluene, and F-HBC and J-HBC in chloroform are representative of the isolated PLE of HBC derivative molecules.

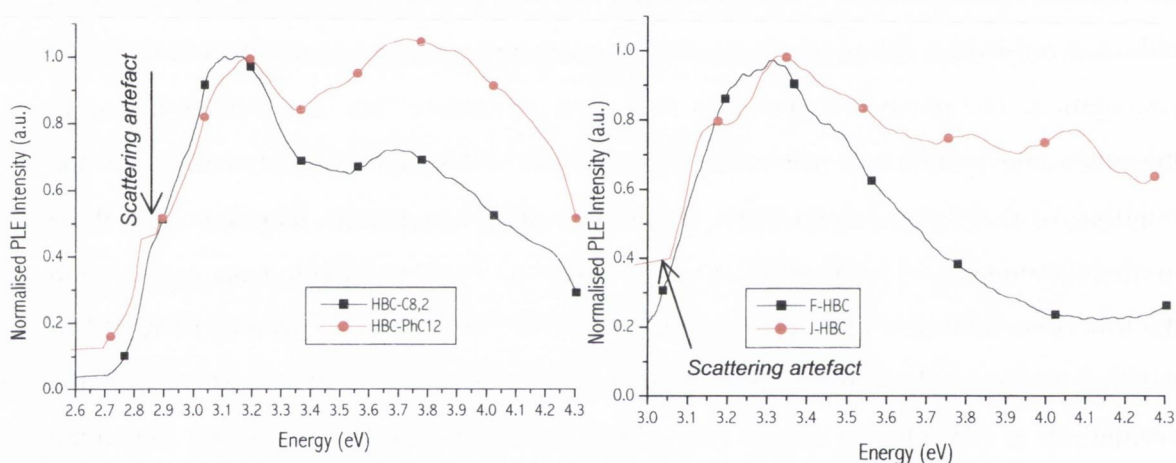


Figure 3.9: Normalised PLE spectra at low concentration $\sim 10^{-13}$ a) HBC-C8,2 and HBC-PhC12 in toluene and b) F-HBC and J-HBC in chloroform. Straight line segments in the spectra indicate where scattering artefacts have been removed for clarity. In the case of HBC-C8,2 the scattering peak is a shoulder and has not been removed (the HBC-PhC12 peak can be seen in Figure 3.14 b)). For J-HBC the spectrum given has been smoothed by averaging, this results in the irregular shape of Peak 1 and the peak at ~ 4.1 eV. The scattering peak, indicated in the plot, arises from the solvent molecules scattering the primary excitation beam of the photo-luminescence spectrometer. The scattering peak is also found in the PL and it is always observed to move in relation to the excitation energy.

The low concentration PLE spectra, of each derivative, are similar. However there is an appreciable difference of ~ 0.2 eV in energy between similar electronic transitions in the chloroform and toluene solutions. From Figure 3.9 a) and b), and Table 3.6, there are two dominant broad excitation peaks in the low concentration species PLE: in toluene there is a high energy peak at ~ 3.7 eV and a lower energy peak at ~ 3.1 eV and in chloroform there is a high energy peak at 3.8 eV and a low energy peak at ~ 3.3 eV. In

Chapter 4, it will be shown that the lower energy peak is the transition to the lowest energy level that is dipole-allowed to the ground level and origin, therefore, of the photo-luminescence. HBC-PhC₁₂ is a slightly different molecule to the other molecules presented in Figure 3.6. HBC-PhC₁₂ has 6 exo-phenyl groups covalently bonded to the aromatic core. From the PLE spectra the PhC₁₂ side-chains have caused both excitation peaks to blue-shift by $\sim 0.03\text{eV}$ relative to the HBC-C_{8,2}.

As both broad excitation peaks probably arise from a superposition of several vibrational-electronic transitions, the general blue-shift implies that the phenyl group has caused an overall change, suggesting that there is very limited electronic coupling throughout the whole HBC-PhC₁₂ molecule. The fact that the phenyl groups don't induce a red-shift implies that in fact the exo-phenyl groups are not extending the π -conjugation. The phenyl groups are free to rotate, therefore they can only contribute to the electronic system when a phenyl group lies in the π -conjugated plane. As the rotations of the six exo-phenyl groups are most likely incoherent, they only contribute to the inhomogeneous broadening of the system. The FWHM of the low energy peaks in the low concentration PLE spectra are compared in Table 3.6. The averaged FWHM of the low energy peak of the four molecules in the spectra is $0.58 \pm 0.05\text{ eV}$ and the normalisation of the higher energy excitation peaks (around 3.7 eV) also reveals that the HBC-PhC₁₂ excitation spectrum is slightly broader relative to HBC-C_{8,2}. The PLE spectra obtained in chloroform have a different spectral profile to those obtained in toluene. These differences arise from the different environments of their respective isolated molecules. For instance the PLE spectra of F-HBC was obtained at 10^{-12} M . Comparison of the PLE spectra of HBC-PhC₁₂ at low and high concentration also reveals differences due to the change in environment¹⁵. The changes in environment, other than the solvent (for instance the presence of aggregates), do not significantly change the energy of the lowest energy transition of the isolated molecules at medium/high concentration. The main change in the PLE spectra with increasing concentration is the intensity of Peak 1 relative to Peak 2.

While the low concentration luminescence and luminescence-excitation spectra suggest the presence of isolated molecules, these spectra alone don't prove that isolated molecules are uniquely being observed. However, as will be shown in the next section,

the change in spectra from low concentration to medium concentration strongly suggests that the isolated molecules of HBC-C_{8,2}, HBC-PhC₁₂, F-HBC and J-HBC have in fact been observed in the region of 10^{-13} M.

MOLECULE	ENERGY (eV)		FWHM (eV)
	<i>PEAK 1</i>	<i>PEAK 2</i>	<i>PEAK 1</i>
HBC-C _{8,2}	3.12 ± 0.02	3.70 ± 0.03	0.54
HBC-PhC ₁₂	3.18 ± 0.04	3.74 ± 0.06	0.59
F-HBC	3.30 ± 0.04	-	0.56
J-HBC	3.33 ± 0.04	3.8 ± 0.03	0.63

Table 3.6: Values of the peak energy and FWHM of low concentration species. For F-HBC no Peak 2 can be discerned, For J-HBC the spectrum given has been smoothed by averaging, this results in the irregular shape of Peak 1 and the peak at ~ 4.1 eV

PLE/ABSORPTION SPECTRA OF MEDIUM AND HIGH CONCENTRATION SOLUTIONS

In order to study how aggregation effects can change the optical spectra of a molecule, optical spectra of all the molecules in chloroform at concentrations ranging from 10^{-8} to 10^{-5} M were taken. It is important to remember that the aromatic cores of each molecule investigated are identical (with the exception of N-HBC). Therefore any differences in the spectra will be as a direct result of differences in the aggregation of the molecules. Aggregation is expected to be heavily influenced by the aromatic cores and, crucially, also by the substituted side-groups. From Figure 3.10, clear differences in the spectra can be observed. However, in order to compare optical spectra, it is often more useful to consider the similarities first, and the differences second.

The optical absorption spectra obtained at high concentration (10^{-4} – 10^{-6} M) are given in Figure 3.10. All the derivatives have a dominant absorption band that falls between 2.4 – 4.0 eV. The considerable bandwidth ~ 1.6 eV of the overall absorption band is a factor 2.76 greater than the observed FWHM for the low concentration species. This suggest that the absorption band for the high concentration species is the result of a broadened super-position of more than one optical transition (from Figure 3.10 more than one transition peak is observed). Resolving the super-position for each derivative is

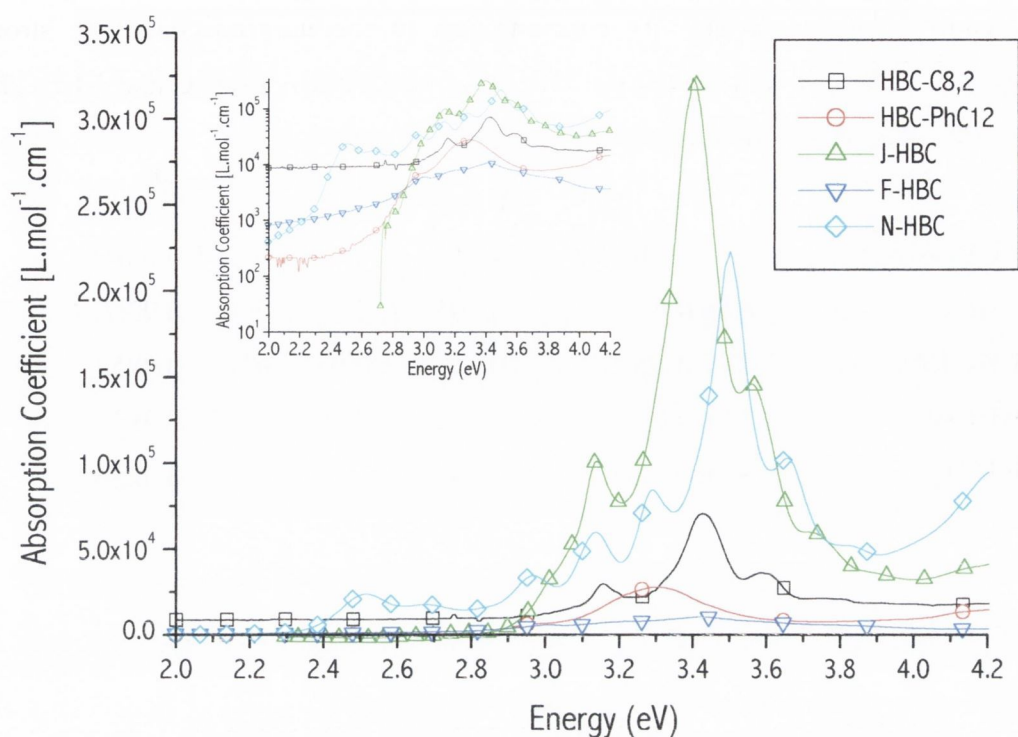


Figure 3.10: Absorption spectra of all derivatives in solution at $\sim 10^{-5}$ M in chloroform. Inset: same spectra but intensity in log scale.

essentially the task at hand, as it is the finer structure of the spectra that holds the key to deciphering the molecular interactions. The similarities of the simpler low concentration spectra have given rise to much more complex high concentration spectra. Listed in Table 3.7 are the main characteristics for each absorption spectrum in Figure 3.10.

From Figure 3.10, 3.12 and Table 3.7, the variability of the band *peak-maximum* energy between derivatives (~ 0.1 eV) is small compared to the FWHM of the dominant peak and very small compared to the total bandwidth (not including N-HBC). This confirms that the variance of one optical transition cannot be the sole contributor to the large FWHM of the spectra of some of the derivatives. The small variability in the band peak-maximum energy is a direct consequence of the aromatic chromophores of each molecule studied being chemically identical (with the usual exception of N-HBC).

In contrast to the band peak-maximum energy, the large variability of the absorption coefficient and FWHM indicate that although there is little difference between the cores of each molecule, there is a large variability in the inter-molecular interactions. Using values from Table 3.7, the overall FWHM can be plotted against the maximum oscillator strength as shown in Figure 3.11. The trend in the graph suggests that the

MOLECULE	BAND MAXIMUM (eV)	MAX ABSORPTION COEFFICIENT [L.mol ⁻¹ .cm ⁻¹]	BAND FWHM (eV)
HBC-C8,2	3.43 ± 0.01	48,014	0.15 ± 0.02
HBC-PhC12	3.30 ± 0.01	28,105	0.36 ± 0.02
F-HBC	3.42 ± 0.02	10,711	0.93 ± 0.04
J-HBC	3.39 ± 0.01	322,753	0.19 ± 0.02
N-HBC	3.50 ± 0.01	221,060	0.15 ± 0.02

Table 3.7: Values of the peak energy, absorption coefficient and FWHM for all derivatives studied.

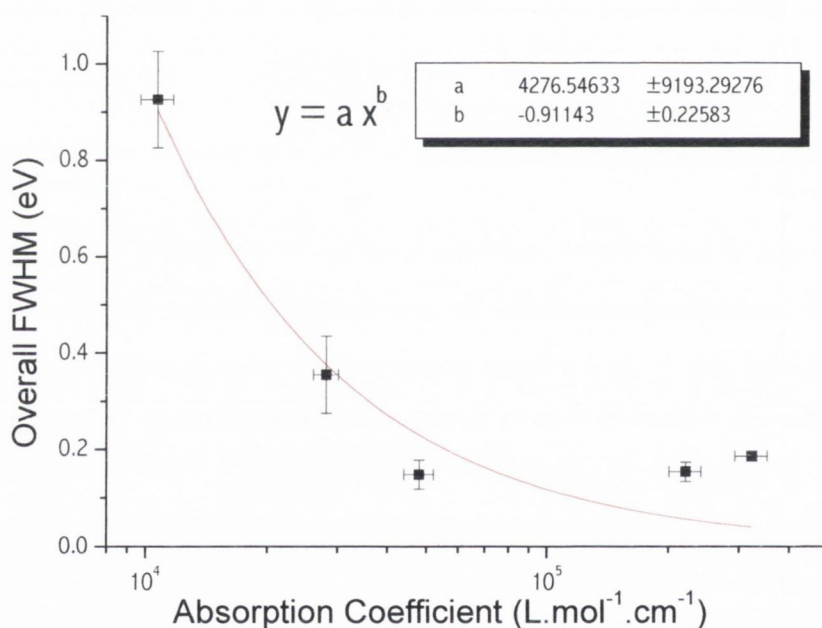


Figure 3.11: A plot of the overall FWHM of the absorption band versus the maximum oscillator strength of the band of all HBC derivatives from Table 3.7.

absorption coefficient roughly varies inversely with the FWHM. The reason for this trend is not trivial when all factors are included, however it is essentially a consequence of observing an ensemble of aggregates, not an ensemble of isolated molecules. It is reasonable to assume that HBC-C8,2, with the smallest FWHM, can be considered as an example of an ordered system of MSAs. On the other hand, F-HBC in the same solvent and at a similar concentration has a much greater FWHM than HBC-C8,2, indicating that F-HBC forms much more disordered species.

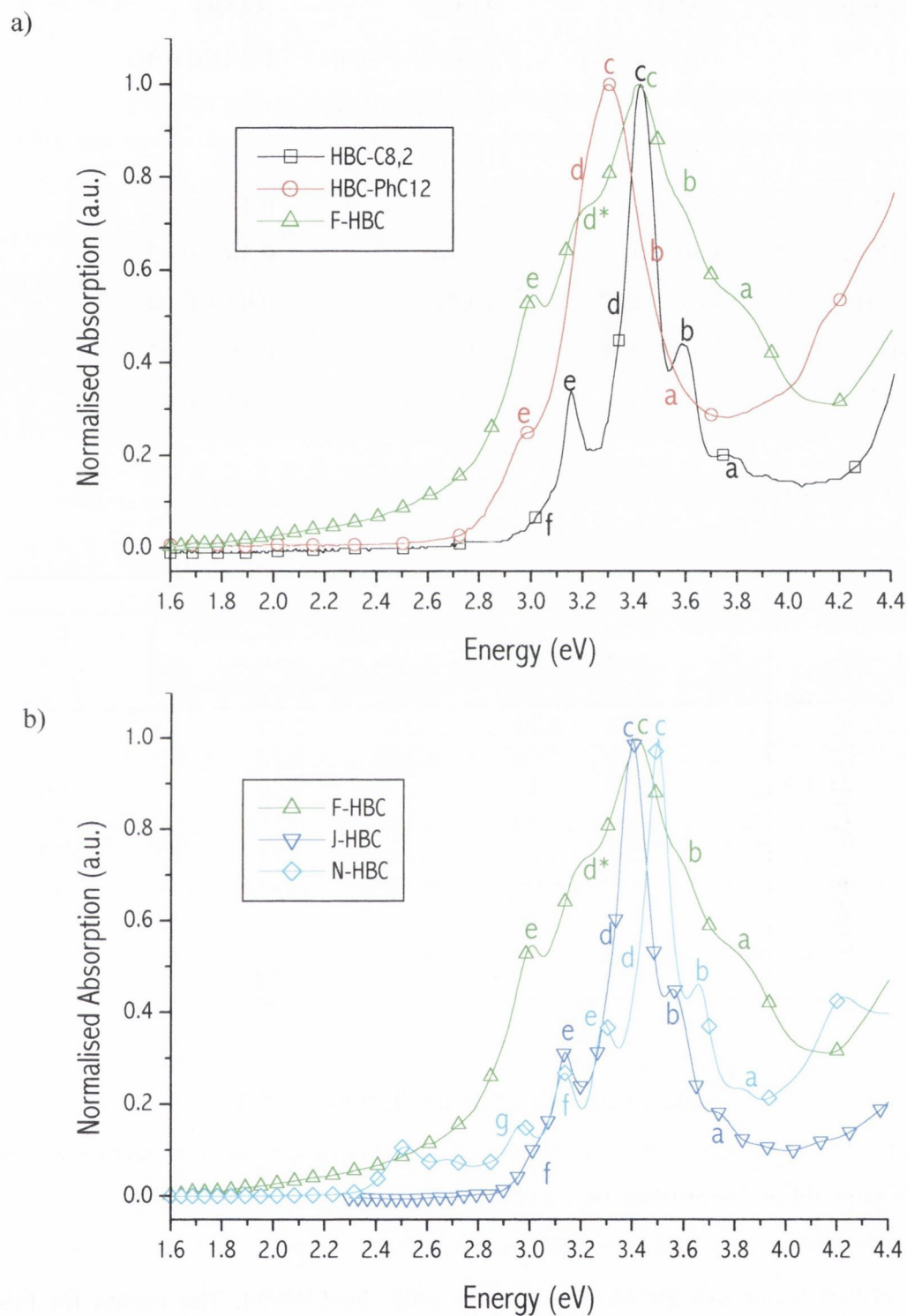


Figure 3.12: Solution Normalised Absorption Spectra at high concentration of all molecules in chloroform a) HBC-C8,2, HBC-PhC12 and F-HBC; b) N-HBC and J-HBC (F-HBC is included to allow comparison). For the moment, the *labelling of the peaks is strictly alphabetical* from high to low energy. The letters are *not* meant to associate one peak of one derivative to a peak of another derivative with the same letter. The association of peaks will be made later in the discussion section. See Table 3.8 for values

measured. The shoulder d* is important in later discussions of the species contributing to the spectrum of F-HBC.

In Figure 3.12, all the absorption spectra, normalised with respect to the absorption maximum, are given. The normalised plot is much more useful when comparing all the molecules as it allows a comparison of the relative peak heights of the fine structure of all the spectra. To accomplish this, all relevant peaks in the spectra are labelled provisionally with a letter. The assignment of a letter to each peak is strictly alphabetical. Correlations between the absorption peaks of different derivatives will be made in the discussion section. The peak energies and normalised intensities of each labelled peak are given in Table 3.8.

MOLECULE	PEAK ENERGY AND INTENSITY						
	a	b	c	Shoulder d	e	f	g
HBC-C8,2 (<i>eV</i>)	3.73	3.59	3.43	3.33	3.16	3.08	2.78
(<i>int.</i>)	0.19	0.43	1.00	0.39	0.34	0.13	0.02
HBC-PhC12		3.43	3.30	3.21	2.98		
		0.65	1.00	0.81	0.24		
F-HBC	3.76	3.58	3.42	*3.21	3.00		2.60
	0.58	0.76	1.00	0.74	0.56		0.11
J-HBC	3.73	3.56	3.40	3.30	3.14	3.07	2.78
	0.18	0.45	1.00	0.42	0.31	0.17	0.003
N-HBC	3.82	3.66	3.50	3.42	3.29	3.13	2.97
	0.23	0.46	1.00	0.5	0.38	0.26	0.15

Table 3.8: The energy and normalised intensities of the absorption peaks for each derivative studied and shown in Figure 3.12.

The fine-structure of the spectra are much more easily explained by taking HBC-C8,2 as the example molecule and comparing all the other molecules to it. The absorption band of HBC-C8,2 is composed of two sub-bands: peaks a-b-c and peaks e-f. The reason for calling them sub-bands is to emphasise that if the spectra of HBC-C8,2 were broader all that would be observed is one dominant band. This is commonly the case for the absorption spectra of a very disordered ensemble of organic molecules, in our case F-HBC at high concentration is approaching this level of disorder. The collection of peaks g at lower energy is discussed in Chapter 4.

At high concentration, all the spectra are similar in that they have two prominent bands, each with satellite peaks. Common to all the spectra (except for F-HBC), the weaker sub-band (peak e) is found to have an oscillator strength that is approximately a factor 0.24 – 0.38 lower than the oscillator strength of the dominant sub-band (peak c). The actual values of the transition energies and oscillator strengths are given in Table 3.8. For HBC-C8,2 and HBC-PhC12, the oscillator strengths of the optical transitions at energies < 2.8 eV are less than $10^3 \text{ Lmol}^{-1}\text{cm}^{-1}$. For a singlet-singlet transition this low oscillator strength usually indicates that the transition is a forbidden-transition¹⁶. These low energy bands have tended to be disregarded in papers describing the optical properties of HBC derivative molecules due to the fact that they are at lower energy than the dominant PL emission peak¹⁷. In the context of this work, these low energy features cannot be ignored. In the inset of Figure 3.13, the lowest energy peak observed is < 2.63 and is located at approximately 2.5 eV. More over, for the polar N-HBC the low energy absorption band is clearly observed at ~ 2.5 eV. For clarity the absorption coefficient has been reduced by a factor 10 in order to compare the spectrum with the other derivatives in Figure 3.13. Although N-HBC should also have a forbidden S_1 transition, the absorption coefficient is a factor between 45 to 200 greater than that of the non-polar HBC derivatives at 2.5 eV. The assignment of these absorption peaks requires the use of the PL spectra. Features in this region are likely to be strongly forbidden as they may originate from the anti-symmetric H-aggregate FER transition of the molecular symmetry forbidden S_1 electronic transition! This will be dealt with in Chapter 4, however, for the moment the *possible* existence of these peaks and their low energy is all that is important.

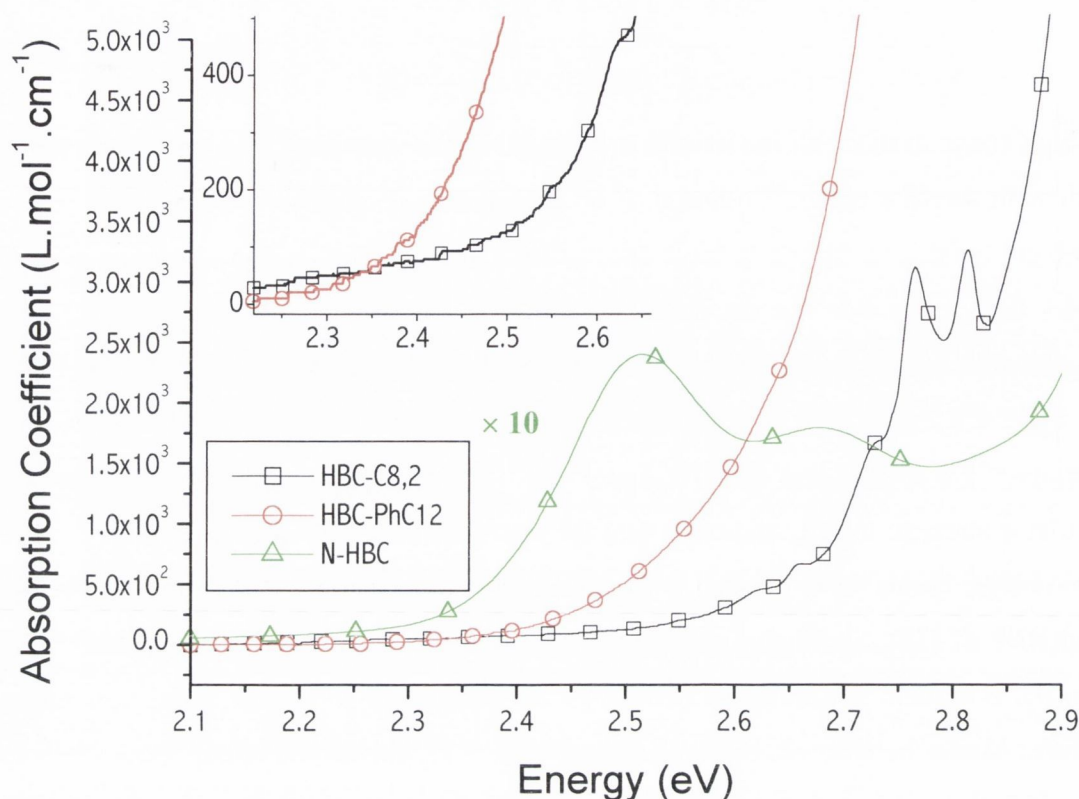


Figure 3.13: Absorption spectra of HBC-C8,2 and HBC-PhC12 at high concentration. Note that the absorption coefficient of N-HBC is a factor 10 larger than illustrated. Inset: Log plot of absorption spectra magnified to show the position of the lowest energy peaks observable. Notice how the lowest energy features are < 2.63 eV. Features in this region are likely to be strongly forbidden as they may originate from the anti-symmetric H-aggregate FER transition of the molecular symmetry forbidden S_1 transition!

LOW CONCENTRATION SPECIES AT MEDIUM AND HIGH CONCENTRATION

For HBC-PhC12 and F-HBC the PLE spectra obtained at medium concentration demonstrated some dependence on the PL emission wavelength. In Figure 3.14 a) and b), the PL and PLE spectra obtained for the low concentration species of HBC-PhC12 are compared to the unusual PL and PLE spectra obtained at higher concentration. The similarities in the energy of the PLE and PL maxima indicates that the low concentration species is still present at higher concentrations. The PLE at 10^{-6} M was collected by detecting the PL from the peak at ~ 2.85 eV.

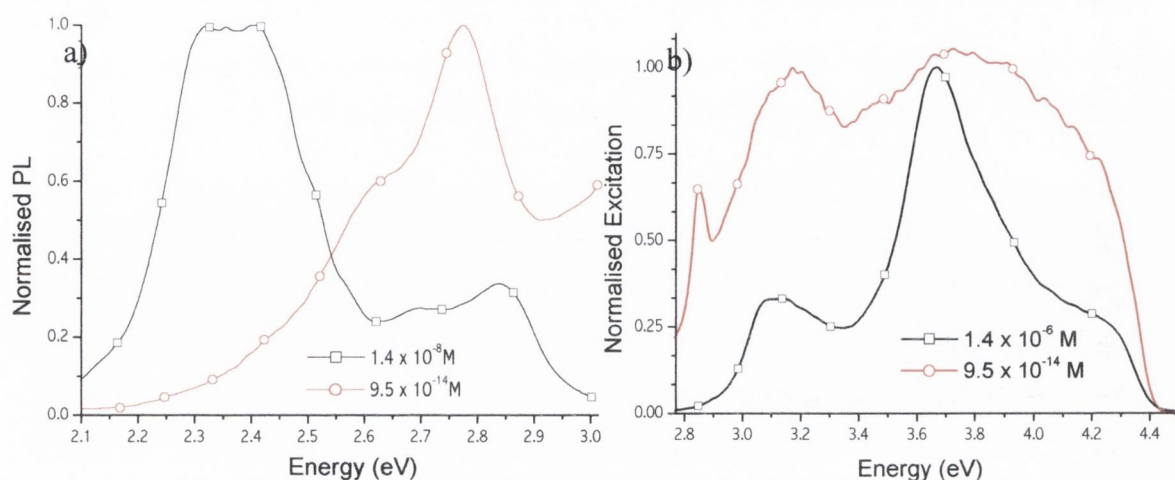


Figure 3.14: a) PL and b) PLE spectra of HBC-PhC12 obtained at medium concentration are compared to the spectra obtained at low concentration. The similarity in the spectra demonstrates that low concentration species are still present at higher concentrations for HBC-PhC12. The sharp peak at 2.85 eV is the solvent scattering peak.

In Figure 3.15 a) and b), the different PL and PLE spectra for the medium concentration species of F-HBC are given. Each spectrum was obtained at the same concentration for the same sample. The difference in the spectra clearly demonstrates, as with HBC-PhC12 at medium concentration, that there are at least 2 species in solution. Comparing the PLE spectra of F-HBC with the spectra obtained at low concentration, from Figure 3.9 b), indicates that the low concentration species of F-HBC is still present at medium concentration.

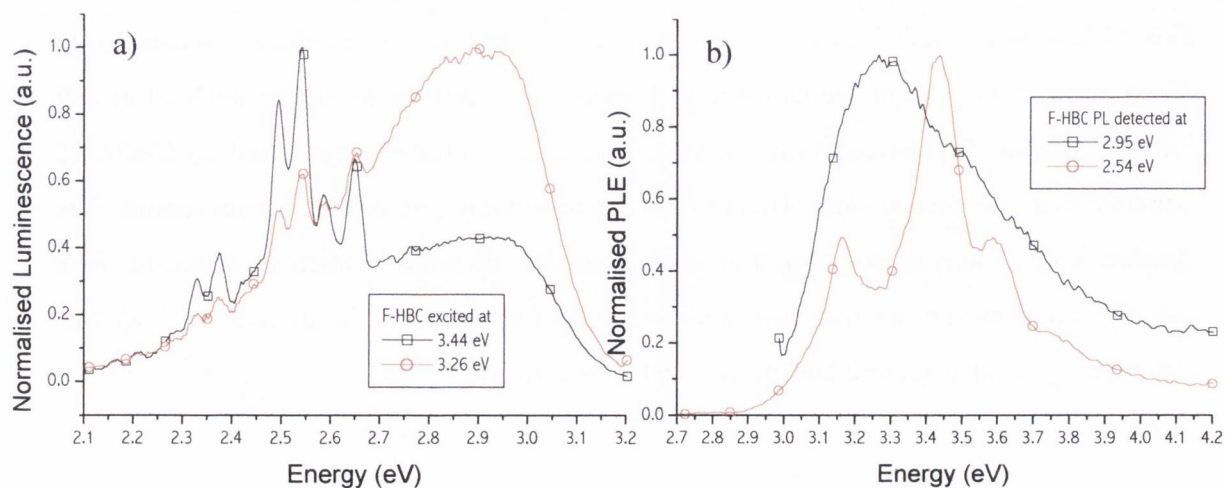


Figure 3.15: a) PL and b) PLE spectra of F-HBC obtained at medium concentration. The different PLE spectra were obtained by changing the PL detection wavelength. Comparison with PLE spectra obtained

at low concentration (see Figure 3.9 b)) indicates that one of the species at medium concentration is in fact the same as the low concentration species.

AGGREGATES IN DIFFERENT SOLVENTS

As a follow up on the low concentration spectra obtained in different solvents, high concentration solutions of two derivative molecules were prepared in toluene and in chloroform. The absorption spectra obtained are presented in Figure 3.16. From inspection, no significant change in the dominant transition energies was observed. It is often observed that for supposedly isolated non-polar molecules in solution, the optical transition energy does not alter upon changes to the solvent molecule polarity. However, the optical spectra of polar molecules, such as NHBC, do often vary as a function of solvent polarity.

For HBC-C8,2 and HBC-PhC12, the total overlap between the normalised absorption spectra taken in toluene and chloroform is striking when one considers that *if* the species being measured is isolated then a significant change in the polarity of the immediate environment of the molecule should give rise to a significant shift in the electronic transition energy. For aggregated molecules, their environment is composed of other identical molecules. Therefore for non-polar molecule aggregates in a polar solvent the aggregate molecules in the bulk of the aggregate will have a non-polar environment. Thus, the lack of a solvent shift for the non-polar HBC derivatives further confirms that the high concentration species are aggregated and not isolated.

For the polar N-HBC molecule there is a small down shift in energy of 0.03 ± 0.01 eV upon changing the solvent from toluene to hexane¹⁸. This energy shift is a factor 6.7 smaller than the energy shift observed for the *non-polar* low concentration species (see Figure 3.9). The relatively small change in energy of polar N-HBC molecules cannot be explained by considering the species in solution as isolated. As will be discussed later, the lack of a significant change in the absorption spectrum is due to the N-HBC species being aggregated.

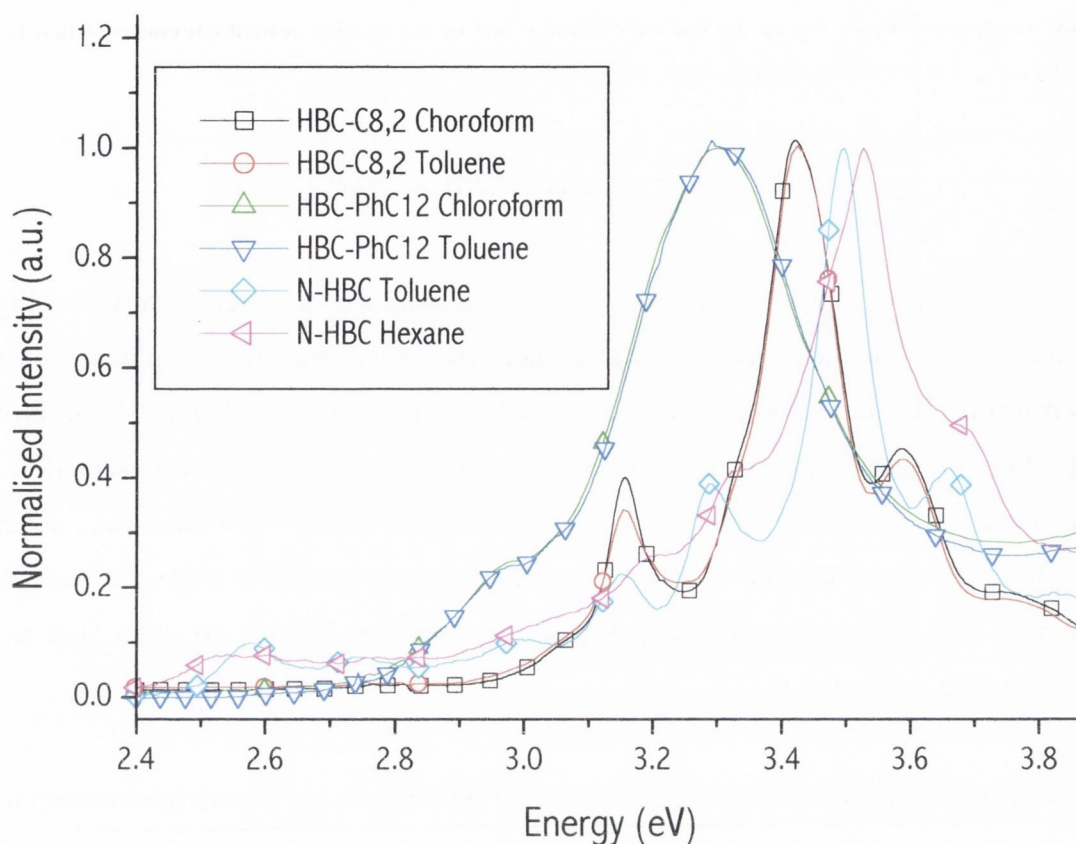


Figure 3.16: Normalised absorption spectra for HBC-C8,2, HBC-PhC12 and N-HBC derivatives. Notice how for the non-polar molecules there is a negligible energy shift in the absorption maximum upon a change in solvent from toluene to chloroform. Only the polar derivative N-HBC has a small shift in energy upon a solvent change from toluene to hexane.

Although the change in solvent does not significantly affect the energy of the optical transition of the high concentration species, the probability that the transition occurs does seem to be influenced by the choice of solvent. This change in transition probability is reflected in the absorption coefficient as shown in Figure 3.17. For both derivatives the species in solution in toluene has a much larger absorption coefficient. For HBC-C8,2 and HBC-PhC12 the change in solvent from chloroform to toluene has increased the absorption coefficient by a factor 12.3 and 20.8 respectively. The larger proportional increase of HBC-PhC12 could be attributed to the higher solubility of this derivative. In the discussion section physical reasons for these changes are suggested.

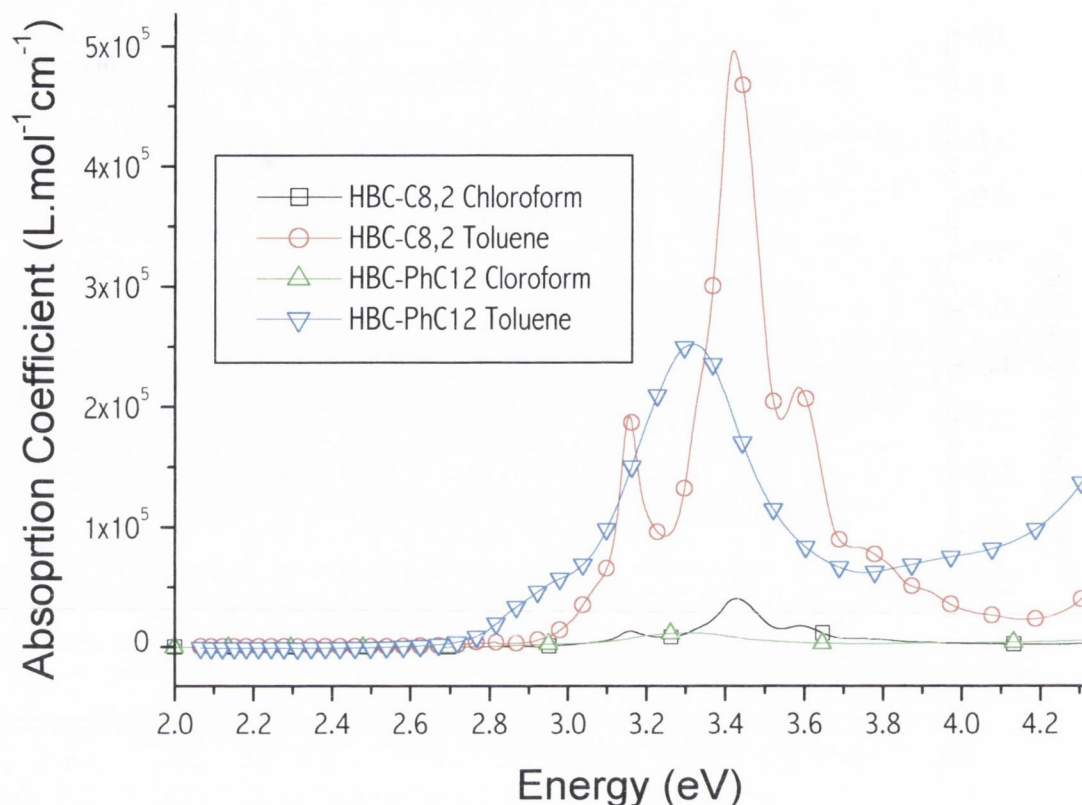


Figure 3.17: Absorption spectra of HBC-C8,2 and HBC-PhC12 in chloroform and toluene at the same concentration.

OPTICAL SPECTRA SOLID STATE

The increase in the density of molecules in the solid state compared to solution often results in fewer well-defined features than in solution. The reason usually given is that there is a marked increase in the number of intermolecular interactions giving rise to inhomogeneous broadening. However, this is a simplification. If a solution is made up of isolated molecules then there will be a large increase in density upon evaporation of the solvent. On the other hand, if the molecules in solution are already aggregated then the increase in density of an aggregate in solution upon solvent evaporation (where density is the average separation between molecules) will be relatively less. The solid state spectra of all the molecules are given in Figure 3.18. The peak positions and relative intensities are given in Table 3.9 using the same letter assignment as for the spectra obtained in solution.

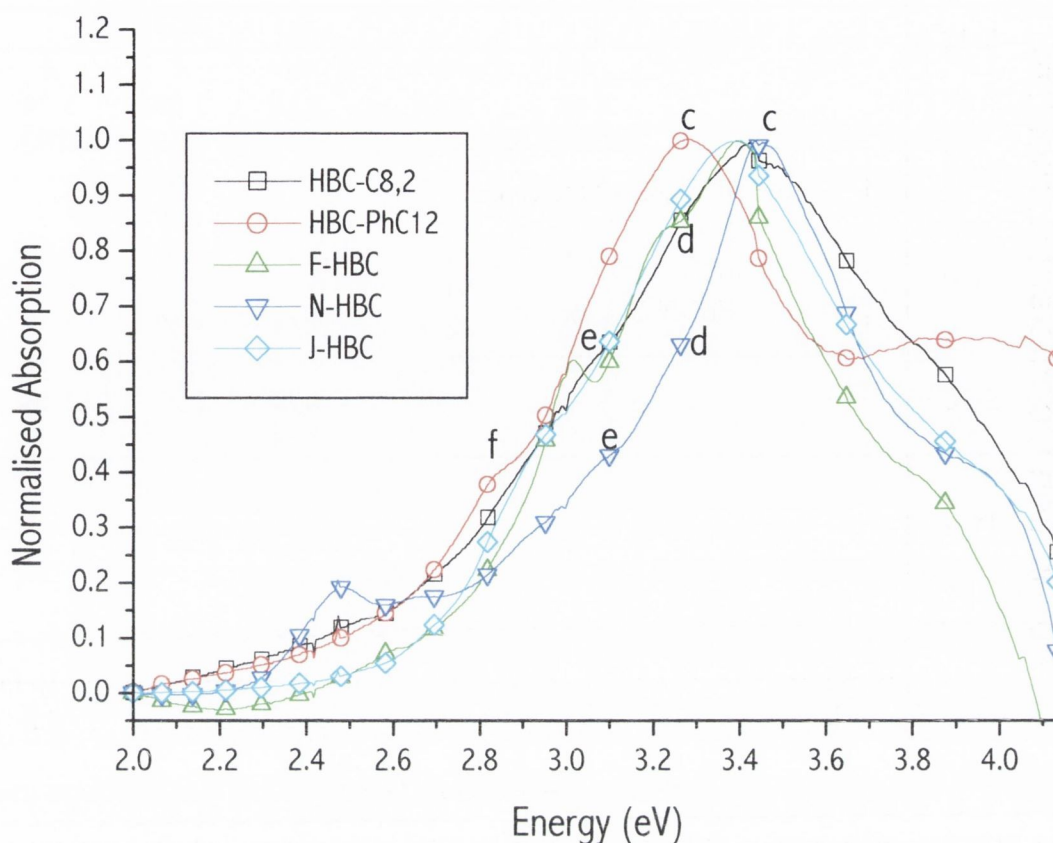


Figure 3.18: Normalised absorption spectra of all derivatives in solid state on glass.

The absorption spectra of all the HBC derivative molecules in the solid state, with the exception of N-HBC, do not differ much from solution. The peaks are broader and with less fine-structure, however the energies of the optical transitions are the same. This simple comparison adds strength to the argument that the molecules are already aggregated in solution. Otherwise the increase in density from isolated molecule to solid state would bring about a large relative increase in the number of electronic interactions that should give rise to FER processes compared to the high concentration solution (i.e. an energy shift). In fact these changes already occur with the change from low to medium concentration in solution. Therefore, the molecules are already aggregated when deposited from solution onto glass to form the solid state samples. Hence the similarity between the high concentration and solid state absorption spectra (with the exception of some additional broadening due to the increased disorder of the ensemble in the solid state). For comparison values of the peak maximum energy and FWHM at high concentration and in solid state are given in Table 3.10. Notice how the peak energies are almost identical. On average the FWHM increases by a factor ~ 4.3 . This change is most appreciable for highly ordered derivatives such as HBC-C8,2.

SOLID STATE PEAK ENERGY AND INTENSITY							
MOLECULE	a	b	c	Shoulder d	e	f	g
HBC-C8,2 (eV)	-	-	3.43	3.33	3.16	3.08	2.78
(int.)			1.00	0.39	0.34	0.13	0.02
HBC-PhC12	-	-	3.28	3.21	2.98	2.84	
			1.00	0.81	0.24	0.4	
F-HBC	-	-	3.41	3.25	3.01		2.60
			1.00	0.85	0.59		0.11
J-HBC	-	-	3.39	3.30	3.14	3.07	2.78
			1.00	0.42	0.31	0.17	0.003
N-HBC	-	-	3.45	3.30	3.12	2.97	2.48
			1.00	0.67	0.44	0.33	0.20

Table 3.9: Values of the peak energy and normalised oscillator strength determined from solid state normalised absorption spectra. Peaks a and b are not observed in the spectra.

The solid state absorption spectra clearly show optical transitions below 2.8 eV. In fact their relative absorption coefficient has increased by up to a factor 1000 at ~2.6 eV compared to the absorption spectra taken in solution. This indicates that a process must be occurring upon increasing the concentration to solid state, that either a) is making the forbidden S_1 transition more allowed or b) increasing the number density of the species absorbing at energies < 2.8 eV. This will be a topic in the discussion section.

MOLECULE	SOLUTION	SOLID	SOLUTION	SOLID
	PEAK c MAXIMUM (eV)	BAND MAXIMUM (eV)	PEAK c FWHM (eV)	BAND FWHM (eV)
HBC-C8,2	3.43 ± 0.01	3.43 ± 0.02	0.148 ± 0.02	0.97 ± 0.02
HBC-PhC12	3.30 ± 0.01	3.28 ± 0.03	0.355 ± 0.02	0.79 ± 0.06
F-HBC	3.42 ± 0.02	3.41 ± 0.03	0.926 ± 0.04	0.70 ± 0.02
J-HBC	3.39 ± 0.01	3.39 ± 0.03	0.186 ± 0.02	0.84 ± 0.02
N-HBC	3.50 ± 0.01	3.50 ± 0.02	0.154 ± 0.02	0.59 ± 0.02

Table 3.10: Values for the peak maximum energy and FWHM of solid state samples and high concentration samples.

COMPARISON OF PLE AND ABSORPTION SPECTRA

The comparison of normalised absorption with normalised PLE spectra can also reveal some information about the nature of the species being observed and the nature of the molecular interactions involved. In the case of non-interacting molecules in solution (isolated molecules) the relationship between the PLE and absorption spectra is simple. The isolated molecular species will absorb photons at a given energy with a given probability which will determine the absorption spectrum. The PLE spectrum will therefore be determined by the photo-luminescence quantum yield (PLQY) and the absorption coefficient. On the other hand, aggregates in solution may have several other factors that may precipitate a difference in both energy and intensity between the absorption and PLE spectra. Differences between the absorption and PLE spectra of a solution of a given molecule often results from the existence of more than one species in solution. Generally speaking, different species will have a differing optical response.

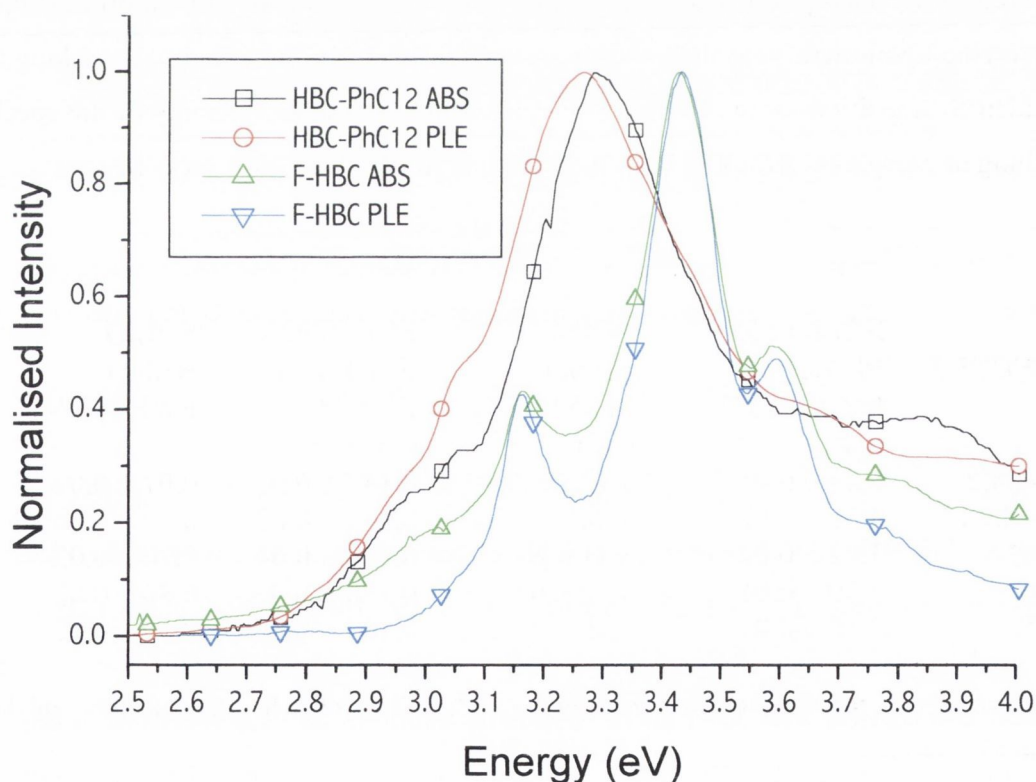


Figure 3.19: The normalised absorption and PLE spectra of HBC-PhC12 and F-HBC.

When comparing the PLE and absorption spectra, certain criteria must be met: a) self-absorption effects must be reduced to a minimum by choosing a suitably low concentration solution (a concentration of $\sim 10^{-5} - 10^{-6}$ M was found to be adequate)

and b) each spectrum must be normalised with respect to each other in such a way that the overlap is maximised. The aim is to discover at what photon energies are the optical responses dissimilar. As PLE spectra are obtained by measuring the photo-luminescence intensity, differences in the PLQY of the species in solution will affect the relative difference in the overlap at a given energy.

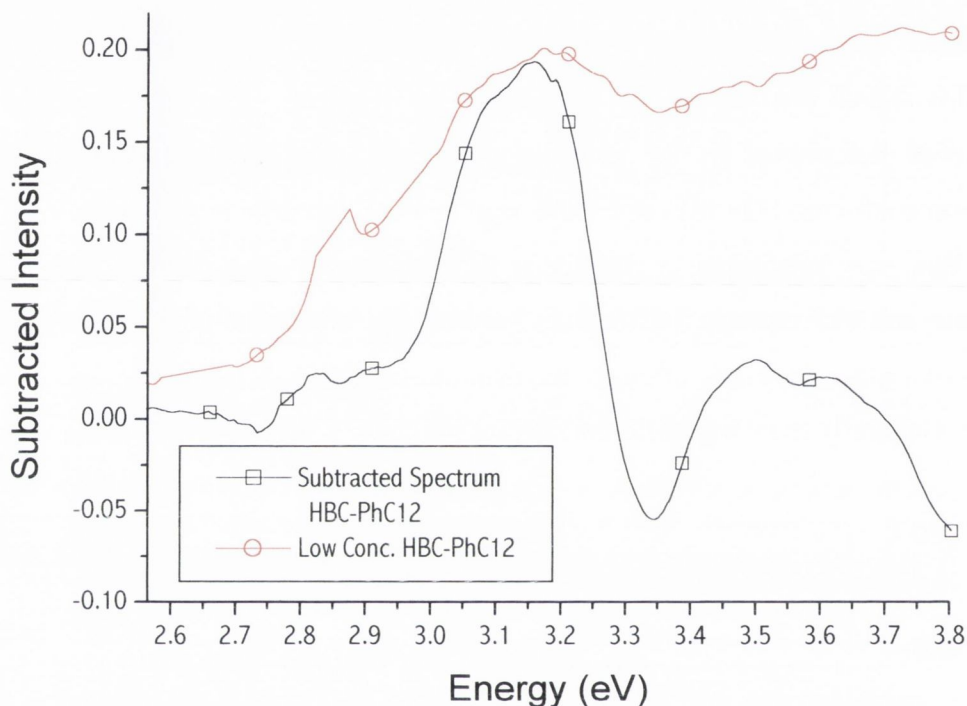


Figure 3.20: The subtracted spectrum for HBC-PhC12. PLE spectrum of low concentration species of HBC-PhC12 is included for comparison. The subtracted intensity is defined as the PLE intensity minus the absorption intensity.

In Figure 3.19, the normalised absorption and PLE spectra of HBC-PhC12 are compared. For HBC-PhC12 there is a notable difference in the intensity of the PLE and absorption spectrum at ~ 3.1 eV and at ~ 3.85 eV. Plotted in Figure 3.20 is the subtracted spectrum, here defined as the PLE intensity minus the absorption intensity. To allow comparison with other known species in solution, the PLE spectrum of the low concentration species of HBC-PhC12 is also given in Figure 3.20. Although the intensities of the low concentration species and the subtracted spectrum are not the same, there is a close match of the peak energies of both spectra. The positive peak in the subtracted spectrum indicates that at this energy the species in solution will contribute more to the photo-luminescence than at other energies. This strongly suggests that there are 2 distinct species in solution. The PLQY of isolated species was

not directly measurable however in Chapter 4 it will be demonstrated that is higher than for an aggregated species. Therefore, a positive peak at the same energy as the low concentration species in the subtracted spectrum indicates that the second species observed is most likely the isolated molecules at high concentration. This is confirmed by the energy dependence of the photo-luminescence and PLE spectra in Figures 3.14 and 3.15.

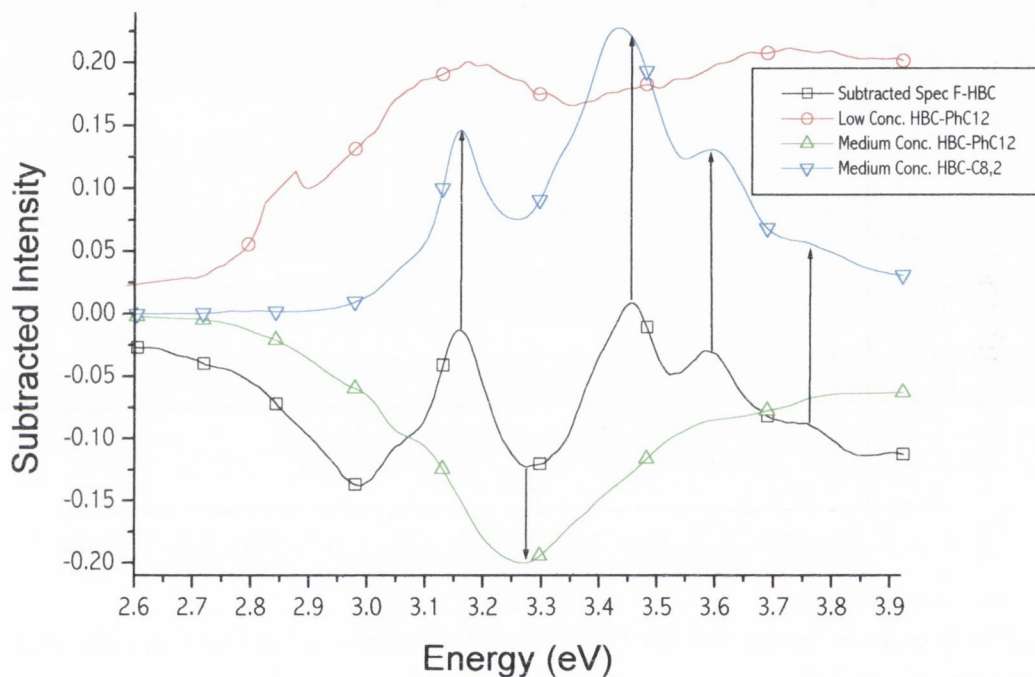


Figure 3.21: The subtracted spectrum of F-HBC and PLE spectra of HBC-PhC12 (at high and low concentration) and HBC-C8,2 at high concentration are given for comparison. Note that the medium concentration HBC-PhC12 spectrum is inverted to allow comparison.

The normalised absorption and PLE spectra of F-HBC are given in Figure 3.19. For F-HBC the subtracted spectrum in Figure 3.21 is more complicated than that of HBC-PhC12 in Figure 3.20. The differences in intensities of the absorption and PLE spectra of F-HBC in Figure 3.19 give rise to negative peaks in the subtracted spectrum. This indicates that at the energies of the negative peak minima, the species is contributing less to the photo-luminescence than at other energies. In other words, at the energy of the negative peak minima the species observed is absorbing photons but not emitting them as efficiently as at other energies.

In order to identify the species responsible for the negative peaks in the subtracted spectrum, the PLE of HBC-PhC12 at low and medium concentration (the latter is inverted to allow comparison), and the PLE of HBC-C8,2 at medium concentration are given in Figure 3.21. Where the subtracted spectrum approaches zero at a given energy, this indicates that there is a good overlap between the absorption and PLE spectra. These maxima, are very well matched in energy with the absorption peaks of HBC-C8,2. On the other hand, the subtracted spectrum minimum is a good match, at 3.27 eV, with the PLE spectrum of HBC-PhC12 at high concentration. The minimum at ~ 3.0 eV is not as straightforward to assign and will be dealt with in the discussion section.

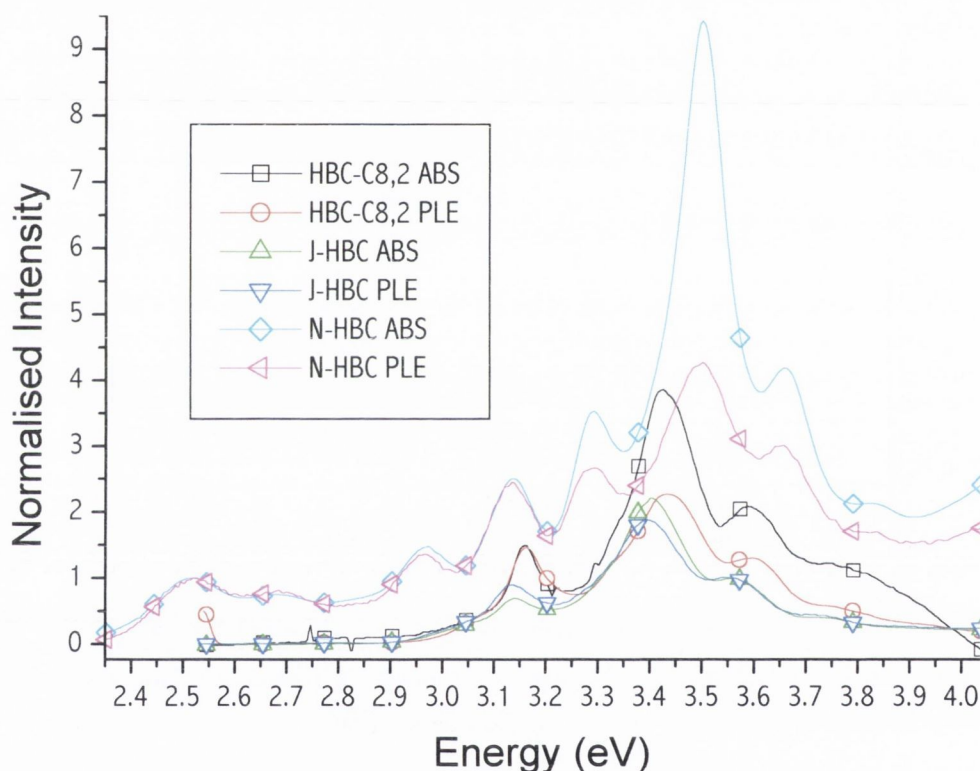


Figure 3.22: Absorption and PLE spectra of HBC-C8,2, J-HBC and N-HBC, normalised to maximise the overlap between PLE and absorption spectra.

The normalised PLE and absorption spectra of HBC-C8,2, J-HBC and N-HBC are given in Figure 3.22. Note how for instance with N-HBC the best overlap is achieved by normalising with the low energy peak at ~ 2.5 eV. For completeness, the subtracted spectra of HBC-C8,2, J-HBC and N-HBC are given in Figure 3.23. For these derivatives all the subtracted peaks are negative. Note how for the subtracted spectrum of N-HBC the real intensity is a factor 3 larger than that shown in Figure 3.23. Interestingly, the energy of the negative peak minima are coincident in energy with the

peak maxima of their respective PLE and absorption spectra. These two factors may indicate that there is one species in solution. However, in each case the discrepancy between the PLE and absorption spectra intensity is greater at higher energies. This suggests that the probability that a photo-exciton will emit a photon is reduced as the energy of the photo-exciton generated is increased. The implications of this will be dealt with in the discussion section.

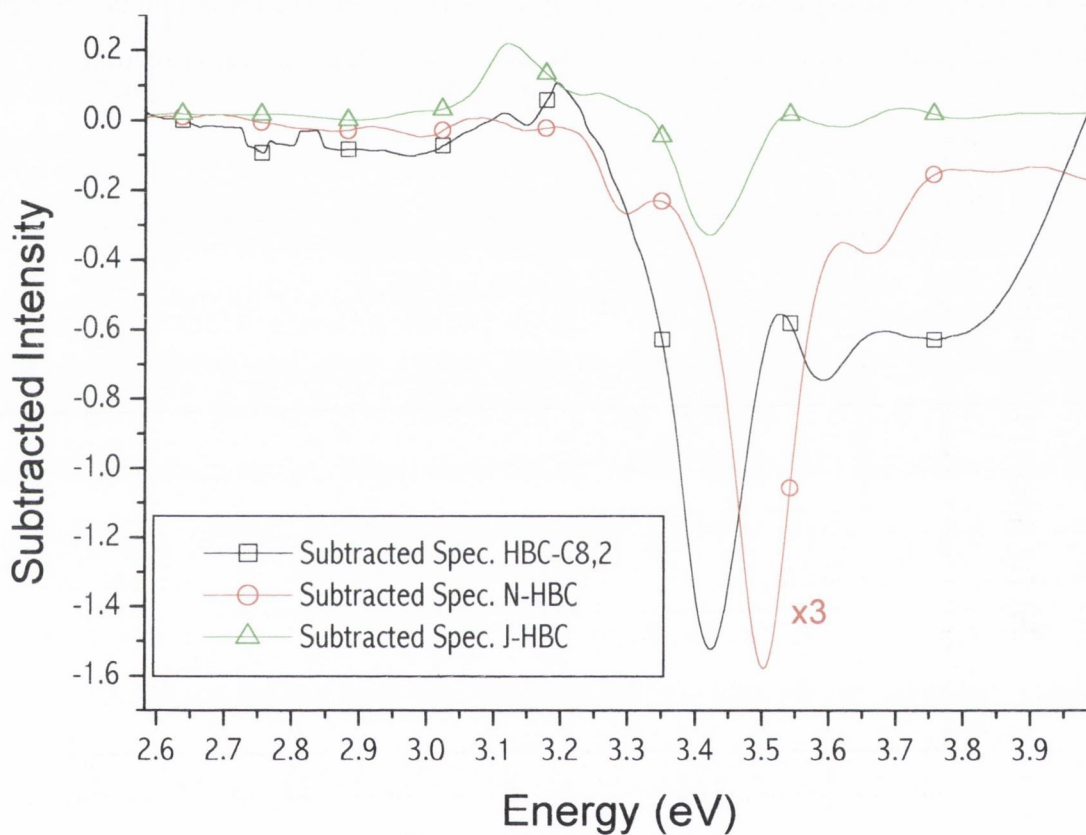


Figure 3.23: Subtracted spectrum for HBC-C8,2, N-HBC and J-HBC derivatives.

3.5 DISCUSSION

ISOLATED MOLECULES

The materials used for these measurements were synthesised in four different labs, dissolved in different solvents and measured repeatedly using different optical spectroscopy instruments. Therefore it is highly improbable that an identical impurity contaminated each and every sample. In this respect, the PLE spectra obtained at low concentration are thus very unlikely to originate from an impurity. In Chapter 4, the concentration dependence study will show how the population of the low concentration species increases as the concentration is lowered, thus confirming that the low concentration PLE spectra are real.

Comparison of the low concentration PLE spectra with the medium and high concentration absorption and PLE spectra demonstrates vast differences in the optical transitions observed. The change in PLE spectra upon increasing the concentration is an indicator that the species observed at low concentration is different to the species observed at medium and high concentrations. Since the solutions measured only contain one derivative molecule, the likelihood is that the low concentration species is the isolated molecule and the medium and high concentration species are the aggregated molecules. This is supported by the fact that the low concentration species is only observed at high concentration for known liquid crystalline molecules¹⁹. Furthermore, conventional photo-physics of isolated molecules stipulates that a change in solvent polarity should give rise to a energy shift in the absorption transition energy

The hyperchromic shift in the low concentration PLE spectra, upon changing from toluene to chloroform, results from solvent molecules stabilising the molecular electronic ground state more than the electronic excited state. If both electronic states are stabilised equally, there would be no net increase or decrease of the transition energy between states. The asymmetrical stabilisation is the result of a) the difference between the spatial electron distributions of the molecular electronic excited and ground states and b) the much faster timescale of the electronic transition compared to the solvent reorganisation. When a molecule is in the electronic ground state, the solvent

molecules are optimally arranged to interact with the electron cloud distribution of the molecular electronic ground state. The favourable interaction between the solvent dipole – molecular electron cloud will therefore reduce the energy of the electronic ground state. Accordingly, the larger the electron cloud displacement during an electronic transition, the less likely the solvent arrangement (optimised to the electronic ground state) will favourably interact with the electronic excited state. This is compounded by the fact that electronic transition is much faster relative to the solvent molecule re-arrangement. The solvent molecules therefore have no time to re-arrange during the electronic transition. The result is an asymmetrical perturbation of the energy of the two electronic states, which increases the electronic transition energy between the states, thus leading to a blue-shift in the absorption spectra. For isolated polar molecules in a polar solvent, the permanent dipoles of the solvent molecules may not necessarily align with the permanent dipole of the molecule. In this case an unfavourable interaction may give rise to an decrease in the transition energy and hence a red-shift in the absorption spectrum.

Chloroform has a larger permanent dipole²⁰ of 1.78 Debye compared to that of toluene 0.375 Debye and for the non-polar HBC derivatives it seems that chloroform stabilises the ground state much more than the excited states, and gives rise to a larger blue-shift in the absorption spectrum. The reverse phenomenon is often observed in the fluorescence where the molecule is in the excited state. In this case the solvent molecules stabilise the excited state more than the ground state. The usual result is an increase in the solvent relaxation and hence a red-shift in the fluorescence spectrum. In conclusion, the solvent dependent energy shift observed for the low concentration species PLE spectra corroborates the finding that the low concentration species are in fact the isolated molecules. In Chapters 4 and 6, further evidence to support the fact that these are the spectra of the isolated molecules will be presented.

TRANSITION ENERGY OF ISOLATED AND AGGREGATED SPECIES

Inspection of the PLE and absorption spectra of the isolated species (Figure 3.9) and aggregated species (Figure 3.12), reveals that there is a large energy difference of ~ 0.6 eV between the lowest energy transitions of both species. There is also a notable difference between the oscillator strengths of the lowest energy transition of the aggregate compared to the isolated molecule. Although it was not possible to measure the absorption coefficient of such a highly diluted sample of isolated molecules, the observation of a highly diluted ensemble of isolated molecules at $\sim 10^{-15}$ M requires that the absorption coefficient be sufficiently high to absorb enough photons so that the photo-luminescence of the isolated molecules, at such a low concentration, can be detected (see Chapter 4). It is therefore likely that the isolated molecule transition at 3.1 eV is a symmetry-allowed transition. On the other hand, the lowest energy transition of the aggregated species is most likely a symmetry-forbidden transition as it has an oscillator strength that is a factor 10 – 100 lower than that of the dominant transition²¹. Therefore, the conclusion is that the lowest energy transition of the isolated species is unrelated to the lowest energy transition of the aggregated species. Instead it is much more reasonable that the isolated molecule absorption peak at ~ 3.1 eV is related to the dominant absorption peak *c*. The nature of the lowest energy transition at ~ 2.5 eV for the aggregate is therefore not straightforward.

Since the non-polar HBC aromatic cores have a D_{6h} symmetry and the polar N-HBC molecule has C_{2v} symmetry, the S₁ transition should be strictly symmetry forbidden. In practice though, a forbidden transition will generally have a small transition probability. The fact that the lowest energy transition of the isolated molecule is observable, even for such a highly diluted ensemble of molecules, strongly suggests that this transition is symmetry-allowed. According to D_{6h} and C_{2v} group symmetry rules the lowest energy symmetry-allowed transition is the S₂ transition. If the peak at ~ 3.1 eV is the S₂ transition, then isolated HBC molecules are fluorescing from the S₂ state (the PL maximum of the isolated species is at ~ 2.8 eV which is at higher energy than the lowest energy aggregate absorption peak at ~ 2.5 eV). This suggests that the usual fast relaxation of excitons to the lowest energy available electronic state, that is implied by Kasha's rule, does not hold for isolated HBC derivative or N-HBC molecules. The

relaxation rate from S_2 to S_1 must be slow enough that most S_2 excitons will radiatively decay from the S_2 state. S_2 emission has been observed previously for molecules such as Azulene²² and S_3 emission has been observed for tetracene in methylcyclohexane²³. Further proof that the dominant PL emission is from the S_2 state for the aggregated species can be found from the absorption and emission spectra of N-HBC in hexane (see Chapter 4 for the PL). The dominant emission peak at 2.63 eV is at higher energy than the lowest energy absorption peak at 2.57 eV for N-HBC in hexane.

The likelihood is that HBC derivatives and N-HBC have strong S_2 absorptions and a weak S_1 absorptions as expected from their respective symmetry group dipole selection rules. Therefore the conclusion is that in both the isolated and aggregated state, the dominant absorption peak and PL peak originate from S_2 transitions. The S_1 transition, observable only for the aggregate state, perhaps becomes more allowed for the aggregated species than in the isolated species because some aggregation effect disrupts the strict symmetry rules, making the S_1 absorption band more allowed. Perhaps then the reason why the lowest energy PL peaks for the aggregate (see Chapter 4) are much lower in energy than for the isolated PL is because the rate of S_2 to S_1 relaxation increases upon aggregation, giving rise to strong transitions in the PL at low energy (< 2.5 eV).

Another possible explanation as to why there are much lower energy features in the aggregated species absorption spectra when compared to the isolated species PLE spectra is dealt with in APPENDIX A but will be discussed briefly here. It is possible that for the isolated molecule the exciton is not fully delocalised over the whole HBC molecule. Instead, an effective conjugation area for planar molecules that is limited to the coronene inner core of the HBC derivatives could explain why the lowest energy transition of the isolated molecules is 0.6 eV higher in energy than the lowest energy aggregate absorption transition. This would also explain why the addition of *exo*-phenyl groups, in the case of HBC-PhC12, does not red-shift the absorption peak. Comparison of the π -bond alternation of HBC and coronene reveals some interesting similarities that may explain why their experimental absorption spectra are similar, whereas their calculated transition energies from PFEO and 2D QB treatments differ so much from experiment. The postulate is that the chemically stable sextet ring current (SRC) of

coronene may persist in the larger HBC molecule, giving rise to a higher energy transition than would be expected for a molecule of the size of HBC. Thus the suggestion is that there is an effective conjugation area for planar molecules²⁴ in an analogous way to the effective conjugation length of conjugated polymers. It may then be possible, that the disruption of this SRC upon aggregation leads to lower energy transitions being observed (the Disrupted SRC state or DSRC). With this explanation Kasha's rule is obeyed for both the SRC and DSRC states. The fact that a variation of the PLE as a function of emission energy is not observed (see Chapter 4) is accounted for by the close proximity of one species to another in an aggregate (i.e. there is intimate mixing of the SRC and DSRC species). This allows excitons to migrate to the disrupted SRC sites with some probability. The number density of these sites is probably low, therefore photon-emission is less probable than from the numerous SRC sites. In this framework the intensity of the low energy DSRC features would be correlated to the number density of molecules in a DSRC state in the aggregate rather than depending on the symmetry selection rules changing upon aggregation.

The overall similarity between the optical absorption spectra of each derivative at high concentration in Figure 3.12 is reasonable when one considers that the active chromophore for each molecule is the HBC core of the molecule and does not include the side groups of the molecule. However, there are some differences in the fine structure of the absorption spectra that cannot be directly correlated to the optical response of the isolated molecule. The question is how do molecules that behave similarly in the isolated form have such different fine structure upon aggregation? Next, the relationship between the molecular interactions in an aggregate and the optical response will be discussed.

From inspection of Figure 3.12 and Table 3.8, the small variability in the transition energy of the dominant absorption peak demonstrates that the size of the quantum box that is being optically probed remains essentially unchanged upon substitution of different side-groups. More importantly, it suggests that aggregation does not lead to strong *inter*-molecular charge delocalisation that may increase the dimension of the isolated molecule 2D quantum box to an aggregate 3D quantum box. As discussed earlier, an increase in the physical size or dimensionality of the confinement space of an electron would be observed spectroscopically. The main signatures of these changes

would be a red-shift of the absorption band and significant broadening (as the number of possible transitions increases) including a large increase in the low-energy absorption tail. There is no spectroscopic evidence, from the high concentration absorption spectra, to support the notion that inter-molecular bonds are forming, upon aggregation, that correlate the π -conjugation of many neighbouring molecules in an aggregate. Although this π -bond correlation does take place when chemical dimers are formed (or for instance when conjugated monomers are polymerised into conjugated polymers), it is unlikely that there are fully delocalised electron states in a van der Waals aggregates such as HBC derivative MSAs.

There are, however, large differences in the FWHM of the absorption spectra of the different HBC derivatives. Interestingly F-HBC at high concentration does appear to have an extended absorption tail unlike the other HBC derivatives. In the following sections, these spectroscopic anomalies and other observations will be explained in terms of the photo-exciton resonance interactions associated with molecular van der Waals aggregates.

The subtraction of the PLE spectra from the absorption spectra of high concentration solutions reveals interesting information about the MSAs. It is clear that HBC-PhC12, and perhaps F-HBC, have isolated species present at high concentration. This suggests that HBC-PhC12 is liquid crystalline at room temperature, which is confirmed by TGA and DSC analysis²⁵. The surprising result is that some of the other molecules exhibit what appears to be a isolated molecule absorption but no fluorescence. This can be explained in terms of the disorder of the MSAs. Isolated molecule fluorescence will only occur if an exciton formed on an isolated molecule does not migrate on to the MSAs nearby. The liquid crystalline nature of HBC-PHC12 ensures that molecules are not strongly bound to any molecular site and are free to displace away from the nanowire axis. This in turn ensures that the isolated HBC-PhC12 molecules are not coupled to the MSA (they might even be present interstitially between the nanowires in a bundle). The lack of any electronic coupling to an MSA ensures that the PLQY is high. Comparatively, disorder in the other non-liquid crystalline MSAs will give rise to molecules that are disconnected from the MSA but not sufficiently that the photo-exciton generated on these disorder induced "isolated" species will not migrate to the

core of the MSA. The result is a low PLQY for excitons generated on these species. If this is the case there will be a contribution to the absorption but not to the PLE (see Figure 3.24).

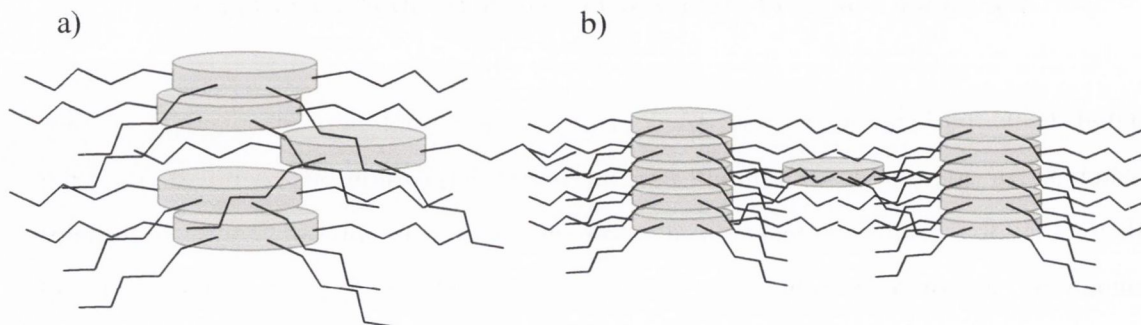


Figure 3.24: a) Disorder induced isolated species at high concentration will give rise to isolated molecules being observed in the absorption but not in the PL b) Liquid crystalline induced isolated species at high concentration.

From Figure 3.16, it is clear that a change in solvent polarity does not affect the absorption transitions of the non-polar high concentration species. This result seems unreasonable if the high concentration species were isolated, however the result is easily explained in terms of aggregates. For a spherical aggregate, the ratio of the number of molecules in the bulk of an aggregate N_B , to the number molecules on the surface of an aggregate N_S , is given by $N_B/N_S \sim r/3$, where r is the radius ($N_B/N_S \sim r/2$ for a cylinder with a large aspect ratio). Therefore in general, the larger an aggregate, the greater the number of bulk molecules to surface molecules. In solution, the surface molecules of an aggregate are stabilised by the presence of solvent molecules, but the molecules in the bulk of the aggregate are not affected due to charge screening effects (i.e. the persistence length of the interaction will be solely determined by the polarisability of the molecule). In the process of photo-absorption, all molecules have a certain absorption cross-section of interaction with the photon. It follows that since there are far fewer surface molecules, there will be a much higher overall probability that a photon will interact with a bulk molecule. The result is that for large aggregates of non-polar molecules, changes in solvent polarity will not give rise to significant solvent shifts in the absorption spectra. For polar molecules like N-HBC, small solvent shifts will be observed due to the persistence length of the solvent stabilisation into the aggregate being greater than for non-polar molecules. This is because polar molecules are

polarisable and also have permanent dipole moments that can align with the solvent molecule dipole.

FRENKEL EXCITON RESONANCE IN AGGREGATES

Isolated HBC molecules are disk-like molecules are made up of a graphitic core surrounded by a number of aliphatic side-groups. The preferred aggregation of the molecules is to self-assemble into columnar stacks (i.e. nanowires), but the optimal arrangement is not a straightforward face-to-face stacking, instead a staggered and displaced arrangement²⁶, which is constrained by the side-chains, is favoured (see illustration in Figure 3.24 a)). However, it must be noted that, in solution and at room temperature, the molecules making up the aggregate are free to rotate about the columnar axis.

The high polarisability and small permanent dipole moment of the large centro-symmetric aromatic core of HBC derivatives (except N-HBC) ensures that the van der Waals interaction, and not the Coulombic (electrostatic) interaction, is the most dominant term in the total ground state interaction energy. Under these conditions the centro-symmetric geometry of the HBC core ensures that the *electronic transition* dipole moments of the isolated molecules point along-the-plane of the molecule. Thus columnar stacking of the isolated molecules will therefore form H-aggregates²⁷.

An aggregate is essentially a collection of coupled molecules. The degree and nature of the coupling interaction can be described by three factors: the Coulombic binding energy of the aggregate ground state W (negative for dimers and larger aggregates, and positive for excimers), the Coulombic interaction energy W' of the excited state of one molecule with the ground state of another and finally the exciton resonance *or transfer* interaction term β . The resonance interaction term will determine the degree of splitting of the aggregate FER energy levels. For H-aggregates, assembled from parallel stacked molecules with a centro-symmetric transition dipole moment, we expect $\beta > 0$ as the moments should lie parallel to each other (see Chapter 1). From the vector addition of the transition dipole moments the higher of the two dimer exciton states is dipole allowed and has the larger oscillator strength. The result is a blue-shift of the aggregate

excitation spectrum peak maximum with respect to the isolated molecule spectrum peak maximum.

The increase in concentration of isolated molecules, from 10^{-13} M to 10^{-8} M, alone cannot explain the dramatic change in the luminescence and luminescence-excitation spectra observed: a new species must be responsible. Formed at medium concentration, H-aggregates will generally blue-shift the excitation spectrum. Using the shift of the absorption/PLE maximum observed, from low to medium concentration, the magnitude of the energy shift ΔE upon aggregation, for all derivatives, can be measured. Initially assuming the values for W and W' for each compound are similar, the ΔE value scales with the observed blue-shift. Values for ΔE of all derivatives given in Table 3.11 are all positive, indicating that the absorption maxima of all derivatives are blue-shifted relative to the isolated PLE peak maximum. This confirms the formation of H-aggregates at high concentration. Calculated in this way, HBC-C_{8,2} and N-HBC aggregates have a relatively larger ΔE value than, say, HBC-PhC₁₂ aggregates (a factor ~ 2.6 larger). At medium and high concentration the dominant sub-band (peaks *a*, *b* and *c*) for each derivative is at higher energy and has a larger oscillator strength than the weaker sub-band (peaks *e* and *f*) at lower energy. On average the weaker sub-band has an oscillator strength that is a factor ~ 0.36 lower in intensity than the dominant sub-band. This behaviour is consistent with that expected from FER systems that are H-aggregates as described in Chapter 1.

MOLECULE	ISOLATED		AGGREGATE		ΔE (eV)	RATIO $\frac{FWHM_A}{FWHM_I}$
	BAND MAX. (eV)	BAND FWHM (eV)	BAND MAX. (eV)	BAND FWHM (eV)		
HBC-C _{8,2}	3.12	0.54	3.43	0.148	(+) 0.31	0.27
HBC-PhC ₁₂	3.18	0.59	3.30	0.355	(+) 0.12	0.60
F-HBC	3.30	0.56	3.42	0.926	(+) 0.12	1.65
J-HBC	3.33	0.63	3.39	0.186	(+) 0.06	0.29
N-HBC	-	-	3.50	0.154	(+) 0.27*	0.26*

Table 3.11: The shift in energy ΔE between the isolated and aggregate absorption maxima and the ratio of aggregate $FWHM_A$ to isolated $FWHM_I$ for each derivative. Notice how the energy shift ΔE is large for all derivatives and with the exception of J-HBC. *Values estimated by taking the average of the isolated molecule absorption spectra of all other derivatives.

The collective exciton states that arise from FER in an aggregate will generally lead to exchange narrowing²⁸ of the absorption and emission bands relative to the isolated molecule absorption and emission bands. From Table 3.11 the decrease in FWHM by a factor 0.27 – 0.29, from low to medium concentration, observed for some derivatives confirms that FER is occurring, and by default confirms the presence of aggregates in solution. The exceptions in Table 3.11 are HBC-PhC12 and most notably F-HBC. The increase in FWHM upon aggregation of F-HBC is a result of measuring the FWHM_A at high concentration from Figure 3.12. However, at medium concentration F-HBC has a FWHM comparable to that of HBC-PhC12 as can be seen in Figure 3.19. The much larger FWHM of HBC-PhC12 relative to HBC-C8,2 is probably due to disorder of the aggregate that arises from the liquid crystalline behaviour of this derivative at room temperature.

Further evidence of FER in the medium and high concentration spectra is discussed by Fleming et al¹⁵. Peak *e* for HBC-C8,2 is observed to sharpen more than peak *c* upon increasing the concentration from medium to high concentration. This is because the dipole-allowed state, peak *c* in Figure 3.12, is lifetime broadened as the exciton can quickly decay to the lower lying, dipole-forbidden state, peak *e*. This labels peak *e* as the dipole-forbidden state (see also Chapter 4).

The establishment of the dipole-allowed and dipole-forbidden transitions in the spectra relative to the FER model makes it possible to measure the resonance interaction and other FER parameters directly. For HBC-C8,2, HBC-PhC12 and J-HBC the parameters are readily measured from the spectra and are given in Table 3.12.

Overall the values measured for 2β are roughly similar for all derivatives. This is because all the derivatives have the same aromatic core (with the exception of N-HBC), therefore the basis states of the collective exciton state for each derivative aggregate are all similar (as confirmed by the low concentration PLE spectra). From the aggregate geometry optimisations, the intermolecular distance for all derivatives are also of the same order, therefore the strength of the dipole-dipole resonance interaction will tend to be alike for all derivatives. A possible explanation for the slightly larger value of 2β for HBC-C8,2 and N-HBC is that the molecules in the aggregate stack are aligned with

greater order, or are held closer together, thus ensuring that the stronger resonance interaction is observed.

However neither W or W' can be independently measured from the spectra. Only the sum $W + W'$ can be measured from the spectra (see Figure 1.4 in Chapter 1). To determine W' is more straightforward for non-polar molecules, because the reasonable assumption that $W \sim 0$ can be made. This is a fair approximation for non-polar molecules as the W interaction is entirely a Coulombic interaction. The Coulombic binding energy W , can be estimated from the point-dipole approximation $W = (1/2\pi\epsilon)(\mu^2/R^3)$, where R is the intermolecular plane distance (~ 3.5 Å) and μ is the permanent dipole moment and all other symbols have their usual meaning. HBC-C_{8,2} has an extremely small permanent dipole moment $\mu \approx 0.06$ Debye²⁹, and thus has an almost negligible shift of ≈ -0.05 meV. The parameter ΔE includes β , W and W' , and is therefore not as well suited for comparison when β can be measured directly from the spectra.

MOLECULE	2β (eV)	W	W'	REMARKS
HBC-C _{8,2}	0.27 ± 0.02	~ 0	0.16 ± 0.04	C aggregated species
HBC-PhC ₁₂	0.23 ± 0.02	~ 0	~ 0	L aggregated species
F-HBC	0.27 ± 0.04	~ 0	0.16 ± 0.04	C aggregated species
	0.21 ± 0.04	~ 0	~ 0	L aggregated species
J-HBC	0.26 ± 0.02	~ 0	0.13 ± 0.04	C aggregated species
N-HBC	0.36 ± 0.02	~ 0	$0.17 \pm 0.04^*$	C aggregated species
	0.32 ± 0.02	~ 0	~ 0	L aggregated species

Table 3.12: FER parameters measured from medium and high concentration spectra. In Chapter 4, the species with $W' \sim 0$ are labelled L and those with $W' > 0$ are labelled C.

Significantly, HBC-C_{8,2} aggregates seem to have a larger Coulombic interaction ($W + W' = 0.16 \pm 0.04$ eV) compared to HBC-PhC₁₂ aggregates (negligible energetic shift). This interaction is also known as the “crystal shift” in the case of molecular bulk crystals, and describes the difference in the transition energy $\hbar\omega_0$ for a isolated molecule compared to a molecule as part of an aggregate. As described above, for non-polar

molecules the Coulombic binding energy W is almost negligible. This implies that W' (due to the high polarisability of the molecules) is the more dominant of the two Coulombic interactions. The large positive value for W' of the HBC-C_{8,2} molecules is possibly due to the greater cohesion and smaller intermolecular distance increasing the magnitude of the Coulombic term and hence increasing $\hbar\omega_0$. On the other hand, the more loosely bound HBC-PhC₁₂ molecules have a similar $\hbar\omega_0$ to when isolated. This would suggest that the HBC-PhC₁₂ molecules in the stack behave in a fashion more similar to the non-aggregated case. However, despite W being negligible for both derivatives, aggregates do form. This is because the van der Waals (dispersion) interaction, and not the Coulombic interaction, is the dominating force binding the aggregates together (for both molecules the permanent dipole moments are small and the polarisabilities are large).

The polar N-HBC molecule has a dipole moment ~ 6 Debye and should therefore have a large Coulombic binding energy $|W| \sim 0.3$ eV if the relative permittivity is taken as $\epsilon \sim 3$ (from polystyrene) and the intermolecular distance is taken as ~ 3.5 Å. Correcting for the angle ϕ between the permanent dipoles of N-HBC, using the maximum value $\phi = 45$ degrees calculated from the aggregate geometry optimisation, reduces W by a factor $\cos^2\phi = 0.5$. This results in a more reasonable Coulombic binding energy of $W \sim 0.15$ eV. Since no isolated PLE spectrum was obtainable, extrapolating values for N-HBC is less straightforward. However, the rough calculation of the Coulombic binding energy of N-HBC indicates that for such a polar molecule the aggregate transition energy should be red-shifted significantly by $0.15 < W < 0.3$ eV if the Coulombic interaction were the dominant interaction influencing the molecular alignment in the aggregate. Since the energy of the dominant absorption peak in the high concentration spectra of N-HBC is equivalent to that of the other derivatives, it seems that the Coulombic interaction is not the dominant binding interaction. This is confirmed by the aggregate geometry optimisations. The molecular alignment seems to be more heavily influenced by the dispersion interaction and the steric hindrance between the t-butyl groups of neighbour molecules, than by the permanent dipole-interaction. This is clearly the case in the aggregate geometry optimisation, because the permanent dipole alignment is symmetric, which would give a positive (repulsive) Coulombic binding energy.

Values for F-HBC in Table 3.12 are measured from the medium concentration spectra presented in Figure 3.19 and not from the high concentration spectra for reasons that will be explained later (including how the N-HBC peak assignment was extrapolated from the medium and high concentration spectra of F-HBC).

The medium and high concentration PLE/absorption spectra of F-HBC reveal an interesting feature that helps explain the aggregate N-HBC absorption spectrum. At medium concentration the PLE/Absorption spectra of F-HBC is very similar to that of HBC-C8,2. The medium concentration spectrum was used to determine the FER parameters of the F-HBC aggregated species C in Table 3.12. In fact the measured FER parameters are identical to those of HBC-C8,2. At high concentration, in Figure 3.12 two new peaks e and d^* emerge in the absorption spectrum that are not present at medium concentration. These peaks are energetically quite close to the allowed (peak c) and forbidden (peak e) transitions of HBC-PhC12. This is not a coincidence. What is happening is that two species of F-HBC are thermodynamically favourable at high concentration. Species C has optical properties that resemble that of HBC-C8,2 whereas species L resembles HBC-PhC12. This is also confirmed by the energetic positions of peaks in the subtracted spectrum of F-HBC. Unfortunately, N-HBC does not demonstrate the same concentration dependence of F-HBC, however the peak positions are remarkably similar to that of F-HBC (if the larger 2β of N-HBC relative to F-HBC is taken into account). Accordingly the FER values for species L and C are given in Table 3.12. Notice how for both N-HBC and F-HBC the L species has a smaller 2β interaction energy relative to the C species. This can be explained by considering how the W' interaction is drastically reduced for the L species for both derivatives. A negligible W' interaction indicates that the molecules' excited state is not interacting with the ground state of the neighbouring molecule. Since this is clearly observed for HBC-PhC12, which is liquid-crystalline at room temperature, and not for HBC-C8,2 which is crystalline, at room temperature, the likelihood is that $W' \sim 0$ for liquid crystalline species. Liquid-crystalline aggregates will tend to have molecules that are not strongly bound in position, therefore the greater displacement of the molecule will increase the distance between the interacting transition dipoles and thus reduce the energy of the resonance interaction of the L species. Conversely, the large Coulombic interactions of C aggregates in Table 3.12 is a manifestation of the aggregates being

physically robust and stable - as confirmed by X-ray diffraction measurements² (HBC-C8,2 is known to be crystalline at room temperature where HBC-PhC12 is a liquid crystal). As a summary of the above peak assignments, the absorption spectra of all derivatives are given in Figure 3.25 with the relevant symmetric (+) and anti-symmetric (-) FER H-aggregate transitions indicated. Also indicated in the Figure are the L and C species assignments.

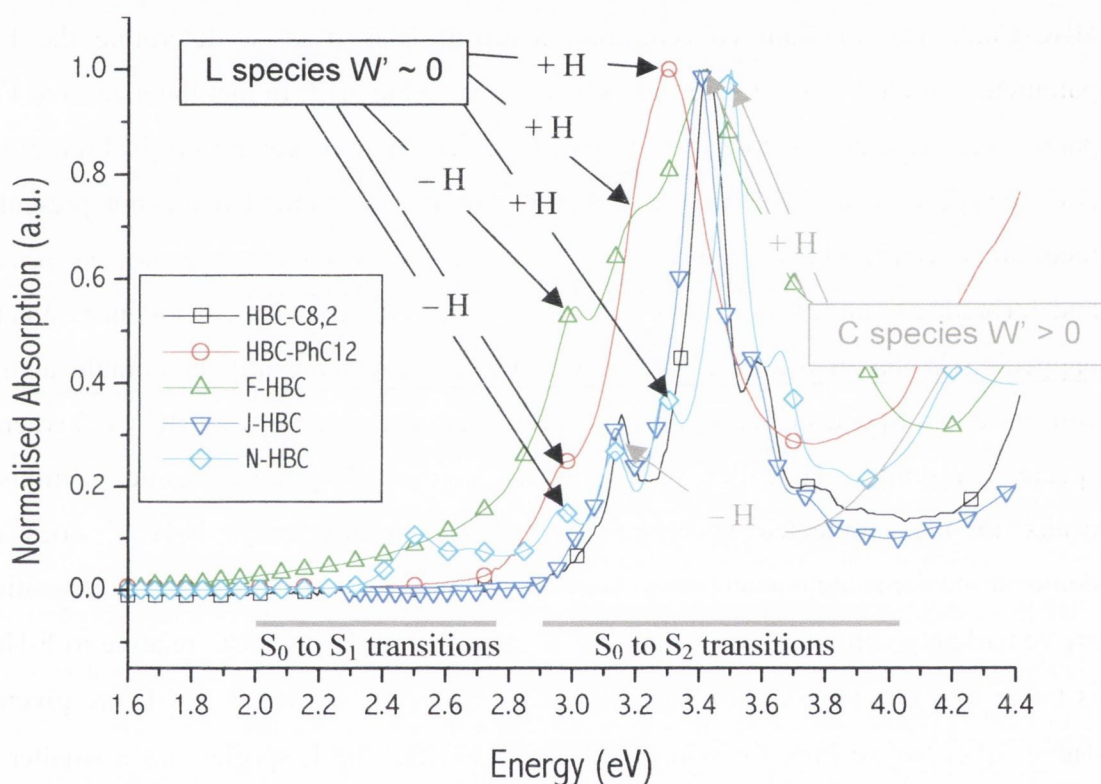


Figure 3.25: Absorption spectra of all HBC derivatives. The FER dipole allowed (+ H) and dipole forbidden transitions (- H) are indicated, as are the peaks corresponding to the C and L species of the relevant species. Note that the S_1 and S_2 transitions are respectively symmetry forbidden and symmetry allowed by the symmetry of the molecular structure not the FER. The FER transitions of an aggregate structure are determined by the symmetry of the transition dipole interaction between transition dipoles of neighbouring molecules in an aggregate.

3.6 CONCLUSIONS

The new synthesis of highly soluble HBC derivatives has made it possible to measure the optical spectra of the HBC chromophore at very low concentrations. This has made it possible to observe the isolated molecular species of HBC spectroscopically for the first time and to confirm the widely accepted, yet not often observed, photo-physical properties of isolated molecules. For example, the hyperchromic shift of the PLE spectrum of HBC-C8,2, and HBC-PhC12 with respect to F-HBC and J-HBC upon changing the solvent polarity.

The identification of the isolated species at low concentration has also made it possible to understand the influence of the self-assembly or aggregation of HBC derivatives on the optical properties. More importantly the effects of different solubilising side-chains on the MSA structure and the accompanying changes to the optical properties have also been determined. The overall similarity of the optical spectra of C aggregates of different derivatives (and L aggregates of different derivatives) confirms that the optical properties are determined by the stacking of the aromatic cores of the molecules. The identification of the L and C aggregate species from otherwise complicated absorption and PLE spectra was only made possible by the comparison of all derivatives presented. This demonstrates the necessity of synthesising various similar derivatives with identical chromophores in order to determine the molecular interactions on the aggregate bundle structural level. As demonstrated by the results presented here, the structural hierarchies above the molecular structure can play a dominating role in determining the final optical response of real solutions of small molecules in solution and can therefore not be neglected.

The observation of the dipole-allowed state and dipole-forbidden state enabled the molecular interaction of the aggregates to be assessed. The measured values for W , W' and β all agree with a system comprised of highly polarisable, closely assembled molecules with a low permanent dipole moment, and therefore support the idea that the aggregates are indeed observed at concentrations above 10^{-9} M. From this, it therefore follows that the low concentration spectra can be attributed to isolated molecular entities in solution. This idea is further supported by the similarity of the excitation

spectra at low concentration to that of the isolated molecules found at medium concentration for known liquid crystalline HBC derivative molecules at room temperature.

The hexabenzocoronene family of compounds are a very suitable class of materials for studying aggregation effects. The high purity attainable and 2-D shape makes an interesting molecule easier to study, and has enabled the demonstration of the photo-physics of isolated and the investigation of the photo-physics of aggregated molecules.

¹ For example, zero E_S is often reported for polymers even though the calculated E_S , from the Huang-Rhys parameter and vibrational-electronic (v-e) transition energy, is clearly non-zero. Experimentally, it is often found that increased solvent polarity doesn't alter the E_S shift of a supposed highly diluted solution of non-polar molecules. More significant though, is the lack of a consensus as to why, for molecular crystals with FER, the v-e structures of resonant excitons are absent.

² U. Brackmann, *Lambdachrome Laser Dyes* (Lambdaphysik 1994)

³ M. Fox, *Optical Properties of Solids* (Oxford Press 2001)

⁴ W. J. Blau, A. J. Fleming, *Science* **304**, 1457 (2004)

⁵ C. Didraga, J. Knoester, *J. Luminescence* **102-103** 60 (2003)

⁶ J. Schütze, B. Brüggermann, T. Renger, V. May, *Chem. Phys.* **275** 333 (2002)

⁷ J. P. Hill, J. Wusong, A. Kosaka, T. Fukushima, H. Ichihara, T. Shimomura, K. Ito, T. Hashizume, N. Ishii, T. Aida, *Science* **304** 1481 (2004)

⁸ I. Baraldi, M. Caselli, F. Momicchioli, G. Ponterini, D. Vanossi, *Chem. Phys.* **275** 149 (2002)

⁹ K. Kirova, S. Brazovski, A. R. Bishop, D. McBranch, V. Klimov, *Synth. Met.* **101** 188 (1999)

¹⁰ J. B. Birks, *Photophysics of Aromatic Molecules*, Wiley, New York (1970)

¹¹ M. Pope, C. E. Swenberg, *Electronic Processes in Organic Crystals and Polymers*, Oxford University Press (1999)

¹² N. Nijegorodov, R. Mabbs, W.S. Downey, *Spectrochimica Acta Part A* **57** (2001) 2673-2685

¹³ B. Servet, *Chem. Mater.* **6** 1089 (1994)

- ¹⁴ Dimer structure of HBC-C8 was calculated by the same method. Geometry optimised structure not shown.
- ¹⁵ A. J. Fleming, J. N. Coleman, A. B. Dalton, A. Fechtenkötter, M. D. Watson, K. Müllen, H. J. Byrne, W. J. Blau, *J. Phys. Chem. B*, **107** 37 (2003)
- ¹⁶ M. Kasha, *Spectroscopy of the Excited State*, Plenum Press, New York (1976)
- ¹⁷ W. Hendel, Z. H. Khan, W. Schmidt, *Tetrahedron*, **42** 1127 – 1134 (1986)
- ¹⁸ In collaboration with Dan Gregg, Chemistry Dept. Trinity College Dublin
- ¹⁹ van der Craats A.M., Warman J.M., Fechtenkoetter A. Brand J.D., Harbison M. A., Muellen K., *Adv. Mater.* 1999, *11*, 1469.
- ²⁰ Lide D. R., *Handbook of Chemistry and Physics*, 77th Ed, CRC, New York, 1996.
- ²¹ M. Pope, C. E. Swenberg, *Electronic Processes in Organic Crystals and Polymers*, Oxford University Press, p 29, 1999
- ²² G. Visnawath, M. Kasha, *J. Chem. Phys.*, **23**, 574 (1956)
- ²³ Nickel B., Roden G., *Z. Electrochem. Ber. Bungsengs. Physik. Chem.* **81** 281 1977
- ²⁴ Sly W.G., *Acta Crystallorg.* **17**, 511 1964.
- ²⁵ Fechtenkötter, A.; Saalwächter, K.; Harbison, M. A.; Müllen, K.; Spiess, H. W.; *Angew. Chem. Int. Ed.* **1999**, *20*, 3039.
- ²⁶ Rodríguez, J.; Sánchez-Marín, J.; Torrens, F.; Ruette, F.; *J. Mol. Struc. (Theochem)* **1992**, *254*, 429-441.
- ²⁷ Knöster, J.; Proceedings International School of Physics “Enrico Fermi” Course CXLIX: Organic Nanostructures
- ²⁸ Abram, I. I.; Hochstrasser, R. M.; *J. Chem. Phys.* **1980**, *72*, 3617
- ²⁹ AM-1 Calculation performed on HBC-C_{8,2}. However, when thermalised to room temperature, the molecule can be approximated as planar and hence has no permanent dipole moment.

Chapter 4: PL AND PLE SPECTRA

4.1 INTRODUCTION

In this Chapter the photo-luminescence spectra of all derivatives at various concentrations are presented. The influence of aggregation on the PL properties of solutions of molecules is explored and found to be most likely determined by structural levels above the molecular structure. Particular spectroscopic signatures, originating from FER in the PL, will be shown to allow an approximate determination of the aggregate structure. To achieve this, a FER photo-absorption-luminescence (p-a-l) cycle relevant to H-aggregates is constructed and the general FER properties of J and H aggregates are explored.

The migration of excitons throughout an aggregate to molecular sites of lower energy can give rise to very different PL spectra for similar compounds. In this manner, PL spectra allow a differentiation of MSA structures formed by similar molecules, such as the HBC derivatives studied here. In fact, the PL spectra can give information that absorption spectra cannot reveal. It will be shown that interactions of molecules in aggregate bundles (i.e. in the super-structure of an aggregate) can profoundly influence the structure of the PL spectra. For instance, at low concentration, the asymmetric substitution of alkyl-oxy chains of J-HBC does not lead to a different emission in the PL compared to the other symmetrically substituted derivatives (for isolated J-HBC molecules, the emission is still from the S_2 state as with the other derivatives). However, from evidence, found in the spectroscopic FER signature of the PL spectra of J-HBC aggregates, the asymmetric substitution does favour a different aggregate super-structure compared to HBC-C8,2, HBC-PhC12 and F-HBC. Likewise, N-HBC aggregates in hexane are found to have a similar PL FER signature to J-HBC. Thus, differences in the PL spectra do allow a distinction between MSA superstructures formed by J-HBC and N-HBC when compared to the symmetrically substituted HBC-C8,2, HBC-PhC12 and F-HBC aggregates. These divergences, in the medium and high concentration PL spectra, are assigned to differences in the FER responses of the aggregates, and not due to differences in the symmetry of the isolated molecule's molecular electronic states (as has been previously suggested in the literature⁵).

The combination of absorption/PLE and PL spectra also allows the assignment of electronic and vibrational-electronic (v-e) transitions of the molecules. This is particularly aided by the comparison of the PL spectra of the five different HBC derivatives studied here. The concentration dependence of the HBC derivatives' PL intensity is explored and helps confirm the identification of the isolated molecular species. Finally the relative photo-luminescence efficiencies of the HBC derivatives are compared and examined in terms of the MSA structure.

4.2 RESULTS

ISOLATED MOLECULES

In Figures 4.1 and 4.2, the low concentration PLE and PL spectra of HBC-C8,2, HBC-PhC12, J-HBC and F-HBC are presented. The isolated species of N-HBC was not obtainable in chloroform or toluene for reasons that will be given in Chapter 5. As discussed in Chapter 3, when the difference in solvent is considered, the PLE spectra of the isolated species of HBC-C8,2, HBC-PhC12, F-HBC and J-HBC are similar in structure. From Figures 4.1 and 4.2, the PL spectra of all the derivatives are also similar in structure. For F-HBC however the PL spectrum has an additional contribution from the aggregate PL at lower energies (the fine structure).

As can be seen from Table 4.1, the major difference between the PL of the isolated species of all derivatives is the energy of the PL intensity maximum. In a similar manner to the PLE spectra, this disparity arises from the different solvents used. The bathochromic blue-shift between the PL spectra of HBC-C8,2 and HBC-PhC12 in toluene and the PL spectra of J-HBC and F-HBC in chloroform is ~ 0.2 eV (this is similar to the bathochromic blue-shift of the PLE). Therefore, when calculating the Stokes shift from the difference in energy between the dominant PLE peak and the dominant PL peak, as given in Table 4.1, the calculated Stokes shifts do not reflect the difference in the solvent environment of the isolated molecule. In theory the increase in solvent polarity of chloroform with respect to toluene should stabilise the excited state and give rise to a larger Stokes shift. This is not observed. Instead it seems, at least for

the non-polar molecules studied here, the Stokes shift is rather similar in both solvents (within the margin of error). To assess this the fine structure in the isolated PL spectra must be examined.

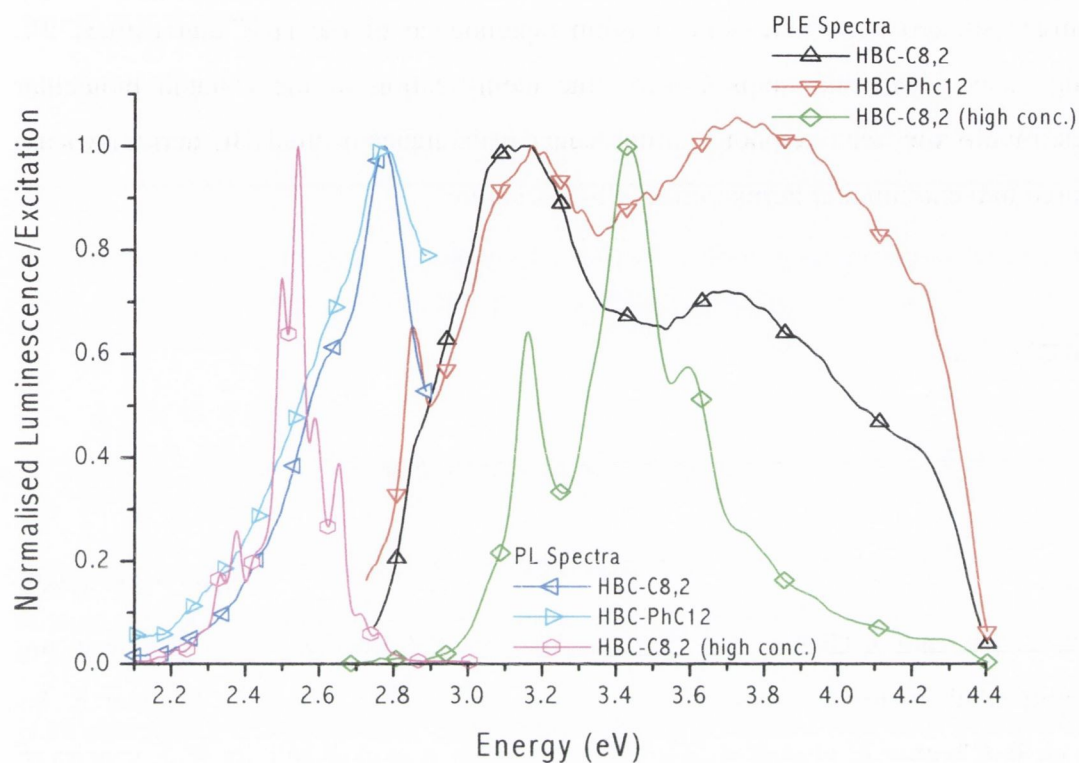


Figure 4.1: The normalised PL and PLE spectra of HBC-C8,2 and HBC-Phc12 of low concentration species at $\sim 10^{-13}$ M. The PL and PLE spectra of HBC-C8,2 high concentration species at 10^{-6} M is also given for comparison. Note that there is a solvent scattering artefact at ~ 2.85 eV.

From inspection of Figures 4.1 and 4.2, a notable difference between the PL and the PLE spectra of the isolated species is the resolution of distinct peaks and shoulders in the former. From Figures 4.1 and 4.2, the plot in Figure 4.3 a), the energy difference between each successive peak in the PL of the most highly resolved PL spectra, of HBC-C8,2, is approximately 0.15 ± 0.01 eV (similarly for the other derivatives). The straight line fit of the data agrees with the expected linear increase of the energy of the successive energy levels of a quantum harmonic oscillator (see Figure 4.3 b)). This energy difference is similar to that expected for aromatic C = C stretches (~ 0.19 eV) and therefore the peaks and shoulders are most likely of vibrational-electronic origin.

MOLECULE	EXCITATION		LUMINESCENCE		
	ENERGY	FWHM	ENERGY	FWHM	STOKES
HBC-C8,2	3.12 (eV)	0.54 (eV)	2.77 ± 0.01	0.32 ± 0.02	0.35 ± 0.03 (eV)
HBC-PhC12	3.18	0.59	2.77 ± 0.02	0.45 ± 0.04	0.41 ± 0.05
F-HBC	3.30	0.56	2.90 ± 0.05	0.44 ± 0.04	0.40 ± 0.08
J-HBC	3.33	0.63	2.98 ± 0.02	0.32 ± 0.04	0.35 ± 0.04

Table 4.1: Values of the transition energies, FWHM and Stokes shifts of the PLE and PL spectra of all derivatives observed at low concentration. The Stokes shift is determined by the difference in energy between the PLE and PL peak maxima.

Therefore the values of the Stokes shifts in Table 4.1, 0.35 – 0.45 eV, are also reasonable when considering that the total Stokes shift is contributed to by the vibrational-electronic (v-e) and solvent relaxation energies (this will be discussed extensively in Chapter 6). The Huang-Rhys parameter for a vibrational envelope such as the PL of HBC-C8,2, calculated by comparing to a Poisson distribution, is $S \sim 0.5$. This is typically observed for isolated conjugated molecules^{1,2,3}. If the isolated molecule PLE were to be mirror symmetric with the PL (this is often the case for non-interacting isolated molecules), the v-e relaxation energy contribution would be given by $2S_{\text{Abs}}\hbar\omega_{\text{pl}} \sim 0.15$ eV. Subtracting this value from the total isolated Stokes shift gives a solvent relaxation energy of $\sim 0.2 - 0.26$ eV. This is a reasonable Stokes shift for isolated molecules that are surrounded by solvent molecules. The isolated molecules of HBC-PhC12 and F-HBC, present at *high concentration* in Figure 4.10 and Figure 4.11, have a Stokes shift that is between 0.1 – 0.2 eV less than the Stokes shift measured for the isolated molecules at 10^{-13} M. This is most likely due to a change in the environment from solvent molecules of chloroform and toluene to alkyl- chains that has a much lower polarity which is closer to that of alkanes (a dipole moment ~ 0 Debye).

As far as the electronic transition involved in the PL of the HBC-derivatives studied, all molecules appear to emit from the S_2 state as described previously in Chapter 3. Note that this is also the case for J-HBC. If the emission were from the S_1 state the energy of the dominant PL transition of the isolated molecule should be much lower than 2.77 eV. This is not the case. In fact, far lower energy transitions exist in the aggregate

absorption spectra 2.4 – 2.8 eV that are much more reasonable candidates for the S_1 absorption transitions.

The FWHM of the PL emission is listed in Table 4.1 for each derivative and compared to the FWHM of the PLE spectra. Clearly the PL is on average a factor 1.3 – 1.7 sharper. This is most likely due to the each of the PLE spectra being a superposition of several electronic transitions whereas the PL spectra are the result of emission from one electronic state.

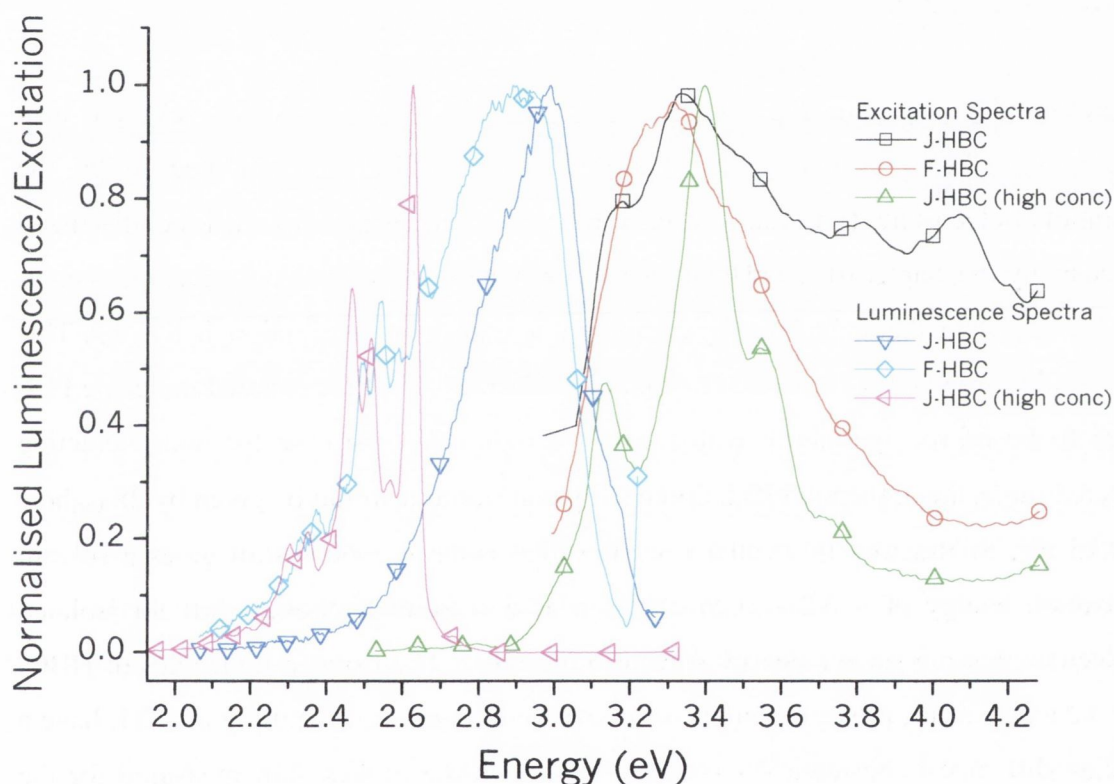


Figure 4.2: The normalised PL and PLE spectra of J-HBC and F-HBC in chloroform at low concentration $\sim 10^{-13}$ M. For comparison the PL and PLE spectra of J-HBC at high concentration $\sim 10^{-5}$ M is also given.

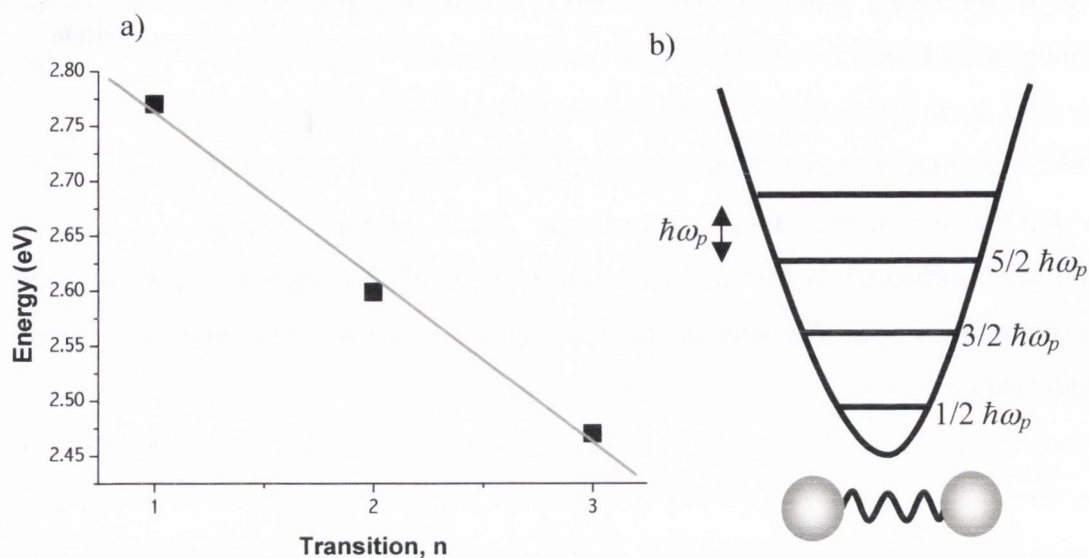


Figure 4.3: a) Plot of the PL peak/shoulder energy of HBC-C8,2 isolated molecules in toluene versus an arbitrary transition number. The straight line fit agrees with the linear increase in transition energy of successive energy levels of a harmonic oscillator. b) The energy levels of a quantum harmonic oscillator. Note the transition energy is $\hbar\omega_p$, where ω_p is the frequency of oscillation.

AGGREGATES

In Chapter 3, the absorption/PLE spectra for aggregated solutions of all derivatives were found to be remarkably similar. Some differences in intensity at given energies, between the absorption/PLE spectra, were related to the relative population of the L and C species (each with a different W' interaction energy). In contrast, on first inspection of the PL spectra for aggregated solutions of all derivatives in Figure 4.5 and 4.7, some PL spectra appear substantially dissimilar to the others.

The peak energies and intensities of each PL spectrum are listed in Table 4.2. The dominant intensity peak of J-HBC and N-HBC is clearly at higher energy than the dominant intensity peak of the other derivatives. The medium and high concentration PL spectra of N-HBC in chloroform are observed to differ substantially from the PL spectra of the same molecules in hexane. The reasons for this dramatic difference are the topic of Chapter 5. More significantly, the dominant PL intensity peak of N-HBC, at 2.59 eV in hexane, is observed to be at higher energy than the lowest energy absorption/PLE peak in Figure 4.6. This negates the possibility that the dominant PL peak of N-HBC originates from the lowest energy peak in the PLE spectrum. The same

is observed for J-HBC from Figures 4.6 and 4.7. The PLE spectrum of J-HBC shows some intensity between 2.4 eV and 2.8 eV (although much weaker than N-HBC it is still higher than for the other derivatives) and has a dominant PL peak at higher energy at 2.59 eV. As described in Chapter 3, the increase in intensity of these low energy features in the absorption/PLE spectra may arise from an increase in the allowed-ness of the symmetry-forbidden S_1 transition. However, from the discrepancy of the dominant intensity PL peak energy compared to the energy of the S_1 state, this increase in allowed-ness has not given rise to a dramatic change in the PL spectra (for instance a dominant PL emission at energies < 2.4 eV). Instead, as will be discussed later, the reason the intensity profile of the PL spectra of N-HBC (in hexane) and J-HBC differs from that of the other derivatives is due to the super-structure of the MSA formed.

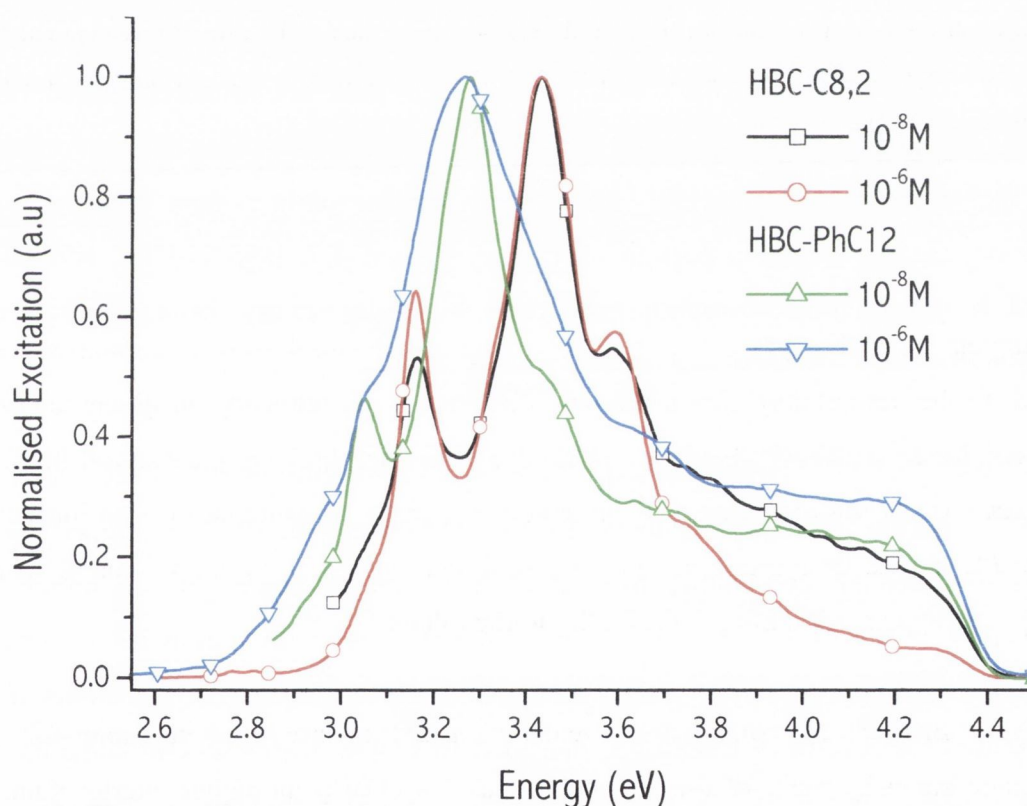


Figure 4.4: Normalised PLE spectra of HBC-C8,2 and HBC-PhC12 at 10^{-6} M and 10^{-8} M in toluene.

On first inspection, the fine structure of the PL of all derivatives appear to be unrelated to the absorption fine structure. However from the mirror spectra in Figures 4.8 and 4.9, when the PL spectrum is inverted and stretched along the energy axis, it superimposes reasonably well with the absorption/PLE spectrum. This in effect demonstrates that the PL peaks $a - e$ originate from the S_2 absorption peaks $a - e$ and confirms that the

dominant aggregate PL peaks *a* – *e* originate from the S_2 to S_0 transition for all derivatives (as is the case for the isolated molecules). The mirror symmetry of the relative energetic positions of the *v* – *e* peaks in the PL and PLE spectra holds reasonably well for HBC-C8,2 and the other symmetrically substituted derivatives (not shown). The exception is HBC-PhC12 at high concentration which will be discussed later.

As can be seen from the mirror spectra in Figure 4.9, for J-HBC there is a major discrepancy in the intensity of several of the peaks. This lack of mirror symmetry in the intensity profile, is also observed for N-HBC (not shown). For N-HBC this is further compounded by the fact that the N-HBC PLE spectrum is the result of a superposition of an ensemble of L and C aggregated species (see Chapter 3). It is interesting to note that overall, the peak energies of N-HBC (in hexane) and HBC-PhC12 are reasonably matched. This confirms that the L and C species of N-HBC are intimately mixed. Since excitons are mobile in these systems, the photo-luminescence is more likely to originate from the species at lower energy - that is the L species (as is evident from the lower transition energy). From inspection of Figure 4.5 and 4.7, both N-HBC and HBC-PhC12 L species have absorption transitions at similar energy, hence the emission energy of the PL *v* – *e* transitions are also similar.

The mirror spectra in Figures 4.8 and 4.9 are useful in determining the FER transitions in the PL spectra. As described above the overlap between the PLE spectra and the PL spectra is reasonably good along the energy axis. A energy axis expansion, rather than contraction, of the PL spectra was chosen to match peaks with similar behaviour (see discussion section) Having designated the allowed and forbidden FER transitions of the absorption/PLE spectra in Chapter 3, the good fit of the mirror spectra suggests that peaks *c* and *e*, in the PL spectra, are the allowed and forbidden H-aggregate FER transitions respectively. The resonance interaction energies can therefore be determined and are given in Table 4.3. The values of the resonance interaction, expressed as $2\beta \sim 0.11$ eV, are smaller than the values in the PLE spectra by a factor ~ 2.4 . Several possible reasons for this decrease will be given in the discussion section.

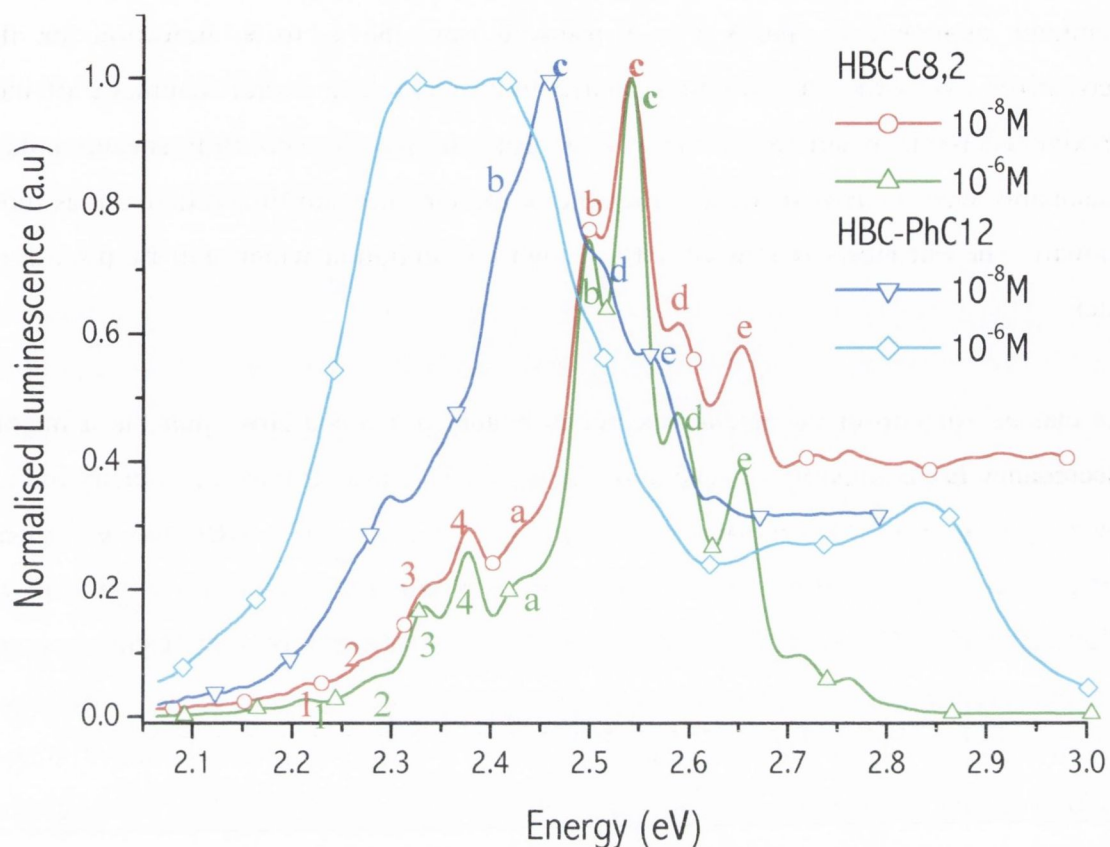


Figure 4.5: Normalised PL spectra of HBC-C8,2 and HBC-PhC12 at 10^{-6} and 10^{-8} M concentration in toluene. The S_2 transition $v - e$ peaks are labelled with letters $a - e$ positioned beside peak maximum or by indicating equivalent peak at high or medium concentration by an arrow. The S_1 transition $v - e$ peaks are labelled with numbers 1 – 4.

PL PEAK ENERGY AND INTENSITY					
MOLECULE	a	b	c	d	e
HBC-C8,2 (eV)	2.43	2.50	2.54	2.59	2.65
(int.)	0.22	0.74	1.00	0.48	0.38
HBC-PhC12	2.35	2.42	2.45	2.50	2.56
	0.42	0.82	1.00	0.72	0.57
F-HBC	2.43	2.45	2.54	2.59	2.65
	0.28	0.85	1.00	0.46	0.50
J-HBC	2.42	2.46	2.52	2.57	2.62
	0.22	0.64	0.56	0.31	1.00
N-HBC	2.37	2.43	2.47	2.56	2.59
	0.28	0.62	0.41	0.42	1.00

Table 4.2: The values of the peak energies of the PL and their normalised intensities of all derivatives. Values are given for the high concentration in toluene spectra. Values for N-HBC correspond to the PL spectra in hexane.

Listed in Table 4.3 are the FWHMs of the dominant peaks in the emission spectra. In general the FWHM are similar in magnitude, with the exception of HBC-PhC12 at high concentration. This derivative is unusual because its PL spectrum evolves with concentration. At medium concentration the PL FWHM and PL fine structure are similar to that of HBC-C8,2 and F-HBC. However, at high concentration the peak at ~ 2.35 eV is observed to increase in intensity, thus contributing to the overall increase in the FWHM. Note the smaller FWHM of J-HBC and N-HBC is because only one peak is measured. For the other derivatives peaks b and c are combined for the FWHM measurement.

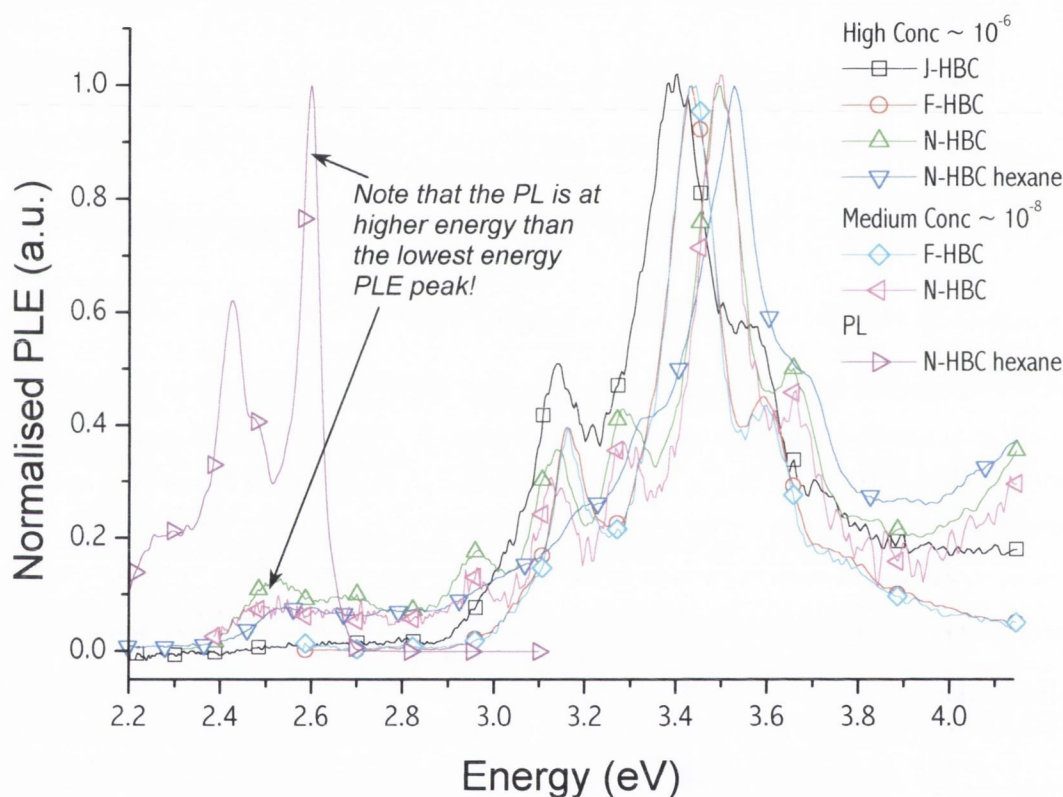


Figure 4.6: Normalised PLE of J-HBC, F-HBC, N-HBC at $\sim 10^{-6}$ M and $\sim 10^{-8}$ M in chloroform. PL and PLE spectra of N-HBC are included to illustrate that the dominant emission of N-HBC cannot originate from the lowest energy peak in the PLE (see text).

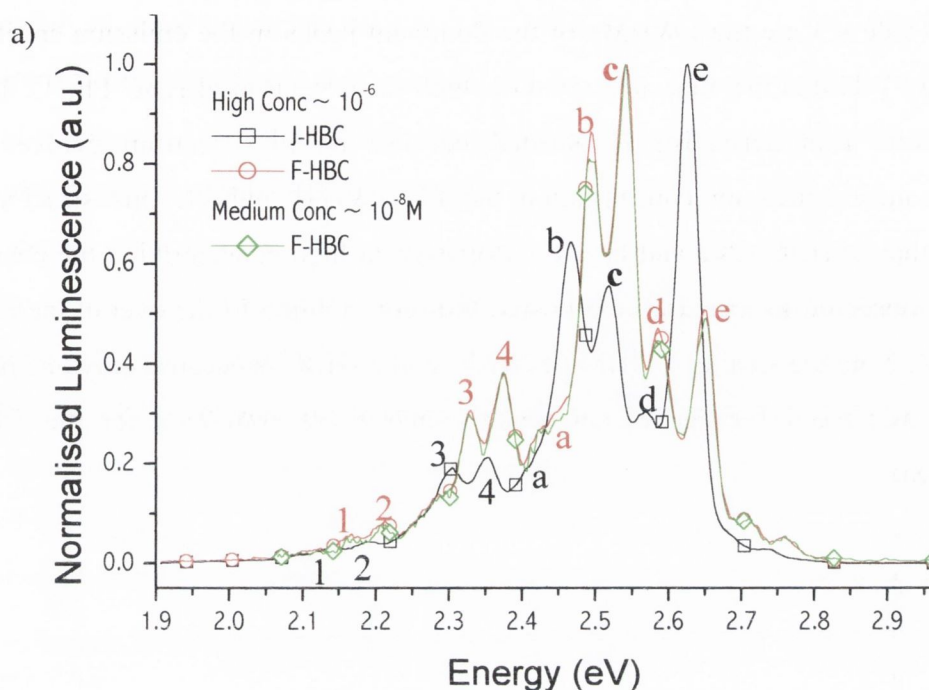


Figure 4.7(a): Normalised PL of J-HBC at 10^{-6} M and F-HBC at $\sim 10^{-6}$ and 10^{-8} M in chloroform. The various peaks of the PL spectrum of J-HBC are labelled by a letter or number as close as possible to the actual peak or shoulder for S_2 or S_1 transitions respectively.

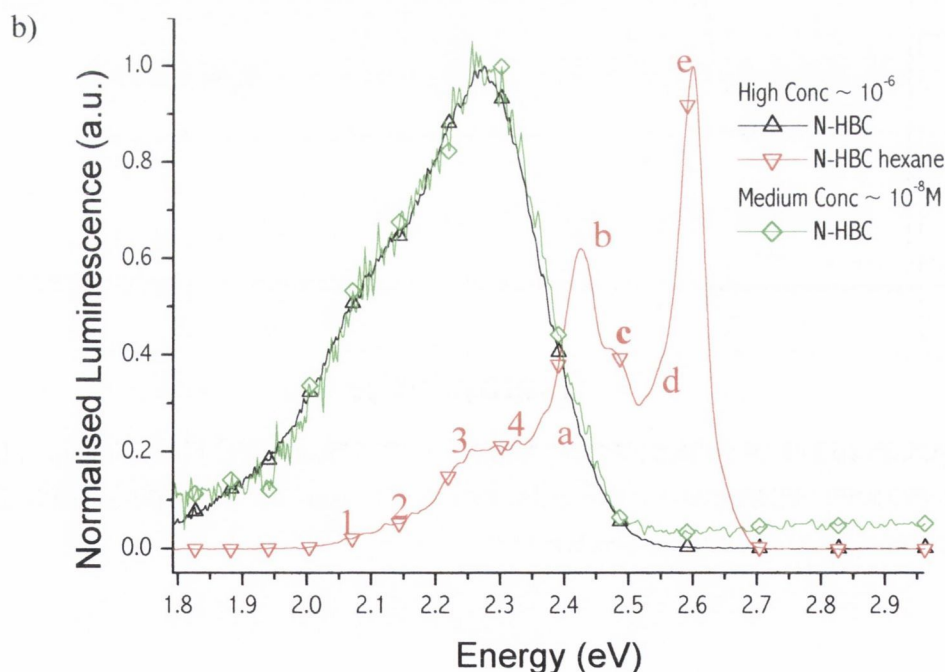


Figure 4.7 (b): Normalised PL of N-HBC at $\sim 10^{-6}$ and 10^{-8} M in chloroform. The normalised PL of N-HBC in hexane is also included. The various peaks of the PL spectrum of N-HBC in hexane are labelled by a letter or number as close as possible to the actual peak or shoulder for S_2 or S_1 transitions respectively. The arrows indicate the equivalent peak in the PL spectrum of N-HBC in hexane. The reason why the PL of N-HBC in chloroform is so different to that of N-HBC in hexane is the topic of Chapter 5.

The Stokes shift of the aggregates given in Table 4.3 are calculated from the difference in the energy between the PLE and the PL intensity maxima. This will be shown in Chapter 6 to be an incorrect way of measuring the Stokes shift of FER systems. In this chapter it is sufficient to say that the Stokes shifts of the HBC derivative aggregates are quite large, however the true values are approximately 0.6 eV (a factor 4 greater than the $v - e$ reorganisation of the HBC isolated molecules ~ 0.15 eV).

The HBC-PhC12 and F-HBC derivatives are unusual, in that the peak, at energies associated with the isolated species, survives at high concentration (see Figures 4.10 and 4.11). PLE spectra collected at this emission energy, given in Figures 4.10 b) and 4.11 b) , demonstrate a striking similarity with that of their respective isolated species.

	FWHM pk $c+b$ or pk e (eV)	2β (pk c to pk e) (eV)	Rough Stokes shift (eV)
HBC-C8,2	0.08 ± 0.01	0.11 ± 0.01	0.89 ± 0.02
HBC-PhC12	0.18 ± 0.02	0.10 ± 0.02	0.83 ± 0.02
F-HBC	0.08 ± 0.01	0.11 ± 0.01	0.99 ± 0.02
J-HBC	0.04 ± 0.01	$0.11 \pm 0.01^*$	0.77 ± 0.04
N-HBC	0.06 ± 0.01	$0.12 \pm 0.02^*$	0.73 ± 0.02 L species 0.93 ± 0.02 C species

Table 4.3: Values of FWHM, 2β and Stokes shift calculated from the PL spectra. The rough Stokes shift calculation is from the PLE maximum to the PL maximum. As will be shown in Chapter 6, this Stokes shift is incorrect for FER systems but is widely used. Note: The rough Stokes shifts of HBC-PhC12 and the L-species of N-HBC are not the same due to the strict criteria used (from the spectra the energies of the PLE and PL peak are a close match). * see discussion - 2β may be larger ~ 0.16 eV

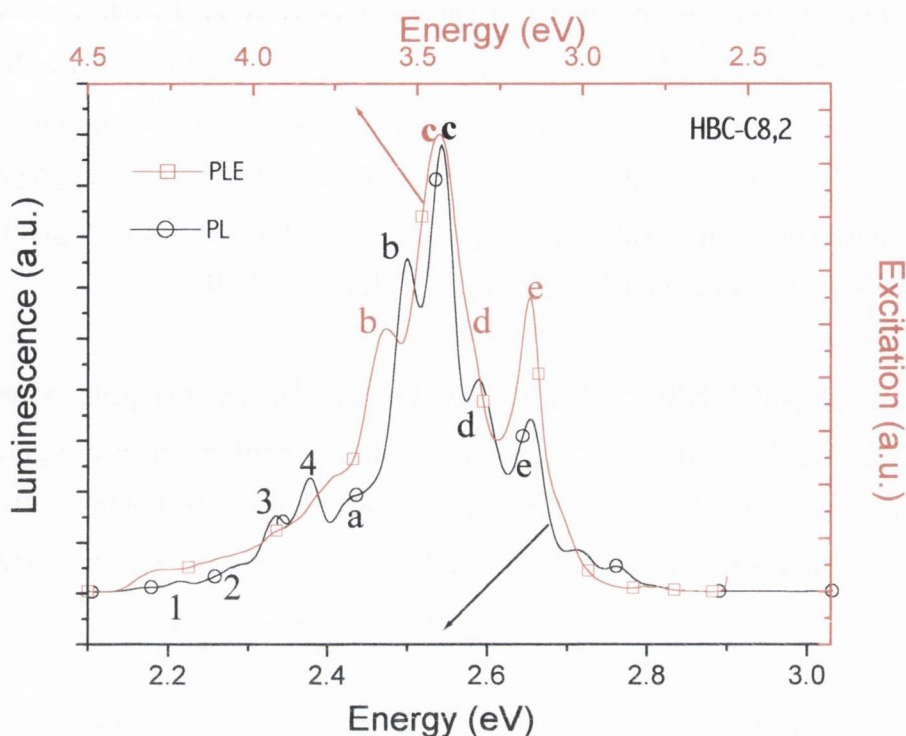


Figure 4.8: Mirror reflection of PL spectrum superimposed over PLE spectrum of HBC-C8,2. Note the general agreement in the peak overlap along the energy axis. As discussed in the text, the lower energy FER state is sharper due to the longer lifetime of this state compared to the FER higher energy state.

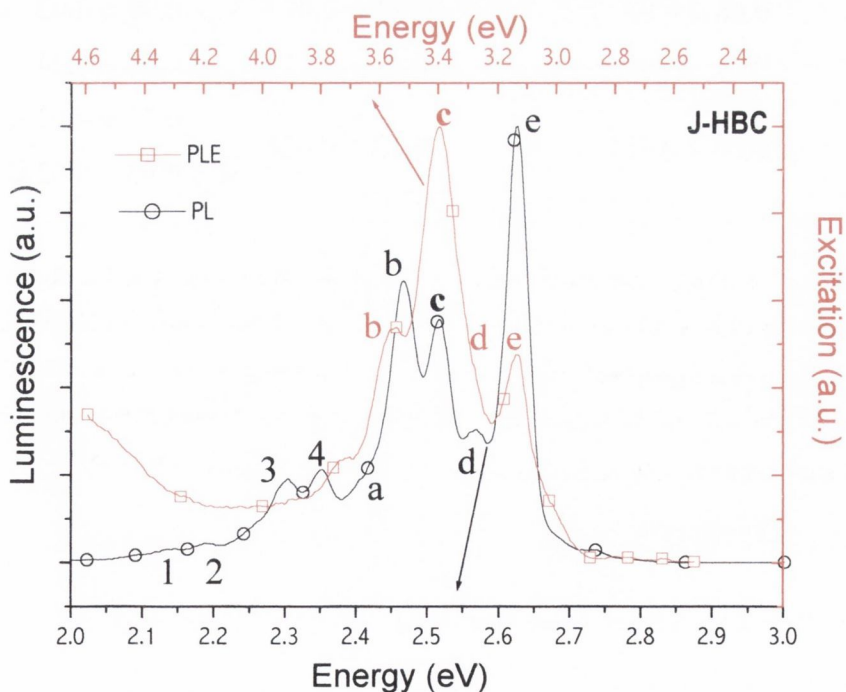


Figure 4.9: J-HBC mirror reflection of PLE spectrum superimposed over a PL spectrum stretched along the energy axis. Note the general agreement in the peak overlap along the energy axis. For J-HBC, and N-HBC (not shown) the major discrepancy is in the relative intensity of the PL peak ~ 2.65 eV. The

equivalent PLE peak has a lower relative intensity. In the discussion section this will be shown to be due to the MSA super-structure.

Plotted in Figure 4.12 are the peak transition energies of the PL and PLE of HBC-C8,2 and HBC-PhC12 versus an arbitrary transition number (the axes are exchanged to allow an easy comparison with the spectra). The linear relationship between the transition energies and the transition number indicates that the peaks are most likely of $v-e$ origin. The values of the transition energies, given in Figure 4.12, are averaged over all the $v-e$ peaks in the spectra. The relationship of some peaks, particularly in the PLE are so different to the other peaks that the transition energy seems to be totally different. Most notable is the reduction in the $v-e$ transition energy of the PL peaks $a-e$ relative to the PLE peaks $a-e$ by a factor 3–4 (the larger value is calculated by comparing more discernable peaks such as a, b and c of both spectra). The dashed boxes in Figure 4.12, are a guide to the eye of the relative decrease of the bandwidth of the PL compare to the PLE. As illustrated above with the mirror image projections of the aggregate PL and PLE spectra, this is a reasonable comparison. The decrease of a factor ~ 3.3 represents a vast change in the bandwidth. This will be shown, in Chapter 6, to be due to changes in the observed $v-e$ transition energies originating from FER.

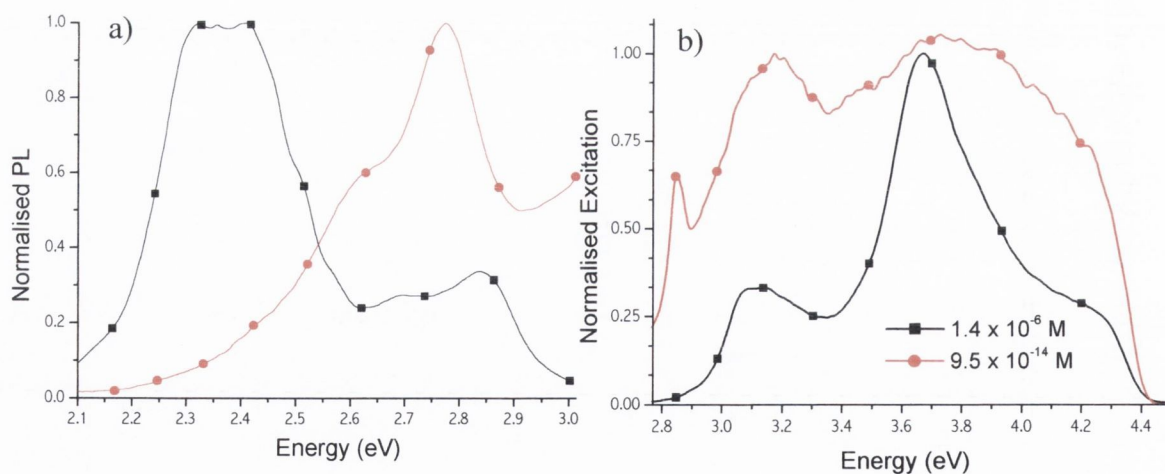


Figure 4.10: a) PL and b) PLE spectra of HBC-PhC12 at 10^{-6} M. Comparison with the PL and PLE spectra of HBC-PhC12 isolated molecules at 10^{-14} M confirms that isolated species of HBC-PhC12 are present at higher concentration.

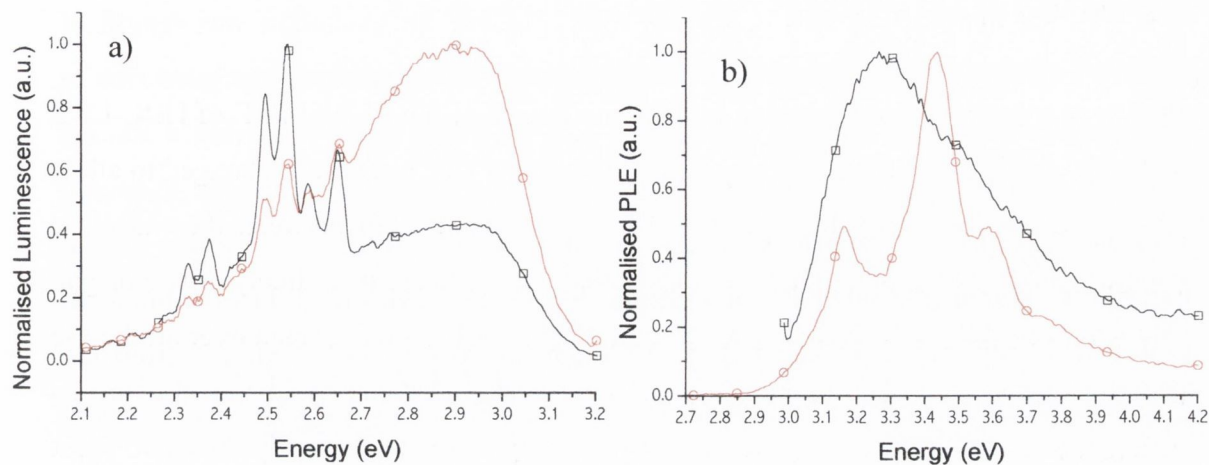


Figure 4.11: a) PL and b) PLE spectra of F-HBC at 10^{-13} Excited (black – 3.44 eV, red – 3.26 eV) and collected (black – 2.95 eV, red – 2.54 eV) at different energies. This demonstrates that there are two species in solution at this concentration: aggregated and isolated species of F-HBC.

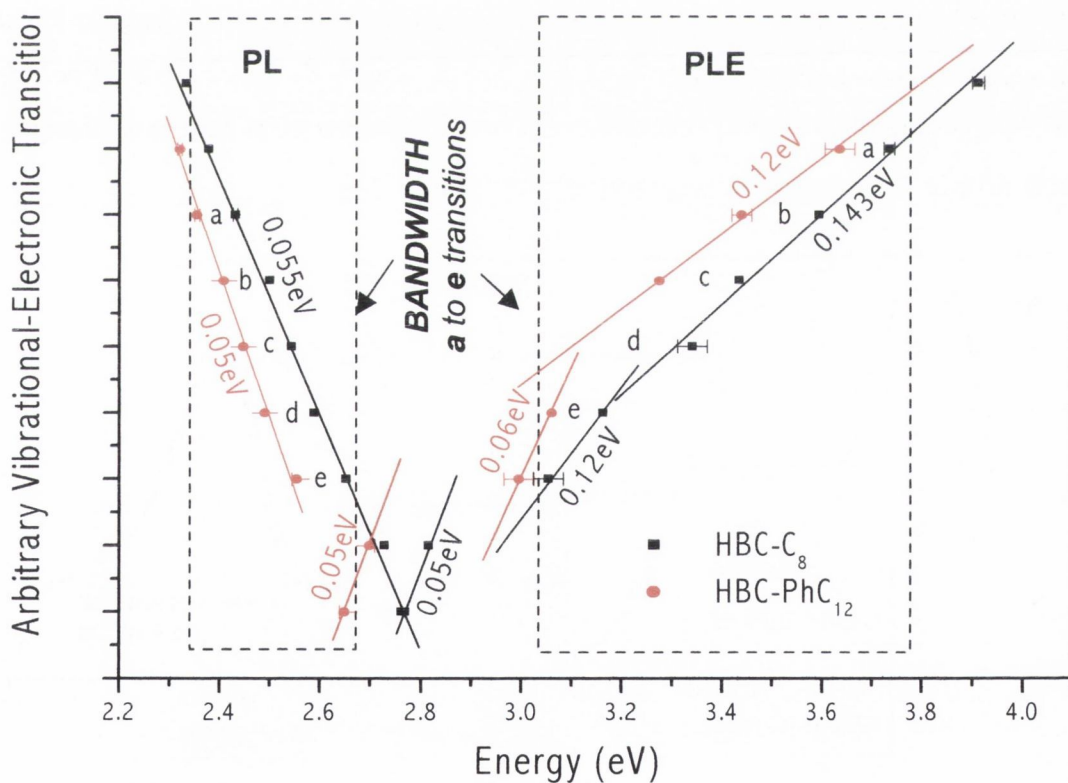


Figure 4.12: A plot of the vibrational-electronic transition energy, of the PLE and PL spectra, versus arbitrary transition number. The slope indicates the energy of a v-e transition. Note, for easy comparison with the PL and PLE spectra, the energy axis is on the bottom therefore transition energy is the reciprocal of the slope observed i.e. the larger the slope in the figure the lower the transition energy. The large reduction in bandwidth of the PL compared to the PLE is also indicated.

Given in Figures 4.13 and 4.14 are the non-resonant Raman spectra and FT-IR spectra of solid state samples⁴ of HBC-C8,2 and HBC-PhC12. An excitation wavelength of 1064 nm (1.16 eV) was required as excitation with lower wavelengths gave rise to luminescence from the samples (even at ~ 1.77 eV) that made collecting a Raman spectrum impossible. The correspondence between the vibrational energies measured from the PLE spectra match those observed, and indicated, on the non-resonant Raman and FT-IR spectra (the latter is coincidental due to the large manifold of vibrational modes of a large molecule like HBC). Although not much can be inferred from the absolute intensities of the peaks in either spectra, the vibrational energies measured correspond to the ground state vibrations of HBC-C8,2 and HBC-PhC12. Noticeably absent in the Raman spectra are any strong features at the wavenumbers corresponding to 0.04 – 0.05 eV. This does not discount that vibrational modes at this energy exist. All that can be inferred is that if they do exist they are much weaker, in the molecular electronic ground state, than the vibrational modes at energies 0.16 – 0.2 eV.

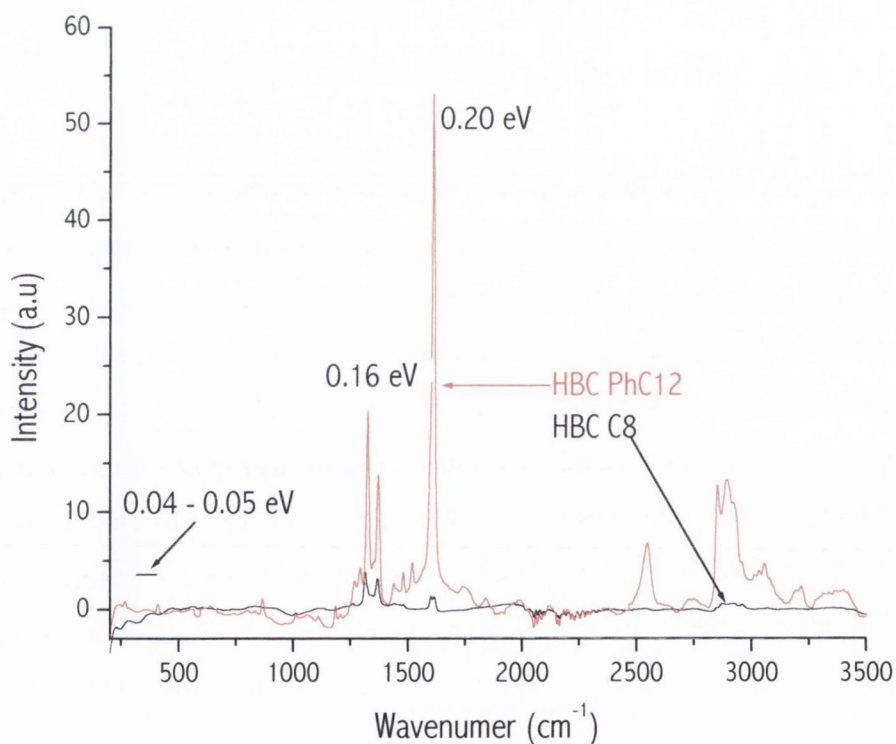


Figure 4.13: Non-resonant Raman spectra of solid films of HBC-C8,2 and HBC-PhC12. The excitation wavelength used is 1064 nm. Energies in eV of major absorption peaks are indicated. Note that there are no noticeable features in the region of 0.04 – 0.05 eV.

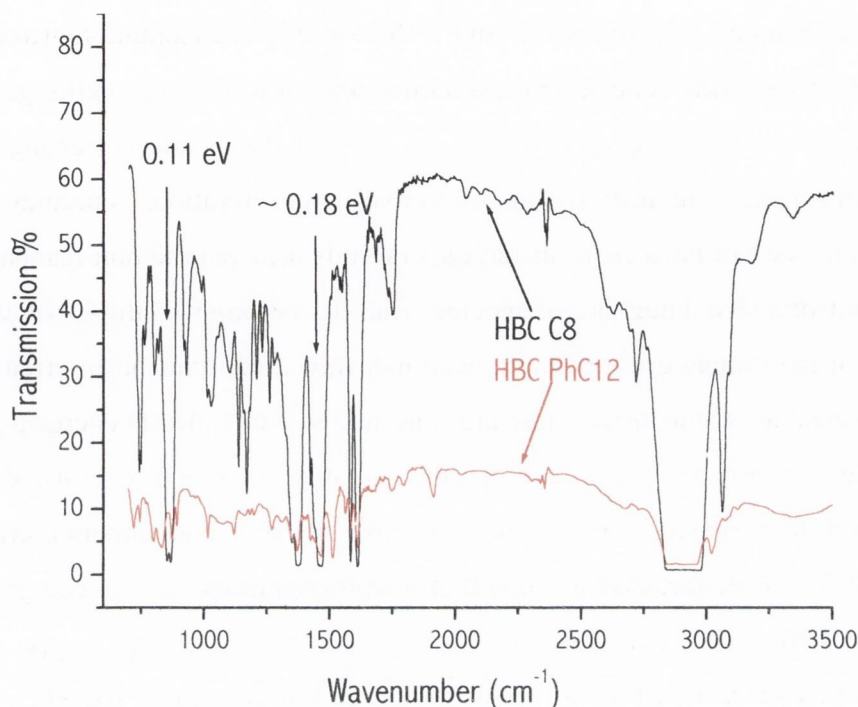


Figure 4.14: FT-IR spectra of HBC-8,2 and HBC-PhC12 in solid state. Energies in eV of major absorption peaks or groups of peaks are indicated.

CONCENTRATION DEPENDENCE

As described in this and previous Chapters, large differences in the optical response of the HBC-derivative molecules are observed as a function of the concentration of the solution measured. In this section these changes, and their relation to the concentration of the molecules will be described. In Figure 4.15, the PLE and PL spectra of HBC-C8,2 in toluene at various concentrations spanning from 10^{-13} to 10^{-7} M are given. As can be seen from the various examples of other derivatives in Figures 4.15 and 4.16, the isolated molecules are eventually replaced by the aggregate spectra as the concentration is increased. In the experimental preparation, the solutions are successively diluted to lower concentrations, and PL and PLE measurements are started at low concentration with higher concentration solutions successively measured to avoid contamination with the higher concentration species of the same molecule.

In Figure 4.16, the PL intensity versus concentration of HBC-C8,2, HBC-PhC12, F-HBC and N-HBC are plotted. As can be seen from the plot, the isolated molecule intensity increases between 10^{-15} M – 10^{-8} M. At high concentrations the intensity

decreases and the aggregate spectrum is observed to increase. The reason for the decrease of the isolated molecule intensity is the depletion of isolated molecular species to form aggregates as the concentration is increased.

In Figure 4.17, the PL intensity per mole of most HBC derivatives is plotted against the concentration. As can be seen from the plot there is a large difference in the PL/mole between the isolated and aggregated species. The PL efficiency of the isolated species is ~ 7 orders of magnitude greater than that of the aggregate. This helps explain why the isolated species are observable at low concentrations $\sim 10^{-15}$ M. This change in the PL efficiency gives rise to a decrease in the isolated molecule PL intensity as the concentration is increased. This is due to highly efficient photo-luminescent isolated molecules being depleted in favour of less efficient aggregates.

The negative slope of the PL/mole versus concentration of isolated species is due to the increase in the total concentration in solution. In the concentration range 10^{-15} - 10^{-8} M, there are isolated and aggregated species in solution and both contribute to the total concentration. However, as the isolated species are the only species observable at this concentration, the PL/mole is observed to decrease monotonically with a slope ~ -1 in the log-log plot. Note that all the derivatives decrease with the same gradient. This indicates that the process giving rise to the decrease in isolated molecule PL/mole is similar for all the derivatives (i.e. the depletion of the isolated molecule population).

In fact, as can be seen from Figure 4.17 the PL intensity of the isolated molecules remains nearly constant. This seems to indicate that the population of isolated species is constant in this concentration range. This may be as a consequence of the 1-D structure of the HBC derivative MSA structures (this 1-D structure will be demonstrated in Chapters 5 and 7). Since the MSA structure only has two effective molecular binding sites at either end of the nanowire (in terms of FER), the collision cross-section of isolated molecules with an aggregate is much smaller than if the HBC molecules were un-substituted. For instance polymer aggregates have a much larger surface area available for effective binding and de-binding compared to the HBC derivative MSAs studied here (and hence the chromophores are more likely to interact upon binding). Therefore isolated molecules are more likely to collide with other isolated molecules in solution as these will have a higher diffusion coefficient than a larger aggregate due to

their smaller mass and volume. If the collision rate between molecules is smaller than the de-binding rate of dimers and small aggregates in solution, the number of isolated molecules will remain high at equilibrium.

At concentrations above approximately 10^{-9} M the aggregate PL and PLE spectra emerge and become more intense than the isolated molecule PL and PLE spectra. This gradual substitution of one species by another confirms that isolated molecules have been observed at low concentration. The fact that the aggregate spectrum only becomes observable at medium concentration indicates that the lower luminescence efficiency of the aggregates requires that many more molecules (in aggregated form) be present in solution in order that the aggregate spectrum be observed.

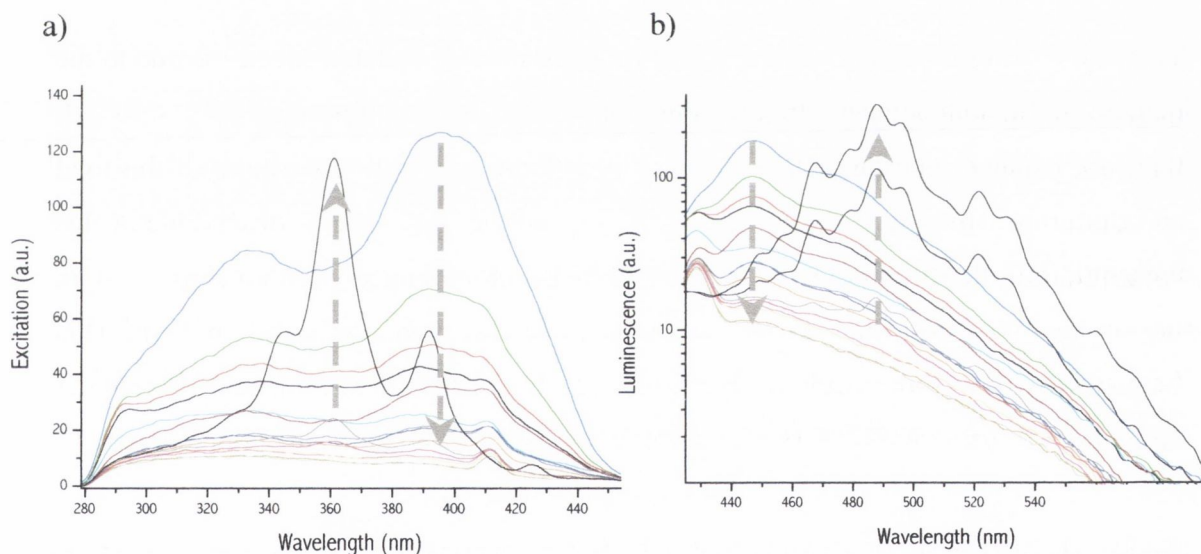


Figure 4.15: a) PLE and b) PL of HBC-C8,2 at various concentrations demonstrating how as the concentration is increased from 10^{-15} M to 10^{-7} M, the isolated molecule spectrum is replaced by the aggregated species spectrum (trend indicated by the dashed arrows).

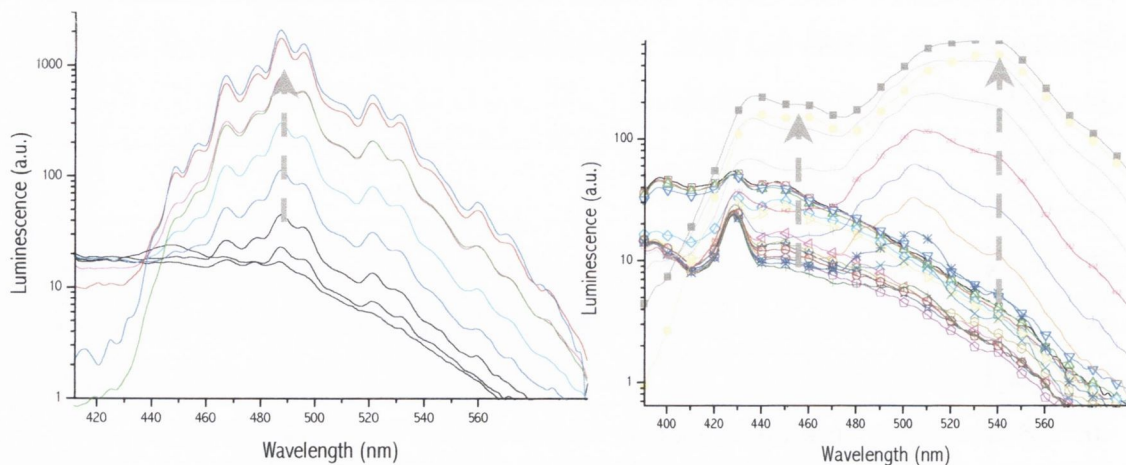


Figure 4.16: a) PL spectra of HBC-C8,2 aggregated species at various concentrations (10^{-9} to 10^{-5} M) and b) PL spectra of HBC-PhC12 at various concentrations (10^{-15} to 10^{-5} M). Increases in PL intensity as the concentration is increased are indicated by the dashed arrows.

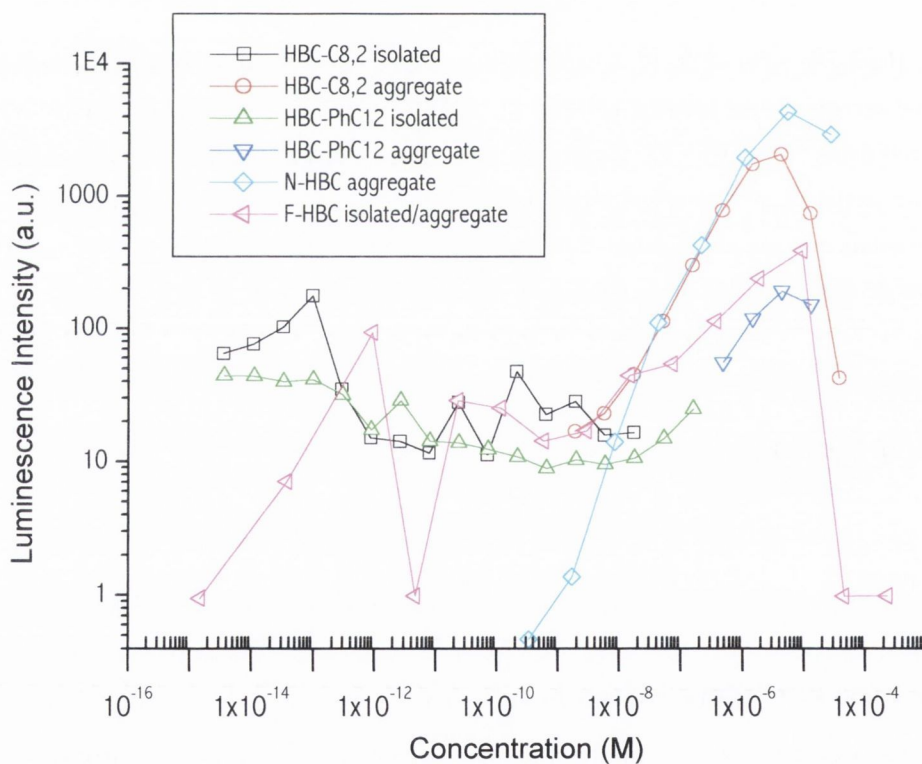


Figure 4.17: Intensity versus concentration plot of the isolated molecule and aggregate PL of all derivatives. Note the steady decrease in the PL intensity of the isolated molecules in the 10^{-15} – 10^{-9} M concentration range and the rapid increase in the aggregate PL above 10^{-9} M. The sharp decrease in PL intensity of the aggregates above 10^{-5} M is due to self-absorption effects decreasing the amount of light reaching the entire volume of the cuvette when exciting at the PLE maximum.

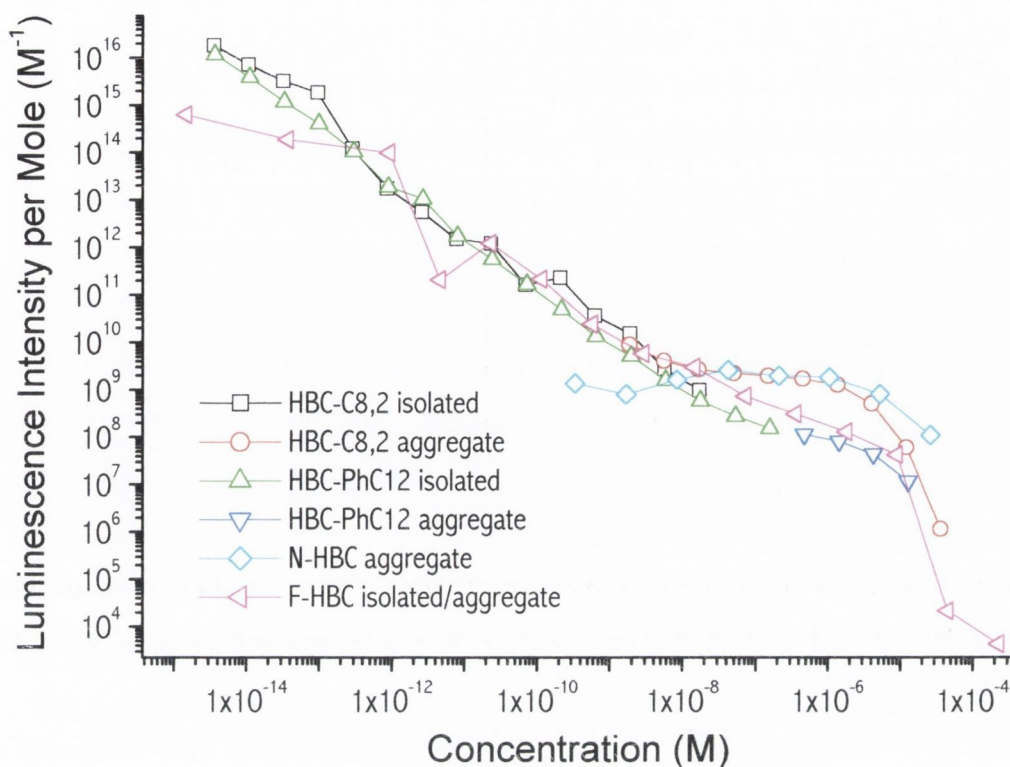


Figure 4.18: The log-log plot of the PL intensity per mole versus concentration for HBC derivatives. Note the monotonic decrease of the isolated molecule PL per mole from low concentrations up to $\sim 10^{-8}$ M. At higher concentrations, up to 10^{-5} M, the PL per mole of the aggregates remains almost constant. The rapid decrease in the PL per mole at concentrations above 10^{-5} M is due to the high absorption of the solution preventing the excitation beam from penetrating the entire volume of the cuvette. Thus, the excited volume decreases and results in a lower PL intensity being detected.

4.3 DISCUSSION:

ISOLATED MOLECULES

In Chapter 3, the PLE of the isolated molecules of HBC-C8,2, HBC-PhC12, J-HBC and F-HBC were found to be similar despite the different side-chain substitution and the symmetry of their substitution. Even the addition of pendant *exo*-phenyl groups to the HBC core, in the case of HBC-PhC12, was not found to profoundly change the electronic transition energy. From the PL spectra presented in this Chapter, the PL spectra of all derivatives also appear to be on the whole similar. This agrees with the findings from the absorption/PLE spectra, that the aromatic core of the molecule is the active chromophore in each case. Thus the similarity in the electronic structure, inferred

from absorption/PLE and PL spectra precludes any contributions arising from the non-aromatic substituted side-chains that could differentiate each HBC derivative from the others. From inspection of PL and PLE spectra of isolated molecules, observable at low concentrations $\sim 10^{-13}$ M, the similar Stokes shifts indicate that in all probability the emission states of the HBC derivatives are the same states.

In Chapter 3, the likelihood that the lowest energy electronic state observed in the PLE spectra is due to an S_0 to S_1 transition was discounted due to the D_{6h} symmetry of the HBC core. The energy of the PLE peaks, for a molecular core the size of HBC, was found to be rather high. Likewise the energy of the PL peaks in Figures 4.1 and 4.2 are also rather high for a molecular core the size of HBC. The most likely scenario is that the symmetry allowed S_2 state is being observed in the PLE as well as in the PL. A S_2 to S_0 transition has been observed previously for azulene and it arises from a relatively faster rate of S_2 to S_0 emission compared to S_2 to S_1 electronic relaxation. If the opposite were the case, isolated HBC derivatives would absorb light but not emit light, as the S_1 to S_0 transition is symmetry forbidden for D_{6h} molecules. However, the fact that isolated HBC molecules can be observed at such high dilutions, indicates that an efficient p-a-l cycle must be occurring.

As briefly described in Chapter 3, the relatively high energy of the PLE and PL peaks in the spectra of the isolated molecules may arise from an effective conjugation area of HBC molecules. This would explain the similarity in the energy of HBC-PhC12 with respect to HBC-C8,2. Note that if the exciton is fully delocalised on the HBC-PhC12 molecule the change from benzenoid to quinoid state of the aromatic rings should planarise the exo-phenyl groups and lead to a larger conjugated area in the photo-excited state and hence give rise to a red-shift in the PL spectrum with respect to HBC-C8,2. This is not observed. Intriguingly, the asymmetrical side-chain substitution of J-HBC does not favour a faster S_2 to S_1 relaxation, or an enhanced S_1 to S_0 radiative transition. If either were true, the PL spectrum of J-HBC isolated molecules would differ substantially from the PL spectra of the other derivatives. The PL energy would be lower and the intensity most likely reduced. This is not observed. In a previous study⁵ it was concluded that an asymmetric substitution of side chains, such as that of J-HBC and N-HBC, should give rise to an enhanced S_1 absorption and emission. However, the results presented here indicate that for the isolated molecules this is

definitely not the case. The fact that the asymmetric substitution of J-HBC does not give rise to a red-shift in the PL spectra either, corroborates with the conclusion that the S_2 transitions are dominant (or an effective conjugation is occurring, see below). The conclusions from the previous study are most likely unreliable due to the fact that the HBC absorption and PL spectra measured were of aggregates of HBC and not the isolated species. The assignment of the S_1 absorption transition in their paper also ignores peaks at lower energy than 2.65 eV that have been described here.

The surprising result for the isolated molecule PL and PLE spectra, is the fact that although a bathochromic shift is observed for the PLE, no difference is observed in the Stokes shift for isolated molecules in solvents of different polarity. This is most likely due to the fact that only the non-polar derivatives of HBC were observed in isolated form. The bathochromic shift in the PLE arises from an asymmetric solvent induced energy relaxation of the initial ϕ_i and final ϕ_f electronic states, $\Delta\phi_i$ and $\Delta\phi_f$ respectively. Thus for HBC derivative molecules the ratio $\Delta\phi_i/\Delta\phi_f > 1$ and is a function of the solvent polarity i.e. the greater the solvent polarity the greater the ratio and hence the transition energy between ϕ_i and ϕ_f increases (this is observed as a blue-shift in the PLE spectrum in chloroform compared to toluene). In the photo-excited state isolated molecules may be substantially relaxed by solvent molecules (the greater the solvent polarity the greater the absolute relaxation of the energy levels). However, if the ratio $\Delta\phi_i/\Delta\phi_f$ is constant throughout the p-a-l cycle, the Stokes shift will not be a function of the solvent polarity. Hence the Stokes shift of isolated non-polar HBC molecules will be the same in chloroform and toluene, for example. This makes sense for non-polar molecules, because the lack of a permanent dipole does not align solvent molecules in a preferential manner (with respect to HBC derivative molecules) in such a way that the ratio $\Delta\phi_i/\Delta\phi_f$ would become solvent dependent.

AGGREGATES

As described previously in Chapter 3, the energy of the dominant electronic transitions in the absorption/PLE spectra are relatively high for a molecular core of the size of HBC. The postulate that the dominant transitions are likely to arise from the symmetry-allowed S_0 to S_2 transition is confirmed by the existence of weak features at lower energy in the absorption/PLE spectra of aggregates. Following this argument, these low energy features (~ 2.5 eV) in the aggregate PLE spectra, that are significantly enhanced in the N-HBC spectra, are most likely due to S_0 to S_1 transitions (for J-HBC a slight increase in the intensity of the PLE spectrum at this energy is also observed). If an enhanced S_1 absorption in the absorption/PLE spectrum is observed for N-HBC, where is the corresponding enhanced S_1 emission? In the PL spectra of Figures 4.5 and 4.7, there are some fine structures at energies < 2.45 eV for HBC-C8,2, HBC-PhC12, F-HBC and J-HBC; and at energies < 2.40 eV for N-HBC. These features are indicated by the numbers 1 – 4 in the PL spectra in Figure 4.5 and 4.7. In the mirror spectra of Figures 4.8 and 4.9, no corresponding PLE peaks are observed at energies > 3.8 eV. This suggests that these low energy emission peaks 1 – 4 correspond to a different electronic state than the S_2 electronic state. Instead they probably arise from transitions from an electronic state lower in energy than the S_2 state, specifically the S_1 state. The emission peaks 1 – 4 are also divided into two sub-bands: peaks 1 and 2, and peaks 3 and 4. If these also correspond to two FER transitions of the S_1 state the $2\beta_{S_1PL}$ value is ~ 0.16 eV which corresponds to $2\beta_{S_1Abs} \sim 0.17$ eV measured from the difference in energy between the 2 lowest energy peaks of N-HBC in Figure 4.6.

Although energetically speaking the assignment of the low energy features of the PL and PLE spectra to S_1 transitions makes sense, the normalised intensities of peaks 1 – 4 for N-HBC and the other derivatives in Figures 4.5 and 4.7 are not so easily explained. If the S_1 absorption is enhanced for N-HBC, compared to the other derivatives, why is the S_1 PL transition energy not higher in intensity? This question may be answered by the effective conjugation model in Appendix A. If the S_1 transition (assigned here) is in fact due to S_1 transitions of a Disrupted Sextet Ring-Current (DSRC) then the PL intensity will merely reflect the probability that an exciton will find such a DSRC site in its lifetime. If DSRC sites only occur in highly disordered segments of a MSA then the

exciton may not be able to reach these sites effectively (the hopping probability is reduced in these segments). This would explain why the intensities of these low energy PL peaks are quite similar for all the derivatives. The higher probability of a DSRC feature in the PLE of N-HBC compared to the other derivatives may be due to the nitrogen substituted heteroatoms (and their lone pair electrons) disrupting the SRC in disordered segments of the MSA.

If excitons are not mobile in a MSA, then the ratio of the intensities of the corresponding PLE and PL features should be close to unity. If on the other hand excitons are mobile, as is the case, the relative intensities of the PL features may differ greatly from the PLE features. This phenomenon will be shown to give rise to the differences in the PL intensity distribution of N-HBC and J-HBC compared to the other derivatives, while at the same time all the derivatives have a similar PLE intensity distribution. For symmetrically substituted molecules such as HBC-C8,2, HBC-PhC12 and F-HBC, the sites probed by the exciton are up and down a nanowire, therefore the exciton will luminesce from a site similar to one upon which it was created. Hence the absorption spectra will resemble the PL.

From the mirror image superposition in Figures 4.8 and 4.9, the PL spectra of all derivatives can also be broken down into two sub-bands corresponding to the symmetric and anti-symmetric FER transitions. The FER signature of the PLE spectra indicates that H-aggregates have formed in solution from a stacking arrangement of the molecules (as corroborated by the aggregate geometry optimisations in Chapter 3). Namely, the signature of FER in a H-aggregate is a higher oscillator strength of the higher energy FER transition (the symmetric state is dipole-allowed and has a higher energy). The increase in the sharpness of the lower energy transition peak at ~ 3.17 eV, from medium to high concentration for HBC-C8,2, also fits into the framework of FER. From the uncertainty principle $\Delta E \cdot \Delta t > \hbar/2$, the longer lifetime of the lower energy FER transition relative to the higher energy FER transition (due to rapid relaxation from the higher to the lower level), makes the lower energy FER transition sharper than the higher energy transition.

From current FER models, largely based on J-aggregates of polar molecules, it is generally believed the photo-luminescence from H-aggregates is not possible. Next, this will be shown not to be the case and an explanation as to why H-aggregate emission is not generally observed, except for quasi 1-D systems like HBC derivative nanowires, will be given.

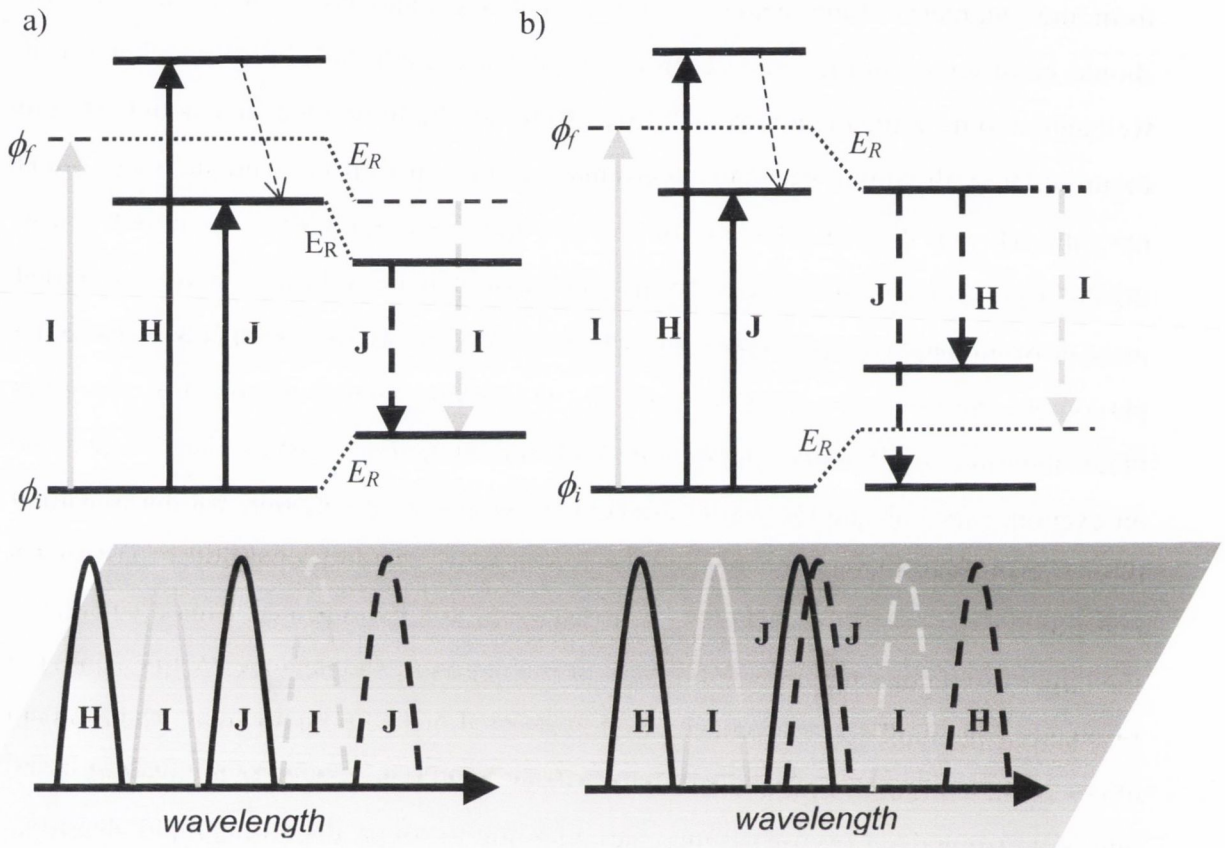


Figure 4.19: a) The conventional photo-absorption-luminescence cycle for FER systems derived from J-aggregate systems. Only the symmetric, therefore dipole-allowed, FER transitions are illustrated for H and J aggregates. The isolated molecule transitions are indicated by the letter I. Solid and dashed vertical arrows represent absorption and luminescence transitions respectively. E_R represents the v-e relaxation of the energy levels in the photo-excited state. As can be seen from the diagram H-aggregate emission is not possible in the conventional p-a-l cycle due to the rapid relaxation of the exciton (thin dashed arrow) to the symmetric J-level. b) The proposed p-a-l cycle that can describe both J and H aggregate emission processes. Note that with this model even for systems that have nearly coincident J-aggregate absorption and emission peaks the system still undergoes a v-e relaxation. With the diagram in a) J coincident absorption and emission could only be achieved if E_R is zero. This latter point is the topic of Chapter 6. For illustration purposes only, the related absorption and emission spectra for each p-a-l cycle is given below the diagram. Note: for vibrational-electronic features do not compare these spectra to the real spectra, use the p-a-l cycle in Chapter 6.

The current energy level diagram for the photo-absorption-luminescence (p-a-l) cycle for an FER system is given in Figure 4.19 a). This p-a-l cycle has been derived for J-aggregate systems⁶ and tested against J-aggregate systems⁷. The cornerstone belief is that an exciton of the symmetric H-aggregate FER state (at higher energy) will quickly relax to the lower energy symmetric J-aggregate state. Thus emission will only occur from the symmetric J-aggregate collective FER state and no H-aggregate emission should be observed in the PL. The problem with this energy level diagram is that it is well suited to describe the absorption process but not the luminescence. As indicated in Figure 4.19 a), the initial state ϕ_i (the ground state) is not FER coupled and therefore is not split, whereas the excited state ϕ_f is split due to the resonance of the exciton between the degenerate electronic states of $2N$ molecules (note that $2N$ from now on is the total number of molecules in resonance – in Chapter 1 it was simply N). This is because the photon electric field wavelength is much greater than the aggregate, so many molecules “feel” the same oscillation of the photon field and are therefore just as likely to generate an exciton. Since all the molecules are coupled with their neighbour, via the transition dipole resonance interaction, this leads to an increase in the probability of creating a one-exciton state over the collective FER state of the $2N$ molecules. This gives rise to the larger oscillator strength as a function of the number of molecules $2N$ that can be in resonance (the number $2N$ is typically limited by disorder). So far so good. The problem arises in the emission. In this energy level diagram it is not possible for symmetric H-aggregate (or anti-symmetric J-aggregate) emission to occur, due to the rapid electronic relaxation to the lower lying state. This energy level diagram only considers the transition dipole alignment as being perfectly parallel or anti-parallel and ignores the more likely case that $\alpha \neq 0^\circ$, where α is the angle between transition dipoles. In this model, even when $\alpha > 0^\circ$, there is no possibility of H-aggregate emission in the PL spectra. Thus in the current FER energy level diagram the PL spectra of J or H aggregates will only display J-aggregate emission in both kinds of aggregates (very weak, if any, J-aggregate - or strictly speaking forbidden H-aggregate - emission in the former).

The mirror image spectra of HBC-C8,2 and J-HBC both show a non-zero intensity of the PL peak that corresponds to the H-aggregate FER transition. Therefore the question is how is this possible? The FER interaction, as observed in the absorption/PLE spectra

is mediated via the photon field. The large wavelength of the electric field couples many molecules together over distances of ~ 50 molecules in some Pseudo-Iso-cyanine J-aggregate systems. The question is: if the initial state in the absorption has no FER coupling and the final state does, what is the case during the reverse process when a photon is emitted rather than absorbed? This is not clear in the literature. It boils down to whether the FER process survives after the photon is absorbed and continues during the excited state of the molecule. The transition dipole of the ground state ϕ_i to excited state ϕ_f of a molecule always exists in theory but perhaps with a zero probability. In the absence of a photon electric field, that is resonant in energy with the transition energy between the ϕ_i and ϕ_f states, the transition dipole probability is zero. This is why in the absorption process the FER ground state is not split in Figure 4.19 a) and b). Upon the arrival of a photon, of the correct energy, the probability of the transition dipole occurring becomes non-zero. Thus the final FER state is split, due to the resonant interaction of two identical, non-zero, transition dipoles of neighbouring molecules. The transition dipoles are therefore momentary and exist only during the electronic transition. This is why the FER states observed in the absorption/PLE spectra are momentary states and not permanent. Thus if the molecular system were probed differently, by say non-optical methods, the measurement obtained would only observe the isolated molecule energy levels and not the FER levels. In the absence of a resonant photon-field all the aggregated molecules are not FER coupled. In order to have a permanent splitting of the ϕ_f state the resonant interaction would have to be permanent, such as a chemical bond forming between the molecules in an aggregate. This is not the case in van der Waals aggregate systems.

Since the FER states are momentarily created, this in itself determines that if the ϕ_f state is split momentarily in the absorption process, then the ϕ_i state must be split momentarily in the luminescence process (notice that technically the ϕ_i and ϕ_f states are the final and initial states respectively in the luminescence process). As illustrated in the energy level diagram in Figure 4.19 b) constructed here to apply to H and J aggregates, there must be a splitting of the HOMO and LUMO levels during FER (for HBC aggregates during S_2 absorption means the LUMO + 1 level is split). This means that there must be a possibility of H-aggregate emission in the PL so long as the probability that the transition dipole vector summation is non-zero (i.e. some oscillator strength).

The construction of the energy level diagram in Figure 4.19 b) is the topic of Chapter 6. It may be noted that if the FER states are momentary, how can solvent relaxation of the excited state occur? Solvent relaxations occur because the electron cloud distribution is different for the LUMO states compared to the HOMO states. A molecule in the excited state is always overall electrically charge-neutral. If the molecule possesses a permanent dipole the electron distribution of the molecule when in the LUMO state may be overall charge-neutral, but local variations will arise due to the presence of the permanent dipole influencing the equilibrium position of the electron distribution of the molecule. Thus the energy levels of polar molecules will be substantially more solvent relaxed than for non-polar molecules (specially for highly polarisable molecules). From the low concentration spectra presented here a solvent relaxation of ~ 0.2 eV was measured for the isolated molecules. Solvent relaxations also arise from the polarisation of the HBC molecules by the solvent molecules' permanent dipoles. HBC molecules are very polarisable, therefore the solvent relaxation contribution to the Stokes shift may also be large. This may be also due to the fact that a S_2 exciton is formed on the HBC molecule and not a S_1 exciton. The difference between the electron cloud distribution of a given exciton state relative to the electronic ground state will be greater the higher the energy of the exciton state.

For pure, perfect H-aggregates the likelihood that the transition dipoles of neighbouring molecules will align in a parallel alignment during photo-luminescence (bright symmetric FER state) is not high due to the un-favourable β energy of repulsion between the transition dipoles (symmetric alignment of the transition dipoles will occur during the absorption process because the photon-field is an external influence). As illustrated in Figure 4.20, the natural induction state of a pure H-aggregate is not the symmetric state. However, for H-aggregates, where the transition dipole alignment is not perfectly parallel, then the probability of the "symmetric" FER transition occurring is non-zero - specially if the transition dipole interaction β is small and say accessible via phonon assistance (i.e. if $\beta \sim \hbar\omega_p$). More importantly, the vector summation of transition dipoles with $\alpha > 0^\circ$ is non-zero. Therefore this imperfect "symmetric" transition will have a non-zero oscillator strength and will give rise to a non-zero intensity in the PL spectra. This is probably how the H-aggregate emission occurs for H-aggregates of HBC derivatives. The imperfect alignment of molecules required for

H-aggregate emission is confirmed by the non-zero oscillator strength of the dipole-forbidden FER state, at ~ 3.17 eV for HBC-C8,2, in the absorption/PLE spectra. Note that the above explanation also explains why for the HBC derivative H-aggregates, $\beta_{S2PL} < \beta_{S2Abs}$ by a factor 2.4 - the H-aggregate emission of HBC derivative aggregates may be phonon assisted.

H-AGGREGATES

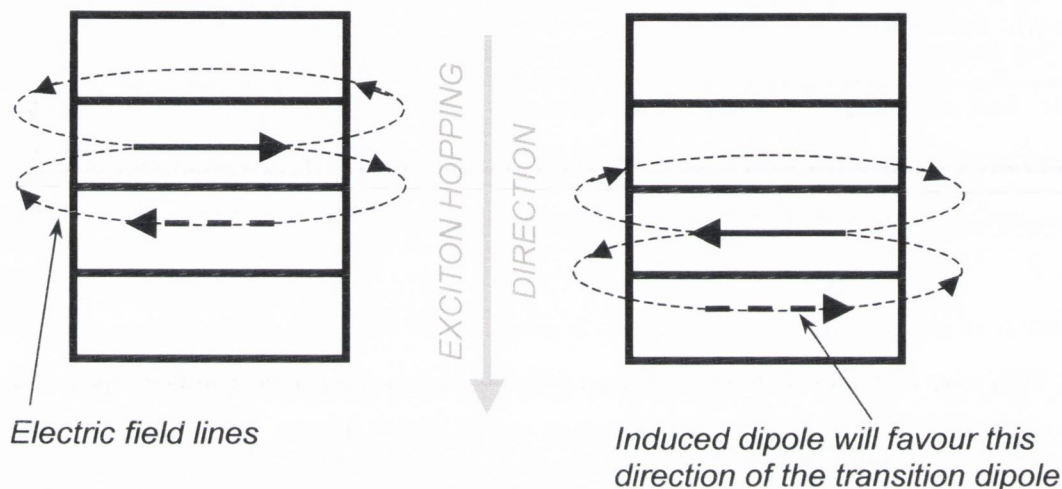


Figure 4.20: Snap-shot illustration of the natural induction state of a pure H-aggregate demonstrating that it is a hopping “state”. The transition dipole (solid arrow) interaction of neighbouring molecules in the stack is more likely to transfer energy from one molecule to another. This natural state is “dark” because the transition dipole alignment is anti-parallel thus ensuring that the anti-symmetric, therefore dipole-forbidden, H-aggregate FER state is the natural state. Thus energy is transferred rather than emitted as a photon and hence exciton diffusion by hopping will therefore be easier in H-aggregates and consequently the photo-luminescence quantum yield will be low.

Thus from the above discussion, the natural induction state of a pure H-aggregate is not the symmetric FER state. In fact, if a transition dipole interacts with a neighbour molecule in pure H-aggregate, it is more likely to create an anti-symmetric FER state. Thus the natural induction state of a pure H-aggregate is dark (i.e. no photon is created/emitted by the natural induction FER state). This means the natural induction state of a pure H-aggregate will not lose energy by photon emission, thus in this case, the exciton is conserved and is passed on to the neighbouring molecule. Hence, the natural induction state of a pure H-aggregate is a travelling state whereby the exciton may be transferred back and forth between molecules, or under the influence of a decreasing potential, travel in a given direction in the stack entirely by FER with

J-AGGREGATES

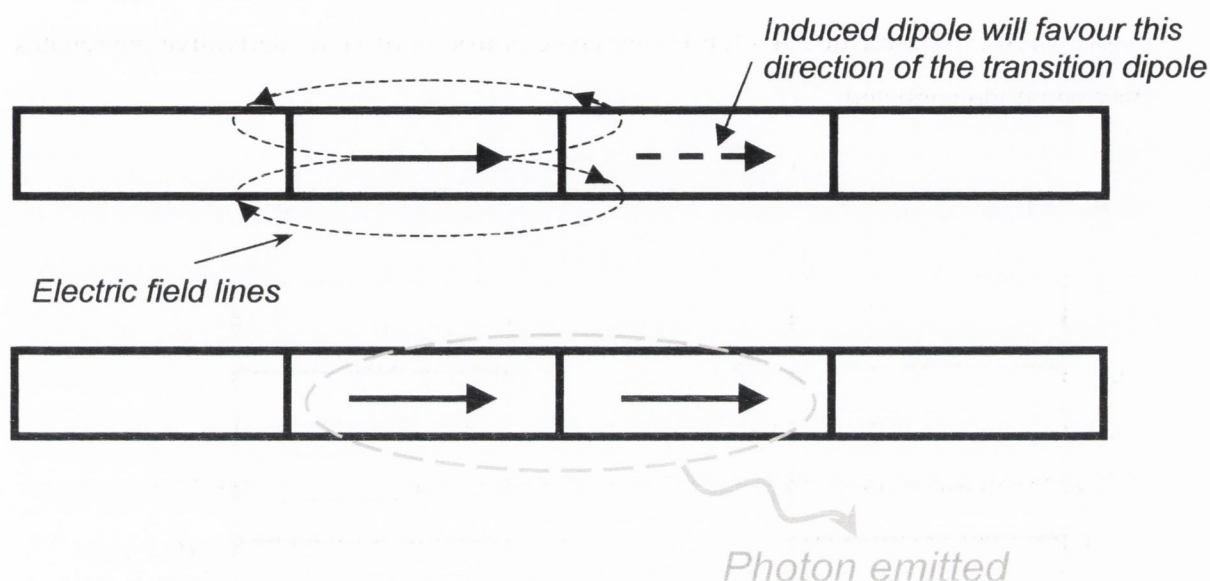


Figure 4.21: Snap-shot illustration of the natural induction state arising from transition dipole (solid arrows) interactions in J-aggregates demonstrating that it is “bright”. The symmetric, therefore dipole-allowed, J-aggregate FER states will give rise to photon emission. An exciton in a pure J-aggregate system is therefore more likely to radiate than to hop along the aggregate. The exciton diffusion in a pure J-aggregate system will therefore be low. This explains why the photo-luminescence quantum yield of J-aggregate systems such as polymers and small polar molecules is high.

neighbouring molecules. The implications of v-e relaxation on this FER transfer process is the topic of Chapter 6 – essentially FER excitons require phonon assistance to surmount the potential barrier between v-e relaxed molecules and the neighbour molecule that is not yet in FER.

For pure J-aggregates on the other hand, the natural induction state, as illustrated in Figure 4.21, involves the parallel alignment of transition dipoles. This is the symmetric FER state and it is bright. Thus for pure J-aggregates the FER exciton is more likely to luminesce than to travel along the aggregate. The last two conclusions explain many features of conjugated molecule/polymer aggregates. For example, due to the fact that FER excitons in J-aggregates are much less likely to travel and are more likely, therefore, to luminesce near the site where the exciton was created explains the higher PLQY of J-aggregates compared to H-aggregates. For H-aggregates, the PLQY is lower due to the fact that the more an exciton travels the more likely it will be interact with a

quenching site or be quenched when travelling, because it is in effect probing many more phonon manifolds in its lifetime. The above discussion was in reference to pure H and J aggregates. In reality aggregates are a mixture of both. Even the 1-D stacked molecules of HBC derivatives are not pure H-aggregates due to the fact that a) the HBC molecule is not a linear molecule b) it has degenerate and 6-fold symmetric states. Thus there will always be a component of the transition dipoles that leads to $\alpha > 0^\circ$. One must take note that the more molecules, $2N$, involved in a given FER state the more likely it will be observed above all the other possible FER states with a lower number $2N$, because the oscillator strength will be larger the more molecules, $2N$, that are involved. Thus in a sense, less efficient FER processes will have their intensity, in the optical spectrum, swamped by the more efficient ones. This also applies to the PL, where in fact an additional remark must be made: the more efficient the process of an exciton reaching a luminescence site, or the less likely the exciton is quenched, will add to the probability that it is this particular FER state that is observed in the PL above all others. In the next section this will be shown to influence the PL spectra of the aggregates of HBC derivatives.

Comparison of the PL spectra of J-HBC and N-HBC (in hexane) with the PL spectra of the other derivatives, demonstrates a much larger intensity of the PL peak that is assigned to the forbidden H-aggregate FER transition from the mirror spectra in Figures 4.8 and 4.9. From the energy level diagram presented above this peak could also correspond to a symmetric J-aggregate transition. The likelihood that this peak corresponds to an S_1 transition is discounted by the S_2 emission of the isolated J-HBC molecule and other reasons given above. It is much more likely that the large intensity of this peak, at ~ 2.62 eV, corresponds to an increase in the correlation between the position of adjacent nanowires in a bundle (the MSA superstructure) giving rise to an increased order.

The symmetrically substituted HBC derivatives are separated by flexible alkyl chains of ~ 10 Å length. Thus the probability of a symmetric transition dipole interaction between molecular cores in adjacent bundles is low – hence the intensity of the corresponding peak in the PL is low. For N-HBC and J-HBC the HBC cores are much closer together in adjacent nanowires ~ 3.5 Å. It is much more likely that a transition dipole interaction

between the cores of molecules in adjacent nanowires are somewhat ordered in their position with respect to each other and are therefore correlated. For the other derivatives, the flexible alkyl-chains give rise to a weak correlation between the molecular cores (the chromophores that interact to give FER) of molecules in neighbouring nanowires in a bundle. The lack of ordered side-to-side aggregation of nanowires in a bundle decreases the likelihood of side-to-side FER (the symmetric J-aggregate transition). For these systems the order of the molecular positions is greater within a nanowire than between nanowires. Since FER is disorder limited, the PL and PLE both have a dominant FER signature of H-aggregates.

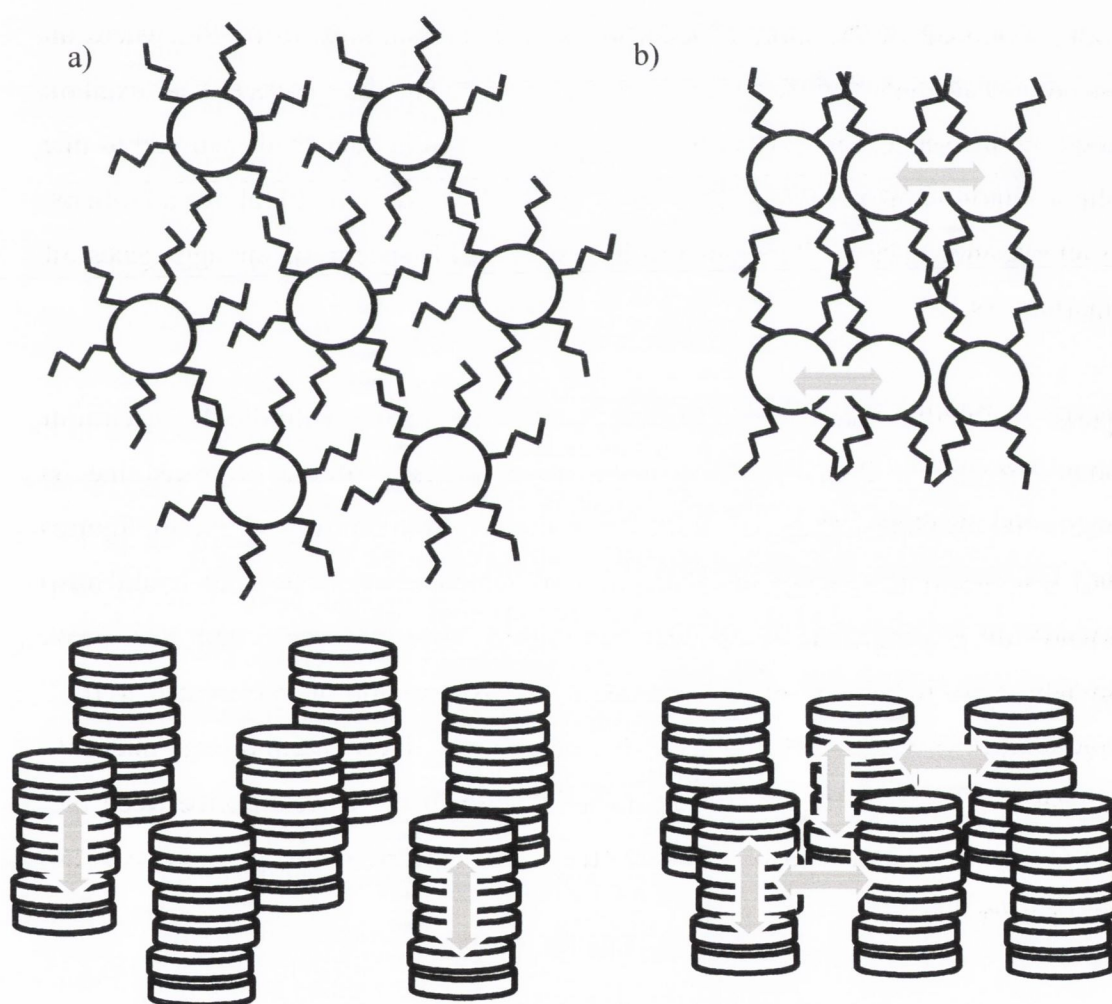


Figure 4.22: Illustration of the two kinds of MSAs detected by the PL spectra of the HBC aggregates. The differences arise from the FER directions possible in the MSAs of the a) symmetrically substituted HBC derivatives (HBC-C8,2, HBC-PhC12, F-HBC) and b) the asymmetrically substituted HBC derivatives (N-HBC and J-HBC). The grey arrows indicate the possible directions of exciton resonance. In the top view, only the MSAs of symmetrically substituted HBC molecules allow side-to-side FER between nanowires

in the bundles. This gives a J-aggregate FER signature in the PL spectra. In the side view, both kinds of MSAs allow for exciton resonance up-and-down a nanowire (note for clarity the alkyl-chains are not shown in the side view). This gives a H-aggregate FER signature in the PL and Absorption/PLE spectra for reasons described in the text.

For N-HBC and J-HBC MSAs the proximity between cores up-and-down a nanowire and side-to-side between nanowires can give rise to both J and H aggregate FER features as illustrated in Figure 4.22. However, the J-aggregate (from side-to-side exciton resonance) features are only observed in the PL and not in the Absorption/PLE spectra. This may be due to the order up-and-down an aggregate being greater than side-to-side order between aggregates in a bundle. As mentioned above the oscillator strength of a FER state is greater the more molecules involved ($2N$). Since the localisation length, $2N$, of an FER state is disorder limited, the shorter localisation range of side-to-side resonance states compared to up-and-down sites will have a smaller oscillator strength and will thus not dominate in the PLE (up-and-down FER localisation range will be greater due to the larger strength of intermolecular interactions ordering the nanowire more). In the absorption, all the molecules are probed, however, since an exciton is mobile during its lifetime, the exciton will migrate and become trapped at lower energy sites. It will therefore spend more time at these low energy sites and is thus more likely to luminesce from these sites. As illustrated in the energy level diagram the symmetric J-state is at lower energy than the H-symmetric state. Thus excitons formed on N-HBC and J-HBC MSAs are more likely to be generated in collective FER states that are resonant up-and-down a nanowire (H-aggregate absorption) but will have a larger relative probability, compared to the absorption process, of luminescing from FER states that are resonant side-to-side between nanowires (J-aggregate and H-aggregate PL).

The fact that most molecules studied for FER are *not* symmetrically substituted in such a way that they have a insulating alky- mantle around the chromophore explains why H-aggregate emission is not frequently observed. Most molecules studied are linear and polar, and have optical spectra more analogous to J-HBC or N-HBC. If one imagines the PL spectra of these molecules to be more inhomogeneously broadened the PL emission appears to be typical of most conjugated molecules (with a dominant peak with 2 - 3 shoulders at progressively lower energy). It is only the quasi 1-D structure of

HBC-C8,2, HBC-PhC12 and F-HBC that restricts the exciton to a H aggregate configuration and has allowed H-aggregate emission (although inefficient) to be detected – there are no efficient J-emission pathways available.

There is one complication with the above explanation of the J-HBC and N-HBC PL spectra: the enhanced peak of J-HBC and N-HBC is also observed in the other aggregates (but with less intensity). If the origin of the peak in the PL spectra of the symmetrically substituted HBC derivatives is also due to side-to-side FER states then the larger inter-nanowire separation of these derivative MSA bundles should surely give rise to a small β of this J-aggregate signature compared to that of J-HBC and N-HBC. This may in fact be the case, since $\alpha \neq 0$ the intensity of the dipole forbidden and allowed J-aggregate FER transitions should have non-zero intensities. In fact in the PL spectra of J-HBC and N-HBC aggregates the peak b is also observed to increase in intensity. Clearly for these derivatives the PL spectra are a superposition of the H and J aggregate signatures, therefore the exact energy of the peak increasing the intensity peak b is not known. But the fact that no other peak at lower energy than peak b is observed to appear or increase in intensity reduces the likelihood that peaks e and b are related vibronically. Therefore it could be that peak b is the anti-symmetric J-aggregate FER state. This would mean that 2β for the J-resonance of molecules in different nanowires in a bundle for J-HBC and N-HBC is ~ 0.16 eV which is greater than 2β of the H-resonance in the PL as would be expected.

The PL spectra of medium and high concentration solutions of HBC derivatives have much more fine structure compared to the PL of the isolated molecules. As discussed in Chapter 3, the emergence of 2 dominant sub-bands in the PLE spectra are typical signatures of FER. Although from first inspection the PL spectra seems unrelated in structure to the PLE spectra, the mirror image superpositions of both PL and PLE spectra in Figure 4.8 and 4.9 do indicate that both are related. The major difference between them is the bandwidth of the PL spectra with respect to the bandwidth of the PLE spectra. The reduction by a factor 3 - 4 is quite large and is generally not observed in non-FER systems. In general the fine structure in the PL is sharper than the PLE but the bandwidth is similar. The reasons for this dramatic change are extensively discussed in Chapter 6.

The v-e transition energies observed from the PLE spectra do match the ground state vibrational energies measured by non-resonant Raman and FT-IR reasonably well. The main discrepancy is the v-e transition energies of the PL (and some low energy peaks in the PLE too). The v-e transition energies measured in the PL spectra are lower than measured by FT-IR and no strong peaks are visible in the non-resonant Raman at energies ranging from 0.04 - 0.05 eV. The origin of this discrepancy may be hinted at by the dramatic decrease in the bandwidth of the PL spectra compared to the PLE spectra. It is possible, and reasons will be given in Chapter 6, that the v-e modes that couple most efficiently to the FER states may be a function of the localisation range $2N$. The large change in bandwidth indicates that in the photo-excited state HBC derivatives behave differently than in the ground state. It is possible that if the HBC derivative MSAs undergo a change in the photo-excited state the FER range may increase. It is well known for Pseudo-Iso-cyanine systems that v-e features become absent in the aggregated state. In isolated form these molecules possess a Stokes shift and v-e transition energy similar to that of isolated HBC derivative molecules. Yet upon aggregation, and FER, the v-e peaks of PIC molecules seem to disappear and the bandwidth decreases dramatically. The HBC derivative spectra appear to be behaving more like PIC in some respects (or at least approaching the same behaviour). This is the motivation of Chapter 6.

CONCENTRATION DEPENDENCE

The linear decrease for all derivatives at low concentration in the log-log plot of the PL intensity per mole indicates that the process governing the behaviour of the derivatives in this concentration regime is the same for all the derivatives. This shows that the exact molecular structure is not important. It is therefore most likely to do with the collision and desorption kinetics of the isolated species – this in effect confirms that isolated molecules are indeed observed.

The plateau region at concentrations above 10^{-9} M, for N-HBC and HBC-C8,2 indicates that the luminescence efficiency of the aggregated molecules is insensitive to the size of the aggregate formed. This indicates that in the lifetime of the exciton the volume explored

does not change. Both N-HBC and HBC-C8,2 seem to be very ordered (from the sharpness of their PLE and PL spectra). This explains why the environment the exciton explores in the MSAs of these molecules does not vary as a function of concentration above 10^{-9} M. On the other hand, the generally more disordered HBC-PhC12 and F-HBC (as described in Chapter 3), both experience a decrease in the PL/mole at concentrations above 10^{-9} . This indicates that for the more disordered derivatives the environment probed by an exciton in its lifetime is changing. If the disorder of an aggregate increases (as confirmed by the increase in FWHM from medium to high concentration of HBC-PhC12) the number of non-radiative pathways is more likely to increase than decrease. This explains the continuous decrease of the PL per mole of these two derivatives.

In fact the increase of the peak at 2.35 eV for HBC-PhC12 upon increasing from medium to high concentration is maybe due to the planarisation of the exo-phenyls. Otherwise this change would be observed for other derivatives. The planarisation may have increased the overall Stokes shift giving rise to a red-shift in the PL spectra. However, the fact that all peaks don't shift down in energy determines that a discreet new planarised species of HBC-PhC12 is forming rather than all molecules in solution planarising in unison. The change is unlike that of N-HBC in chloroform compared to hexane (this is the topic of Chapter 5). It may be possible that an enhancement of the S_1 symmetric J-transition, arising from an asymmetric planarisation of the six exo-phenyls. This would likely break the D_{6h} symmetry and enhance the PL intensity of the S_1 transition. The reason this would not be observed in the PLE spectrum is because, as described earlier, the exciton is mobile. If the phenyls become planarised it is entirely likely that HBC-PhC12 molecules can slide over each other. This would explain the increase in FWHM associated with a decrease in the positional order of molecules in the HBC-PhC12 MSA. If the molecules are sliding in particular segments of the MSA enhancing S_1 emission, mobile excitons will become trapped at these low energy sites and are more likely to luminesce from these sites. If the molecules do slide over one another it is likely that the aggregate configuration will change from a H-aggregate to a J-aggregate. This could explain the why the higher energy S_1 PL peak also at ~ 2.35 eV could contribute to the HBC-PhC12 PL spectrum at high concentration.

The reason the PL efficiency of an aggregate is significantly lower than that of an isolated molecule is because a resonant exciton is coupling to many more vibrational manifolds. The decrease by 7 orders of magnitude cannot be accounted for by the change in the absorption coefficient (the absorption cross-section actually increases). Instead it is likely to arise from the doubling (for $2N = 2$) of the vibrational modes coupled to the exciton (see Appendix B). It may also arise from the exponential increase in the number of physical pathways available to an exciton. The 2 orders of magnitude difference between N-HBC and HBC-C8,2 aggregates compared to HBC-PhC12 and F-HBC aggregates at 10^{-7} M is most likely due to the disorder of the MSA structures formed by the latter two.

4.5 CONCLUSIONS

HBC derivatives have been investigated before with spectra published⁸ that are remarkably similar to the medium and high concentration spectra presented here. Typically the concentration range explored by others has been above 10^{-7} M and/ or in solid state. The results presented in this chapter demonstrate that in previous studies aggregates of HBC were measured and not the isolated HBC molecules. In fact many publications of HBC spectroscopy have used photo-physics of isolated molecules to describe - what we now know to be - aggregates. The detection of the isolated HBC derivative molecules is confirmed in many ways: a) the similarity to known spectra of isolated molecules, b) the isolated molecules at high concentration for known disordered systems of F-HBC and HBC-PhC12, c) the FER splitting of the medium concentration species d) a Stokes shift that is greater than the v-e relaxation contribution, e) the linear dependence of the intensity per mole versus concentration suggesting a dependence on the collision cross-section f) the very high photo-luminescence efficiency and the much lower efficiency of the species at high concentration and g) the bathochromic shift of the isolated molecule PLE that is not observed for aggregates.

The formation of aggregates as the concentration is increased reveals a very complicated PL spectrum. However, comparison with the mirror image of the PLE spectrum indicates the relationship between the two. The distinction between H- and J-

aggregate emission allowed the distinction between the MSAs formed between the symmetrically and asymmetrically substituted HBC derivatives. In fact the detection and assignment of H-aggregate emission has led to the construction of a new energy level system diagram for FER that is relevant to both J and H aggregates. It was found that the reason H-aggregate emission is so elusive is that excitons, like running water, will always find the path of least “resistance”. Hence H-aggregate emission will be easily masked by efficient J-aggregate emission. This is compounded by the fact the natural induction state of a H-aggregate is a travelling state that is more likely to enable the exciton to migrate than to luminesce. Hence, the low PLQY (of H-aggregate emission) arises from excitons in H-aggregates migrating easily to sites of J-emission and/or being quenched along the way.

The distinction in the PL/mole versus concentration plot between ordered and disordered MSAs serves to illustrate the sensitivity of PL spectra to the MSA superstructures formed. In light of this, perhaps the PL spectra of many molecular systems should be revised to see if a FER model would better explain the spectra.

¹ Proc. Enrico Fermi Sch. Phys., *Organic Nanostructures: Science and Applications*, IOS Press, Course CXLIX, p150

² H. Fidder, PhD. Thesis, University of Groningen (1993)

³ H. Fidder, D. A. Wiersma, *J. Phys. Chem.*, **97** 11603 (1993)

⁴ In collaboration with Dr. Alan Dalton, FOCAS DIT, Dublin.

⁵ W. Hendel, Z. H. Khan, W. Schmidt, *Tetrahedron*, **42** p1127-1134 1986

⁶ R. Bosisio, C. Botta, A. Colombo, S. Destri, W. Porzio, E. Grilli, R. Tubino, G. Bongiovanni, A. Mura, G. Di Silvestro, *Synth. Met.* **87** 23 (1997)

⁷ I.G. Scheblykin, M. M. Bataiev, M. Van der Auweraer, A. G. Vitukhnovsky, *Chem. Phys. Lett.* **316** 37 (2000)

⁸ M.A. Biasutti, J. Rommens, A. Vaes, S. De Feyter, F.D. de Schryver, *Bull. Soc. Chim. Belg.* **106**, 659, 1997

Chapter 5: EXCIMER AND SOLUBILITY

5.1 INTRODUCTION

In this chapter the optical properties of MSA ensembles are explored. Observed changes to the emission spectrum for high concentration solutions, solutions in bad solvents and solid state samples are described and explained in terms of MSA interactions.

Compared to isolated molecules, aggregates have a large number of interactions with neighbouring molecules. The transition dipole interactions of molecules in an MSA were described in Chapter 3 and shown to produce distinct signatures in the absorption/PLE and emission spectra. In this chapter, the MSA super-structural level is explored and spectroscopic signatures of molecular interactions at this level are investigated. Three methods were used to control the MSA interactions a) increasing the concentration, b) increasing the MSA dopant loading of solid state matrix samples and c) gradual substitution of a good solvent with a bad solvent. In addition, the latter method conveniently allows a rough determination of the Hildebrand solubility parameter for MSAs. Low temperature emission spectra are presented and shown to support the finding that the red-shifted emission observed arises from excimer emission at disordered sites in percolation networks and disordered agglomerates of MSAs.

For clarity, in this Chapter the general term *emission spectrum* is employed to allow a later distinction between the contributions, from photo-luminescence and excimer emission processes, to the emission spectrum.

5.2 RESULTS

HIGH CONCENTRATION ANOMALIES IN THE PL OF F-HBC

In Chapter 4, the medium concentration emission spectra of all the HBC derivatives, except F-HBC, was shown to vary little over the medium and high concentration range of $10^{-9} - 10^{-4}$ M. Given in Figure 5.1 are all the emission and PLE spectra of F-HBC at the characteristic concentrations at which they can be observed. The low concentrations PL and PLE spectra have previously been described in Chapters 3 and 4. However from Figure 5.1, a characteristically featureless red-shifted broad emission peak doublet is observed to emerge at 2.07 ± 0.02 eV and 2.24 ± 0.02 eV for the higher concentration spectra of F-HBC at 2.3×10^{-5} M. The nature of the peak was unclear and this motivated the search for more controlled experiments to determine its origin. The FWHM of this peak doublet is 0.51 ± 0.04 eV which is a factor 6.4 broader than the FWHM of F-HBC, 0.08 ± 0.02 eV of the PL emission band, between 2.3 and 2.8 eV, as determined in Chapter 4. The red-shifted emission is quite distinct from the other emission spectra observed. The PLE spectrum for this emission, collected at 2.00 eV is also broad and featureless. It must be noted that the slight depression in intensity at the exact energy of the usual PLE spectrum described in Chapter 4 (3.43 eV) is observed to become more prominent for higher concentration solutions of F-HBC. It is certain that the origin of this depression is self-absorption in the PL cuvette at these elevated concentrations. Thus, even though the red-shifted emission displays two peaks due to self-absorption, the PLE has one very broad peak with a FWHM of 1.2 ± 0.04 eV. This is considerably larger than the usual PLE recorded at medium concentration. The PLE of the red-shifted emission nevertheless does contain a new shoulder at ~ 3.0 eV and a peak at ~ 3.2 eV. This was previously observed in the high concentration absorption spectra F-HBC. The emergence of these features was attributed, in Chapter 3, to the increase in the number of L species in solution.

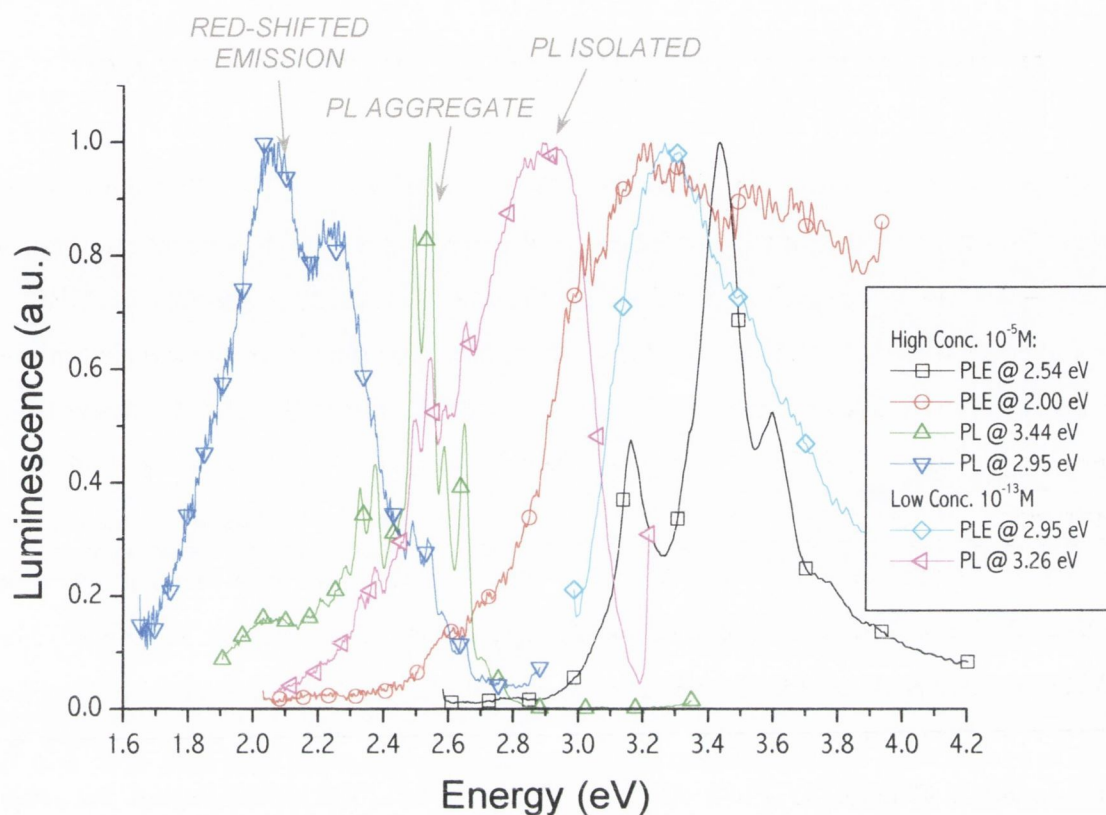


Figure 5.1: All the observed PL and PLE spectra of F-HBC at the characteristic concentration and energy at which they are recorded. Of particular interest in this chapter is the red-shifted emission at $\sim 2.0 - 2.3$ eV.

In Figure 5.2, the PL spectra of F-HBC at high concentration illustrate the increase in the relative intensity of the red-shifted emission with respect to the PL. It should be noted that upon increasing the concentration, the energy of the PL peak maximum is not observed to change - although the red-shifted emission becomes more dominant in intensity. Thus the red-shifted emission is much more sensitive to the concentration, typically, above 10^{-5} M for F-HBC.

A plausible argument at this point is that a new species is responsible for the red-shifted emission. This possibility and other likely explanations will be explored in the discussion section. However, the changes observed for F-HBC will be shown, in the next section, to be reproducible by other sample preparation techniques.

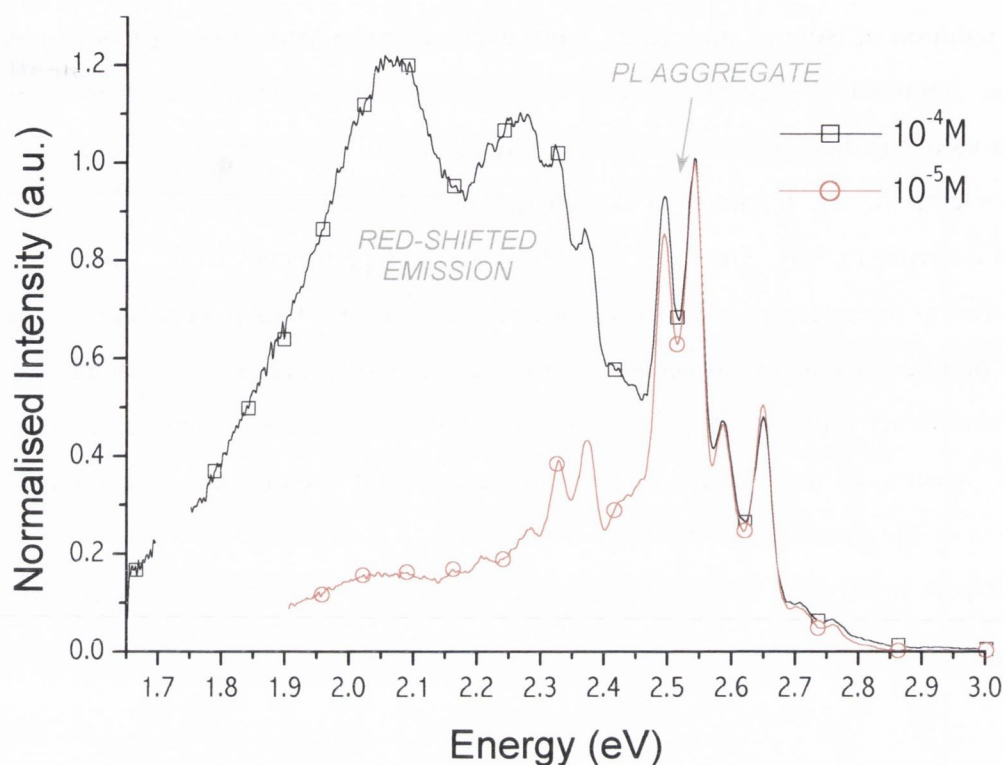


Figure 5.2: PL spectra of F-HBC at 10^{-4} M and 10^{-5} M. Note the increase of a red-shifted emission at lower energies than the dominant PL peak. For clarity scattering peaks and 2nd harmonics of the primary excitation beam have been deleted.

HILDEBRAND SOLUBILITY MEASUREMENTS

To assess the suitability of spectroscopic methods to determine Hildebrand solubility parameters, the solubility parameter of HBC-C8,2 isolated and aggregated species was measured from the emission spectra by the method of solvent mixtures¹. Emission spectra of other derivatives in the presence of acetonitrile and hexane were collected for comparison. Values for the Hildebrand solubility parameter of the solvent mixtures were calculated using data from references [1] and [2]. The upper limit of the solubility was easily obtained by the titration of a solvent with a higher solubility parameter than chloroform such as acetonitrile. The choice of the solvent must be such that the Hansen parameters are similar³. For example a hydrogen bonding solvent should not be mixed with a solvent with no hydrogen bonding.

From Chapter 4, the PL efficiency of aggregates was found to be several orders of magnitude lower than that of isolated species. Therefore the titration of a bad solvent

into a solution of isolated molecules is not expected to induce a red-shift as is observed for the aggregated species. Instead isolated molecules behave as very sensitive indicators of their solvent environment. If aggregation is induced by the titration of a bad solvent, the PL intensity at the energy of the isolated molecules PL maximum should decrease rapidly. The large difference in the PL efficiency of the isolated species compared to the aggregated species makes the emission intensity particularly sensitive to the number of isolated molecules and therefore allows precise determination of the upper and lower limits of the Hildebrand solubility parameters. In Figure 5.3 a) and b), the PL spectra of the isolated species in hexane and acetonitrile, respectively, as a function of the amount of titrated poor solvent is given. Each spectrum is normalised with respect to the total volume after a given amount of hexane or acetonitrile is added to the toluene solution.

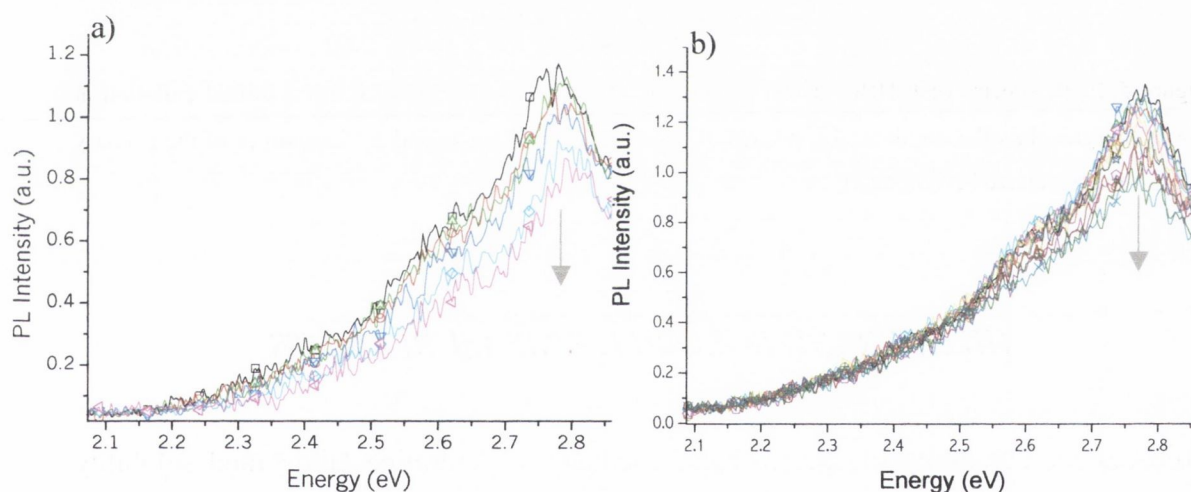


Figure 5.3: PL spectra of isolated HBC-C8,2 molecules at 10^{-13} M in toluene with varying amounts of a) hexane and b) acetonitrile titrated into solution. Note the initially slow and then sharper decrease of the PL intensity as the bad solvent is titrated. Each PL spectrum has been corrected for the decrease in concentration arising from increasing the total volume as more bad solvent is added. Arrow indicates trend as more bad solvent is added.

As can be seen from both Figures 5.3 a) and b), upon initial titration of a small amount of bad solvent the intensity remains rather constant. After a sufficient amount of bad solvent is added, aggregation is promoted and the PL intensity is observed to decrease steadily as more bad solvent is added. To quantify these changes, the Hildebrand solubility parameter of each good/bad solvent mixture was calculated as was the PL

intensity normalised with respect to the initial PL intensity of the pure toluene solution. The latter value was plotted against the solvent mixture Hildebrand parameter and is given in Figure 5.4. From the plot a clear plateau between $\delta_L = 17.28$ and $\delta_U = 18.44$ can be seen. At either side of this plateau the normalised PL intensity, which is proportional to the number of isolated molecules still in solution (i.e. that have not aggregated), is observed to decrease steadily. This clearly indicates that if the solubility parameter of the solvent used decreases below 17.28 or increases above 18.44 then the number of isolated molecules present is depleted in favour of forming aggregated species. The value calculated agree with the observation that isolated species of HBC-C8,2 were only observable at low concentrations in toluene ($\delta = 18.3$) and not chloroform ($\delta = 18.7$). Since a photo-luminescence photo-multiplier detector has a finite sensitivity, a certain number of isolated molecules must be present in the cuvette in order to enable detection above the noise level. Thus dilution in a bad solvent will not give rise to a sufficient number of isolated molecules for a given total concentration.

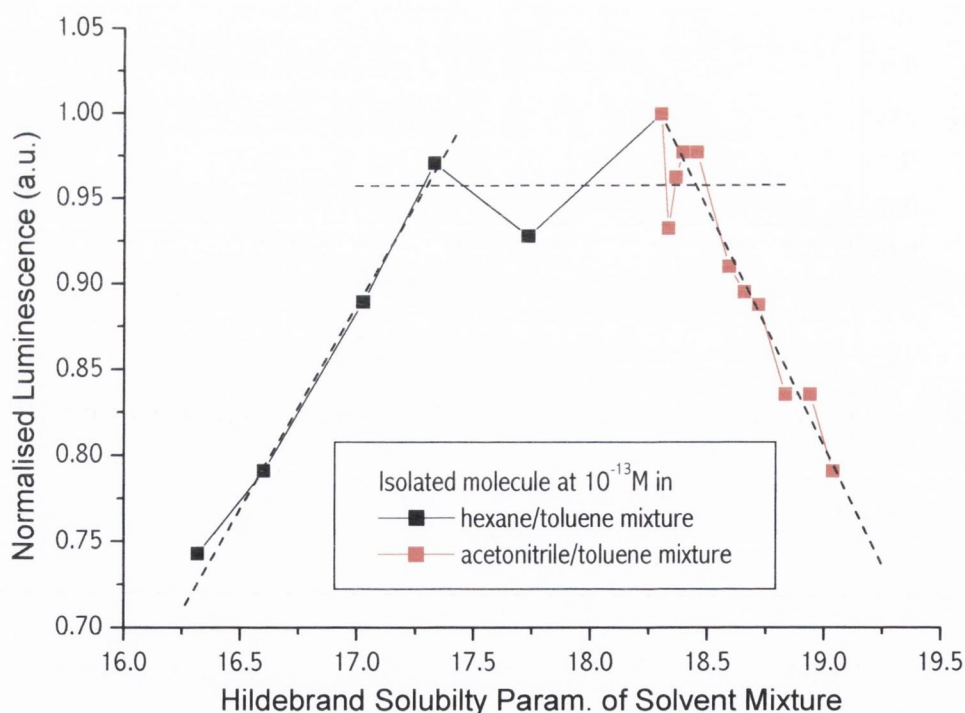


Figure 5.4: Plot of the normalised PL versus Hildebrand solubility parameter, δ , of the good/bad solvent mixture. High and low δ values were obtained by titration of acetonitrile and hexane respectively. The decrease of the normalised luminescence of isolated molecules indicates that the number of isolated molecules is depleted in favour of forming aggregates upon titration of a bad solvent.

The same procedure for measuring the Hildebrand solubility parameter was applied to a high concentration solution of HBC-C8,2 at 10^{-5} M in chloroform. Figure 5.5 shows the evolution of the PL spectra upon titration of acetonitrile. The emergence of a red-shifted broad emission double peak at 2.0 and 2.25 eV is clearly observed. This is very similar to the red-shifted emission observed for F-HBC at high concentration presented above.

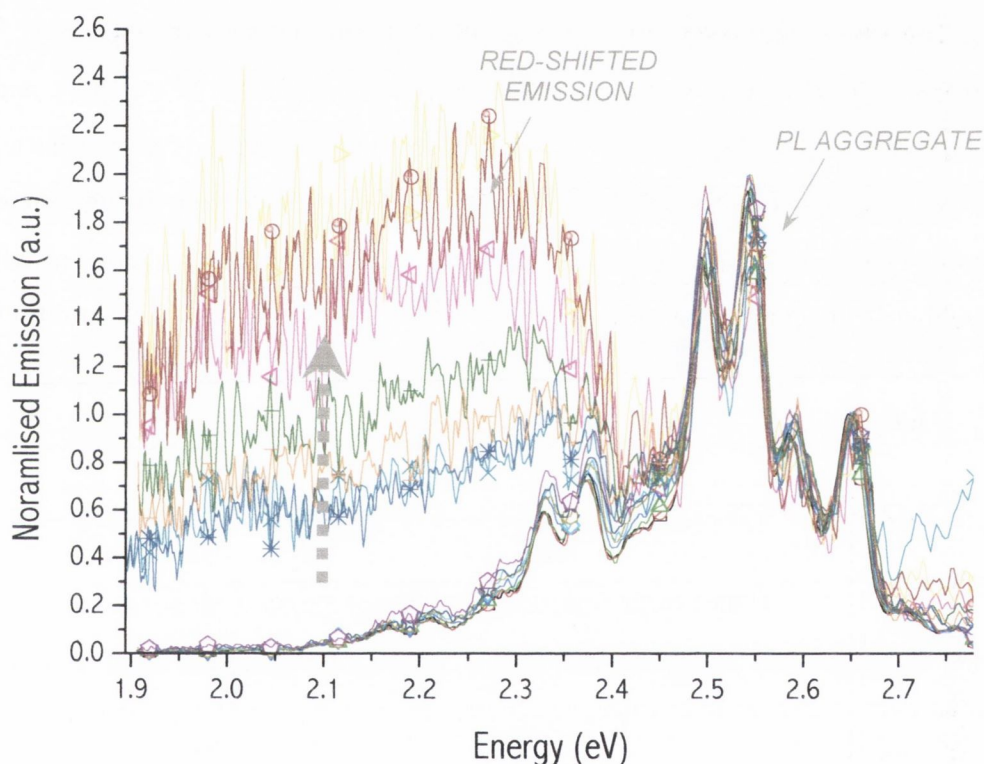


Figure 5.5: PL spectra of HBC-C8,2 aggregates at 10^{-5} M in chloroform/acetonitrile mixtures. The dashed arrow indicates the increase in the intensity of the red-shifted emission upon increasing the amount of acetonitrile titrated into solution.

At high concentration, solutions of HBC-C8,2 are composed of aggregated species. The spectroscopic measurement of the Hildebrand solubility parameters of the aggregates proved harder to achieve than for isolated molecules. Perhaps this confirms that molecules in the centre of aggregates are less sensitive to the nature of the solvent molecules. As can be seen from Figure 5.5 the upper limit of the solubility was attained by titrating in acetonitrile. The lower limit proved much more elusive, probably due to the fact that some small trace amounts of chloroform present helped to maintain the solubility of the HBC-C8,2 MSAs in hexane. The spectra of HBC-C8,2 titrated with

hexane is therefore not included. However, the plot of the normalised red-shifted emission intensity, obtained from Figure 5.5, is given in Figure 5.6 shows a demonstrable change at $\delta \sim 20.6$. This value is higher than the upper limit of the solubility of the isolated species and may indicate the difference between the surface of an HBC derivative aggregate and a HBC derivative isolated molecule (the aromatic core is exposed in the latter case).

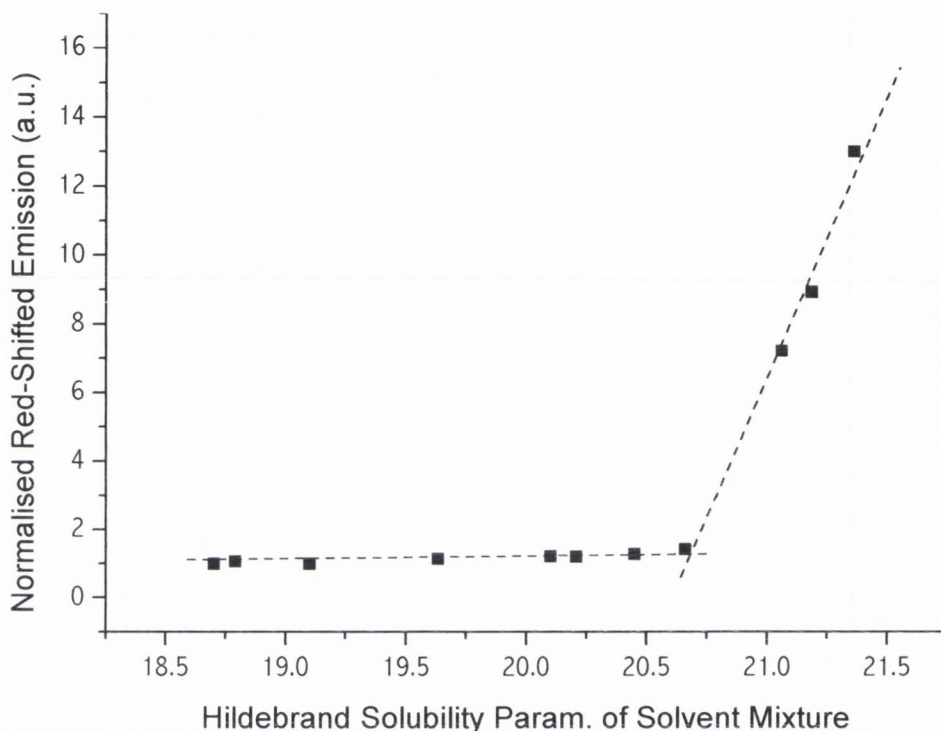


Figure 5.6: Normalised Red-Shifted emission intensity of HBC-C8,2 aggregates versus the Hildebrand solubility parameter of a chloroform/acetonitrile mixture. Note the sharp increase at ~ 20.6 .

In order to demonstrate that changes to the PL spectra do occur upon titration of hexane, very small volumes (< 10 microlitres) were added directly to hexane. Such small volumes could not be measured accurately, therefore an estimation of the lower limit of the solubility parameter was not achieved. An estimation of the upper and lower limit of the solubility parameters of HBC-C8,2 was possible, however, by using the cloud-point test method for solvent mixtures. In the cloud point test δ , is determined by inspection of the formation of visible particles/aggregates in the solution upon titration of a bad solvent. This requires the use of very high concentration solutions $\sim 10^{-3}$ M. This concentration is too high for PL spectroscopy due to the prohibitive amount of self-absorption modifying the real structure of the PL. The upper and lower limit were measured, using the cloud point test, as 15.66 and 18.95 respectively. These values span

a broader range than the values calculated from the spectroscopy of the isolated species at 10^{-13} M. Therefore, this demonstrates the higher precision, if not accuracy, of the isolated species spectroscopic measurement method. From Figures 5.7 – 5.10 similar spectral features were observed in the emission spectra of all derivatives in bad solvents such as hexane and acetonitrile.

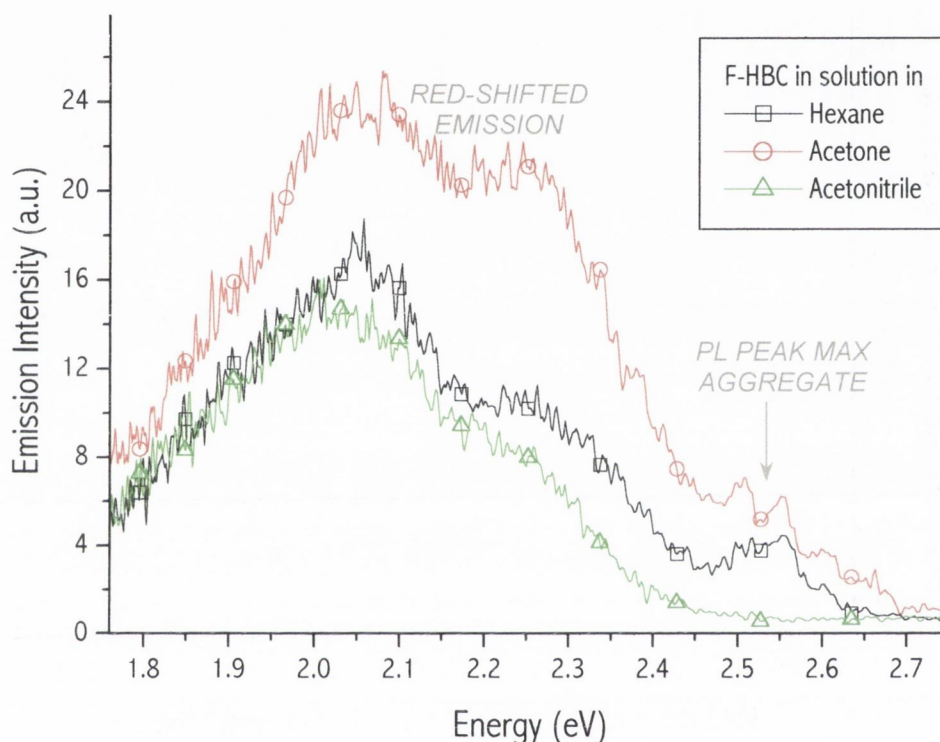


Figure 5.7: Emission spectra of F-HBC in Hexane, Acetone and Acetonitrile. Note the similarity of the spectra to the high concentration F-HBC solutions in chloroform and the MSA dopants in polymer matrices presented above.

As shown in Figure 5.7, the titration of a bad solvent, such as acetonitrile or acetone, to medium concentration solutions of F-HBC is observed to induce similar spectral changes as observed for the high concentration solutions of F-HBC. Clearly the energy of red-shifted emission peak is similar to that observed for the high concentration spectra. As will be shown later, the fact that the red-shifted emission appears for N-HBC in hexane, discounts the possibility that the red-shifted emission arises from a solvatochromic/bathochromic shift of the PL.

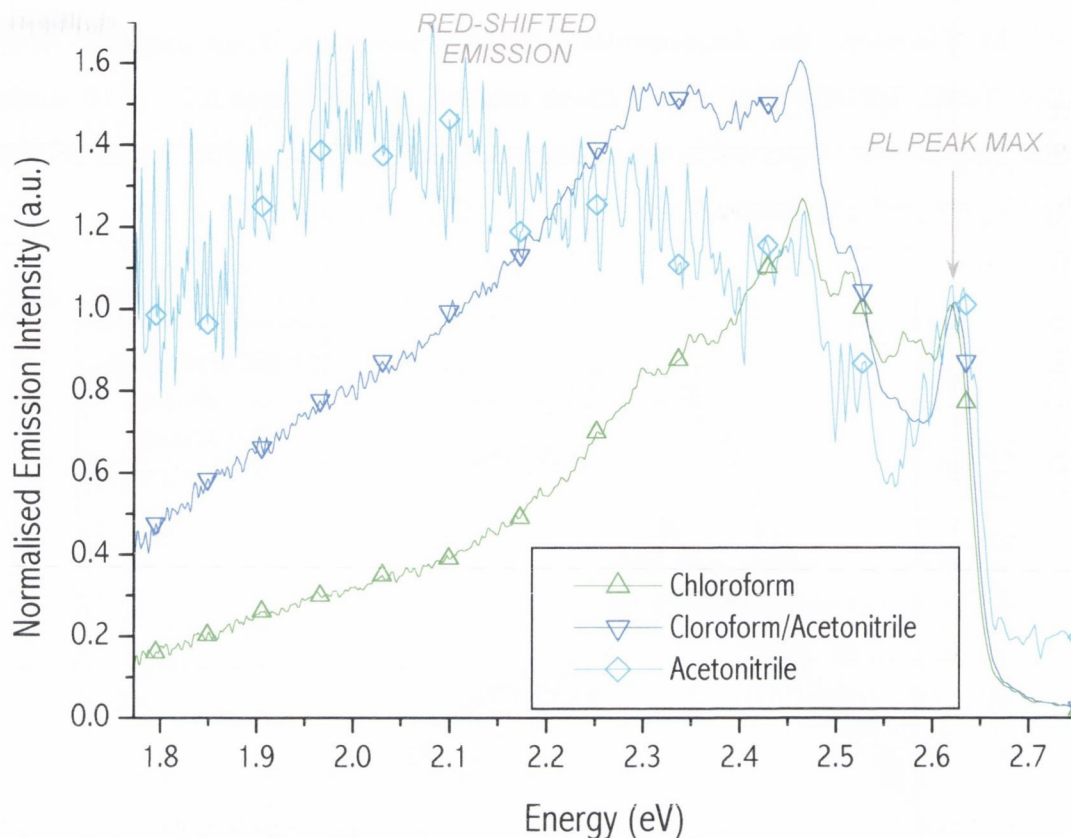


Figure 5.8: Emission spectra of J-HBC in Chloroform and Acetonitrile.

The emission spectra of N-HBC in the presence of various solvents is given in Figure 5.10. As described in Chapter 3, N-HBC is a polar molecule. It should therefore allow the distinction between solvent induced bathochromic shifts arising from a stabilisation of the excited state by solvent molecules and other red-shifts in the emission spectra. The permanent dipole moment of the various solvent molecules used is given in the figure key. As can be seen from inspection, the energy of the emission maximum does decrease with increasing solvent polarity. As described in Chapter 4, the relaxation of the excited state by the solvent molecule permanent dipoles reduces the energy of the radiative transition. This is observed as a solvent polarity dependent red-shift in the spectra.

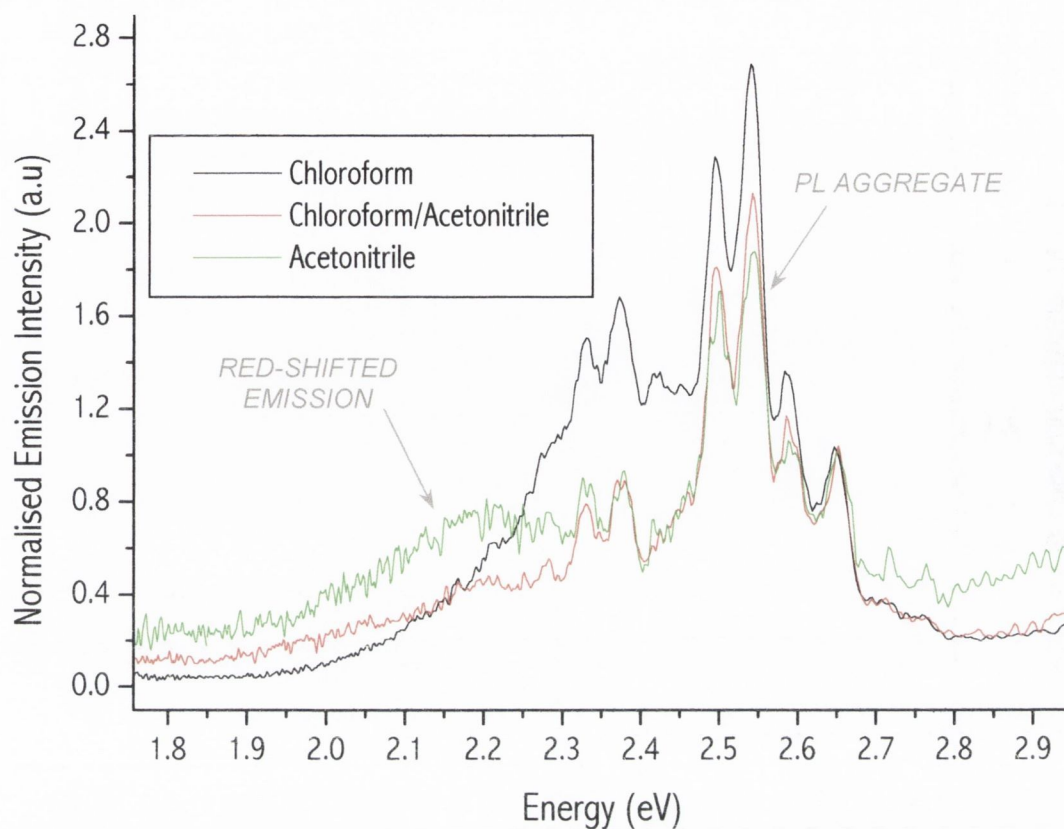


Figure 5.9: The emission spectra of HBC-PhC12 in chloroform and acetonitrile. Note the emergence of a red-shifted emission at ~ 2.2 eV for the acetonitrile solution.

However, from Figure 5.10, it should be noted that the energetic position of the peak maximum of N-HBC in chloroform appears very close to the peak for N-HBC in acetone despite a relative increase of the solvent polarity by a factor 2.76. This confirms that there must be two distinct emission processes contributing to the emission spectra, namely, the aggregate PL and a red-shifted emission process. These will be assigned in the discussion section.

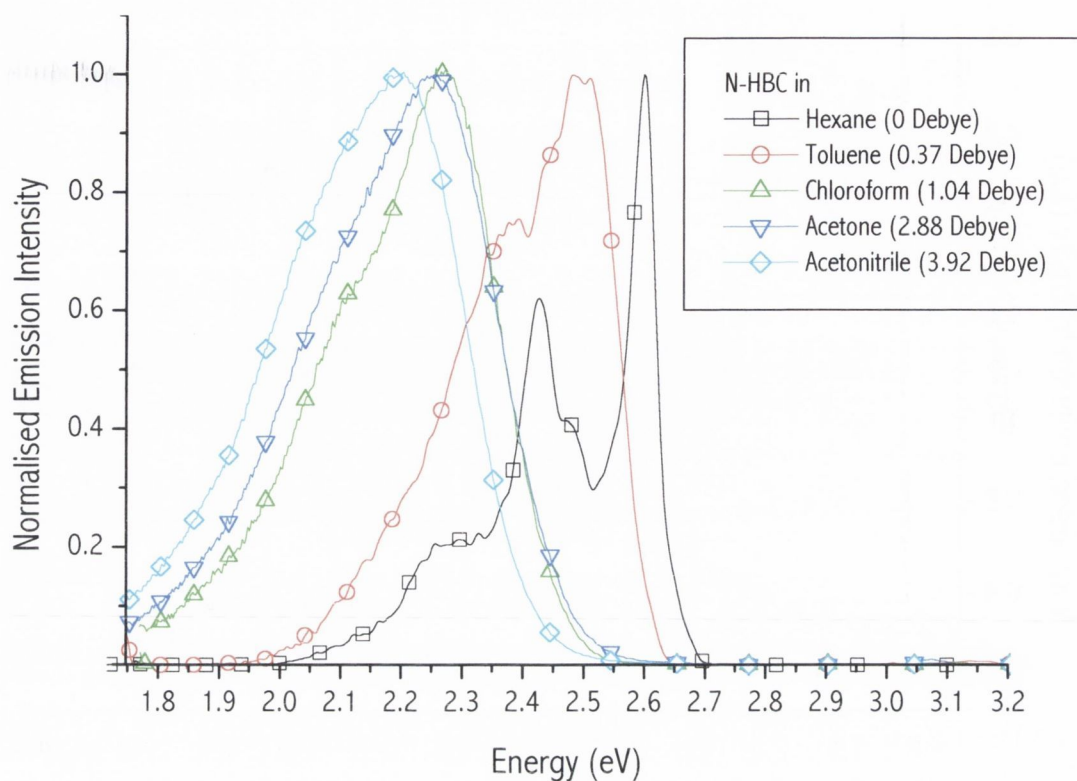


Figure 5.10: Emission spectra of N-HBC in various solvents of different polarity (values of the polarity are given in the key).

INERT MATRICES DOPED WITH MSAs

Similar changes to the optical spectra, as observed at high concentration exclusively for F-HBC, can also be achieved by doping inert polymer matrices with any of the HBC derivative MSAs. In Figure 5.11 and 5.12, the variation of the emission and PLE spectra with increasing dopant loading can clearly be seen. The energy of the dominant PL peak of low dopant loadings is similar to values obtained for the dominant PL peak at medium concentration in solution presented in Chapter 4. This demonstrates that no self-absorption effects are responsible for the overall red-shift of the emission spectra at high dopant loadings.

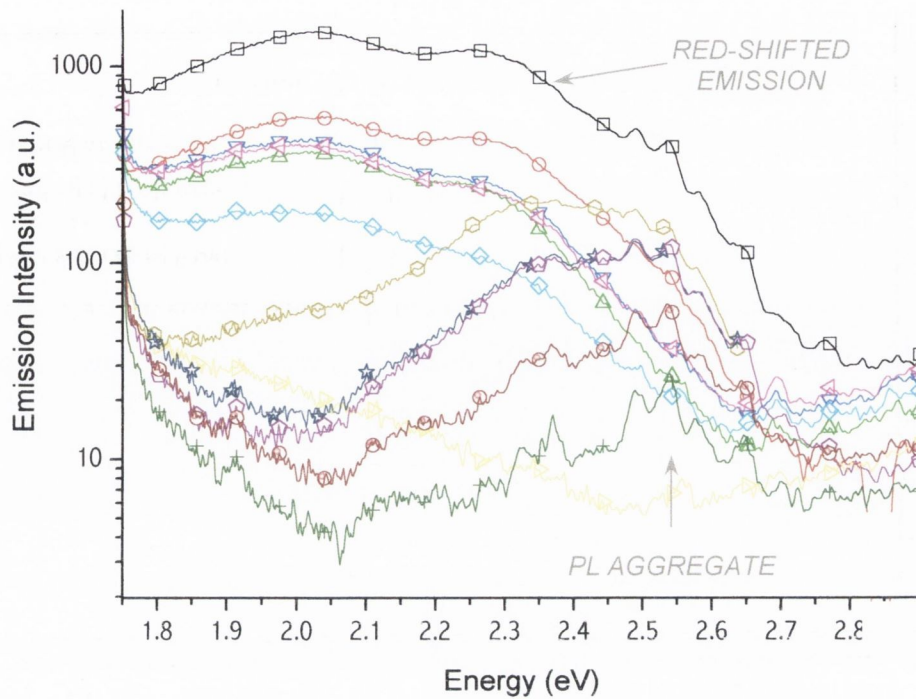


Figure 5.11: Emission spectra of HBC-C8,2 MSA doped matrix at various loading ratios (Note: vertical axis is in log scale). As the loading ratio is increased the PL (max. at 2.54 eV) is gradually superseded by a broad red-shifted emission at lower energies (2.0 – 2.3 eV).

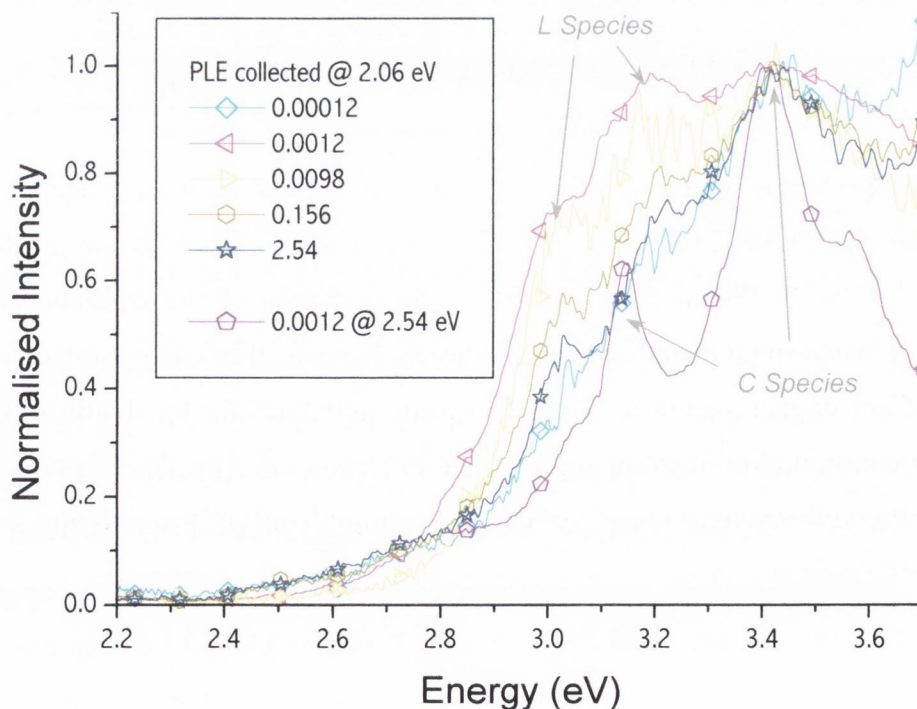


Figure 5.12: The PLE spectra collected for different loadings of HBC-C8,2 MSA in inert polymer matrices. For comparison the PLE spectrum collected at 2.54 eV (the PL) is given. This latter spectrum is not observed to change upon changing the loading of MSA. Note the similarity in the peak positions with the spectra collected at the emission maximum of the red-shifted emission at 2.06 eV. Also visible are the two new peaks at ~ 3.0 eV and ~ 3.2 eV.

Self-absorption of the emitted light can lead to an apparent red-shift in the peak position of the emission spectra by reducing the intensity of the blue-edge of the emission. The fact that the change from the dominant peak emission energy from higher to lower energies is not gradual (i.e. from the PL to the red-shifted emission) negates the possibility that this change arises from self-absorption effects as the dopant loading is increased. Instead the emission at lower photon energies, between 2.0 – 2.2 eV, is observed to emerge rapidly while the PL intensity decreases as the dopant loading is increased.

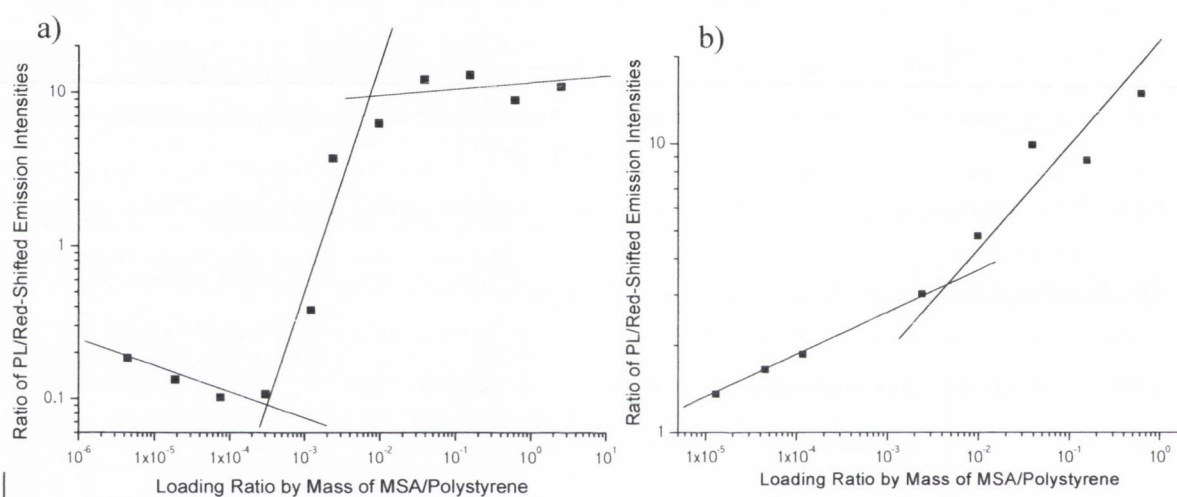


Figure 5.13: Log-log plot of the red-shifted emission versus the dopant loading of a) HBC-C8,2 and b) HBC-PhC12.

A qualitative comparison of the FWHM of the PL with the FWHM of red-shifted emission in Figure 5.11 indicates that PL FWHM remains constant whereas the FWHM of the red-shifted emission increases. Although the magnitude of the observed FWHM will vary depending on how many transitions are included, the relative change of the FWHM of the PL and the red-shifted emission, from low to high loading, can indicate whether the processes leading to broadening are the same in each case. The fact that the increase in FWHM of the red-shifted emission is far greater than that of the PL indicates that disorder is being introduced without significantly changing the order of the constituent parts. For HBC derivatives, this means that the order of the nanowire/nanotubule MSAs is for the most part preserved when used as dopants,

however the manner in which the MSAs interact is more disordered – there is an increase in the geometric disorder of the network. An analogy can be found in a pile of toothpicks. The pile is disordered even though the individual toothpicks remain structurally ordered (e.g. they stay straight no matter how much the pile is disordered).

Plotted in Figures 5.13 and 5.14 are the red-shifted emission intensity versus dopant loading. A clear transition can be observed for some of the MSA derivatives. For instance HBC-C8,2 and N-HBC both have a distinctive change between 0.03 – 0.7 % and 0.04 – 0.07 % loading respectively. On the other hand the change in intensity of the red-shifted PL of HBC-PhC12 in Figure 5.13 b) is more gradual and has a less clear transition at 0.04 % loading compared to HBC-C8,2 and N-HBC. A sharp transition in the relative intensity of the red-shifted emission with respect to the PL, as a function of the dopant loading, indicates that the probability of red-shifted emission from a photo-exciton begins to increase non-linearly at dopant loadings above ~ 0.03 %. Although the lower limit of the transition was not observed for J-HBC, the slope of the plot in Figure 5.14 b), at dopant loadings between 1 – 10 % does match that of the other MSA HBC derivatives. The implications of these results will be dealt with in the discussion section.

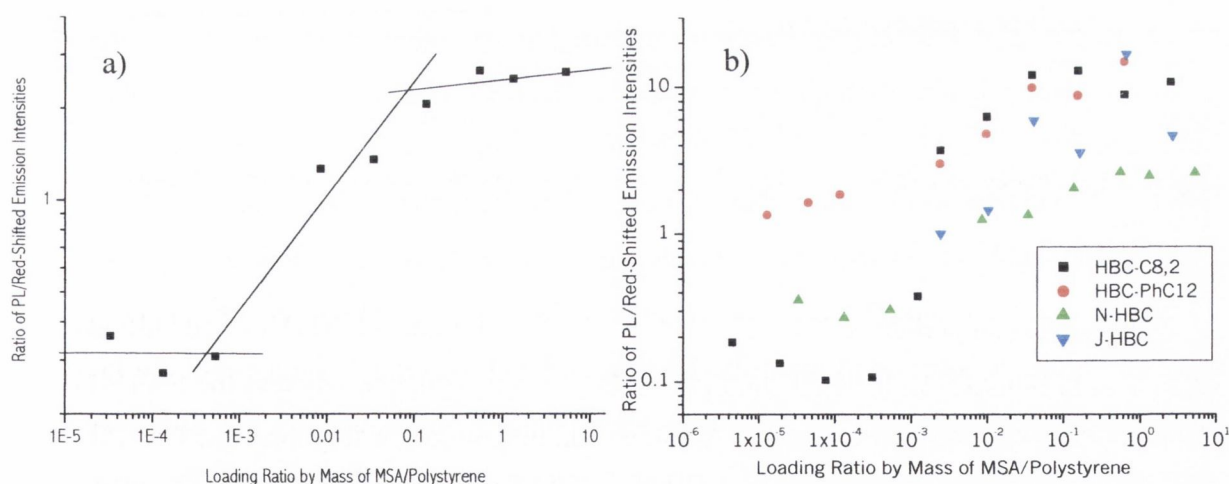


Figure 5.14: a) Log-log plot of the emission intensity versus loading of N-HBC doped matrix. B) Multi-log-log plot of the intensity versus loading of J-HBC doped matrix samples. For comparison other molecules are included.

LOW TEMP EMISSION OF MSA DOPED MATRICES

To assess whether the mobility of an exciton plays a role in the red-shifted emission process, the emission spectra of the MSA loaded matrices was measured at liquid nitrogen temperature 77 K and compared to the room temperature spectra at 300 K. Significant increases in the intensity of the emission spectra at 77 K were recorded for all derivatives. Comparison of the relative increases of PL and red-shifted emission demonstrates that they are the result of different processes. In Figure 5.15, the intensity of the red-shifted emission of a HBC-C8,2 doped matrix at 0.98 % loading is observed to increase by a factor 15.8 by cooling from 300 K to 77 K (the trend is clearer when comparing between the $77 < T < 300$ K and the 77 K spectra). Due to the large FWHM of the red-shifted emission it is hard to compare the red-shifted emission and PL relative increment in intensity. However from Figure 5.16, the relative increase of the red-shifted emission intensity with respect to the PL intensity of HBC-PhC12 can clearly be seen. The red-shifted emission intensity increases by a factor 6.9 relative to the PL at 300 K. From Figure 5.16 the isolated molecule PL and aggregate PL of the liquid crystalline HBC-PhC12 is also observed to increase by a factor 3.09 and 4.12 respectively. These values make sense if the red-shifted PL occurs from discrete sites at which migrating excitons may become trapped. On the other hand, the PL of the isolated molecule is already high if the isolated molecules are not interacting with other chromophores – the PLQY is already high and can't increase above 1. However the factor 3.09 increase would imply that at room temperature the PLQY is at most 0.33. This is too small for an isolated molecule that can be detected as low as 10^{-15} M. Therefore the likelihood is that the large FWHM of the red-shifted emission is contributing to the increase in intensity. Having said that the relative increase of the PL intensity of the aggregate PL should increase slightly more due to the fact that aggregated molecules are coupled to a larger vibrational manifold. A low temperature induced de-population of the phonon manifold should decrease the likelihood of an exciton in-elastically scattering with a phonon and decaying by non-radiative processes.

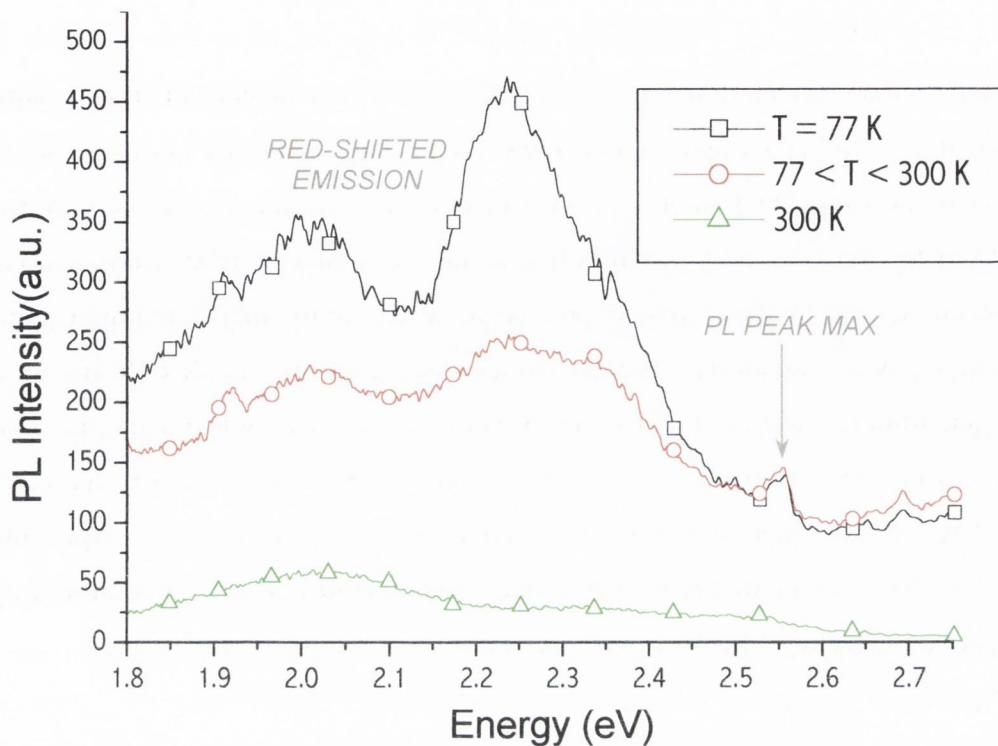


Figure 5.15: Emission spectra of HBC-C8,2 doped polymer matrix at 0.98 % loading at various temperatures, including 77K and room temperature 300 K.

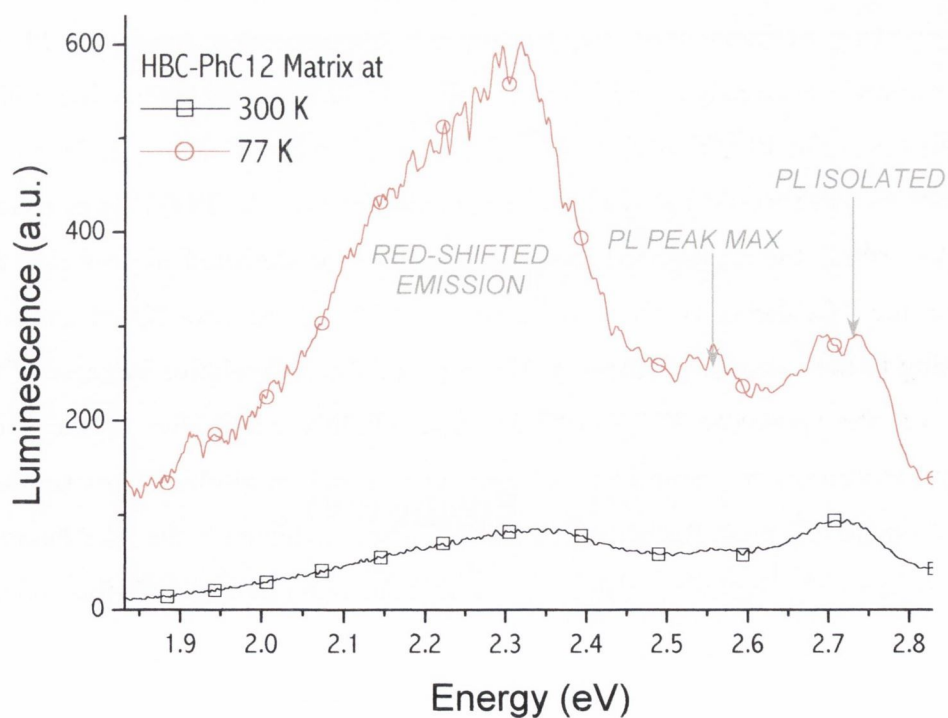


Figure 5.16: Emission spectra of HBC-PhC12 doped polymer matrix at 0.98 % loading at 77 K and 300 K.

From Figures 5.17 and 5.18, similar increases of the red-shifted emission are also observed for N-HBC and J-HBC. The relative increase of the red-shifted emission is 2.07 and 5.95 respectively. For J-HBC the relative increase of the PL is 3.7. Thus the increase of the red-shifted emission is always larger than that of the PL for all derivative molecules. At low temperatures, excitons can perform more intermolecular hops without being annihilated by inelastic scattering with phonons. This translates into the exciton being able to travel further and probe a larger volume of an aggregate. The increase in the PL intensity reflects the fact that excitons are less likely to lose coherence while on a nanowire/nanotubule. In the discussion section, the fact that the red-shifted emission increases above and beyond the PL is due to red-shifted emission sites being located at junctions between nanowires/nanotubules. At low temperature the increase in the number of excitons reaching nodes means that excitons are effectively funnelled to these red-shifted emission sites.

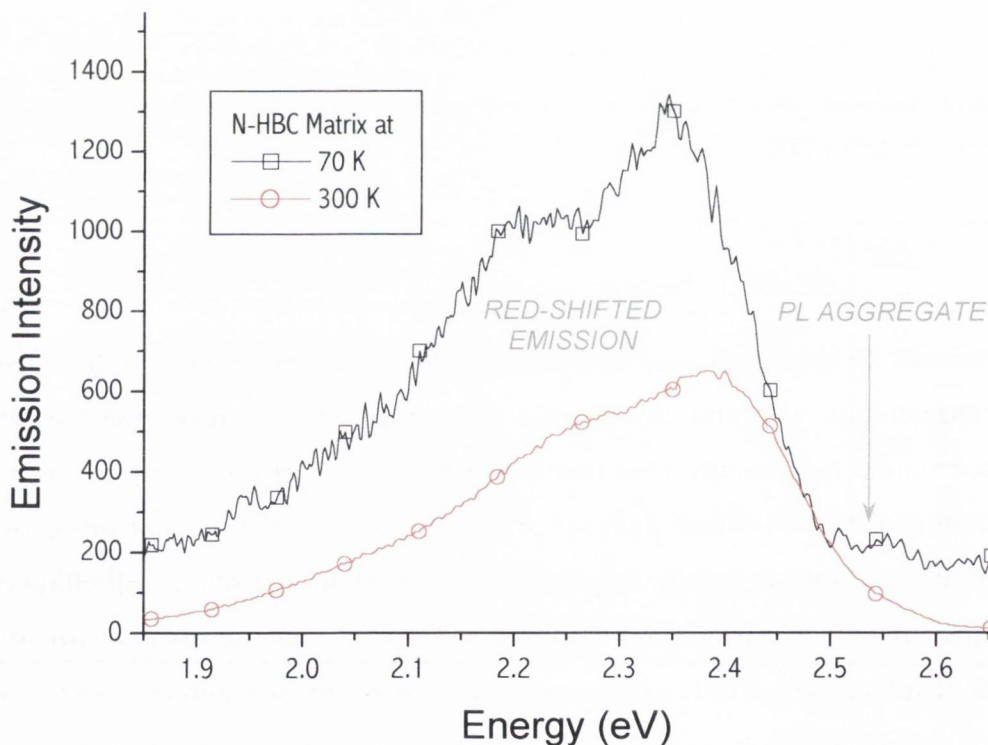


Figure 5.17: The red-shifted emission spectra of N-HBC doped matrix at 5.3 % loading. Notice the large increase in intensity at 77 K compared to room temperature.

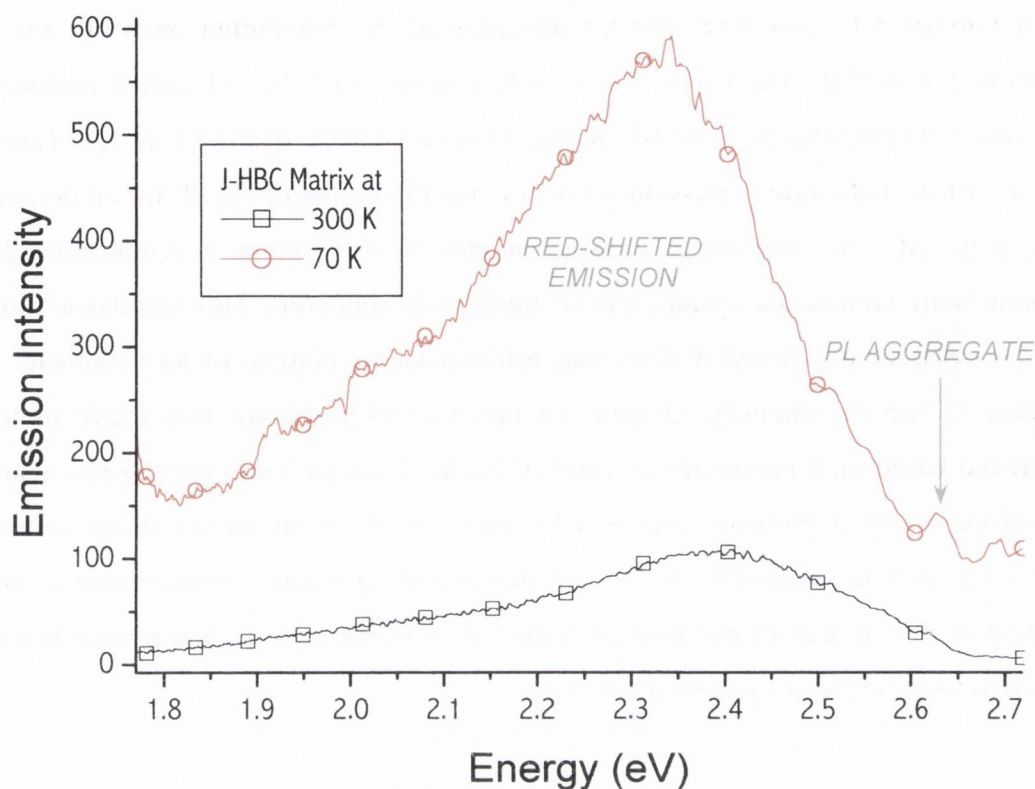


Figure 5.18: Emission spectra of J-HBC Matrix at 1.1 % loading at 70 K and 300 K.

5.3 DISCUSSION

The similarity in the energy and shape of the red-shifted emission peak between the high concentration solutions, matrix and Hildebrand measurement samples, points towards a similar process governing the changes to the emission spectra in each case. The tailoring of the red-shifted emission of aggregates by doping a polymer matrix, by titration of a bad solvent and by varying the concentration of a solution all allowed the red-shifted emission to be studied in a controlled manner. There are several possibilities that may explain the red-shifted emission: an increase in S_1 emission arising from a breaking of symmetry of the molecule, phosphorescence or excimer emission. The former two can be easily discounted by the fact that the energy of the red-shifted emission is different to that of the S_1 emission peaks ascribed in Chapter 4, and because phosphorescence is usually an intensity that is 6 – 7 orders of magnitude lower than an allowed singlet-singlet transition⁴. It is also unlikely that either process would be dopant

loading dependent. As will be shown in the following section excimer emission is much more likely to be the emission process.

The increase in the dopant loading of an inert polymer matrix is observed, in Figure 5.11, to increase the red-shifted emission intensity in a manner that would be expected from the formation of a percolation network. This is confirmed by features such as the lack of change in the red-shifted emission intensity up to a critical dopant level, whereupon there is a rapid non-linear increase to a saturated level (reached at a slightly higher dopant level than the critical concentration). From percolation theory, inclusions with a large aspect ratio are expected to have a percolation threshold⁵ of the MSA network at dopant levels of $< 1\%$. The percolation threshold $\sim D/L$ where D is the diameter and L is the length. From Figure 5.11 and the plots of the normalised red-shifted emission to dopant loading, all derivatives have a threshold of emission that lies within expected for a matrix doped with 1-D structures such as nanowires/nanotubules. Although this does not directly explain the red-shifted emission it does determine that the intensity of red-shifted emission is dependent on the connectivity of the inclusions in the matrix. This implies that the red shifted emission does not originate from a general change of all the molecules that leads to a higher probability of red-shifted emission with respect to the PL. Instead, the dependence on the connectivity, as demonstrated in Figures 5.13 and 5.14, suggests that the mobility of excitons in an aggregate plays a role in the process leading to red-shifted emission. Since excitons are mobile⁶ in molecular aggregates, the large non-linear increase in the number of pathways above the percolation threshold will allow excitons to probe more of the volume of an aggregate during the exciton's lifetime. As the red-shifted emission is related to the ability of an exciton exploring more pathways in the network, it is feasible that the red-shifted emission could arise at distinct molecular sites. Plausible candidates for these sites are the network nodes that form where an aggregate touches another aggregate in the percolation network (see Figure 5.19). The existence of a network is supported by the low-temperature emission spectra where the red-shifted emission is observed to increase more quickly than the PL. This arises because excitons will tend to survive more molecular site hops at low temperature, due to the reduced number of inelastic phonon collisions that may lead to non-radiative emission (i.e. exciton quenching). Therefore at low temperatures, the probability that an exciton will reach a red-shifted emission site in its lifetime will increase, and hence the red-shifted emission

will be determined by the level of interconnectivity in the network. The fact that the normalised red-shifted emission intensity saturates above a critical dopant loading also confirms that a percolation network has formed. The critical dopant loading, or percolation threshold, of all the derivatives is measured to be between 0.03 - 0.7 %. This percolation threshold is similar to that measured for 1-D carbon nanotubes⁷ in polymer matrices $p = 0.037$ %. Thus the doped matrix results suggest that the HBC MSA inclusions in the matrix have a large aspect ratio. This finding is further confirmed by electrical percolation, AFM and SEM data of HBC-derivatives presented in Chapter 7.

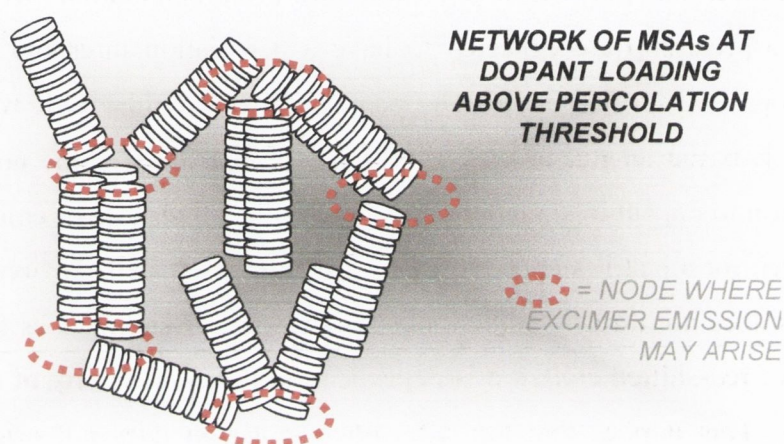


Figure 5.19: Illustration of part of a percolation network of nanowires (or nanowire bundles) in a polymer matrix. Above the percolation threshold an exciton can migrate between nanowires via the connecting nodes that have formed. Excimer emission is likely to occur at the interface between nanowires at junctions that are generally more disordered than the rest of the nanowire. PL emission will still occur when excitons radiatively decay at sites other than the junctions. Note that the percolation network can be formed from networks of aggregate bundles and not necessarily individual nanowires.

Since the formation of a percolation network of MSA inclusions in the polymer matrix can give rise to the same red-shifted emission that is observed in the other systems, it is therefore likely that a similar process is occurring at high concentration for F-HBC or in bad solvents. In solution, it is entirely possible that the local density of molecules may reach densities levels found in solid state samples of the pure compound (so long as the aggregate remains soluble). As illustrated in Figure 5.20 aggregates (and agglomerates of aggregates) are essentially nano- or micro- particles in solution and are therefore already in approximately solid state form - with each molecule roughly stacked with a periodicity of ~ 3.5 Å. The exception is that a molecule, in an aggregate in solution, may have a slightly higher mobility - certainly for liquid-crystalline molecular aggregates in solution. It is important to note that aggregates already form at

concentrations $< 10^{-9}$ and become observable in the PL at medium concentration $\sim 10^{-9}$ M. However no red-shifted emission is observed. Therefore the size of the aggregate, which will increase in size with increasing concentration, does not seem to influence the level of red-shifted emission (see Chapter 4).

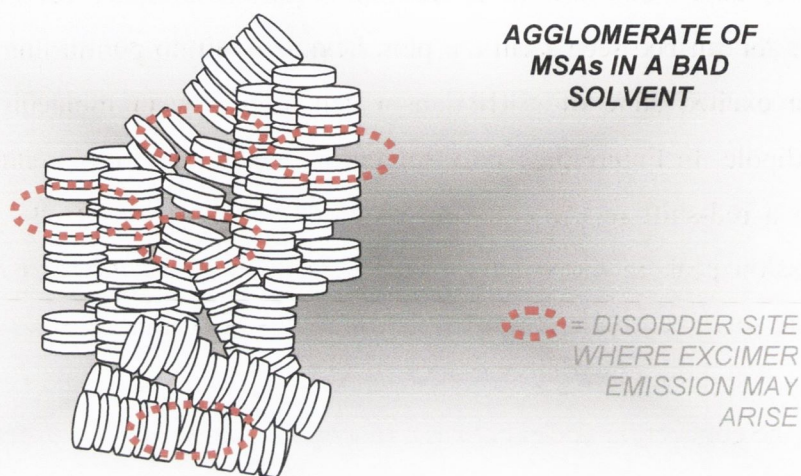


Figure 5.20: Illustration of an agglomerate of MSA nanowires in a bad solvent. The lack reorganisation ability of an aggregate in a bad solvent leads to many disorder sites that may act as excimer emission sites. Shown in the diagram are examples of network formation (above the percolation threshold) and molecular site dislocations that will effectively make a single nanowire into two nanowires with a disordered junction connecting them.

The titration of a bad solvent generally induces aggregation or agglomeration of any particles that are insoluble in the titrated bad solvent. Therefore aggregates in solution at medium concentration, that emit the usual PL explored in Chapter 4, can be induced to agglomerate into larger particles by the titration of a bad solvent (in this case of hexane or acetonitrile). As can be seen from Figure 5.5 and Figures 5.7 – 5.10, the agglomeration of the MSAs to form larger particles does lead to an intense red-shifted emission. The difference is that the reorganisation process of an aggregate in a bad solvent is severely hindered, by the fact that the volume of space available for the equilibrium binding de-binding kinetics is much more smaller and restrictive, and therefore does not allow an effective re-ordering process. The result is that the titration of a bad solvent can lead to disordered agglomeration of otherwise ordered MSAs. This effectively forms a percolation network in the agglomerate that gives the same spectral

features in the emission spectra as the solid state percolation network of MSAs in a polymer matrix. As can be seen from Figure 5.7 – 5.10, the titration of solvent molecules with a large or small permanent dipole moments will give rise to the same spectral features. Therefore this discounts the possibility that the red-shifted emission occurs because of a bathochromic shift of the PL. This conclusion is confirmed by the solvent dipole dependent shift of N-HBC in solution in Figure 5.10 and plotted in Figure 5.21. As can be seen from the plot, hexane, with no permanent dipole, cannot stabilise the excited state of N-HBC as much as a solvent molecule with a large permanent dipole. In Figure 5.21 only solvent molecules with a permanent dipole > 0 give rise to a red-shift in the emission spectra. Therefore, the appearance of a red-shifted emission peak in the spectra of the hexane solutions cannot be ascribed to a bathochromic/solvatochromic shift. Instead, the red-shifted emission most likely arises from excitons migrating along ordered MSA nanowires/nanotubules to disordered sites that exist at the connection nodes between nanowires/nanotubules in the network (this is illustrated in Figure 5.20). From the curve fit in the plot in Figure 5.21, the energy shift of the emission maximum is observed to scale roughly to the power ~ 0.5 with the permanent dipole of the solvent molecule. This progression has previously been used to determine the dipole of the excited state of N-HBC to be ~ 40 Debye⁸. This value, although comparable to other compounds such as 4-dimethylaminobenzil-4'-nitroanilin, is rather large. In fact, from the plot and emission spectra in different solvents, there appears to be two distinct emission processes centred between 2.2 – 2.3 eV and 2.5 – 2.6 eV, the red-shifted emission and PL respectively. Each of these emissions become more stabilised by an increase in the solvent molecule dipole, however the progression from one to another is not continuous, but rather is discreet. The straight line fits to each emission centre, in Figure 5.21, indicate the relationship of the PL or the red-shifted emission to the solvent dipole.

The conclusion is therefore that red-shifted emission is in fact excimer emission. Excimer emission has been described previously^{9, 10} for high concentration solutions 0.2 M of anthracene. The characteristically broad red-shifted emission of anthracene is found to have a longer lifetime by a factor 1.8 relative to the monomer emission (0.8ns). This increase in the lifetime would agree with our findings that the excimer emission arises from mobile excitons probing a percolation network until they become trapped at an excimer emission site¹¹. Excimer emission is generally agreed to happen at

dislocation sites in a crystal¹² which correlates with the finding that the excimer emission intensity is dependent on the number of nodes in the percolation network. The temperature dependent increase of the excimer emission observed for HBC derivatives, has also been found for anthracene¹³ excimer emission. However in general excimer emission of molecules has been used as an indicator of the transition from monomer to aggregate state. The results presented here, however, confirm that this is a simplification. In fact excimer emission does not indicate aggregation is occurring, rather it indicates that disordered agglomeration of aggregates is occurring. From investigating HBC derivatives, it is clear that aggregates form at much lower concentrations than 0.2 M. The emission from the aggregates does not exhibit any excimer emission at concentrations as high as 10^{-4} M. It is only at higher concentrations or in bad solvents, that the disordered agglomeration leads to red-shifted excimer emission. This is confirmed by spectra of pyrene in cyclohexane¹⁴, which displays a usual PL up to 10^{-4} M. At concentrations above this an excimer band is observed to increase in intensity. Our results therefore suggest that the pyrene spectra, say, at 10^{-5} M is that of the aggregate species of pyrene and not that of the isolated species.

The dislocation sites in crystals are analogous to the disordered junction sites between MSAs. Therefore it is possible that excimer emission is an indicator of the formation of a disordered mesoscopic structure. This would explain why the transition to exciton percolation in the generally more disordered liquid-crystalline HBC-PhC12 doped matrices is less clear than for the much more ordered HBC-C8,2 and N-HBC case. The latter molecules have a clearer percolation threshold because the change to a more disordered system, upon the formation of a percolation network (in terms of what the exciton probes in its lifetime), is much more noticeable if the system is very ordered to begin with. Interestingly Figure 5.12 demonstrates this. The PLE spectra collected at the energy of the red-shifted emission maximum is observed to change upon increasing the dopant loading. Two new peaks emerge in the PLE spectrum of HBC-C8,2 doped matrices at ~ 3.0 eV and 3.2 eV. The spectral position of these peaks are the same as for HBC-PhC12 at medium concentration in solution. In fact the species responsible for these new peaks is the L species of HBC-C8,2. The increase of the positional disorder of molecules in the MSA network nodes and agglomerates has led to the observation for the first time of the L species of HBC-C8,2 (see Chapter 3). Only the C species of HBC-C8,2 is observed in solution, because it is the thermodynamically favourable structure

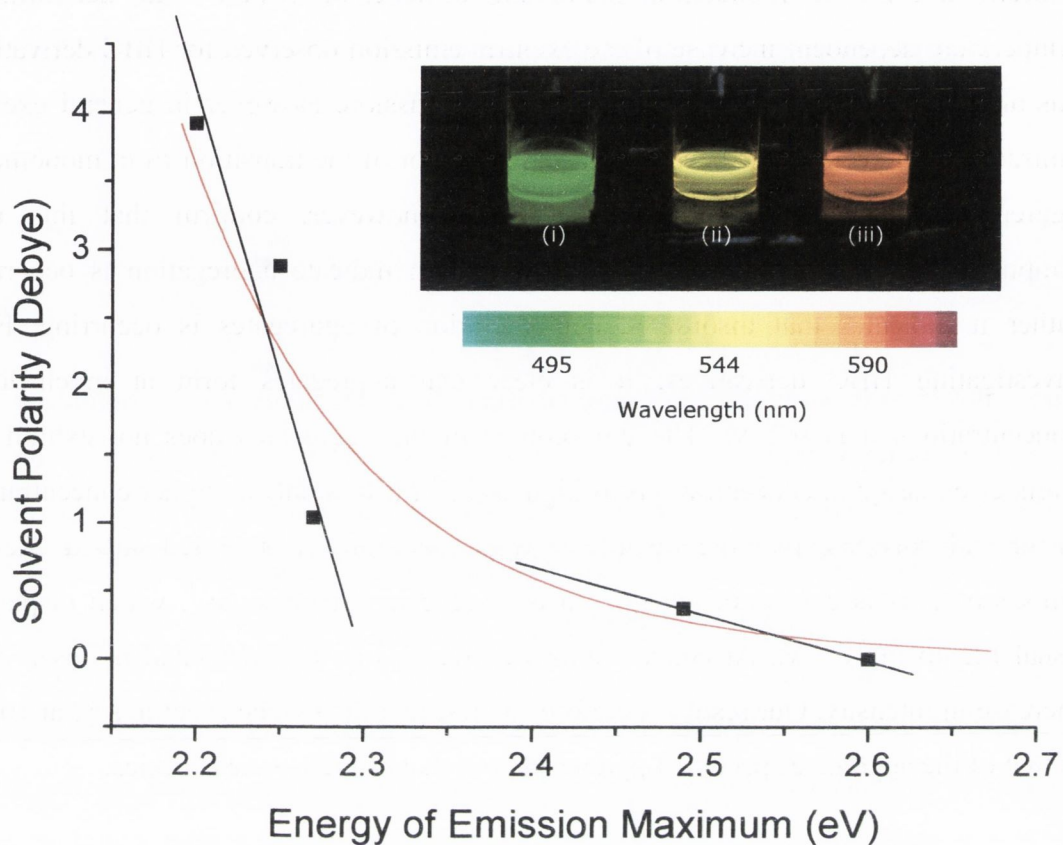


Figure 5.21: A plot showing the relationship between the polarity of the solvent used and the energy of the emission maximum of N-HBC. Inset: a photograph, courtesy of ref [6], illustrating the control of the emission colour of N-HBC by changes in the solvent polarity (i – toluene, ii – chloroform and iii – methanol).

for HBC-C8,2 if allowed to re-organise and equilibrate. The L species was previously observed for F-HBC at high concentration and it is the equilibrium species of HBC-PhC12 in solution. The emergence of this feature does not, however, suggest that the L species are directly responsible for the red-shifted emission. If this were so then medium concentration solutions of HBC-PhC12 would also display the red-shifted emission. This is not the case. Instead the emergence of the L species in the PLE spectra is symptomatic of the formation of disordered networks. These sites may well give rise to more excimer emission but it is the increase in the total disorder of the system, either by a) the formation a disordered networks of ordered MSAs or b) by the agglomeration ordered MSAs into larger particles in a disordered fashion induced by the titration of a bad solvent.

Thus, in conclusion, the reason that the red-shifted emission is observed for high concentration F-HBC solutions in chloroform is that chloroform is a bad solvent for F-HBC. This is confirmed by the fact that sedimentation of aggregates of F-HBC from solution in chloroform is observed for sample solutions at 10^{-3} M.

5.4 CONCLUSIONS

The control of the red-shifted emission via three different sample preparation techniques has allowed the emission processes to be determined. The similarity between the red-shifted emission at high concentration for F-HBC, in bad solvents for all derivatives and in percolation networks, indicates that a similar emission process occurs in all samples. The measured percolation threshold of $\sim 1\%$ is consistent with the formation of percolation networks by 1-D inclusions which have aspect ratios > 100 . Therefore the dependency of the re-shifted emission with the increase in connectivity between nanowires (or nanowire bundles) in the polymer matrix suggests that the red-shifted emission arises from excitons probing these junction sites. Excimer emission arises from the stabilisation of the excited state of one molecule by the ground state of another molecule, therefore these sites will be at lower energy than other non-excimer sites. Migrating excitons that are able to percolate through the nanowire network, are more likely to become trapped at these lower energy sites and therefore radiatively decay at the same sites. The increase in connectivity above the percolation threshold, in essence, funnels excitons to the excimer emission sites. This is confirmed by the large relative increase of the excimer emission compared to the PL at 77 K. The increased survivability of a hopping exciton at low temperature ensures that more excitons may therefore reach an excimer emission site.

From the Hildebrand solubility measurements, the increase of excimer emission was found to be correlated to the degree of aggregate agglomeration induced by the titration of a bad solvent. The agglomerates are in effect disordered networks of aggregates. The disorder is however, only observed for the excimer emission and not the aggregate PL. This indicates that although the nanowire structure may remain ordered, the network formed is disordered. It must be noted that wherever a break in a nanowire occurs, say

by a molecular dislocation, a network junction may form. Therefore any disorder induced in the nanowire structure may lead to the formation of partial networks and therefore contribute to the excimer emission and not the PL intensity.

The spectroscopic measurement of the HBC-C8,2 isolated molecule solubility parameter was found to be much more precise than the high concentration measurements and cloud-point test generally used. The high sensitivity of the desorption rate of isolated molecules to the solvent environment gives rise to sharp decreases in the isolated PL intensity as a function of the solubility parameter of the solvent mixture. For instance the value calculated agrees with the observation that isolated species of HBC-C8,2 were only observable at low concentrations in toluene ($\delta = 18.3$) and not chloroform ($\delta = 18.7$). The slight differences in the Hildebrand parameters measured for the isolated and aggregated species, may indicate the different nature of the surface exposed. This could open the possibility to distinguish between the aliphatic side chains exposed on the surface of a HBC aggregate and the aromatic core that becomes exposed to the solvent in the isolated case.

Finally, the percolation measurements presented are in great measure possible thanks to the quasi 1-D structure of HBC derivatives. The fact that the stacked aromatic cores of the MSA are insulated by an aliphatic mantle, reduces the likelihood of excimer emission occurring from individual bundles (see Chapter 4). The geometry is such that excitons can only freely travel up and down a nanowire/nanotubule. It is because of this quasi one-dimensionality that such a low percolation threshold is achieved. For polymers for instance, excimer emission may occur at considerably lower concentrations due to the fact that polymer aggregates are generally much more disordered. The emergence of excimer bands in the emission spectra of organic molecules has usually been used as an indicator of aggregation. Perhaps because for very disorder aggregate systems, excimer emission may coincide with aggregate formation. However, it is generally believed that at concentrations below the critical concentration for excimer emission, molecules in solution are in the isolated state. This is frequently the litmus test for aggregation. However, the results from HBC derivatives presented here clearly indicate that excimer emission is not a good indicator of the isolated to aggregated state transition. Rather, excimer emission is a good indicator of

the formation of exciton percolation networks in disordered mesoscopic agglomerates of aggregates.

¹ J. Burke, Solubility Parameters: Theory and Application, AIC Book and Paper Group Annual, Vol 3 1984.

² Data from J. Appl. Polym. Sci., **5**(15), 339 (1961)

³ J. Burke, Solubility Parameters: Theory and Application, AIC Book and Paper Group Annual, Vol 3 1984.

⁴ M.Pope, C. E. Swenberg, Electronic Processes in Organic Crystals and Polymers, 2nd Ed, Oxford University Press (1999) p 29.

⁵ I. Balberg, C.H. Anderson, S. Alexander, N. Wagner, Phys. Rev B. **30**, 7, (1984)

⁶ M. Tomura, Y. Takahashi, A. Matsui, Y. Tohji, J. Phys. Soc. . Jpn. 25 1968 647.

⁷ B.E. Kilbride, J. N. Coleman, J. Fraysse, P. Founet, M. Cadek, A. Drury, S. Hutzler, S. Roth, W. J. Blau, J. Appl. Phys, **92** 7 (2002)

⁸ D. Gregg, Ph.D. Thesis, Chemistry Dept. Trinity College Dublin (2004)

⁹ J.K. McVey, D.M. Shold, N.C. Yang, J. Chem. Phys. 65 . 1976 3375.

¹⁰ T. Kobayashi, S. Nagakura, M. Szwarc, Chem. Phys. 39. 1979 105.

¹¹ T. Seko, K. Ogura, Y. Kawakami, H.Sugino, H. Toyotama , J.Tanaka, Chem. Phys. Lett. 291(1998) 438 –444.

¹² M.Pope, C. E. Swenberg, Electronic Processes in Organic Crystals and Polymers, 2nd Ed, Oxford University Press (1999) p 50.

¹³W. Arden, L.M. Peter, G. Vaubel, J. Lumin. 9 1974 257.

¹⁴ J.B Birks, L. G. Christophorou, Spectrochim. Acta, 19 401 (1963)

Chapter 6: New Spectroscopic Insights into the Resonance of Frenkel Excitons in Self-Assembled Molecular Aggregates

In this chapter a new interpretation of optical absorption and luminescence spectra of organic molecules is presented. Reviewing spectra previously published indicates that the prevalence of molecular aggregates and Frenkel exciton resonance (FER) has to date been grossly underestimated. Taking examples from different van der Waals systems such as polymers, molecular self-assemblies (MSA) and molecular crystals, variations of the vibrational-electronic (v-e) transition energy (previously unexplained) can now be interpreted in the framework of disorder-limited FER. Applying the principle of conservation of energy, the photo-absorption-luminescence (p-a-l) cycle of resonant Frenkel excitons in aggregates is explained in terms of the p-a-l cycles of isolated molecules. The method employed to measure the Stokes shift of FER systems, derived from our model, is found to differ significantly from that employed currently. Our postulate, that the aggregate v-e transition energy, in the frame of reference of a resonant exciton, decreases as function of the localisation length of the exciton, is demonstrated by the good agreement of the model with existing data. This has allowed the determination of the localisation length of resonant excitons from readily available absorption and luminescence spectra. As the localisation length is a good indicator of the order of a system, this result will be useful in molecular self-assembly (MSA) research. Results from the model suggest that Frenkel exciton resonance is vibrationally modulated, and the collective exciton eigenstate of a resonant Frenkel exciton can couple the v-e manifolds of $2N$ molecules together via the electronic resonance interaction, even in the absence of direct intermolecular vibrational coupling. In essence, it is demonstrated that the photo-physics of an exciton that is resonant over many molecules is fundamentally determined by the photo-physics of the isolated molecule just as one would expect. Our contribution is to highlight the necessity of a reinterpretation of many published molecular spectra in terms of exciton resonance in aggregates.

6.1 INTRODUCTION

It is generally accepted that control of molecular interactions leading to tailored molecular aggregation will soon provide the complexity and economy-of-scale required for advanced nanotechnology applications. This is part of a natural progression of research, from atomic interactions and the formation of molecules, to the study of molecular interactions and the formation of molecular aggregates. Historically more attention has been devoted to the detrimental effects of uncontrolled aggregation, as in laser dyes¹. However, today the advent of controlled aggregation², inspired by self-assembly in biology³⁻⁵ suggests the ability to create complex and functional structures using molecular self-assembly⁶ (MSA). Optical spectroscopy is a useful tool to investigate molecular aggregation⁷⁻⁹ and other molecular phenomena. However, its usefulness to date is limited because experimental optical spectra are generally incompatible with the photo-absorption-luminescence (p-a-l) cycle described by the Stokes model for isolated molecules¹⁰⁻¹¹. Comparing optical spectra of many similar dye molecules¹² reveals variations that are much better explained by the next step in complexity: the molecular aggregate structure and Frenkel exciton resonance (FER). Taking general examples of molecular optical spectra in solution and solid state, it is demonstrated that a conservation of energy model, in the framework of disorder-limited FER, typical of van der Waals aggregates, successfully explains observed trends in the spectra as a function of aggregate morphology order (such as the variation of the vibrational-electronic (v-e) transition energy). The aim is to link together all organic, van der Waals materials under one general exciton model to describe the electronic and v-e structures of optical spectra of organic molecules from isolated to crystalline form. These materials are characterised by weak intermolecular charge sharing, weak intermolecular vibronic coupling, large effective charge screening and strong FER. From the model, the p-a-l cycle of 1D resonant Frenkel excitons and the correct method for measuring the Stokes shift (E_S) are determined and shown to agree with experimental evidence. Mechanisms of FER, exciton migration and photo-exciton quenching, elucidated from the model, are also found to correlate well with general observations. However, the most useful result from the model will facilitate MSA research. With molecular aggregation, the most obvious measure of order is given by the coherence length of the ordered alignment of molecules in an aggregate. In terms of the optical response of a system, this measure translates into the FER range (localisation

length). Using our simple model, now it is possible to extract the localisation length of resonant excitons from the electronic and v-e structure of easily available optical spectra. Our model indicates that, as expected, the v-e relaxation of a resonant exciton is fundamentally determined by the v-e relaxation of the isolated molecule. It will be shown that the resultant E_S is in fact independent of the localisation length of 1-D resonant excitons, due to the decrease of the v-e relaxation energy per molecule as a function of localisation length. In summary, the properties of spectra of small molecules, polymers and large macromolecules are in agreement with the model, indicating that the prevalence of FER has been underestimated to date. Our assessment is that a given molecule has an overwhelming tendency to form aggregates of a particular structure (with some characteristic variance in the order). The main conclusion is that a re-interpretation of many published optical molecular spectra is required in terms of molecular aggregates and, more specifically, resonant photo-excitons.

FER describes the process whereby one excitation quantum^{13,14} is distributed over $2N$ molecules. The ideal conditions for FER are found wherever there exists a collection of identical molecules e.g. solution or solid state samples. It should be noted that in contrast to inorganic crystals, delocalisation does not necessarily involve electron-hole separation. No separation is required for exciton resonance as only the energy of the intra-molecular Frenkel exciton is resonant^{15,16}. The total aggregate size can be much larger than $2N$ because FER is limited by the degree of disorder in the alignment and position of the optical transition dipoles of molecules in an aggregate. The influence of the resonance range on the electronic structure of spectra has been shown to determine the oscillator strength and full-width-half-maximum (FWHM) of optical transitions (through exchange-narrowing¹⁷), and the increase/decrease of symmetric/anti-symmetric transitions energies with respect to the isolated species transition energy¹⁸. FER effects have been extensively studied and reported in the literature. Overall, however, the origin of E_S for resonant Frenkel excitons has not been conclusively determined¹⁹. Similarly, there is no satisfactory p-a-l cycle for resonant excitons^{20,21} that can explain observed changes to v-e structure upon aggregation²². Two examples of inconsistencies with current interpretations are: first, the unrealistically small $E_S \sim 0$ that is often reported for organic molecules – upon aggregation the dominant absorption and emission peaks can be coincident in energy, giving the impression that E_S has reduced

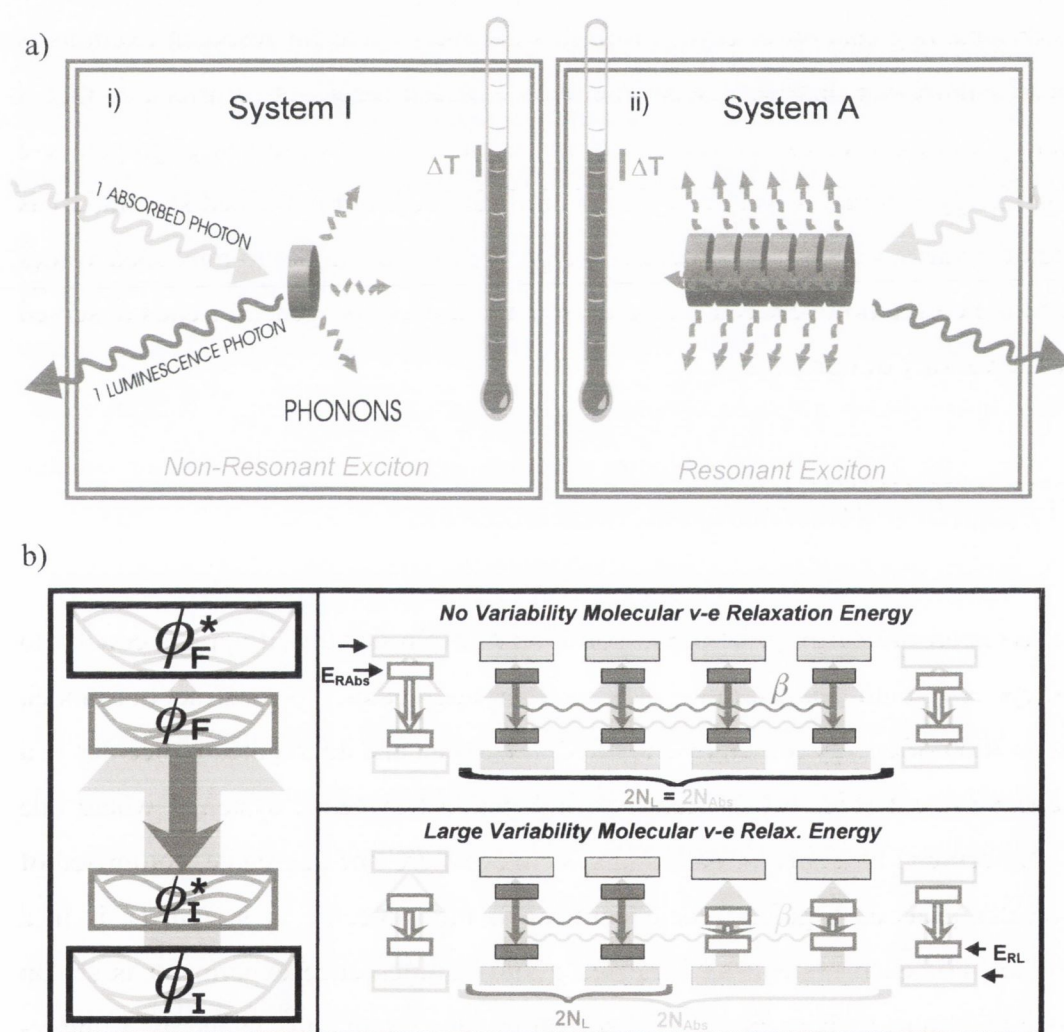
practically to zero^{23,24,11}. Secondly, the un-explained morphological dependencies of the relative intensities of fine structures in optical spectra – which is ascribed to the variability of the aggregate structure influencing the relative intensities of J and H aggregate FER v-e peaks.

It will be shown that by applying the conservation of energy principle, the relationship between the energy losses of an exciton on an isolated molecule, and the energy losses of a resonant exciton on an aggregate, can be determined, regardless of the exact underlying mechanisms involved. It is demonstrated that the total energy converted to phonons by a resonant exciton is predetermined by the non-resonant case (including some additional aggregation effects). From this the p-a-l cycle for resonant excitons is constructed, indicating that the current method of measuring E_S is incorrect, in that it significantly underestimates its value. From the model, the observed aggregate v-e transition energy is found to vary as a function of $(2N)^{-1}$. From published spectra, $2N$ is calculated for various aggregate systems. The good fit of the model to published values of $2N$ and the correlation between predictions of the model and general trends observed indicate the validity of our model.

6.2 GEDANKENEXPERIMENT

The conservation of energy principle is paramount in physics and it applies equally to the p-a-l cycles of both isolated molecules and their aggregates. To construct our model, the conservation of energy principle is applied to isolated and aggregated molecules in a gedankenexperiment (Fig. 6.1a). Take two independent systems: system I where one isolated molecule is in a solvent bath and system A where one aggregate, comprised of $2N$ molecules grouped together (each identical to the molecule in system I), is in a solvent bath. For each system, an idealised photo-luminescence experiment is set up where one photon of a given energy is absorbed by the system and the energy of the re-emitted photon is measured. The difference in energy between the absorbed and emitted photons is equal to the total vibrational relaxation (V-R) energy of the molecules in a system, E_S (for this gedankenexperiment molecule-solvent relaxation interactions and rotational relaxation mechanisms are ignored). During V-R, a certain number of phonons of a given energy are emitted by the photo-excited molecules and subsequently

absorbed by the solvent bath. The solvent bath is monitored and any temperature increase is recorded after one photon is absorbed and emitted. The temperature is used as a guide and is not to be thought of as a precise way of comparing both systems. The energy absorbed by each solvent bath is comparable. However, the temperature increase of the solvent bath, ΔT , is convenient to describe changes to each system as it is related to the total energy gained (and the gain in entropy of the bath). The total energy gained by each solvent bath will be dependent on the total V-R energy emitted by the relaxing exciton on the molecules, where the total V-R is equal to the total number of phonons emitted \times the energy of each phonon.



the temperature of the solvent bath. Conservation of energy dictates that if values of E_S for both systems are equal then the temperature increase of the solvent baths should also be of the same order magnitude (there will be a slight difference in the entropy gained by each system due to system A having more molecules in resonance). However, the energy absorbed by the solvent bath in both systems will be equal regardless of the exact underlying v-e relaxation mechanism (therefore $\hbar\omega_{pA} < \hbar\omega_{pI}$) if the Stokes shifts are the same. b) Illustration of how the localisation length $2N$, for resonant excitons in real systems with fixed (top) and variable (bottom) v-e relaxation energies, depends on how many molecules have the same transition energy. Light grey arrows represent electronic transitions from the ϕ_I to ϕ_F^* states (absorption) and dark grey arrows represent electronic transition from the ϕ_F to ϕ_I^* states (luminescence). Filled arrows represent transitions that are in resonance. Notice how, for the system with variable v-e relaxation $N_L < N_{Abs}$.

The absorption of one photon of $\hbar\omega_{00Abs}$ energy by system I promotes an electron from the ϕ_I to ϕ_F^* molecular electronic state generating one exciton on the isolated molecule (Fig. 6.1b). In the new force-field, the excited molecule then undergoes V-R, releasing excess energy by emitting S_{Abs} phonons of $\hbar\omega_{pAbs}$ energy each during the change of the isolated molecule configuration from the ϕ_F^* to ϕ_F state. The exciton then decays by changing from the ϕ_F to ϕ_I^* state by emitting a photon of $\hbar\omega_{00L}$ energy. Again in a new force-field, the molecule emits S_L phonons of $\hbar\omega_{pL}$ energy each during V-R from the ϕ_I^* to ϕ_I state. The Stokes energy balance equation for the p-a-l cycle of an isolated molecule, neglecting solvent relaxation effects is therefore

$$\underbrace{\hbar\omega_{00AbsI} - \hbar\omega_{00LI}}_{\text{Electronic Energy}} = \underbrace{S_{AbsI}\hbar\omega_{pAbsI} + S_{LI}\hbar\omega_{pLI}}_{\text{Vibrational-Electronic Energy}} \quad (6.1)$$

where the subscripts I represents isolated molecules, Abs refers to absorption, L refers to luminescence, p represents phonons, 0-0 is the phonon transition of an electronic transition and the variable S is the Huang-Rhys (H-R) parameter (see also Table 6.2). The H-R parameter is a measure of the number of phonons involved in the V-R of a molecule^{25,26}. With the general assumption that both halves of the p-a-l cycle are symmetrical i.e. $S_I = S_{AbsI} = S_{LI}$, then for system I, $2S_I$ phonons are emitted during V-R (an example of an asymmetrical p-a-l cycle is discussed later). E_S is therefore given by the sum of the v-e relaxation terms for both halves of the p-a-l cycle²⁷ $E_S = E_{RAbs} + E_{RL} = 2S_I\hbar\omega_{pI}$.

For system A on the other hand, the absorption of a photon by the aggregate leads to FER. Resonance will only occur if each of the $2N$ molecules has the same electronic transition energy $\hbar\omega_{00}$. A good review of the physical principles of FER can be found in references¹³⁻¹⁵. The general equations, describing the electronic transition energies of a 1-D resonant one-exciton^a $|\Phi_{\pm}\rangle = \frac{1}{\sqrt{2N}} \sum_{-N}^{+N} |\phi_n\rangle$, are given by¹³,

$$\text{a) } |\Phi_{\pm}\rangle = \frac{1}{\sqrt{2N}} \sum_{-N}^{+N} |\phi_n\rangle \quad \text{b) } \hbar\omega_{\pm} = \left(\frac{1}{2N} \sum_{-N}^{+N} \hbar\omega_{n00l} \right) \pm \beta \quad (6.2)$$

where $|\Phi_{\pm}\rangle$ are the symmetric and anti-symmetric exciton eigenstates, $|\phi_n\rangle$ are the basis eigenfunctions of the individual molecules, $\hbar\omega_{\pm}$ are the symmetric and anti-symmetric eigenvalues, $\hbar\omega_{n00}$ is the isolated molecule electronic transition energy of the n^{th} molecule (Fig. 6.1b) and β is the resonant transfer interaction energy. The one-exciton collective eigenstate in Eq. 6.1a, is the result of a normalised superposition of the individual molecule basis states. In Eq. 6.2b, the eigenvalues for the collective exciton eigenstates are given. The averaging of $\hbar\omega_{n00l}$ leads to a process known as exchange-narrowing¹⁷ that reduces the observed variance in the electronic energy. Variances of the resonance interaction energy term β in Eq. 6.2b and exchange-narrowing of β are not considered here because this model is more concerned with V-R. The interaction energy β , will increase or decrease the amount of energy a photon must have in order to photo-excite the molecule into its molecular electronic excited state ϕ_F^* . This state is $\hbar\omega_{00Absl}$ higher in energy than the energy of the ϕ_l electronic state, although when probed optically it will be measured as $\hbar\omega_{00Absl} + \beta$. Therefore, although there is a transition dipole-dipole interaction, the photo-physics of a resonant exciton is fundamentally determined by the basis states of $2N$ isolated molecules²⁸. During resonance, Eq. 6.2a states that the one exciton has equal probability of residing on any of the $2N$ molecules, therefore the V-R of the electronic energy levels of all $2N$ molecules must be equal (see Fig. 5.1b). This ensures that the electronic transition energy of each of the $2N$ molecules is monoenergetic, allowing resonance to occur during luminescence with $2N_{Abs} \sim 2N_L$ (as is generally observed). If the opposite case is considered briefly, the collective exciton state, delocalised over $2N$ molecules, would have a localised V-R relaxation, say on only one molecule of the $2N$ molecules. If only one molecule of the $2N$ molecules emits phonons, then the exciton would become localised on this molecule. If this were the case, then the luminescence would not have

the spectroscopic signature of FER. However FER signatures are observed in the luminescence. Therefore in the above framework, the condition for resonance requires that every molecule in resonance emits phonons. The number of phonons emitted during V-R in system A will therefore be $2N2S_I$. For the moment $S_A = S_I$ will be assumed. In fact, the number of phonons emitted per molecule S typically increases from monomer to dimer¹³ i.e. experimentally $S_A > S_I$. However, the lack of charge sharing and weak intermolecular vibronic coupling gives rise to very weak intermolecular vibronic modes. Consequently, the dominant vibronic modes observed are the intramolecular vibronic modes. This means that the observed H-R parameter in the optical spectra is an average of the number of phonons emitted by each molecule and not the sum over all $2N$ molecules. In fact since each molecule has $1/2N$ probability of having the exciton on it, then the probability of emitting a phonon must be the same for each molecule of the $2N$ molecules. Hence, each molecule in system A emits S_A phonons, giving a total V-R energy of $2N2S_A\hbar\omega_{pA}$. The energy of the emitted phonons is the unknown factor, but it must be the same for each molecule in order for all the molecules in the aggregate in system A to vibrationally relax to the same energy (Fig. 6.1b). This is the condition for FER in the luminescence. If each $2N$ molecule relaxes by emitting a different number of phonons then each molecule will relax to a different energy - this would make FER in the excited state impossible.

From Eq. 6.1, if the temperature increase for a system is determined by the total energy absorbed by the bath, then the temperature increase is determined by the total v-e relaxation energy of the resonant exciton. According to the principle of conservation of energy, if values of E_S recorded for system I and A are the same then the temperature increase of the solvent bath for system I and A must also be of the same order of magnitude i.e. if $E_{SA} = E_{SI}$, then $\Delta T_A \sim \Delta T_I$. Otherwise, a system with $2N = 2000$ molecules will heat up roughly by a factor 1000 more than a system with $2N = 2$ - even for the same Stokes shift! The latter can't be the case, therefore the experiment becomes interesting, because for resonance to occur in system A, a factor $2N$ more phonons of correspondingly lower energy must be emitted by system A compared to system I without any change to the total V-R energy, $2N2S_A\hbar\omega_{pA} = 2S_I\hbar\omega_{pI}$ (Fig. 6.1a). The conservation of energy principle dictates that in order to compensate for the increase in the total number of phonons emitted (the condition that FER can be observed in the

luminescence), the energy of each phonon emitted in system A must be less than the energy of the phonons emitted in system I i.e. $\hbar\omega_{pA} < \hbar\omega_{pI}$. This is an important result, as it describes a change to the observed aggregate v-e transition energy as a function of the number of molecules in resonance. In turn, this will allow $2N$ to be determined from absorption and luminescence spectra.

To demonstrate the validity of above result, consider the opposite case, where each molecule in system A relaxes by emitting the same number of phonons of the same energy as in system I. As briefly described above, this un-physical result implies that for one photon and the same E_S (the energy absorbed by the system), the increase in temperature of the solvent bath for system A is a factor $2N$ more than for system I (i.e. for the same E_S , $\Delta T_A \gg \Delta T_I$). This contradicts the conservation of energy principle and, as will be shown, it doesn't correlate with real experimental results. It could be argued that in order to satisfy the conservation of energy, S_A decreases as a function of $(2N^{-1})$ and $\hbar\omega_{pA} = \hbar\omega_{pI}$ (see Appendix B). However, as will be shown this is not observed experimentally. Therefore, the gedankenexperiment demonstrates that the observed aggregate v-e transition energy, $\hbar\omega_{pA}$, must be a function in some respect of the number of molecules in resonance in an aggregate.

6.3 RESONANCE IN REAL AGGREGATE SYSTEMS

To a first-order approximation the vibrational frequency ω_{pI} is unperturbed by aggregation if there is no strong intermolecular vibronic coupling. However, according to the model the v-e transition energy of the aggregate, in the frame of reference of the resonant exciton, is lower in energy than $\hbar\omega_{pI}$. If the aggregate v-e transition energy were to remain the same as the isolated v-e transition energy, the p-a-l cycle superposition would increase E_S unrealistically as a function of $2N$. In this case, the natural variance in $2N$ would result in very broad PL from an ensemble of FER aggregates (because the energy of the luminescence maximum would be a function of $2N$, thus any variability in $2N$ would broaden the PL spectra but not the absorption spectra). Characteristically, this is not observed. As the aggregate v-e transition energy

$\hbar\omega_{pA}$ is different to the isolated molecule v-e transition energy $\hbar\omega_{pl}$, the Stokes energy equation of an aggregate in terms of the experimental observables, ignoring β in Eq. 6.2b, is given by

$$\frac{1}{2N} \sum_{-N}^{+N} \hbar\omega_{00,AbsI} - \frac{1}{2N} \sum_{-N}^{+N} \hbar\omega_{00,LI} = \sum_{-N}^{+N} S_{AbsA} \hbar\omega_{pAbsA} + \sum_{-N}^{+N} S_{LA} \hbar\omega_{pLA} \quad (6.3)$$

where all subscripts have their usual meaning and A represents aggregates. In Eq. 6.2a only the purely electronic energy is normalised as the equation describes a one-exciton state. The lack of a direct intermolecular vibrational coupling results in no normalisation of the overall vibrational energy. Therefore, the electronic transition energy is averaged while the v-e relaxation is summed over the contributing molecules. To generalise the gedankenexperiment and allow comparisons to real experiments, the possibility that E_S of system I and A are not equal must be incorporated. To achieve this, the ratio of the aggregate to isolated E_S , R , is included in the expression describing the conservation of the *total vibrational energy*. This is constructed by equating the total V-R energy of Eq. 6.1 and Eq. 6.3, with the usual assumption that the absorption and luminescence processes are symmetric,

$$\begin{aligned} R2S_I \hbar\omega_{pl} &= 2N2S_A \hbar\omega_{pA} \\ R \frac{S_I \hbar\omega_{pl}}{2N} &= S_A \hbar\omega_{pA} \end{aligned} \quad (6.4)$$

This equation describes the inverse scale relationship of the reorganisation energy per molecule for each half of the p-a-l cycle, $S_A \hbar\omega_{pA}$, with respect to the resonance range $2N$ (see Fig. 6.2). From the expression for the V-R energy per molecule (Eq 6.4.) and using the ratio $k = S_A/S_I$, the *energy per phonon* of system A with respect to system I is

$$\hbar\omega_{pA} = \frac{R}{k} \frac{\hbar\omega_{pl}}{2N} \quad (6.5)$$

This equation describes the v-e transition energy of the resonant exciton with respect to the v-e transition energy of the isolated molecule for $N \geq 1$ where R/k is the energy partitioning coefficient. If this is the case then Eq. 6.3 becomes:

$$\begin{aligned}
 \text{a) } \frac{1}{2N} \sum_{-N}^{+N} \hbar\omega_{00Absl} - \frac{1}{2N} \sum_{-N}^{+N} \hbar\omega_{00LI} &= \sum_{-N}^{+N} S_{AbsA} \frac{R\hbar\omega_{pAbsl}}{2kN} + \sum_{-N}^{+N} S_{LA} \frac{R\hbar\omega_{pLI}}{2kN} \\
 &\text{or} \\
 \text{b) } \frac{1}{2N} \sum_{-N}^{+N} \hbar\omega_{00Absl} - \frac{1}{2N} \sum_{-N}^{+N} \hbar\omega_{00LI} &= R \left(\sum_{-N}^{+N} \frac{S_{Absl} \hbar\omega_{pAbsl}}{2N} + \sum_{-N}^{+N} \frac{S_{LI} \hbar\omega_{pLI}}{2N} \right)
 \end{aligned}
 \tag{6.6}$$

Eq. 6.6(a) and Eq. 6.6(b) describe the p-a-l cycle of a collective one-dimensional exciton eigenstate localised over $2N$ molecules, in terms of the isolated molecule electronic and v-e transition energies, by taking into account changes to the e-p coupling and other V-R processes via the ratios k and R . By comparing the aggregate p-a-l cycle in Eq. 6.6(b) with that of the isolated molecule in Eq. 6.1, it is evident that in both cases the total V-R of the exciton is determined in some respect by $S_I \hbar\omega_{pI}$. This statement reflects the fact that when integrating over all space the amount of energy lost by the collective exciton (by the molecules upon which it resides emitting phonons with a certain probability) must be equal within a factor R/k to the total energy lost by the isolated molecule – otherwise there is no conservation of energy. To illustrate this, *if* say, a resonant exciton *could* be re-localised onto just one molecule in an aggregate, one would expect $2N-1$ molecules to un-relax and 1 molecule to fully relax by an amount equivalent, within a factor R/k , to the isolated V-R. This is because the probability of finding an exciton on the $2N$ molecules is unity for a one-exciton FER state. Therefore from Eq. 6.6, with FER, the individual molecule reorganisation energy $S_A \hbar\omega_{pA}$, given by the normalised v-e relaxation of the isolated molecule, now scales inversely with $2N$, making the experimentally observed E_S invariant with $2N$. An ensemble of aggregates with FER will therefore have a sharp PL, as is observed.

Illustrated in Fig. 6.2 is the p-a-l cycle of a resonant exciton constructed from Eq. 6.6. With charge sharing unfavourable, the electronic transition energies of the collective eigenstates are not permanent energy levels of the system, but momentary levels arising from nearest-neighbour transition dipole interactions during photon absorption and emission i.e. in the presence of the photon electric field. For example, a symmetric optical transition of an H-aggregate requires β extra energy to do work on the transition dipoles in order to overcome the energetically unfavourable symmetric transition dipole interaction and excite a collective exciton eigenstate of $\hbar\omega_{00Absl}$ energy. However the only states that are observable when probed optically are the $\hbar\omega_{00Absl} \pm \beta$ states. If there

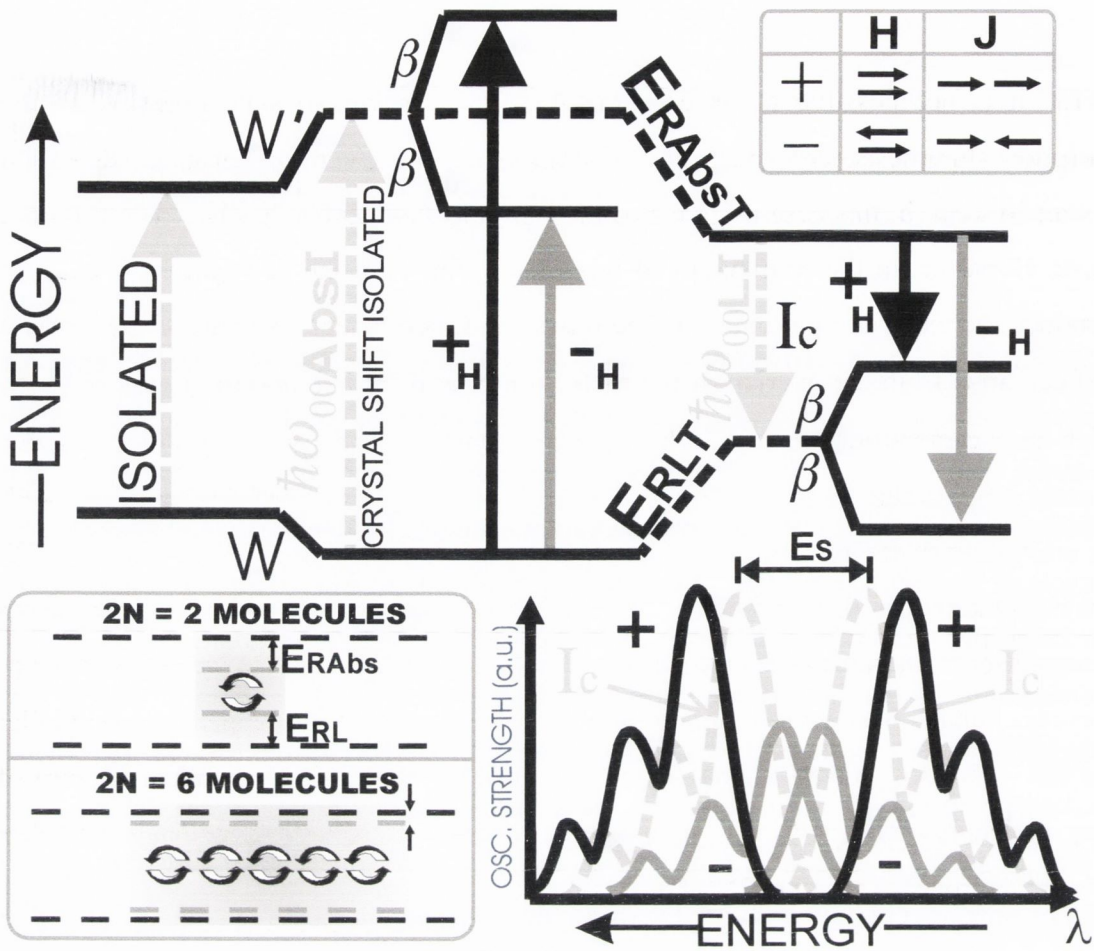


Figure 6.2: Photo-absorption-luminescence cycle of resonant Frenkel excitons showing how E_S is related to the relaxation of the “crystal shifted” isolated molecule energy levels (I_C). All symbols have their usual meaning. W is the ground state Coulombic interaction or intermolecular ground state binding energy (tends to zero for non-polar molecules), W' is the excited state-ground state interaction (can be positive or negative). For the electronic transitions in the p-a-l cycle, + is the symmetric and - is the anti-symmetric electronic transition of an H-aggregate (opposite for J-aggregates e.g. $+_H$ transition is re-labelled $-_J$ etc.). An illustration of the non-convoluted optical spectrum of the p-a-l cycle is also given (from transition dipole interactions, the + transition will have most of the oscillator strength). Experimentally, the spectrum is a superposition of the + and - transition (I_C is illustrated but not observed). Often, this superposition, and especially any significant inhomogeneous broadening, will make the v-e peaks unresolvable. For coincident J absorption and PL, $E_{RAbsT} = E_{RLT} = RS\hbar\omega_{pl} = \beta$. The effect of the resonance range $2N$ on the potential barrier, $2S_A\hbar\omega_{pA}$, between relaxed and un-relaxed molecules that will influence exciton migration is also shown. Care must be taken when interpreting a diagram involving probabilities. The energy levels shown represent the relaxation is the probability is unity, however other arrangements are possible (see Appendix B).

is FER it is not possible to observe the $\hbar\omega_{00AbsI}$ (or $\hbar\omega_{00LI}$) state optically in the absorption (luminescence) spectrum. A splitting of the electronic ground state of a resonant system, in this case to give two FER ground state levels, has not been reported before. However, in the framework of this model, this splitting is required in order to reproduce the experimental data. On the other hand, permanent splitting of the HOMO level can arise from the overlap of the π -electron orbitals of neighbouring molecules. In which case π -electrons can readily be exchanged between neighbouring molecules in a resonant process that leads to splitting (although in our case no particles are exchanged, just energy from the transition dipole). Evident in Fig. 6.2 is the absorption and PL mirror-symmetry of the symmetric and anti-symmetric transitions that often causes aggregate spectra to be mistaken for isolated molecular spectra. More importantly the p-a-l cycle explains how with an interaction β , the Stokes shift will appear much smaller than the isolated molecule Stokes shift. This could explain why the optical spectra of many molecules with a clearly visible vibrational-electronic structure have a Stokes shift that approaches zero i.e. $2NS\hbar\omega_{pl} \gg E_S$.

Typically, when the absorption symmetric transition of a J-aggregate is coincident in energy with the PL symmetric transition (anti-symmetric transition for H-aggregates), E_S is incorrectly measured as zero. The lack of a significant solvent relaxation of non-polar aggregated molecules and the mistaken belief that the e-p coupling decreases because the aggregate is a rigid system, akin to inorganic crystals, has fuelled this incorrect idea. In order for a molecular aggregate system to become rigid, intermolecular covalent bonds would have to form. This is not the case for van der Waals systems. For large aggregates, the vast majority of molecules do not lie on the surface, hence the negligible solvent relaxation¹⁰. From our model and Fig. 6.2, coincident absorption and PL can only occur when $E_{RabsT} = E_{RLT} = \beta$ therefore,

$$2NS_A\hbar\omega_{pA} = \beta \tag{6.7}$$

This is often termed J-resonance, however from Fig. 6.2 it is clear that this condition only arises when the crystal shifted isolated molecular electronic states vibrationally relax by an amount equal to β . The condition of J-resonance can be used to calculate $2N$ from Eq. 6.7. For J-resonance $2N = \beta / (S_A\hbar\omega_{pA})$ or using the relationship $S = g^2$, where g is

the e-p coupling, $2N = \beta / (g_A^2 \hbar \omega_{pA})$. This is very similar to a qualitative function²⁹ f used to describe the v-e properties of resonant excitons $f = \beta / g_A \hbar \omega_{pA}$ (derived from the ratio β / g_A where β is in units of $\hbar \omega_{pA}$). Our equation is quantitative and has similar limits. If β is very small, the molecules in an aggregate are essentially electronically uncoupled, therefore the vibrational properties of the exciton are those of the isolated molecule. If β is very large, compared to $g_A^2 \hbar \omega_{pA}$, the v-e structure of resonant excitons digresses from that of the isolated molecule. Our model arrives at the same conclusions in a quantitative manner that matches data from the whole spectrum of FER ranges of different molecular van der Waals systems.

If the isolated E_S is unknown or difficult to measure experimentally, the special case of coincident J absorption and emission peaks can be used to determine R/k . Substituting Eq. 6.5 into Eq. 6.7 gives:

$$\frac{R}{k} S_A \hbar \omega_{pl} = \beta \quad (6.8)$$

This expression describes the relationship between the ratio of E_S and the ratio of the H-R parameter for J-coincident absorption and emission peaks. Thus, the isolated molecule vibrational frequency ω_{pl} , the e-p coupling ($g_I^2 = S_I$) and the aggregate morphology (sets β and modifies $g_I \rightarrow g_A$) all determine if J-resonance occurs. If Eq. 6.8 is substituted into Eq. 6.6, E_S for J-resonance is 2β and therefore invariant with N . Therefore a notable result of this model is that for any given β the FER range can assume any value, not only in the case of J-vibrationally assisted resonance (N.B. FER is disorder-limited).

A significant outcome of the model and the p-a-l cycle in Fig. 6.2 is that the method of measuring E_S of an isolated molecule³⁰ is not correct for aggregates per se. In optical spectra of aggregates, both the symmetric and anti-symmetric transition peaks must be considered and typically both are observable (for polar molecules the permanent dipole-permanent dipole interaction tends to align the molecules in favour of one of the transitions). Measuring from the lowest energy absorption peak to the highest energy luminescence peak is incorrect as this ignores the symmetric/anti-symmetric transition of H/J aggregates respectively (see Fig. 6.2). It creates the false impression that E_S has

reduced practically to zero upon aggregation and FER, and incorrectly suggests that E_S of the symmetric and anti-symmetric transitions differ by an amount 2β . There is no reason why a dimer should have zero V-R, when as a monomer it significantly relaxes with an appreciable E_S . Unfortunately this has been the method applied to the optical spectra of known FER aggregate systems as well as many spectra where it was believed the species observed was isolated. Our model indicates that experimentally, E_S should be taken as the difference between the average of the symmetric and anti-symmetric absorption transitions and the average energy of the symmetric and anti-symmetric emissive transitions. In this framework, transitions of both symmetries have the same total reorganisation energy (and hence E_S) determined by the relaxation of the isolated molecule energy levels (Fig. 6.2).

What is surprising is that experimentally $\hbar\omega_{pA} = \hbar\omega_{pI}$ is generally not observed (except, as will be shown, for systems with $2N \sim 2$ molecules). For large FER range systems, the v-e peaks seem to disappear (see PICa in Figure 6.3(b)). From the gedankenexperiment, either S or $\hbar\omega_{pA}$ must decrease with respect to the isolated molecule if resonance is to satisfy the conservation of energy principle. A reduction in S would lead to a decrease of the V-R per molecule, although it does imply that aggregation makes the system more rigid. With FER this is unlikely to be the case. FER is a dipole-dipole interaction that can occur between molecules that are physically not in contact with each other. Instead, as will be shown, it appears that S increases slightly from nearest-neighbour interactions. Therefore to conserve energy $\hbar\omega_{pA} < \hbar\omega_{pI}$. The conclusion is that although the observed $\hbar\omega_{pA}$ varies inversely with $2N$, the resonant exciton total V-R, E_S , is fundamentally determined by $S\hbar\omega_{pI}$.

6.4 COMPARISONS TO EXPERIMENT

To demonstrate changes in $\hbar\omega_{pA}$ as a function of N , the absorption/photo-luminescence-excitation (Abs/PLE) and photo-luminescence (PL) spectra of three materials, methyl-substituted ladder-type poly-(para-phenyl) (mLPPP)³¹, alkyl-substituted hexa-*peri*-hexabenzocoronene^{32,33} (HBC-C8,2) and a Pseudo-Iso-Cyanine dye analogue³⁴⁻³⁶ (PICa), are shown in Fig. 6.3a and 6.3b. The optical spectra in Fig.6.3, from the author's

laboratory or reproduced from published spectra (references are given), demonstrate the wide distribution of FER ranges possible and help to illustrate the variances of $\hbar\omega_{pA}$ that are typically observed for planar aromatic compounds (despite weak intermolecular vibronic coupling of van der Waals systems). In Table 6.1, values of the experimental observables obtained from the spectra and an additional two molecules PIC³⁷ (Pseudo-Iso-Cyanine) and TBDC^{38,39} (another cyanine based dye) are given.

According to our model, when aggregation begins, system order will increase in many cases. This initial ordering, increments the FER range $2N$ from 1 to 2. The change, from monomer to dimer, is exemplified by exchange-narrowing of absorption and PL peaks, and splitting of isolated absorption and PL peaks into two peaks separated by 2β . From our model, changes to the v-e transition energy can be very small if $R/k \sim 2$; even though an increase of E_S is observed. For example, for mLPPP, $R/k = 2$, therefore from Eq. 6.5, $\hbar\omega_{pA} = \hbar\omega_{pI}$ for $2N = 2$.

For $2N > 2$, the following changes are expected: further exchange-narrowing of absorption and PL peaks, a decrease of $\hbar\omega_{pA}$ and no further change to E_S . Therefore, the larger N (for $N \geq 1$), the smaller the FWHM of the v-e peaks and the closer the v-e peaks become, without any change to the aggregate E_S .

The PLE and PL spectra of HBC-C8,2 isolated molecules, obtained at 10^{-13} M in toluene, are typical of molecular monomer species (including those of TBDC and PIC). These are characterised by inhomogeneously broadened peaks, with $S_I \sim 0.5$, a large $\hbar\omega_{pL}$ (compared to higher concentration aggregated species) and hence an appreciable E_S . It should be noted for isolated HBC-C8,2 molecules, the observed E_{SI} is greater than the calculated E_{SI} because of the extra solvent relaxation⁴⁰ of an isolated species. As the concentration of HBC-C8,2 molecules is increased from 10^{-13} M to 10^{-6} M, FER leads to splitting of isolated absorption and PL peaks into two peaks separated by 2β , and

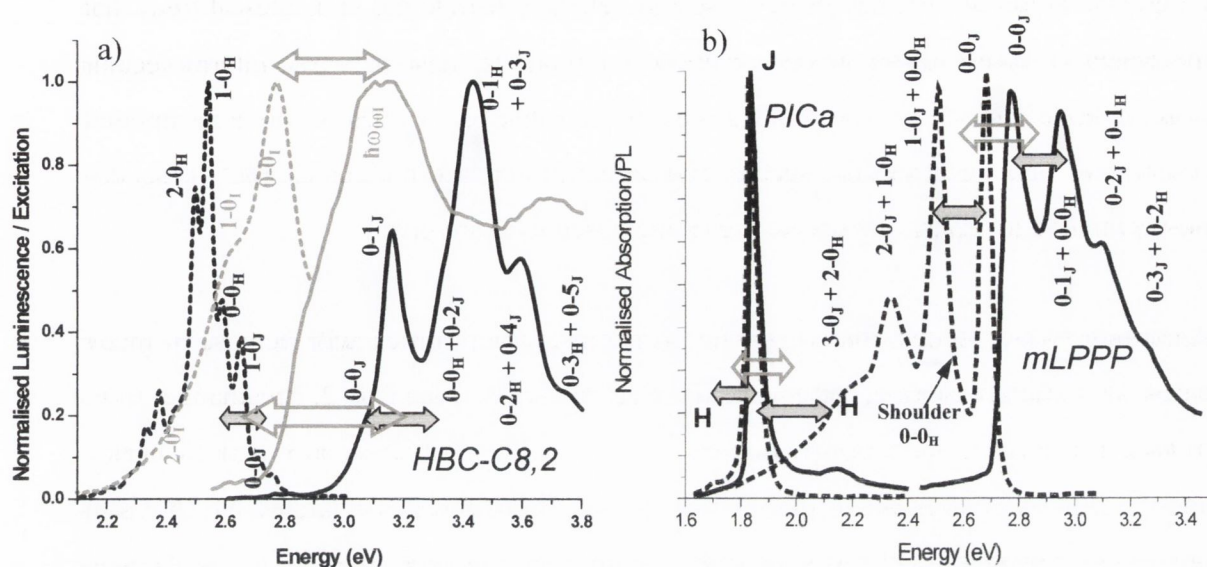


Figure 6.3: The absorption/PLE (solid line) and PL (dashed line) of a) isolated molecules at 10^{-13} M of HBC-C8,2 (grey) and its MSA aggregate at 10^{-6} M (black) from (32) b) Spectra reproduced from ref [28] and [31-33] of mLPPP polymer and PICa small molecule in solid state. The v-e transitions associated with an electronic transition are shown. Most peaks observed in the spectra are a super-position of 2 v-e peaks: one from H and one from J transitions (see Fig. 6.2). The slight mismatched overlap of the v-e transition peaks, from both collective exciton transitions, leads to broadening of the observed peaks. Notice how for mLPPP the higher vibrational H transitions are always broader. Space permitting, the first v-e peak transition label's subscript refers to the dominant electronic transition: H = symmetric H aggregate transition, J = symmetric J aggregate transition and I = Isolated molecule. Filled arrows show resonance interaction energy 2β , hollow arrows show from where E_S should be measured. Changes to the observed v-e transition energy as a function of the order of the aggregate system are clearly visible. For HBC-C8,2 PLE and PL at 10^{-13} M, shoulders between 2.8-2.9 eV are solvent scattering artefacts only observable at this low concentration.

considerable exchange-narrowing of all v-e peaks. The e-p coupling also increases to $S_A \sim 1$. As predicted by the model in Eq. 6.5, and particularly noticeable in the PL, is the decrease of $\hbar\omega_{pA}$ with respect to $\hbar\omega_{pI}$ (the same applies to TBDC and PIC). Comparing the HBC-C8,2 MSAs spectra to the well known spectra of mLPPP and PICa (both in solid state) reveals striking similarities. These include the sharp v-e peaks (relative to inhomogeneously broadened isolated HBC-C8,2 PL and isolated PIC absorption³⁷), and the separation of the isolated absorption and PL peaks into two transitions separated by 2β (this is less obvious for the polar PICa molecular aggregate). More strikingly in the PL, is the almost complete disappearance of v-e features for PICa, making it very

similar to HBC-C8,2 PL. These typical characteristics, together with the mirror-symmetry of the absorption and PL spectra as predicted in Fig. 6.3, indicate that the species observed are aggregates (see Appendix B).

	← Aggregate Order →					
	C_{8,2} Isolated	mLPPP	C_{8,2} MSA	TDBC	PICa	PIC
S_I	0.5	<i>0.45 – 0.5</i>	-	0.5	<i>0.25</i>	0.25
$\hbar\omega_{pl}$ [eV]	0.16	<i>0.15</i>	-	0.17	<i>0.19</i>	0.19
S_A	-	<i>0.45 - 0.5</i>	$1^{Abs}, 1^{PL}$	<i>0.5</i>	<i>0.39(calc)</i>	~ 0.5
$\hbar\omega_{pA}$ [eV]	-	<i>0.15</i>	$0.16^{Abs}, 0.04^{PL}$	0.01	<i>0.01</i>	< 0.01
$E_S=2N2Sh\omega_p$ [eV]	<i>0.16(calc)</i>	<i>0.3(calc)</i>	<i>0.64(calc)</i>	<i>0.22(calc)</i>	<i>0.225(calc)</i>	N/a
E_S (Meas.) [eV]	0.36	0.27	0.64	0.22	0.225	N/a
R/k	-	2	2	1.34	1.52	N/a
β [eV]	-	0.08	$0.135^{Abs}, 0.045^{PL}$	0.114	0.145	N/a
$\beta/S_A\hbar\omega_{pl}$	-	1	$0.84^{Abs}, 1.12^{PL}$	1.34	1.52	N/a
FWHM ^c [eV]	$\sim 0.2^{PL}$	~ 0.1	$\sim 0.15^{Abs}, \sim 0.05^{PL}$	≤ 0.05	≤ 0.05	≤ 0.01
FWHM ^o [eV]	$\sim 0.3^{PL}$	~ 0.25	$\sim 0.3^{Abs}, \sim 0.1^{PL}$	~ 0.05	~ 0.05	~ 0.01
$2N$ (Calc.)	1	~ 2	$\sim 2^{Abs}, \sim 8^{PL}$	~ 22	~ 29	~ 40 (Corr.)
$2N$ (Lit.)	-	-	-	15-18	~ 50	50
Reference	(32)	(31)	(32)	(38,39)	(34-36)	(37)
Comment	Monomer species in solution at 10^{-13} M	Disordered polymer aggregates in solid state	Molecular nanowires in solution at 10^{-6} M that undergo an ordering process in the photo-excited state	J-resonant, ordered mol. aggregate in solution at 10^{-4} M	J-resonant, very ordered molecular aggregate in solid state	J-resonant, very ordered mol. agg. at 1.5K in an ethylene/Glycol glass

Table 6.1: Name and structure of molecules studied are given. Values obtained from spectra in Fig 6.2 and the literature are in normal type. For clarity, estimated values are given in *italics*, and values calculated or corrected are indicated. FER localisation lengths, $2N$, calculated from the model (see text) using values in the table, are as expected to be larger for more ordered aggregates. This trend is confirmed by the decrease in FWHM. The fact that $\beta/S_A\hbar\omega_{pl} \sim 1$ for all molecules suggests that FER is vibrationally modulated. Values of R/k are measured or extrapolated from J-resonant conditions. FWHM^c is the measured full-width-half-maximum of an individual v-e peak, whereas FWHM^o is taken from the overall spectral envelope. As described in the text, for large FER range systems FWHM measurements are unreliable.

In Table 6.1, values of the ratio $\beta/S_A\hbar\omega_{pl}$ are given for each molecule. The fact that for all the materials this ratio is ~ 1 suggests that FER is modulated by the vibrational frequency $\hbar\omega_{pl}$ and e-p coupling of the molecule, in all systems (see Appendix B for explanation). This is likely to be a characteristic of van der Waals systems in general, perhaps due to the lack of strong intermolecular vibrational modes and weak charge sharing not enabling a faster exciton transfer, and hence limiting β . This makes sense when one considers that the molecular electronic energy levels, and thus $\hbar\omega_{00nl}$, are modulated by the nuclear motion via the e-p coupling. In Fig. 6.3, only PICa is J-resonant (TBDC is as well^{38,39}). J-resonance occurs when $E_{RAbsT} = 2NS_A\hbar\omega_{pA} = \beta = RS_A\hbar\omega_{pl}/k$. Therefore, the resonant exciton is undergoing the usual v-e relaxation associated with an exciton on an isolated molecule; with the exception that g_l increases to g_A may make $R > 1$ (solvent relaxations may also contribute). This demonstrates the validity of the model and shows how the optical properties of an aggregate are fundamentally determined by the optical properties of the isolated molecule. Values of R/k measured (and calculated where possible from J-resonance conditions in Eq. 6.8) are given in Table 6.1. As expected values of R/k are much greater than 1 for non J-resonant systems such as mLPPP and HBC-C8,2. This is probably related to secondary effects of FER coupling other intra-molecular v-e relaxation modes to the resonant exciton or a difference between the sharp boundary FER distribution range used in this model and a more realistic smooth distribution. For polar molecules especially, R/k will be larger than unity due to solvent relaxation interactions contributing to R and not k .

Values of S and $\hbar\omega_p$ in Table 6.1 (see Appendix B) were measured directly from the spectra (or in the case of PIC analogue, values are estimated from PIC spectra) by comparison to a Poisson distribution (values are reasonable approximations). The FER range, $2N$, was then calculated for each molecule from either measured values of E_S ($E_{SA} = 2N2S_A\hbar\omega_{pA}$) or measured β values using Eq. 6.7 and compared to values of $2N$ published in the literature. PICa, PIC and TBDC are small polar molecules that form ordered aggregates that are well known for their large FER ranges. Polymers, on the other hand, although known to form small aggregates in most solutions have tended to be disregarded for FER, with some exceptions^{41,42}. Our model indicates that mLPPP, with optical spectra typical of polymers (although a little sharper at 70K in Fig. 6.3b) is

in fact forming large aggregates with FER ranges, limited by disorder, to approximately a dimer, $2N = 2$ (see Appendix B). This is a plausible FER range for polymer systems, which usually have many degrees of freedom. If, in general, polymers form highly disordered aggregates with FER ranges $2N \sim 2$, then the frequently observed variation of the relative peak intensities of the fine structure in optical spectra^{31,41}, of different samples of the same molecule (without a large variation of $\hbar\omega_{p,A}$), can be explained. It is plausible that morphological differences, between samples, could give rise to variations of the relative oscillator strengths of the symmetric and anti-symmetric transitions of aggregates (and their respective v-e progressions).

Even if the variance of $\hbar\omega_{00l}$ is small, the FER range can be disorder-limited by variations in β , deriving from the angular dependence of β with the alignment of the interacting molecular electronic transition dipoles. Typically, a variance in the FWHM of peaks in the absorption or PL is observed experimentally. The general trend in the PL is that the lower the peak energy, the broader the FWHM (the opposite for the absorption). The superposition of the v-e peak progressions of the two electronic transitions H and J, implied by this model, will give rise to observed trend (see Fig. 6.2 and Fig. 6.3). This is frequently observed experimentally.

HBC-C8,2 is a planar aromatic molecule. It forms 1-D molecular nanowires in solution³², indicating a limited degree of positional freedom available to HBC-C8,2 molecules in a nanowire aggregate. HBC-C8,2 molecular aggregates therefore have a larger $2N$ than mLPPP, but differ from the others in that they have a calculated localisation length of 2 molecules and a delocalisation length (here, the FER range during PL) of 8 molecules⁴³ (see Table 6.1, $\hbar\omega_{pAbsA} > \hbar\omega_{pL}$). This correlates well with the observation that the FWHM of the v-e peaks decreases from absorption to PL (from increased exchange-narrowing as $2N$ increases in the photo-excited state). This suggests an ordering process of the HBC-C8,2 molecules during the p-a-l cycle. Finally values of $2N$ in Table 6.1, calculated from the model for TBDC, PICa and PIC (all studied extensively for their FER), are very close to accepted values published in the literature⁴⁴. Therefore, overall, the progression of the optical spectra in Fig. 6.3 with respect to $2N$ calculated from the model, compares very favourably with published values of $2N$ and the expected general trends.

Inspection of Fig. 6.3 also allows a comparison of values calculated for $2N$ with a variable that is independent from this model, such as the change in FWHM resulting from exchange-narrowing (for identical aggregate FER systems the smaller the FWHM the larger $2N$). In Table 6.1, the trend is that the electronic variance of a single v-e peak (FWHM^e) decreases with decreasing $\hbar\omega_{pA}$. This confirms the assumption that $\hbar\omega_{pA}$ scales inversely with $2N$. However, care must be taken when estimating the FWHM, because an ensemble of aggregates can have variances in the aggregate morphology³⁷ that will lead to additional broadening (this is generally more pronounced in disordered systems such as polymers). With an increase of $2N > 2$ the v-e transition energy is observed to decrease more rapidly than the FWHM of each v-e peak. For instance with PIC analogue aggregates in Fig. 6.3b this leads to overlapping v-e peaks, making the v-e features less prominent in the spectra. If this is the case, then for systems such as PIC analogue aggregates, the most dominant factor in the overall FWHM^o of the main absorption or PL peak is roughly $\hbar\omega_{pA}$ and not the variance in electronic transition energy. This would explain why localisation lengths calculated using FWHMs generally give huge overestimates, even though in principle it should work very well. For PIC aggregates, N_{loc} ($2N$ in this thesis) is hugely overestimated^{45,46} as 1600 molecules compared to its accepted^{47,48} value of 50 molecules (from spontaneous emission rates). The former incorrect value is determined from exchange-narrowing: in the weak disorder regime $N_{loc*} \sim (\sigma_I/\sigma_A)^2$ where σ is the observed FWHM. If the value $N_{loc*} = 1600$ was calculated from FWHM, of which the main contributor was $\hbar\omega_{pA}$ and not the variance in electronic energy, then by comparing this expression to our postulate $\hbar\omega_{pA} \sim (\hbar\omega_{pl}/2N)$, the true value of the localisation length can be extracted $2N \sim (\hbar\omega_{pl}/\hbar\omega_{pA}) \sim (\sigma_I/\sigma_A) \sim \sqrt{N_{loc*}}$. Therefore, the corrected localisation length for PIC, using our model, is $2N \sim 40$ molecules; which is very close to the accepted value of 50. This confirms the assumption that overall the PL peaks of PIC and HBC-C8,2 MSA are similar, in that they are both composed of several closely energetically spaced v-e peaks (inhomogeneous broadening does not resolve the closely spaced v-e peaks of PIC, see Fig. 6.3). This agrees with our conservation of energy argument that the observed aggregate v-e transition energy must decrease as a function of $2N$ for van der Waals systems.

Physically speaking, $\hbar\omega_{pA} < \hbar\omega_{pI}$ may arise during the process of exciton resonance due to a preference of the resonant exciton to couple to lower energy intra-molecular vibrational modes. In other words, the probability of a resonant exciton coupling to high energy intramolecular modes decreases, whereas the probability of coupling to low energy intramolecular modes remains constant or increases in order to satisfy the conservation of energy – see Appendix B). From Eq. 6.4, the total reorganisation energy of the exciton is partitioned over $2N$ molecules by distributing the probability of low energy phonon emission over $2N$ molecules (the integration over all space is still a constant energy, and within a factor R/k to the isolated molecule V-R relaxation). As illustrated in the gedankenexperiment, there are two choices to conserve energy, reduce S or reduce $\hbar\omega_p$. In this model, Eq. 6.5 suggests that a resonant exciton can couple to a continuum of vibrational energies $\hbar\omega_{pA}$. However, in reality a molecule will have discrete intramolecular vibrational modes as observed in resonant and non-resonant Raman spectra. An exciton therefore has two choices to conserve energy; it can either emit high-energy phonons with very little probability ($\hbar\omega_{pA} \sim \hbar\omega_{pI}$ and $S_A \ll S_I$), or, it can emit low energy phonons with a high probability ($\hbar\omega_{pA} \ll \hbar\omega_{pI}$ and $S_A > S_I$). From the multiplicity function of $2N$ oscillators, the latter case is more favourable entropically speaking (see Appendix B), and it correlates with our observations that the observed aggregate v-e transition energy decreases as a function of $(2N)^{-1}$. This agrees with the observed enhancement of low energy vibrational modes of FER systems compared to non-FER systems¹⁹. For FER systems with large $2N$ the resonant Raman spectrum has a peak at much lower energy than expected. In this framework, the discreteness of the intra-molecular vibrational modes available to the resonant exciton may explain the variance in R/k observed.

Since the FER range is disorder limited, the smaller the resonant exciton v-e transition energy the more ordered a system is. Therefore, in terms of the ordered alignment of molecules in an aggregate the following trend is observed: PIC > TBDC > HBC-C8,2 > mLPPP. This demonstrates that the differences in the v-e structure of optical spectra of these materials arise from differences in the ordering of their systems. Our model also indicates why exciton diffusion by hopping, typical of van der Waals aggregates, is easier in systems where the exciton is resonant over many molecules e.g. in molecular crystals. From Eq. 6.5, the larger $2N$, the higher the probability that the V-R of each

individual molecule is smaller. This decreases the potential energy barrier that exists between a molecule outside the resonance range and its neighbour molecule that is part of the collective exciton eigenstate (as shown in Fig. 6.2). Thermally assisted hopping, which allows the collective exciton eigenstate to diffuse along an aggregate, is more probable as the potential energy barrier height becomes smaller. Another commonly observed property of aggregates is the reduced PL quantum yield (PLQY) compared to the isolated molecule. In this model, the distributed nature of the collective exciton v-e relaxation, as exemplified by the sum over $2N$ of the individual molecule reorganisation energy in Eq. 6.6, determines that a resonant exciton probes many more molecular vibrational manifolds than an exciton of an isolated molecule. The increased number of non-radiative pathways available to the collective exciton eigenstate in an aggregate reduces the PLQY⁴⁹. This quenching could be a result of dephasing of vibrations in a collective eigenstate (see Appendix B), or the larger availability of pre-existing non-radiative pathways originating from the individual molecule.

6.5 CONCLUSIONS

In this Chapter, it has been shown that although the conservation of energy principle cannot reveal the detailed mechanisms involved with FER, it can clarify how the V-R energy of a resonant exciton is distributed over $2N$ molecules. This approach successfully describes the v-e properties of resonant excitons, and now allows the determination of localisation lengths of resonant Frenkel excitons solely from absorption and PL spectra of aggregates. For J-resonant systems, this has eliminated the need to carry out challenging measurements of FWHMs and spontaneous emission rates from isolated molecules. In fact, solutions of non-polar isolated molecules can be very difficult to prepare, and as the model suggests, many spectra published of non-polar planar aromatic compounds are of aggregates and not isolated molecules. The reason might be that usually samples are prepared for absorption measurements and not PLE or PL, so the lowest concentration explored is $\sim 10^{-7}$ M, which is in general too high²⁹. An outcome of the model is that the p-a-l cycle for resonant excitons can now be understood in terms of the v-e relaxation of isolated molecules (the building blocks of the aggregate), thus allowing E_{SA} to be correctly measured. Finally, the model also

indicates that FER is perhaps rate-limited or modulated by the e-p coupling and vibrational frequency of the isolated molecule. Interpreting all optical spectra of polymers, small molecules, poly-aromatic hydrocarbons and bio-molecular assemblies in terms of an effective resonance range will also enable a more complete understanding of the photo-physics of organic materials. In light of the above, other measurements derived from optical spectra may have to be reviewed. For instance, measurements of exciton binding energies calculated from the band gap peak of the absorption and photocurrent spectra may, if mistaken for the isolated molecule, give an overestimate. The correct peak to measure from is in fact the crystal shifted isolated molecule transition energy – not the FER transition.

<i>I</i>	Isolated	<i>Abs</i>	Absorption
<i>A</i>	Aggregate	<i>L</i>	Luminescence
Resonance Range	$2N$	Resonance Interaction Energy	β
Reorganisation Energy	E_R	Stokes shift	E_S
Phonon Frequency	ω_p	Huang-Rhys parameter	S
Photon Frequency	ω_{00}		

Table 6.2: List of symbols used in this chapter. Subscripts are given in the top two rows. For example: $E_{R,L}$ is the reorganisation energy of the luminescence part of the cycle for an isolated molecule.

- ¹ F. P. Schäfer, *Dye Lasers* (Springer-Verlag 1990)
- ² W. J. Blau, A. J. Fleming, *Science* **304** 1457 (2004)
- ³ C. Didraga, J. Knoester, *J. Luminescence* **102-103** 60 (2003)
- ⁴ J. Schütze, B. Brüggermann, T. Renger, V. May, *Chem. Phys.* **275** 333 (2002)
- ⁵ V. May, R. Scheller, T. Renger, *J. Luminescence* **87-89** 803 (2000)
- ⁶ J. P. Hill, J. Wusong, A. Kosaka, T. Fukushima, H. Ichihara, T. Shimomura, K. Ito, T. Hashizume, N. Ishii, T. Aida, *Science* **304** 1481 (2004)
- ⁷ I. Baraldi, M. Caselli, F. Momicchioli, G. Ponterini, D. Vanossi, *Chem. Phys.* **275** 149 (2002)
- ⁸ K. Kirova, S. Brazovski, A. R. Bishop, D. McBranch, V. Klimov, *Synth. Met.* **101** 188 (1999)
- ⁹ X. Chen, Q. B. Xue, K. Z. Yang, Q. Z. Zhang, *Thin Solid Films* **286** 232 (1996)
- ¹⁰ For example, zero E_S is often reported for polymers even though the calculated E_S , from the Huang-Rhys parameter and vibrational-electronic (v-e) transition energy, is clearly non-zero. Experimentally, it is often found that increased solvent polarity doesn't alter the E_S shift of a supposed highly diluted solution of non-polar molecules. More significant though, is the lack of a consensus as to why, for molecular crystals with FER, the v-e structures of resonant excitons are absent.
- ¹¹ M. Fox, *Optical Properties of Solids* (Oxford Press 2001)
- ¹² U. Brackmann, *Lambdachrome Laser Dyes* (Lambdaphysik 1994)
- ¹³ M. Pope and C. E. Swenberg, *Electronic Processes in Organic Crystals and Polymers* (Oxford Science Publications, 1999)
- ¹⁴ D. P. Craig, S. H. Walmsley, *Excitons in Molecular Crystals* (Benjamin 1968)
- ¹⁵ A. J. Stone, *The Theory of Intermolecular Forces* (Oxford 1996)
- ¹⁶ It is worth noting that excitons can also be in resonance over large distances e.g. Förster energy transfer
- ¹⁷ E. W. Knapp, *Chem. Phys.* **85** 73 (1984)
- ¹⁸ A. S. Davydov, *Theory Molecular Excitons* (Plenum Press, 1971)
- ¹⁹ H. Kano, T. Kobayashi, *J. Lumin.* **100** 269(2002)
- ²⁰ I.G. Scheblykin, M. M. Bataiev, M. Van der Auweraer, A. G. Vitukhnovsky, *Chem. Phys. Lett.* **316** 37 (2000)
- ²¹ R. Bosisio, C. Botta, A. Colombo, S. Destri, W. Porzio, E. Grilli, R. Tubino, G. Bongiovanni, A. Mura, G. Di Silvestro, *Synth. Met.* **87** 23 (1997)
- (22) P. W. Atkins, *Physical Chemistry* (Oxford Univ. Press. 1990)

- ²³ T. Kobayashi, K. Nishimura, E. Tokunaga, *J. Mol. Struct.* **735** 179(2005))
- ²⁴ A. Hauser, *Chem. Phys. Lett.* **192** 65 (1992)
- ²⁵ N. Verdal, J. T. Godbout, T. L. Perkins, G. P. Bartholomew, G. C. Bazan, A. M. Kelley, *Chem. Phys. Lett.* **320** 95(2000)
- ²⁶ E. J. W. List, J. Partee, J. Shinar, U. Scherf, K. Müllen, E. Zojer, K. Petrisch, G. Leising, W. Graupner, *Phys. Rev. B* **61** 10807 (2000)
- ²⁷ G. C. Schatz, M. A. Ratner, *Quantum Mechanics in Chemistry* (Prentice Hall 1993)
- ²⁸ Experimentally, the eigenvalue corresponds to the energy of an absorption or PL peak. The normalisation of the sum of all the basis states reduces the variance of the eigenvalue in an exchange-narrowing process. Variances in both $\hbar\omega_{00l}$ and β can be exchanged-narrowed, however for this paper β will be approximated as constant
- ²⁹ M. Hoffmann, Z. G. Soos, *Phys. Rev. B*, **66** 24305 (2002)
- ³⁰ The correct way to measure E_S for an isolated molecule is from the 0-0 vibronic peak of the absorption peak to the 0-0 vibronic peak of the luminescence.
- ³¹ D. Hertel, H. Bässler, U. Scherf, H. H. Hörhold, *J. Chem. Phys* **110** 9214 (1999)
- ³² A. J. Fleming, J. N. Coleman, A. B. Dalton, A. Fechtenkötter, M. D. Watson, K. Müllen, H. J. Byrne, W. J. Blau, *J. Phys. Chem. B*, **107** 37 (2003)
- ³³ A. Fechtenkötter, N. Tchebotareva, M. Watson, K. Mülleren, *Tetrahedron* **57** 3769(2001)
- ³⁴ D. G. Lidzey, J. Wenus, D. M. Whittaker, G. Itskos, P. N. Stavrinou, D. D. C. Bradley, R. Murray, *J. of Lumin.* **110** 347 (2004)
- ³⁵ D. G. Lidzey, D. D. C. Bradley, M. S. Skolnick, S. Walker, *Synth. Met.* **124** 37 (2001)
- ³⁶ E. O. Potma, D.A. Wiersma, *J. Chem. Phys.* **108** 4894 (1998)
- ³⁷ Proc. Enrico Fermi Sch. Phys., *Organic Nanostructures: Science and Applications*, IOS Press, Course CXLIX, p150
- ³⁸ H. Fidder, PhD. Thesis, University of Groningen (1993)
- ³⁹ H. Fidder, D. A. Wiersma, *J. Phys. Chem*, **97** 11603 (1993)
- ⁴⁰ The variation of E_S for HBC-C8,2 aggregates with solvents of different polarity is negligible, indicating that solvent relaxation can be excluded for HBC-C8,2 aggregates. The principal reason is that for large aggregates the majority of the molecules do not lie on the surface. The other molecules are in solid-state form and hence have no solvent relaxation.

- ⁴¹ M. Knupfer, J. Fink, E. Zojer, G. Leising, U. Scherf, K. Müllen, *Phys. Rev. B* **57** 8 (1998)
- ⁴² K. Kemnitz, N. Tamai, I. Yamakazi, N. Nakashima, K. Yoshihara, *J. Phys. Chem.* **90** 5094 (1986)
- ⁴³ The HBC-C8,2 molecule and its close analogue HBC-PhC12, have been critical in the conception of this model and are the topic of a more extensive and thorough paper on this model.
- ⁴⁴ Calculated by comparing spontaneous emission rates of solutions of aggregated and isolated molecules.
- ⁴⁵ S. de Boer, D. A. Wiersma, *Chem. Phys. Lett.* **165** 45 (1990)
- ⁴⁶ S. De Boer, K. Vink, D.A. Wiersma, *Chem. Phys. Lett.*, **137** 99 (1987)
- ⁴⁷ M. Schreiber, Y. Toyozawa, *J. Phys. Soc. Jpn.* **51** 1528 (1982)
- ⁴⁸ H. Fidder, J. Knoester, D. A. Wiersma, *J. Chem. Phys.* **95** 7880 (1991)
- ⁴⁹ A. Yu. Nollau, M.Hoffman, K. Floreck, T. Fritz, K. Leo, *J. Appl. Phys.* **87** 7802 (2000)

Chapter 7: ELECTRICAL PROPERTIES AND MICROSCOPY

7.1 INTRODUCTION

In this Chapter the electrical properties of pure (pristine) and composite films of HBC derivatives are examined and compared. The optical probing of the HBC derivatives measures the transition levels between occupied (HOMO) valence levels and unoccupied (LUMO and LUMO+1) conduction levels of the molecules. The large overlap between the molecular orbitals of the HBC molecules in their respective MSAs (as demonstrated by the aggregate geometry optimisations), is expected to give rise to a large conductivity. The A.C. microwave charge carrier mobility of HBC derivatives has been measured previously by others¹ and was found to be very large, $0.1 \text{ cm}^2\text{V}^{-1}\text{s}^{-1}$. With this high charge carrier mobility, the conductivity of HBC derivatives is expected to be fairly large even if the density of intrinsic charge carriers is quite low. Graphite is a useful molecular system for comparison with HBC aggregates. The conductivity of graphite² along the c-axis is approximately $2 \times 10^4 \text{ Sm}^{-1}$.

The measurement of the conductivity of electrical percolation networks of HBC MSAs, in an analogous way to the exciton percolation networks of Chapter 5, is also undertaken. The comparison of the results from both percolation networks is expected to reveal more information on the connectivity and dimensionality of the MSA aggregates or MSA aggregate bundles.

Lastly, Atomic Force Microscopy and Scanning Electron Microscopy images are compared and the results are found to complement previous findings about the MSA structure and dimensionality from this and other Chapters.

7.2 RESULTS

PRISTINE FILMS

The measurement of the electrical conductivity of the pristine films was conducted on asymmetrical sandwich devices of Au/HBC-derivative/Al. Symmetrical devices made from Au/HBC-derivative/Au did not generate reproducible current-voltage plots. Generally the latter devices tended to have a large amount of short-circuited pads, probably due to the larger temperature that was required to evaporate gold top electrodes. The lack of substantive amounts of starting material did not allow for more devices to be made. The choice of two different metal electrodes is therefore not ideal for accurate measurements of the electrical conductivity magnitude, however, the accuracy of homo-polar devices was sacrificed in order to ensure that relative measurements of the HBC derivatives were achieved. The measurements presented here are thus order-of magnitude measurements. Typically, electrical measurements of any molecular compound in a sandwich device have a large variability between chemical batches, and sample batches of the same chemical batch. Variances in the electrical behaviour of samples are known to arise from the differences in the morphology and electrode/molecule interface. The morphologies of samples are sensitive to the spinning speed of spin cast films, the solvent used and generally the sample history. Since the subject of this thesis is the optical differentiation between the MSA morphologies of similar compounds, the measurement of the electrical properties, albeit approximate, is nevertheless useful. The sample preparation techniques are given in Chapter 2.

In Figure 7.1, the current versus voltage (I-V) log plots of most of the HBC derivatives are given. Note that forward bias is when the Au and Al electrodes are biased +ve and -ve respectively. The I-V graphs of each derivative are directly comparable as each device was spin cast from 20g/L in chloroform at 2000 r.p.m, with an average thickness of ~ 200 nm. However, in reality, variances in the conductivity, between samples of a given HBC derivative, spin-cast at the same speed, are of the order of one order of magnitude. Even different contact pads of the same sample gave rise to such variances. Therefore the plots presented in Figure 7.1, were chosen because they are representative of the other samples (and pads) of a given HBC derivative. In fact, repeated I-V scans

of the same contact pad yielded a non-linear decrease in the current achieved per I-V run. This will be explained later. Upon first inspection of Figure 7.1, most derivatives appear to behave similarly. However, the diode behaviour of pristine J-HBC films is unusual because chemically, the core of the molecule is identical to most of the other derivatives. It may be that the oxy-groups on the side-chains have given rise to a different electrode/molecule interface compared to the other derivatives. The diode behaviour is the result of an asymmetrical charge injection behaviour of the contacts. From the relative decrease in the current flowing in reverse bias, it appears as though the injection of electrons or holes is more difficult when the Au and Al electrodes inject electrons and accept electrons respectively.

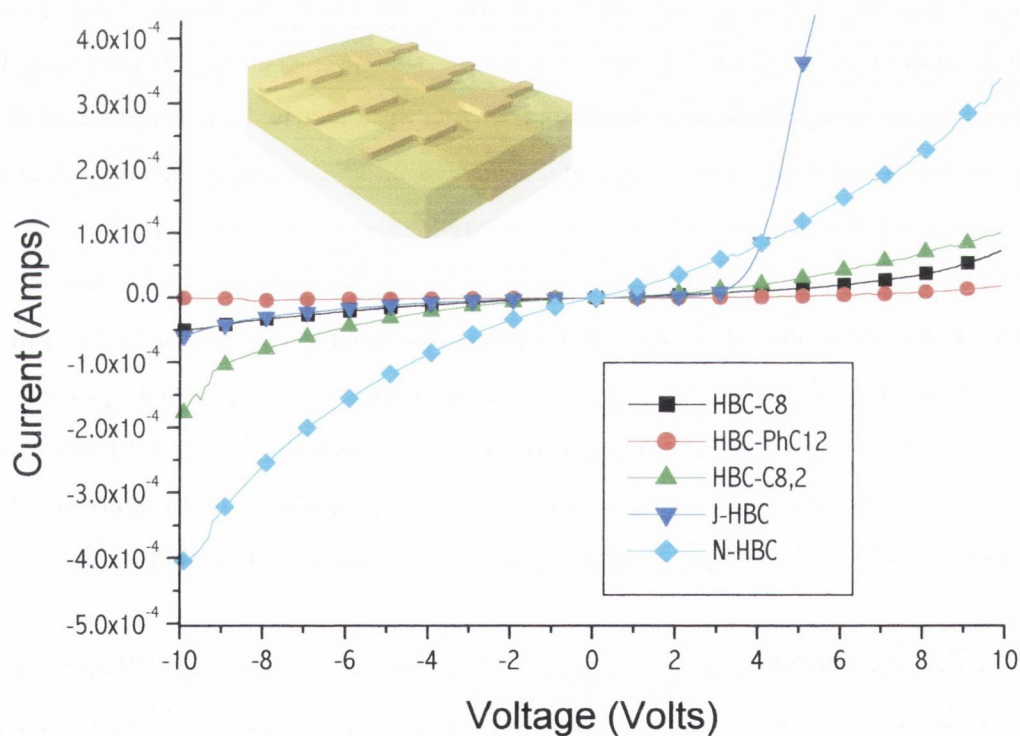


Figure 7.1: Current versus voltage, in reverse and forward bias, for pure HBC derivative films ~ 200 nm thick. Note the diode behaviour of J-HBC. All other derivatives are for the most part symmetric under positive and negative bias. Inset: Graphic illustrating the device planar construction.

As can be seen in Figure 7.2, plotting the I-V curves in a log-log scale indicates that all derivatives behave roughly similar to the other derivatives, with the exception of J-HBC. The I-V curves used in Figure 7.2 are different to those in Figure 7.1 but were chosen because they too are representative of the samples.

The space-charge-limited-current (SCLC) conduction regime occurs when space charge neutrality is violated during conduction. An inexhaustible supply of charge carriers accumulates as a reservoir near one electrode. Therefore all electric field lines will end on charges in the bulk, and the reservoir will be field-free at the electrode. Therefore when one charge leaves the bulk on the opposite electrode, another charge is injected by the electrode and picked up by the field line that has become free. Therefore the number of injected charge carriers and their velocity is proportional to the applied field. In this regime the current flowing I displays a square-dependence with the applied voltage and is determined by the following relationship:

$$I = \left(\frac{9}{8} \right) \frac{\epsilon \mu V^2}{L^3}$$

where ϵ , μ and L are the dielectric constant, charge mobility and film thickness of the organic layer of a metal/organic/metal sandwich device. It is possible to obtain the charge carrier mobility from the intercept of an I-V curve in the log-log scale so long as the slope is approximately = 2 (indicating a square dependence of the current on the applied voltage). This describes a conduction regime where the current is related to the square of the voltage as required by SCLC and will usually only occur when the current exceeds the trap-filled limit. Generally a super linear dependence on the *field* is observed for disordered materials where field-assisted de-trapping or surmounting of potential barriers is involved. A mobility sub-linear field dependence indicates that the charge velocity is saturating at high applied fields. The latter case is thought to arise from an increase in the scattering of charge carriers (as is the case in a band model transport regime) and tends to occur in well-ordered materials.

Values of the charge carrier mobilities were calculated for the HBC derivatives from the intercept of the straight lines with slope = 2. Only portions of the I-V curves are in the SCLC regime. The average charge mobility measured for the HBC derivatives is of the order of $3 \times 10^{-12} \text{ cm}^2/\text{Vs}$. This value is much smaller than the charge mobility of holes $\sim 10^{-7} \text{ cm}^2/\text{Vs}$ and electrons $\sim 10^{-8} \text{ cm}^2/\text{Vs}$ in MEH-PPV³. The problem with measuring the mobility from I-V plots is that at the voltage required to get to the SCLC region may be high enough that the charge mobility is a function of the field. The behaviour of the charge mobility at high electric fields is described by the Poole-Frenkel equation:

$$\mu \cong \mu_0 \exp\left[\gamma\sqrt{E}\right]$$

where μ_0 and γ are the linear and exponential coefficients respectively whose value is sample dependent. This field-dependence of the charge mobility is what gives rise to the marked increase of all the derivatives in Figure 7.1. For organic light-emitting-diodes the large increase of the current flowing, at a given voltage, gives rise to a sharp increase in the electro-luminescence observed and is known as the onset voltage. From inspection of Figure 7.2 the slope of most of the I-V plots tend to increase as the applied field increases. This indicates that the HBC-derivatives are not ordered enough that a sub-linear mobility-field relationship is observed. Instead, as with J-HBC in particular, the HBC derivatives seem to tend towards slope ≥ 1 , indicating that the systems are to some degree disordered. However, as detailed in Chapter 4 local order can give way to disordered percolation network formation.

To determine the relative conductivities, and an estimation of the absolute conductivity, of the pristine HBC derivative films, the first derivative of the I-V plots was determined and is given in Figure 7.3. Using the conductivity at zero bias as a reference, allows all HBC derivatives to be compared.

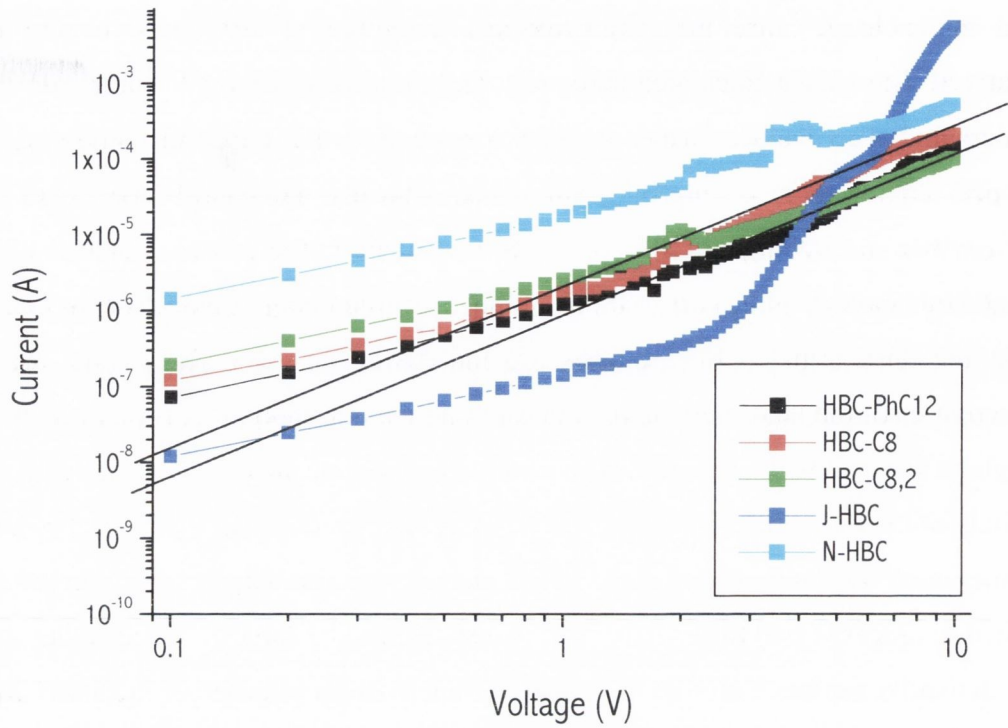


Figure 7.2: Log-Log current versus voltage plots of pristine films of HBC derivatives ~ 200 nm thick. Straight lines indicate a slope = 2 region in several of the I-V curves

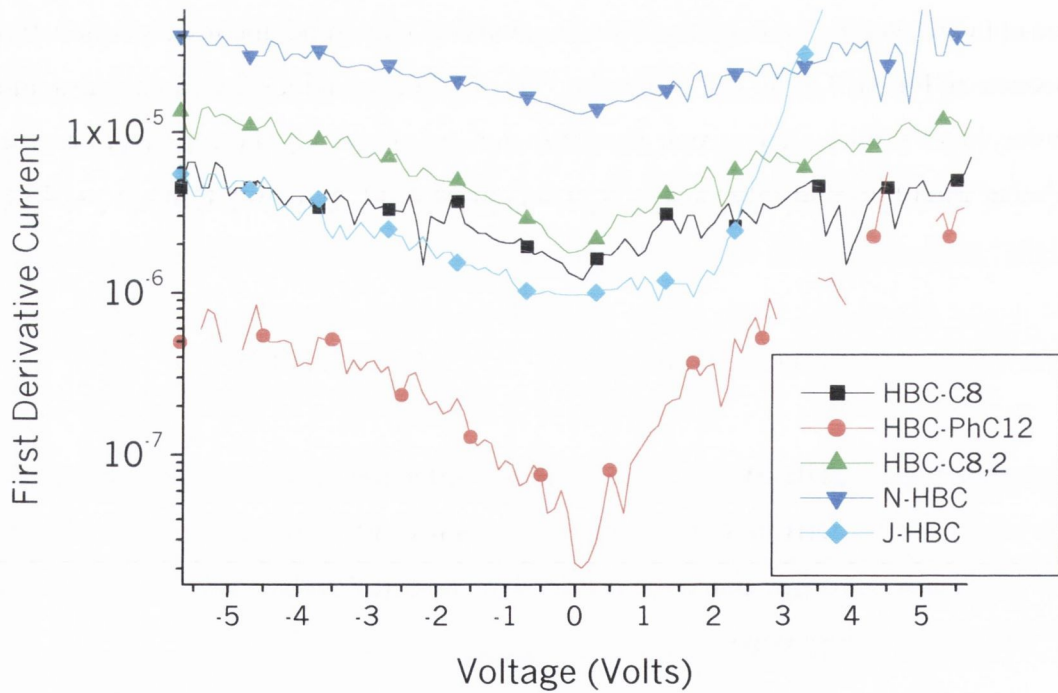


Figure 7.3: First derivative of the current versus voltage of the I-V curves in Figure 7.1.

Listed in Table 7.1, are the conductivities, measured at zero bias, of the HBC derivatives. The values calculated here are larger than the typical values for conjugated polymers and other van der Waals molecular systems. For instance the conductivity of un-doped anthracence is $\sim 10^{-15} \text{ Sm}^{-1}$ and typically conjugated polymers have conductivities⁴ in the range of 10^{-14} to 10^3 Sm^{-1} . Although there is good spatial overlap of neighbour molecules in HBC MSAs, the lack of true charge delocalisation does not enable the fast transfer of electrons up-and-down the nanowire. Thus the low conductivities of the HBC derivatives indicate that the likelihood that Bloch waves exist throughout the nanowire is small. The conduction regime in the HBC derivatives, is definitely not ballistic. It is most likely a hopping type mechanism of charged polarons. The measured conductivities of the HBC derivatives are larger than that of most undoped conjugated polymers. It is very plausible that the larger conductivities of the HBC derivatives arises due to a larger molecular positional order in the HBC MSAs compared to the generally disordered aggregates formed by polymers.

It is interesting to note that the typically most ordered MSA N-HBC, from the sharpness of the optical spectra, is the most conductive. On the other hand, the lowest conductivity is measured for HBC-PhC12. From the optical spectra, HBC-PhC12 displays more disorder than the other derivatives. Thus it seems that it is really the degree of order in a MSA that determines how quickly a charged polaron can hop its way through an MSA.

MOLECULE	CONDUCTIVITY (S/m)
HBC-C8	3.0×10^{-5}
HBC-C8,2	4.6×10^{-5}
HBC-PhC12	5.1×10^{-7}
N-HBC	3.2×10^{-4}
J-HBC	2.4×10^{-5}
Graphite	2×10^{-4}

Table 7.1: The conductivities of pristine films of HBC derivatives.

PERCOLATION SAMPLES

For the percolation studies only one HBC derivative was used, N-HBC, as it was synthesised locally and therefore larger amounts of material were available. As with the results for the pristine HBC devices, the conductivity measurements presented next are meant to be compared on an order-of-magnitude basis. It was found that for devices near the percolation threshold the variability between samples, contact pads and I-V scans was very large indeed. However from the plots in Figure 7.5, a clear trend is observed. The lowest loading that could be measured is 0.0003 (0.03%). In fact many of the 0.03% samples were noisy and flat in their response to an increase in applied bias. Therefore as before, the plots given in Figure 7.5 are meant to be illustrative of the other samples measured at the same loading ratio. However, for the 0.03% this was the only plot that was good.

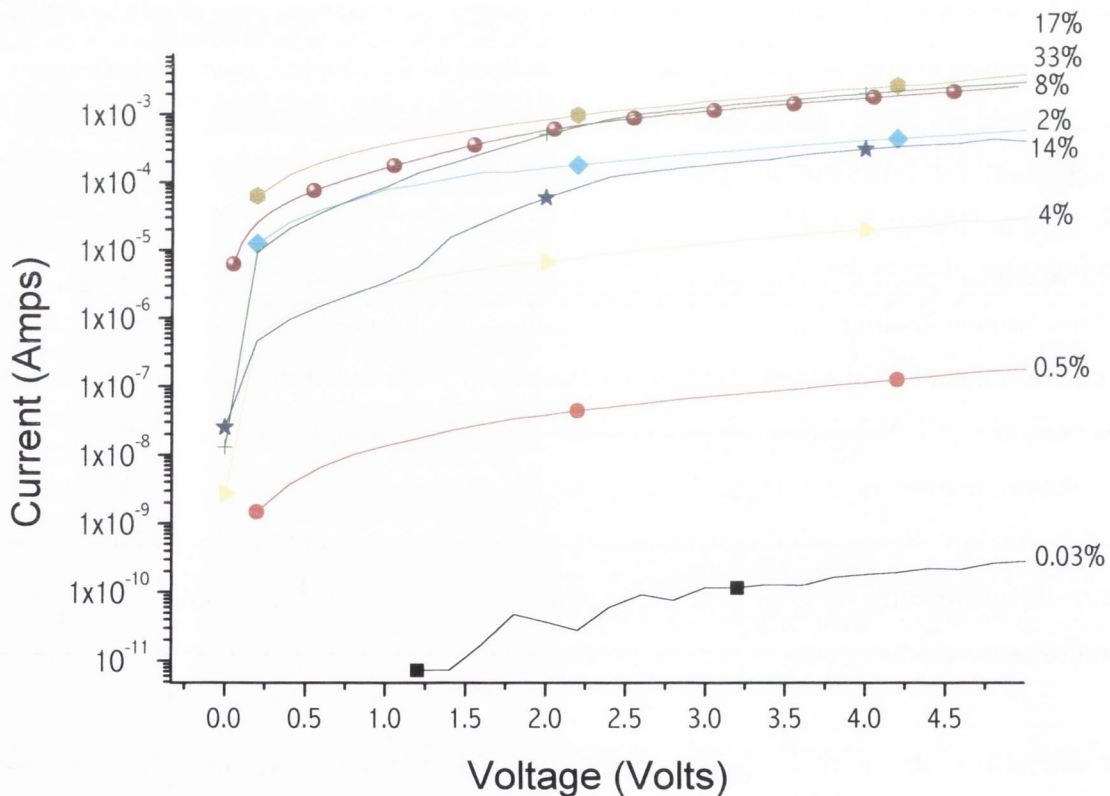


Figure 7.5 a): Log plot of the current versus voltage plots of N-HBC doped matrices (polystyrene) at various doping concentrations.

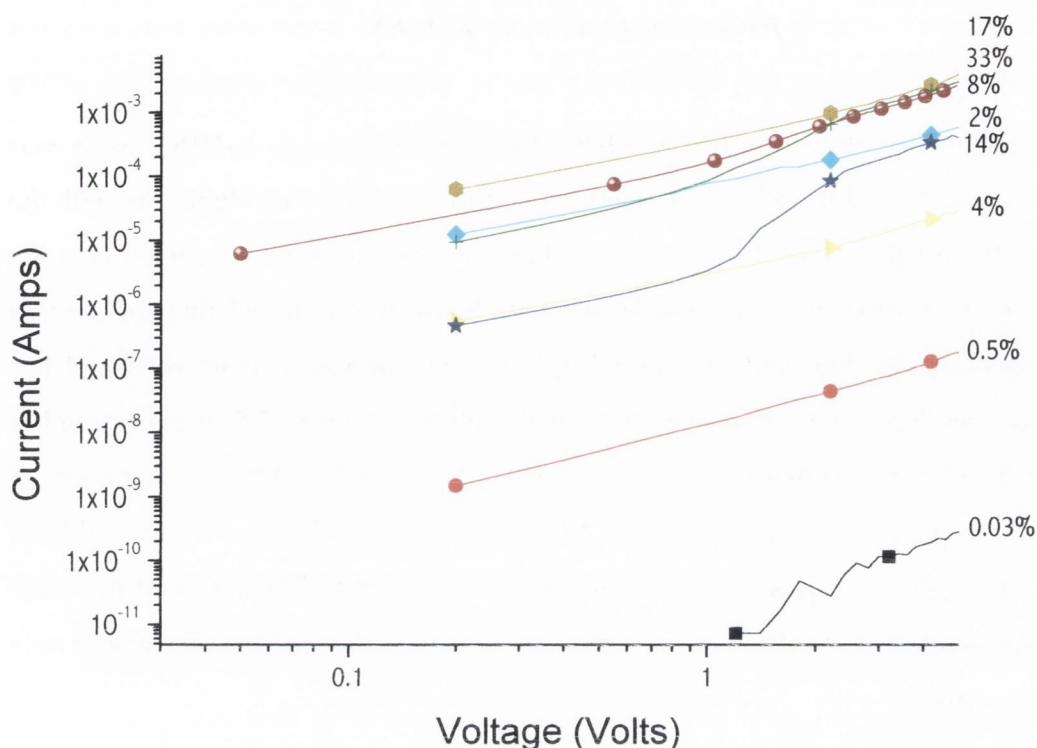


Figure 7.5 b): Log-Log I-V plots of N-HBC doped polymer matrices (polystyrene) at various doping levels.

In Figure 7.5 there appears to be a rapid increase in the current at any given voltage as the dopant loading is increased. To illustrate the dependency of the current on the loading ratio (the conductivity plot is given below), a log-log plot of the current at 4.0 V bias versus loading ratio is given in Figure 7.6. From the log-log plot a clear percolation threshold where the current increases non-linearly with the dopant loading is observed at $< 0.1\%$ loading. In fact it seems that only the upper limit of the onset of percolation regime is observed. This is due to the signal to noise ratio decreasing quickly for low dopant loading samples. This is because the current magnitude in the lower dopant loading samples is at the measurable limit of the instruments (the signal-to-noise ratio was too low).

For comparison the normalised plot of excimer to PL emission ratio from Chapter 5 is given in Figure 7.7. Clearly the behaviour of each plot is similar in that the percolation threshold is $< 0.01\%$. This indicates that the conditions required for efficient charge transport are similar to those required for efficient excimer emission. Namely, the formation of a percolation network is required in both cases. This is evident from the saturation of the current obtained at 4 volts bias for samples with a loading $> 2\%$.

Above this dopant loading the formation of more nanowire interconnections does not significantly contribute to the conductivity of the samples. The conductivity of the percolation samples versus dopant loading is presented below.

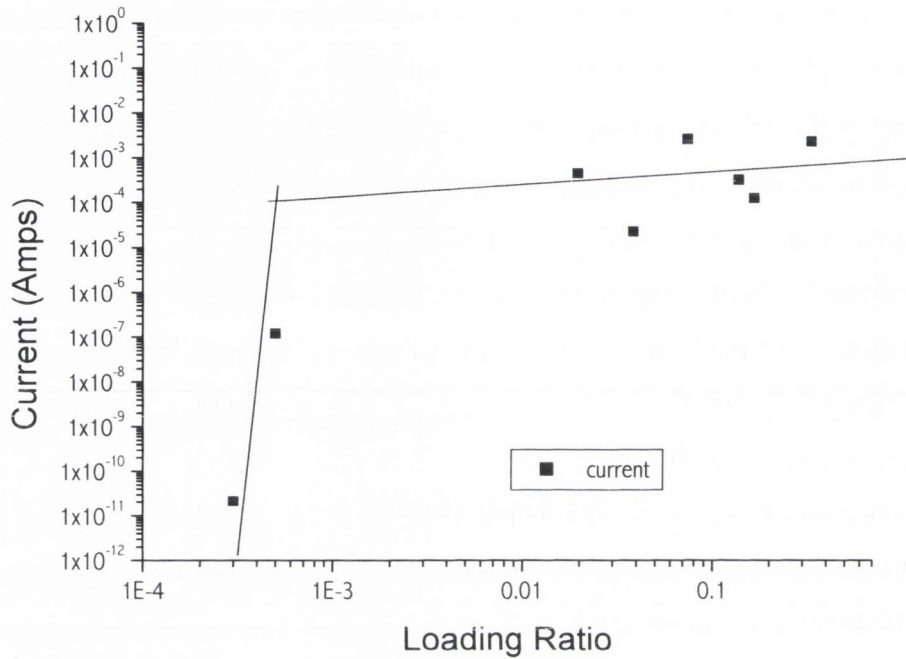


Figure 7.6: Plot of the current passing through a composite of N-HBC MSAs in a polymer matrix (polystyrene) at various loadings biased at + 4 Volts. This plot indicates that the percolation threshold (see linear fits) is < 2 % loading and is likely to be around ~ 0.04 %.

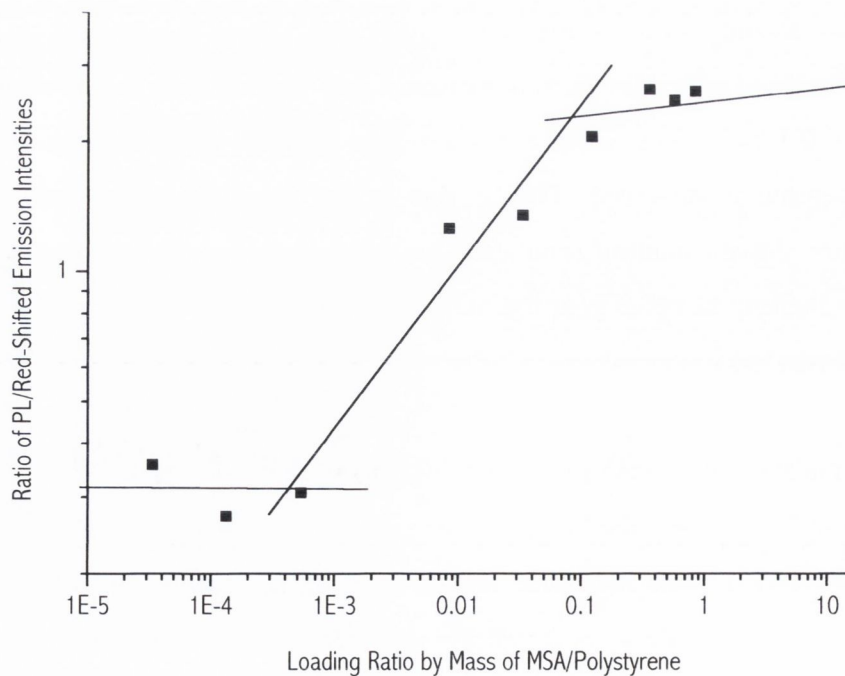


Figure 7.7: Normalised excimer to PL intensity ratio. Multiply loading ratio by a factor 100 to get percentage doping.

To determine the conductivity of each representative sample of the various loadings, the first derivative, of each plot in Figure 7.5, is given in Figure 7.8. As can be seen from the plot, the behaviour is rather similar to the first derivative, in Figure 7.3, of the I-V plot of the pristine film of N-HBC. The conductivities measured for N-HBC in a percolation sample above the percolation threshold $\sim 1 \times 10^{-3} \text{ Sm}^{-1}$ is comparable to the conductivity of the pristine N-HBC samples $\sim 3 \times 10^{-4} \text{ Sm}^{-1}$ (from Figure 7.9 and Table 7.1). This demonstrates that at high dopant loadings the conductivity of the sample is not hampered by the presence of the inert polycarbonate. The only observed difference between the two kinds of samples, pristine and percolation, was the more rapid decrease of the conductivity of the N-HBC nanowires in a percolation network after successive I-V scans. This is due to the limited number of inter-connections in the percolation sample burning out due to Joule heating at the node sites. These locations have a locally high resistance compared to the nanowires themselves, thus joule heating will be more significant between nanowires. The burning out of junctions thus limits the number of paths available for conduction and has the same effect as decreasing the loading ratio of the percolation network.

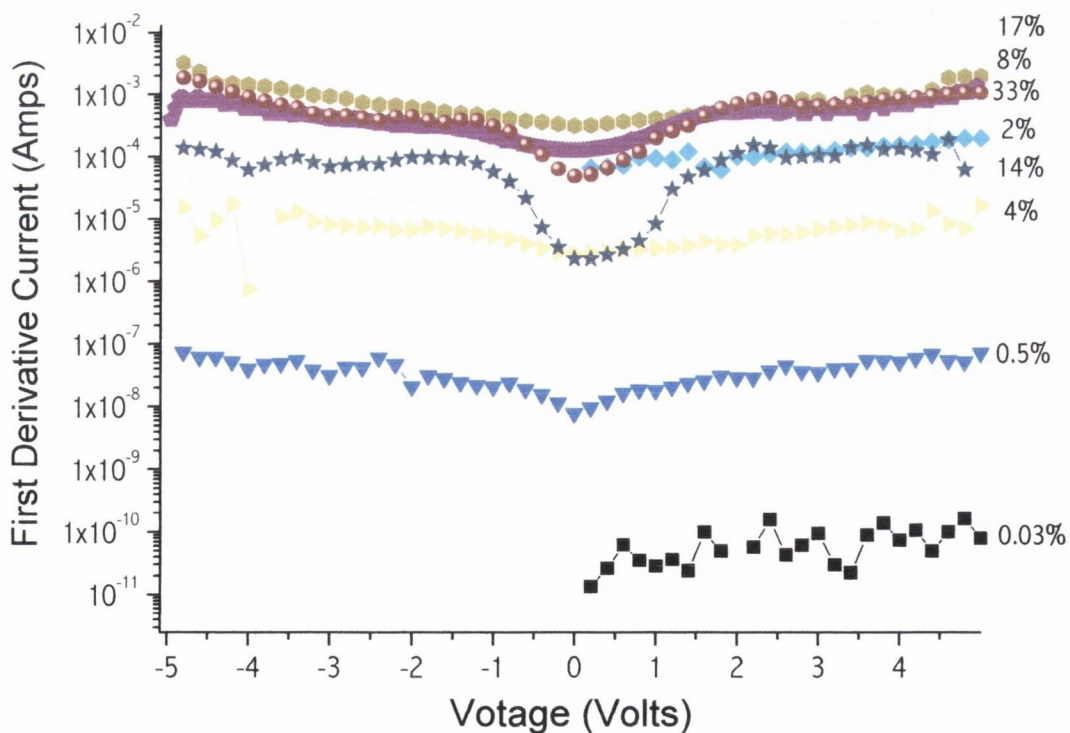


Figure 7.8: First derivative of the current versus applied bias for various loadings of NHBC MSA doped in a polymer matrix.

As can be seen from Figure 7.9, the behaviour of the conductivity versus dopant loading is similar to that of Figure 7.6. The percolation threshold is also observed to be $< 2\%$. The saturation of the maximum conductivity is achieved at dopant loadings $> 2\%$. As described above the maximum conductivity of the N-HBC percolation samples is comparable to that of pristine films of N-HBC. The percolation network formation was also confirmed by the erratic behaviour of the I-Vs of samples of dopant loading $\sim 0.5 - 2\%$. After repeated I-V scans, of the $0.5 - 2\%$ samples, it was often observed that at a given bias voltage the I-V curve would jump up to higher currents and continue along a I-V curve of a previous I-V scan. This can easily be explained in terms of a percolation network. Joule heating from the previous I-V scan burns out several connection nodes at high current. These pathways become unavailable for conduction in the next I-V scan at low bias voltages. Upon reaching a sufficiently high bias voltage, the burnt out interconnects (nanoscale gaps in the conduction network) could be bridged again and conduction along the paths resumes. This could explain why I-V curves, of samples around the percolation threshold will be seen to jump up to higher currents and join the previous I-V scan at a given bias voltage. This behaviour would seem to confirm the dependency of the conductivity on the connectivity of a network. Thus it seems that the increase in bias can effectively increase the connectivity of the network – although it is not stable.

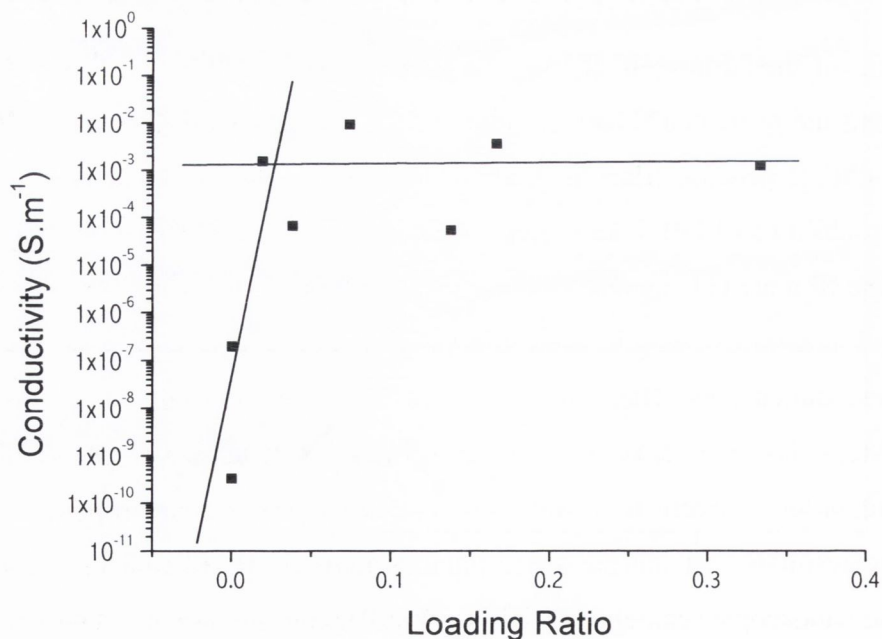


Figure 7.9 a): The log plot of the conductivity of N-HBC doped percolation samples at various loadings. The straight lines are a guide to the eye to indicate that the percolation threshold $\sim 1\%$.

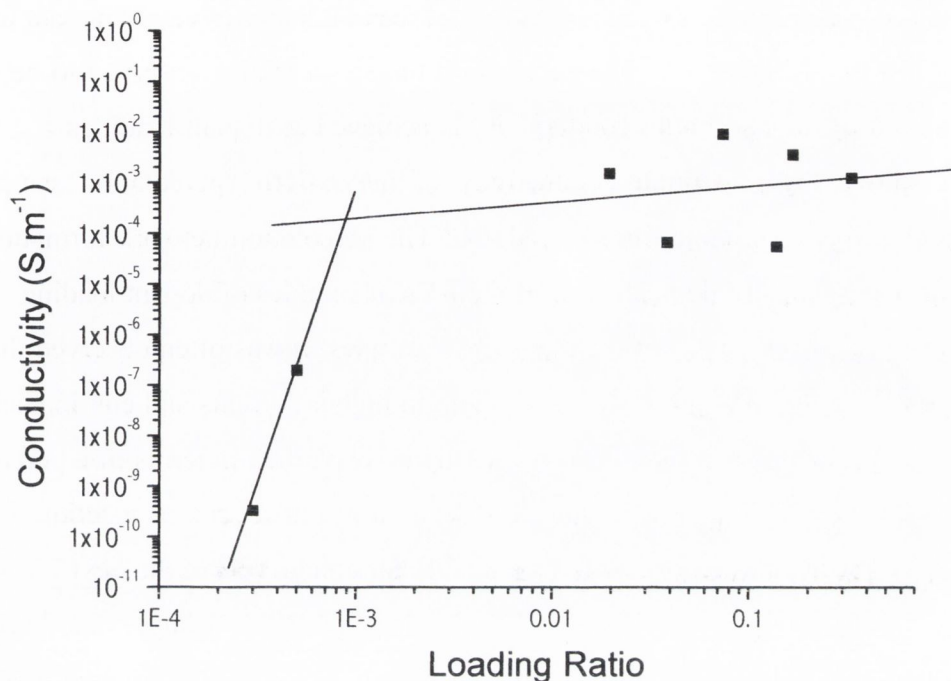


Figure 7.9: The log-log plot of the conductivity of N-HBC doped percolation samples at various loadings. The straight lines are a guide to the eye to indicate the percolation threshold $< 2\%$.

MICROSCOPY

AFM images of the surface of the pristine HBC derivative films used in the electrical measurements are presented below in Figures 7.9 – 7.17. The AFM image of the surface of a HBC-PhC12 pristine film on glass in Figure 7.9 clearly demonstrates the self-organisation abilities of HBC derivatives. The columnar structures protruding from the surface of the film are corrugated on the order of micrometers. These are clearly not due to individual nanowires being imaged, but rather the nanowire bundles are more likely to be of these dimensions. The homogeneity of the sample corrugation suggests a well ordered system, however from the optical spectra and electrical measurements, this macroscopic order is likely to result from the liquid crystalline properties of HBC-PhC12. The result is that the nanowire bundles may seem ordered on a microscopic scale, on the nanoscopic scale the HBC-PhC12 molecules are less ordered than the other HBC derivatives.

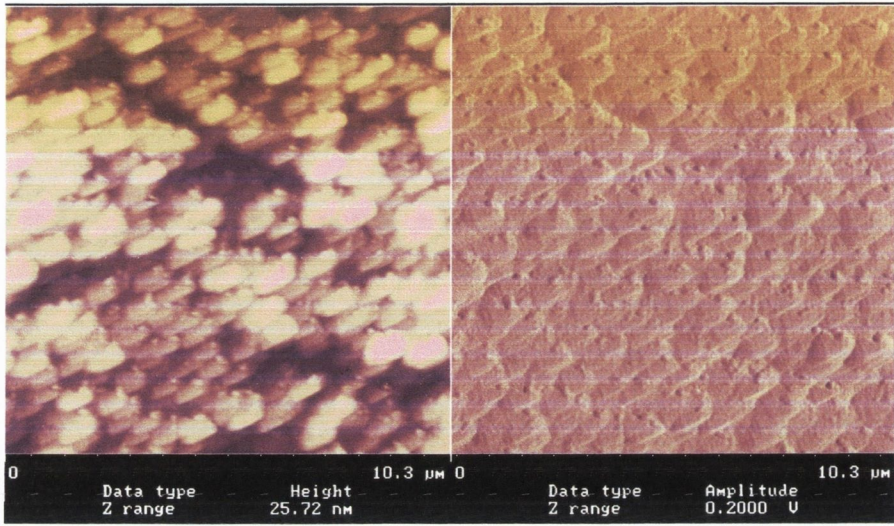


Figure 7.9: NC-AFM images of HBC-PhC12 pristine film on glass.

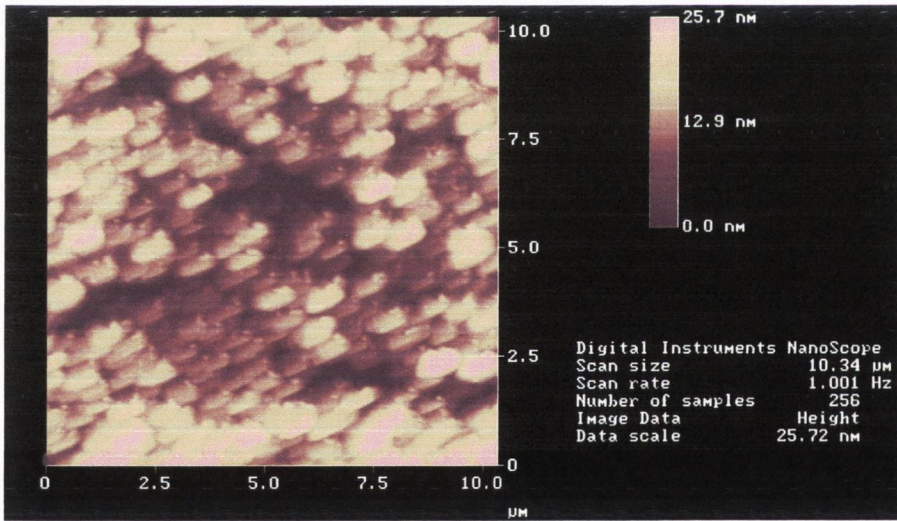


Figure 7.10: NC-AFM images of HBC-PhC12 pristine film on glass.

In the line section, given in Figure 7.11, the vertical distance of the columnar structure is of the order of 16 nm. Line sections of film surfaces are not so useful to determine structural dimensions, however this Figure helps to illustrate the lateral dimensions to be of the order of 1 micrometer. Thus the this size nanowire bundle has a diameter of ~ 300 HBC-PhC12 nanowires.

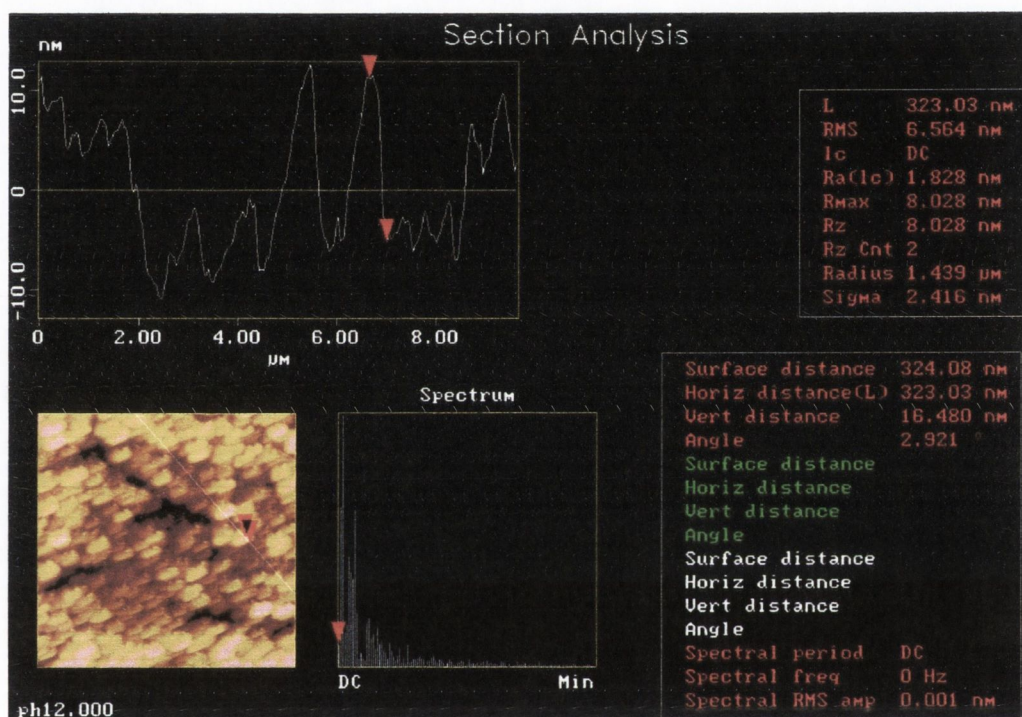


Figure 7.11: NC-AFM images of HBC-PhC12 pristine film on glass. Section profile.

The AFM images obtained for HBC-C8,2 in Figure 7.12 and 7.13 are interesting in that the morphology of the film surface is quite distinct from that of HBC-PhC12. The nanowire bundles are smaller, of the order of 100nm diameter, and are much more disorganised in their orientation on the surface of the film. However, the HBC-C8,2 nanowires are straight and of the order of 2 – 5 micrometers length. The position of the molecules in the HBC-C8,2 nanowire appears to be ordered as indicated in the absorption and PL spectra, however as described in Chapter 5, the agglomeration of the nanowires appears to be disordered

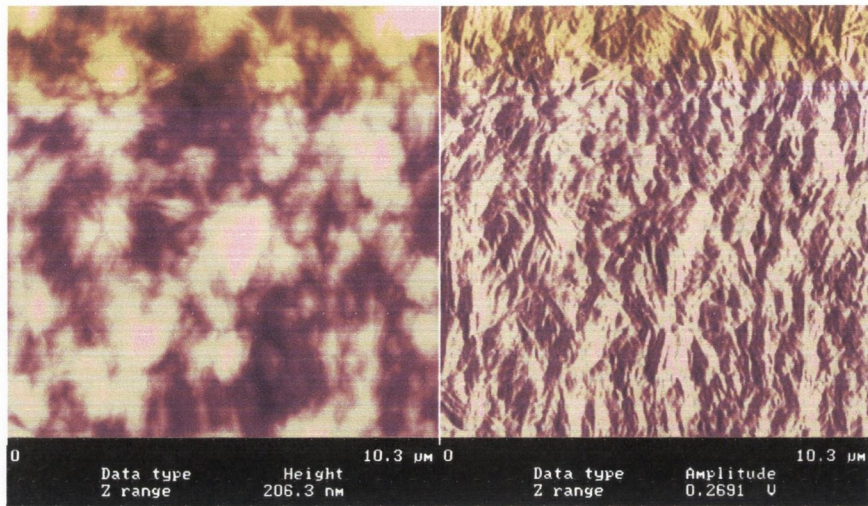


Figure 7.12: NC-AFM image of HBC-PhC8,2 pristine film on glass

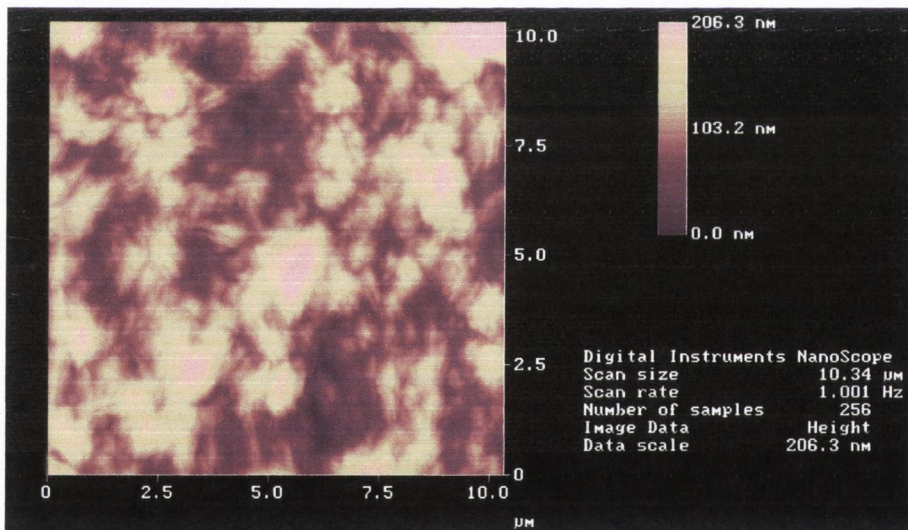


Figure 7.13: NC-AFM image of HBC-C8,2 on glass.

In Figures 7.14 and 7.15, the morphology of the J-HBC film surface is more similar to that of HBC-C8,2 than HBC-PhC12. The nanowire bundles are of the order of 100nm diameter and 2 –5 micrometers long. From the images their appears to be some helicity or twisting in the J-HBC nanowire bundles that distinguishes them from the straighter HBC-C8,2 nanowire bundles.

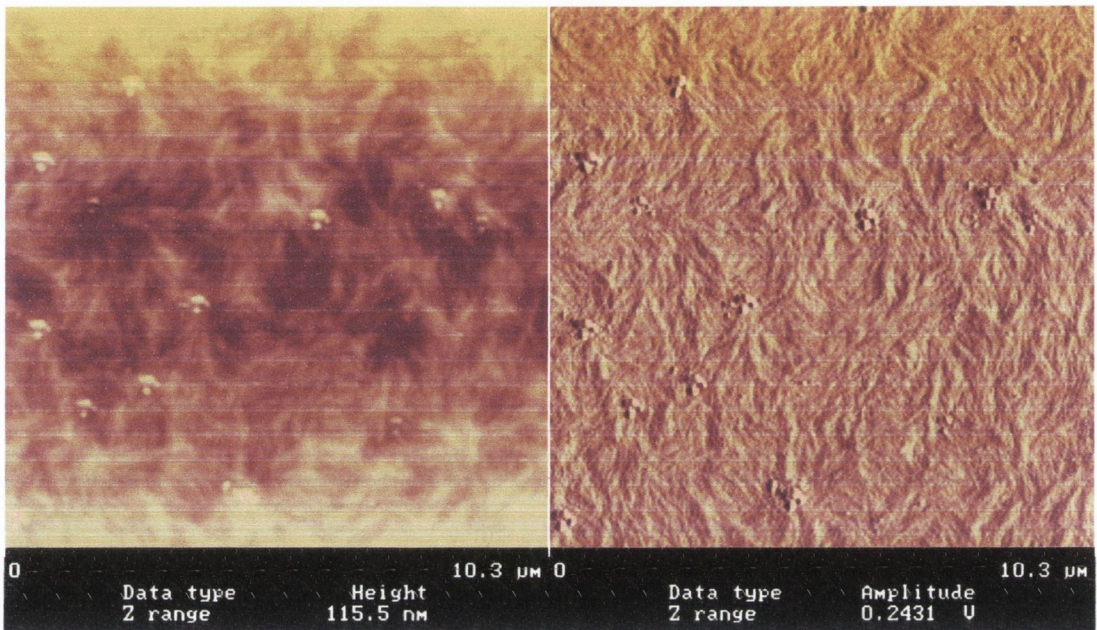


Figure 7.14: NC-AFM image of J-HBC pristine film on glass.

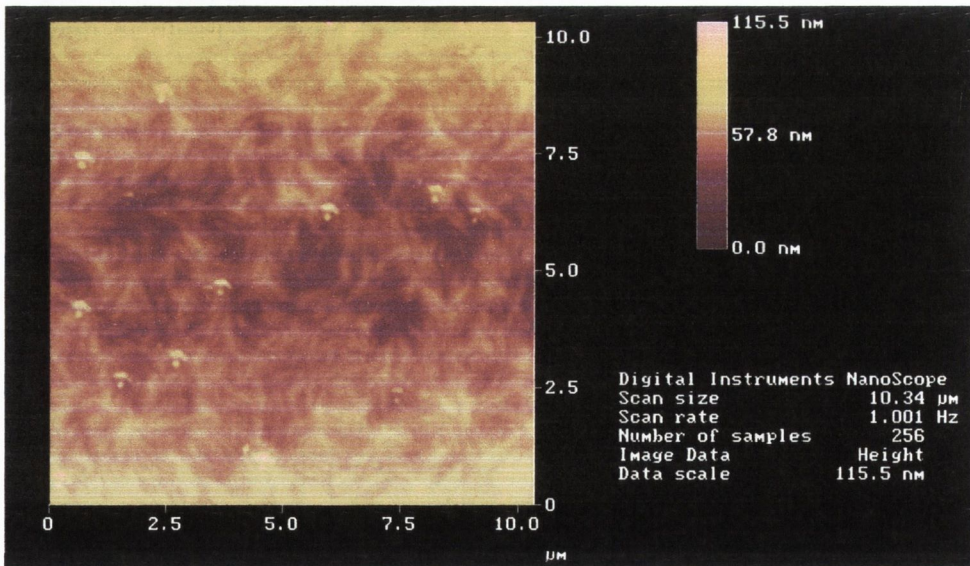


Figure 7.15: NC-AFM image of J-HBC pristine film on glass.

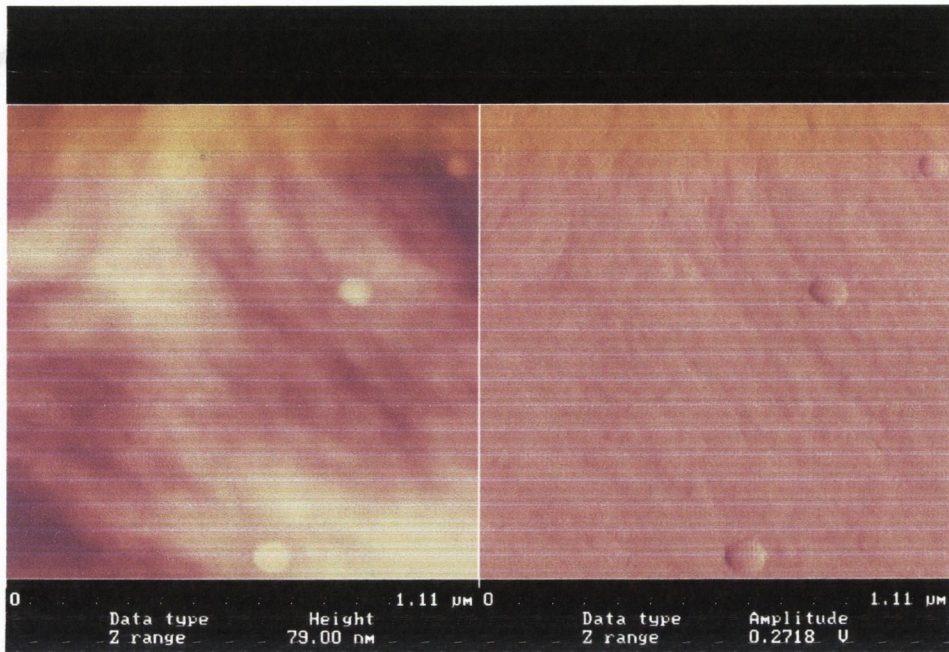


Figure 7.16: NC-AFM image of N-HBC pristine film on glass.

From inspection of Figure 7.14 and 7.15, the J-HBC MSAs appear to have physical dimensions similar to that of HBC-C8,2. However an appreciable difference can be found in the finer structure of the MSA. The J-HBC MSAs appear to be less straight, indicating that J-HBC nanowires are flexible. From Figure 7.14, there may even be some helicity to their structure.

The AFM images of N-HBC in Figure 7.16 show that the film surface is much more homogenous and less rough than the other derivatives. Structures are barely visible and seem to be of the order of 100 nm dimensions (note the smaller scale of the image). This correlates with the electrical measurement conducted whereby this derivative had the highest conductivity of all the HBC derivatives. This is most likely due to the higher order of the N-HBC films.

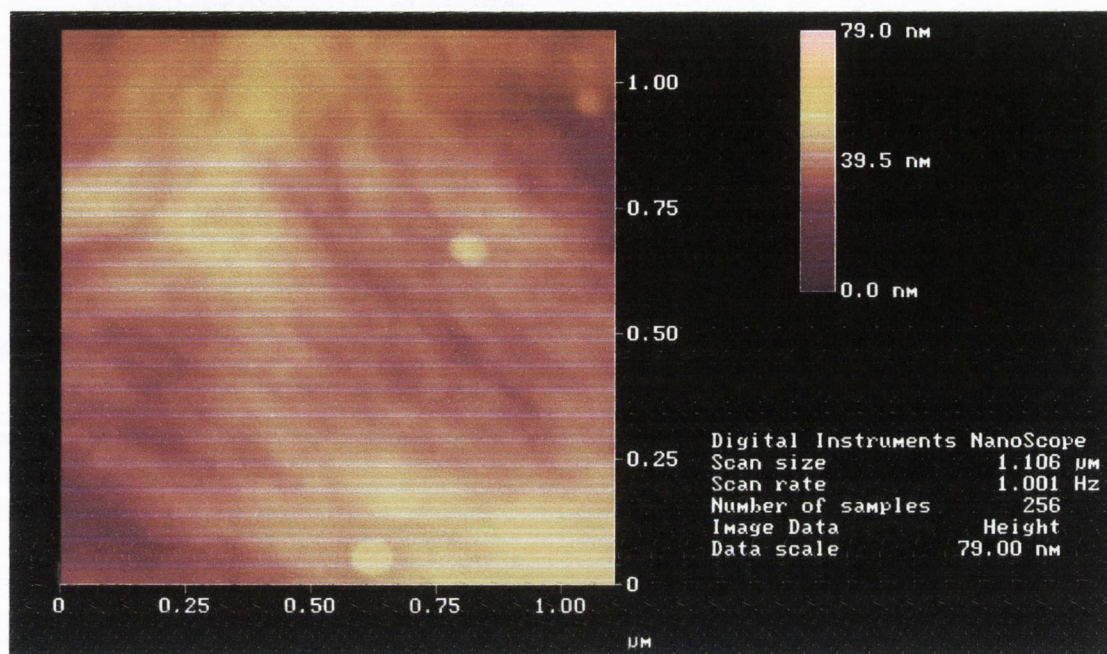


Figure 7.17: NC-AFM image of N-HBC pristine film on glass.

SEM images of HBC-C8,2, HBC-PhC12 and are presented below⁵ in Figures 7.18 – 7.21. The structures observed correlate well with the structures observed from AFM. In general the structures measured by SEM are of the order of micrometers long and hundreds of nanometers diameter. The general straightness of the nanowires does not indicate that the HBC-derivative nanowires are strong, but rather than the nanowires are easily sheered due to the weak van der Waals forces binding the molecules together. Therefore lateral forces, resulting in bending of the nanowire, will likely break the nanowire into two straight segments rather than flex the nanowire. From the SEM images, especially in Figures 7.18, 7.20 and 7.21, a range of nanowires of varying dimensions are observed. This results from the broad distribution in the size of nanowire bundles formed. The globular particles in some of the images result from the deposition of a thin 10Å film of gold in order to make the sample conductive.

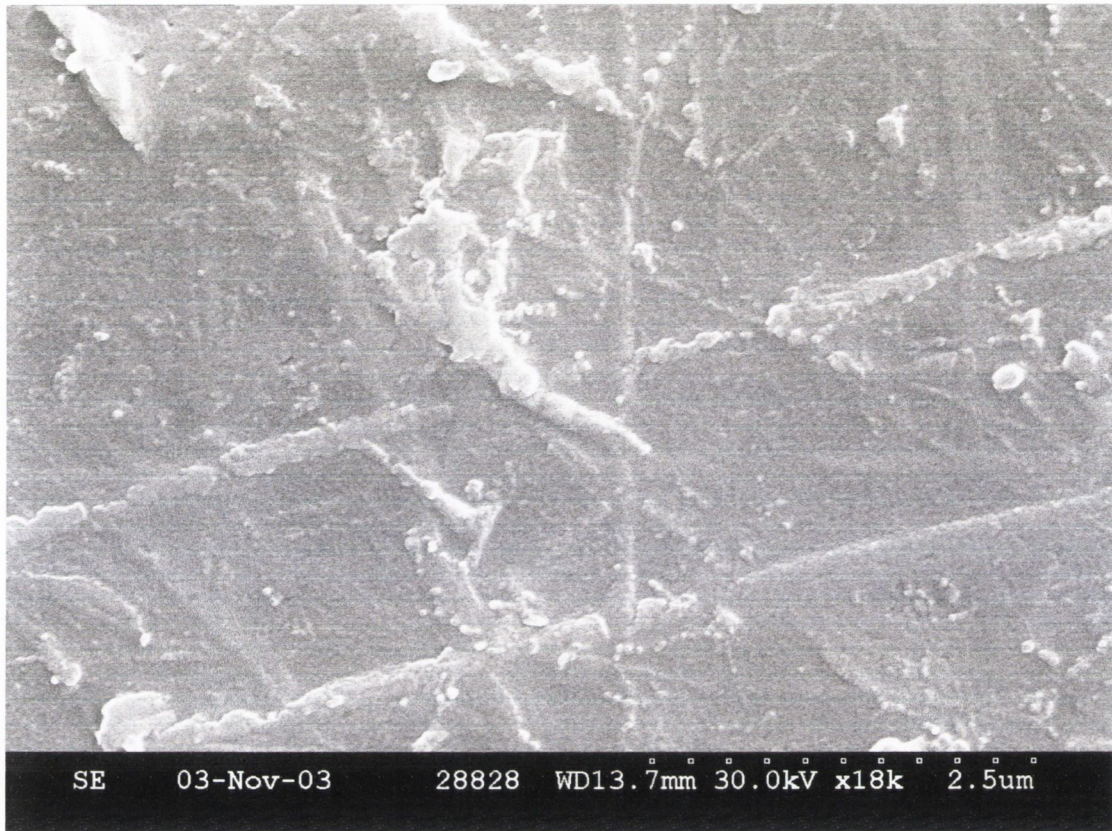


Figure 7.18: HBC-C8,2 nanowire bundles imaged by SEM.

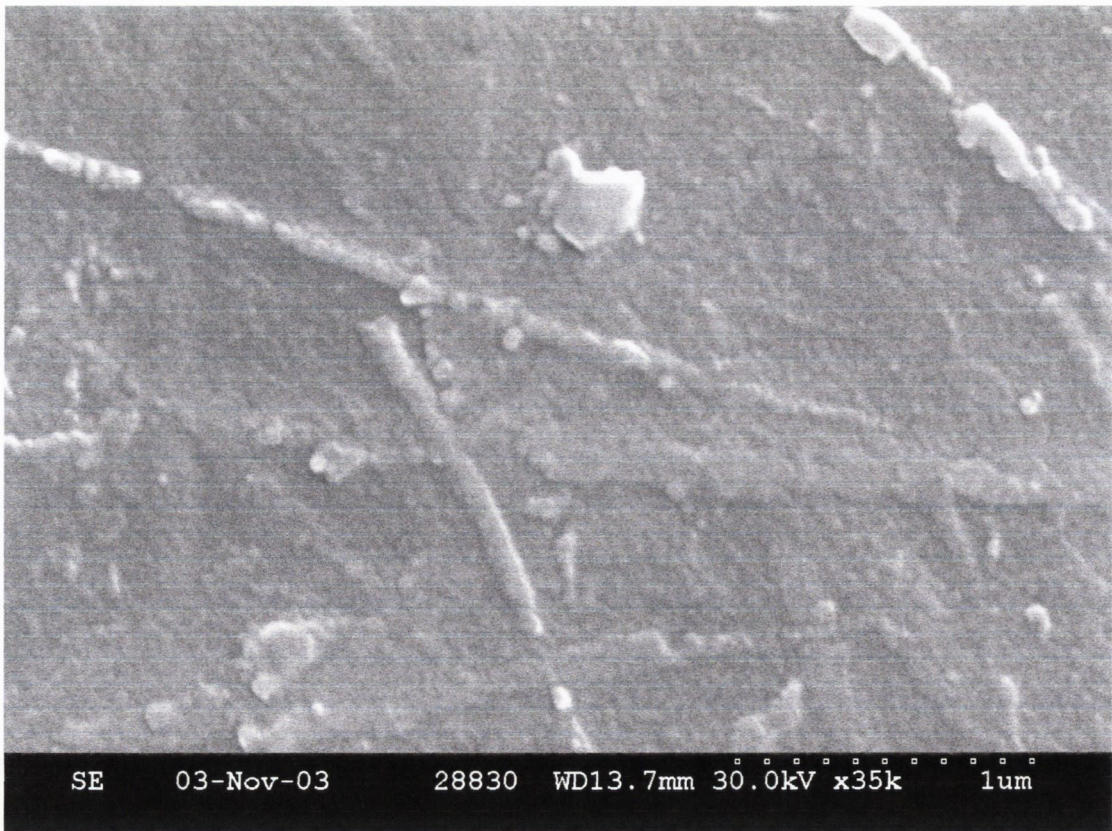


Figure 7.19: HBC-C8,2 nanowire bundles imaged by SEM.

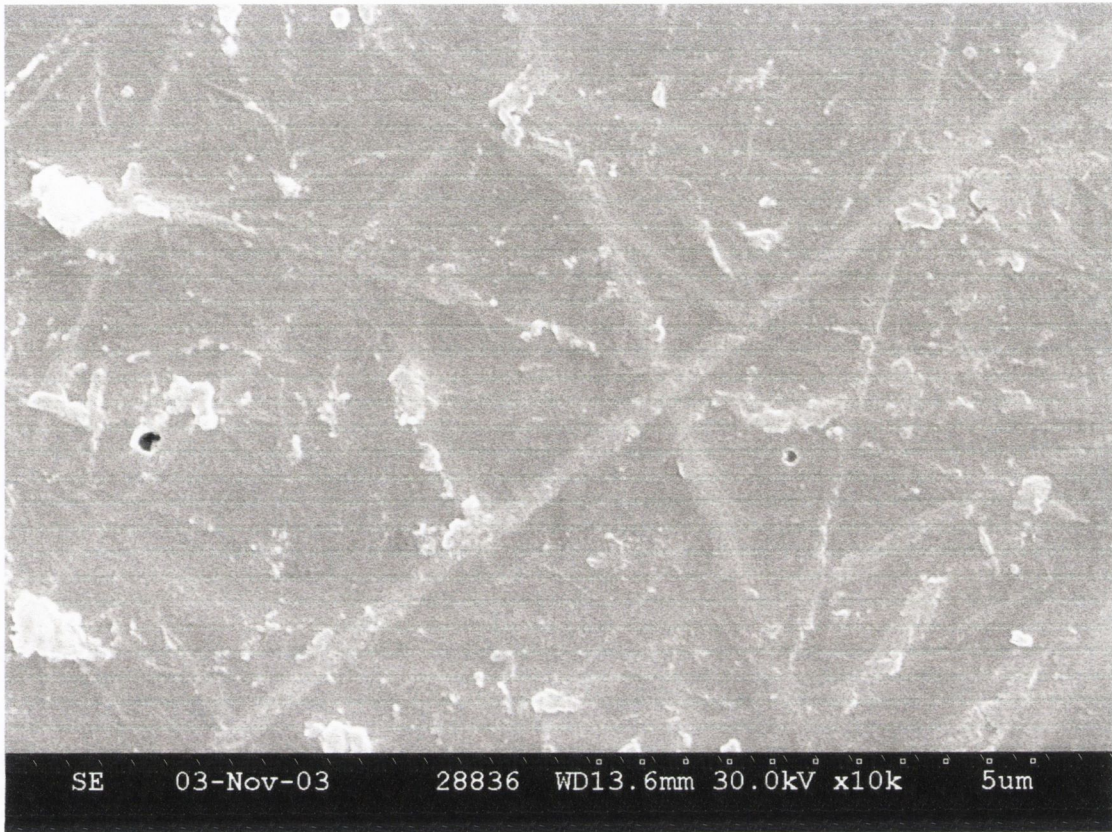


Figure 7.20: HBC-PhC12 nanowire bundles imaged by SEM.

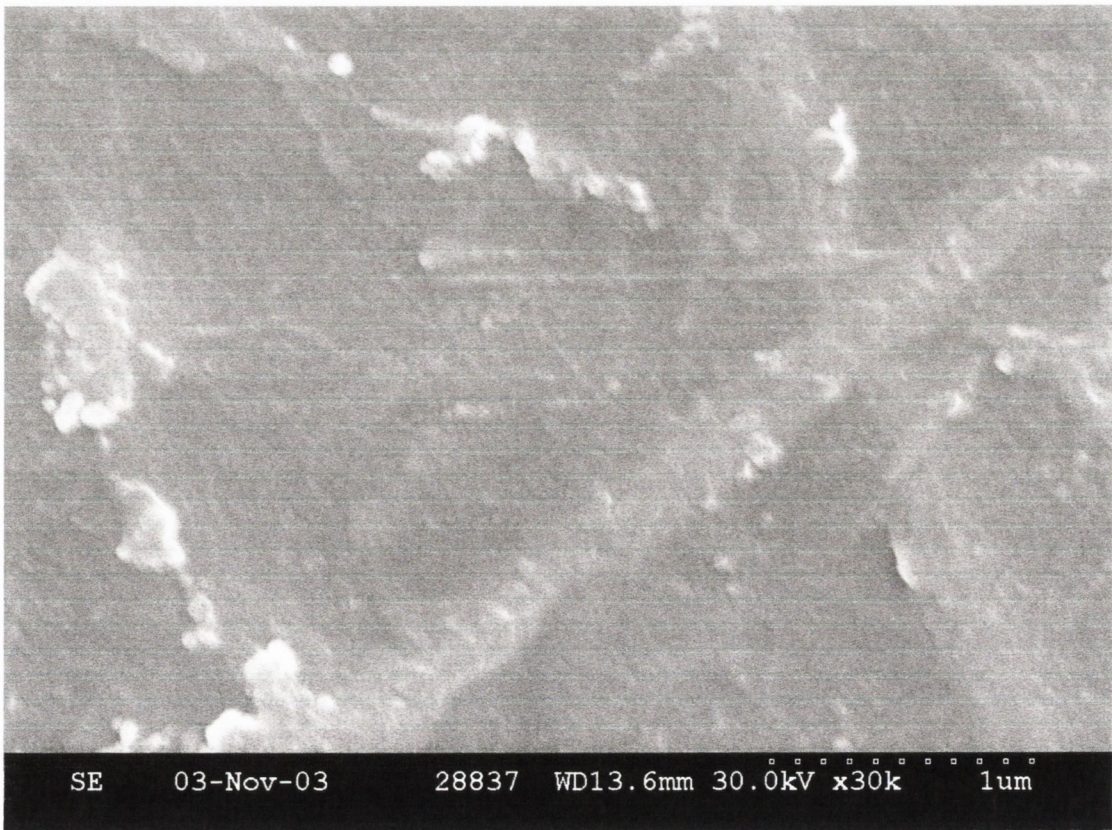


Figure 7.21: HBC-PhC12 nanowire bundles imaged by SEM.

7.4 DISCUSSION

The I-V behaviour of the HBC derivative MSAs from Figure 7.2 is un-expected, given that the A.C. microwave charge carrier mobilities values are very high. The rough charge mobility of HBC-C8,2 and HBC-PhC12, calculated from Figure 7.2, is approximately 11 orders of magnitude smaller than the value calculated from A.C. microwave conductivity measurements. This indicates that although the A.C. microwave charge mobilities may be accurate they in fact are only relevant on a nanoscale. At high A.C. frequencies (e.g. microwaves frequencies at $\sim 10^{10}$ Hz), the intrinsic charge carriers of all materials become larger due to the fact that the displacement of the charge carriers under the microwave frequency A.C. electric field is severely restricted. Thus it is quite possible that the charge carriers may not even be required to hop from one molecule to a neighbour molecule at these high frequencies. Instead the A.C. microwave charge mobilities may be representative of the mobilities of charge carriers on a molecule, not on an aggregate. Thus the A.C. microwave conduction regime is far from that of D.C. conductivity measurements. In the latter, charge carriers must be injected and travel throughout the thickness of the film in a hopping process. This explains why the conductivities measured for the HBC-derivatives are similar to that of conjugated polymers.

The fact that the conductivities of HBC derivatives are not similar to that of crystalline materials, confirms that delocalised electronic states (Bloch waves) are not established in the HBC aggregates. This is most likely due to, the lack of strong coupling (there is no FER during electron/hole transport) disorder in the nanowires inducing Bloch wave de-coherence. Thus the coherence length of the delocalised states is roughly of the order of a molecular spacing. This is confirmed by the lack of sharp peaks at low energies < 2.4 eV in the optical absorption spectra in Chapter 3.

The results from the electrical percolation network agree with the previous findings, from the exciton percolation network, that the HBC derivative MSAs have a large aspect ratio. This gives rise to the very low percolation threshold of HBC derivatives in inert polymer matrices. It also suggests that the HBC MSAs do not agglomerate to form large islands in the presence of the polymer (i.e. the HBC MSAs are soluble in the

polymers used). This confirms that the excimer emission does arise from nanowire (or nanowire bundles) inter-connecting, and not from the creation of localised disorder in a nanowire upon mixing with a polymer. The fact that conductivity through percolation samples is possible at dopant levels $< 0.1\%$ also confirms that nanowires are not breaking up upon introduction into a polymer matrix. Likewise the nanowires in the excimer percolation samples maintain their structural integrity in the polymer. If the structure of the nanowire were to change, say to a spherical inclusion, the expected percolation threshold⁶ would be closer to 20%. The fact that the upper limit of the percolation threshold, measured optically and electrically, is an order of magnitude lower, confirms that 1-D nanowires are the thermodynamically favourable MSA structure formed by HBC derivatives (at least at room temperature).

The relationship between the efficiency of charge carrier conduction and excimer formation is interesting. Not only does the latter method offer a more accurate way of measuring the percolation network formation at low dopant loadings, but it confirms similarity of the transport processes of both species measured in each case. An exciton in molecular systems is a neutral bound polaron pair, formed by the combination of a negative polaron and a positive polaron on a molecule. The charge carrier species for molecular systems are negative and positively charged polarons. Polarons are essentially structural relaxations of the molecular lattice in the presence of a charge. The combination of both charged polarons on one molecule gives rise to a neutral species, a Frenkel exciton. The main differences between the transport of charged polarons and a neutral polaron pair are the fact that the former has a charge and the latter is neutral. They are both common in that they always flow in the direction of a descending potential. For excitons this arises when the band gap decreases. Both species are mobile by diffusion and charged polarons can be influenced by an electric field. The fact that the behaviour of both species in percolation networks is similar confirms that both species are indeed mobile.

The mobility of excitons and charged polarons are equally influenced by the disorder in the HBC MSAs. For instance the conductivity of the more disordered HBC-PhC12 is a factor ~ 1000 lower than the more ordered N-HBC. The relative orders of these two materials was determined from the optical spectroscopy in Chapters 3, 4 and 5. The electronic processes of FER and electron transport are thus influenced by the degree of

positional order in a given structure. In both cases the overlap in the molecular position in an aggregate and/or the energetic overlap of the energy levels will limit the transport ability of excitons or charge carrier species. In both cases, the spatial/energetic integral between the molecular orbitals of neighbouring molecules (from the position in an aggregate) will determine β and hence the exciton or charge carrier hopping probability. The mobility of the charge carriers is dependent of the hopping rate. Hence the conductivity is a function of the quality of spatial and energetic overlap between molecules in an aggregate. Thus, regions of disorder in an aggregate will give rise to small integrals and hence a reduced hopping rate of excitons and charged polarons. The consequence for disordered aggregates is the limited mobility of excitons and low conductivities.

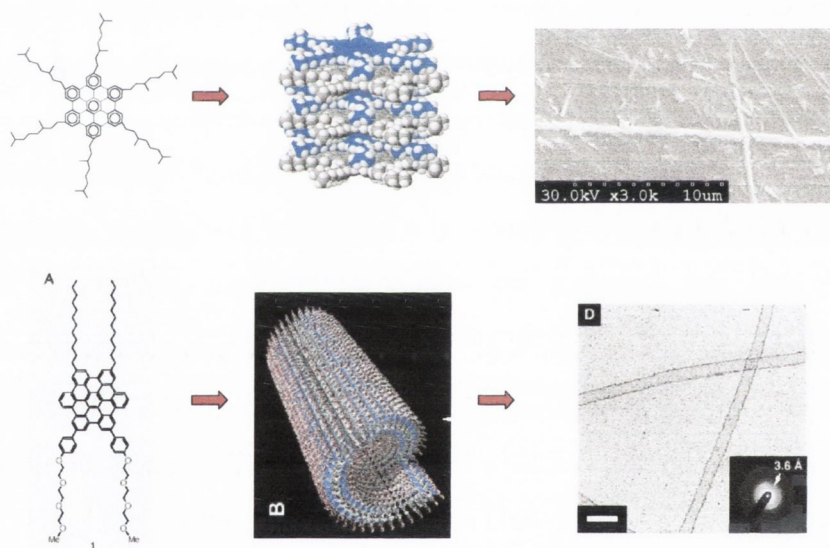


Figure 7.22: Illustration of the two kinds of MSAs formed by the HBC molecules studied: Nanowires (top) and Nanotubes (bottom). J-HBC TEM image taken from ref [7].

The AFM and SEM images confirm that the inclusions in the optical and electrical percolation networks have a large aspect ratio and are 1-Dimensional. The fact that the nanowires are all very straight confirms that the molecules are stacked in a horizontal alignment. If they were arranged parallel to the nanowire, the nanowires would be more elastic and curved nanowires would be observed. Thus the AFM and SEM images confirm the H-aggregate alignment of the molecules as predicted by the optical

properties. TEM data from Hill et al⁷, confirms the twists or helicity observed in the AFM images of the more flexible J-HBC MSAs. They have been demonstrated to produce nanotubules in solution by the bundling of the J-HBC nanowires. The amphiphilic nature of these molecules creates nanotubular micelles as demonstrated in Figure 7.22. This demonstrates the proximity of the J-HBC cores in the lateral direction required for side-to-side J-resonance as described in Chapter 3. The similarity of the PL of N-HBC in hexane to the PL of J-HBC may indicate that N-HBC is forming a nanotubular bundle.

The ordered film of N-HBC is more likely to have contributed to the high conductivity measured for this derivative. In comparison HBC-PhC12 films demonstrate a good macroscopic ordering, but from the optical properties this masks the underlying intrinsic disorder of the alignment of the HBC cores of the molecules in a stack. Thus the alignment factor, as described above, is more crucial in determining the electrical conductivity of a molecular aggregate.

7.5 CONCLUSIONS

In this Chapter, results of electrical measurement and microscopy have been presented that corroborate with results presented in previous chapters. The 1-D structure of the HBC-derivative aggregates is confirmed by the AFM/SEM images as well as by the electrical percolation network threshold of < 0.1 %. The latter result also correlates well with the previous results from the exciton percolation network. The H-aggregate structure of the nanowires is confirmed by the microscopy images. The formation of nanowire bundles, predicted by the side-to-side J-resonance of J-HBC and N-HBC, is also confirmed by the microscopy images acquired.

¹ A. M. Van der Craats, J. M. Warman, A. Fechtenkoetter, J. D. Brand, M. A. Harbison, K. Muellen, *Adv. Mater.* 1999, 11, 1469.

² A. Powel, G. E. Childs, *American Institute of Physics Handbook* (1972)

³ L. Bozano, S. A. Carter J. C. Scott, G. G. Malliaras, P. J. Brock, *Appl. Phys. Lett.*, **74** (1999) 1132

⁴ “Organic Nanostructures: Science and Applications” Proc. Enrico Fermi School of Physics, Course CXLIX (2002) p 67.

⁵ SEM images were obtained with the dedicated assistance of Valeria Nicolosi.

⁶ I. Balberg, C. H. Anderson, S. Alexander, N. Wagner, *Phys Rev. B.*, **30**, 7 (1984)

⁷ J.P. Hill, W. Jin, A. Kosaka, T. Fukushima, H. Ichihara, T. Shimomura, K. Ito, T. Hashizume, N. Ishii, T Aida, *Self-Assembled Hexa-peri-hexabenzocoronene Graphitic Nanotube*, *Science* **304**, 2004.

Chapter 8: CONCLUSIONS

In this thesis it has been demonstrated that the fine tuning of the molecular structure of HBC derivative molecules can give rise to ordered molecular aggregate superstructures. Instead of trying to construct a superstructure using outside influences, such as heating, electric fields or physical manipulation, the HBC derivative molecules have demonstrated that the thermodynamic equilibrium phase of this family of molecules can be very ordered and stable.

The confirmed detection of the isolated HBC derivative molecular species by PL and PLE techniques at $\sim 10^{-13}$ M has been aided by the solubilising substituted chains. Previously it has been assumed that the HBC aggregate spectra was that of the isolated species, and the indicator of aggregation was the inhomogeneous broadening of the aggregate optical spectra. From the results described here, this has been clearly demonstrated not to be the case. In fact, the photo-physical behaviour of the isolated HBC molecules has been demonstrated to conform more to the expected photo-physical behaviour of isolated molecules than the aggregates. The Hildebrand solubility measurement of HBC-C8,2 isolated molecules proved to be more sensitive than the typically used cloud-point test. Therefore, the isolated molecule technique employed here would be a useful technique in measuring the solubility of novel solvents.

This thesis emphasises the need to apply a further litmus test to the optical spectra of conjugated molecules. It has been demonstrated that simply assuming that all molecules in solution are isolated, or if there are aggregates that there is no FER, is wrong. Ideally the optical spectra should be tested to see if an isolated molecule or aggregate with FER interpretation fits the data better. Typically optical spectra have been interpreted solely in terms of the isolated molecular structure, in this thesis it has been demonstrated that the molecular aggregate structure and the molecular aggregate superstructure must be considered when interpreting optical spectra of molecules.

From the spectroscopic measurements performed, the PL and PLE techniques have been shown to be sensitive enough to be able to distinguish the various HBC derivative MSAs formed. In fact the comparison of the well defined features of the HBC

derivative optical spectra has enabled the deciphering of FER signatures that would typically be smeared out by in-homogenous broadening in other, less ordered, molecular systems. The comparison of the symmetrically and asymmetrically substituted HBC derivatives MSAs (quasi 1-Dimensional and quasi 1-2 Dimensional respectively) has allowed a good insight into the behaviour of photo-excitons in these systems. Particularly it has helped determine that in real H-aggregates, quasi-symmetric FER state emission is possible, and is perhaps phonon-assisted. This is observable in the symmetrically substituted HBC MSAs, because J-emission is unfavourable due to the insulating n-alkyl mantle surrounding the HBC cores of the quasi 1-D nanowires. Typically, if J-emission is possible, in an aggregate, it will swamp the PL due to the fact that excitons will migrate and emit from lower energy J-emission sites.

The analysis in Chapter 6, of the typical optical properties of isolated and aggregated molecules, of various molecular systems as well as HBC derivatives, indicates that the prevalence of FER has to date has been underestimated. Various anomalies in the interpretation of molecular optical, in terms of the photo-physics of isolated molecules, have been overlooked and had remained unexplained. However, from the conservation of energy model constructed here, these anomalies can be explained in terms of FER in molecular aggregates. The likelihood is that FER occurs in most molecular systems, the main variable between molecular systems is the localisation range $2N$. The disorder limited localisation length varies from around 2 molecules for very disordered systems (polymers) to > 50 molecules in ordered systems (some small polar molecules). The degree of disorder at thermal equilibrium, as illustrated by some of the HBC derivatives, can be very sensitive to the molecular structure. This allowed the molecular-structure optical-properties relationship to be determined for the HBC derivatives and this was found to be applicable to other molecular systems.

The investigation of the red-shifted emission demonstrated that excitons are mobile in these systems and thus the PL properties of an MSA are even more sensitive to the MSA superstructure than the absorption process. The formation of percolation networks, by either inducing agglomeration of aggregates by titration of a bad solvent or by the doping of an inert matrix, proved to be crucial in determining the final fate of photo-excitons formed in these systems. The migration of excitons to disordered excimer emission sites, was found to be substantially aided by the formation of

connected networks (and not just an indicator of aggregation as has been commonly assumed). This is confirmed by the conductivity measurements of the same percolation networks. The passage of charge carriers through the matrix was found to be as sensitive as the exciton percolation measurements. This may prove to be a quick and simpler way to test for the percolation threshold of novel MSAs. From these same measurement techniques the large aspect ratio of the HBC MSAs was determined. This, together with the AFM and SEM images acquired, confirmed the quasi 1-Dimensionality of the HBC MSAs formed.

Finally the construction of a p-a-l cycle for resonant excitons that is relevant to both absorption and luminescence process indicates that the Stokes shift for aggregates is determined by the isolated molecules primarily. In fact the model explains why it has usually been assumed the Stokes shift is zero, when in fact it has been measured incorrectly. The model was tested against published data and was found to agree with previous values calculated for $2N$. The observed trends of the v-e features of absorption and luminescence spectra can now be explained in terms of the larger oscillator strength of FER states that are coupled to lower vibrational modes that are coherent.

ACKNOWLEDGEMENTS

I would like to thank Prof. Werner Blau for creating a friendly and creative working environment and Dr. Johnny Coleman for his support and interest in my work. I would especially like to thank everyone in Group BU for their support over the years, particularly Rebekah Darcy, Valeria Nicolosi, Take Kobayashi and Roberto Matassa.

I want to thank Dr. Dan Gregg, Dr. Jonathan Hill, Dr. Hugh Byrne, Dr. Jishuan Wu and Alan Dalton for their scientific collaboration and support. Many thanks to John Kelly and, Mick and David from the workshop for their help.

Finally, I'm truly grateful for the enduring support of my parents and sister, and Anna deserves a medal for her love and devoted patience with me. Last but not least, I would like to thank Julien and Damien for their friendship and for having listening to me ramble on and on...

Appendix A: EFFECTIVE CONJUGATION AREA OF HBC MOLECULES

The electronic transition energies measured from the low concentration PLE spectra can be compared with the calculated transition energies obtained from treating the HBC derivative molecules as a 2D quantum box as well as from PFE0 theory. For ease of comparison, the S_1 and S_2 transition energies measured and calculated for HBC and coronene are listed in Table 1A. A surprise result of the quantum box and PFE0 treatment of HBC is the mismatch between the calculated and experimental values. The two theoretical methods give values for the S_1 transition that are within 0.7 eV of each other, indicating that at the very least the S_1 transition energy of HBC should be around 1 – 2 eV. However, the experimental value is considerably higher at 3.1 eV in toluene.

	2D QB eV	S_1 PFE0	Experimental	Ratio Int. $S_1: S_2$
Isolated HBC	1.13 (S_1)	1.84	3.1 (S_1)	~ 1
	2.26 (S_2)		3.7 (S_2)	
	2.63 (S_3)			
Coronene	3.43 (S_1)	3.16	3.0 (S_1)	~ 0.01
	4.12 (S_2)		3.6 (S_2)	
	6.17 (S_3)			

Table A1: The calculated and experimental values of the electronic transitions of HBC and Coronene.

The large discrepancy between the calculated and experimental values for HBC needs to be addressed. There are two possible reasons why there is such a mismatch: a) the lowest energy transition observed for isolated HBC molecules is not the S_1 transition but is the S_2 transition or b) the lowest energy transition is the S_1 transition but the energy is higher than expected due to an effective delocalisation length in the HBC molecule. The former case implies that the S_1 transition is forbidden. This conforms with the allowed and forbidden transitions expected for a molecule of D_{6h} symmetry. However, in order for the isolated HBC molecules to be observable at such low concentrations, Kasha's rule must not apply. For isolated HBC molecules to be

observed the rate at which S_2 excitons generated relax to the S_1 state must be very slow, otherwise no emission from the symmetry allowed S_2 state would be observed. The latter case implies that the S_1 transition energy arises from a delocalisation of the exciton that does not fully extend over the whole HBC molecule. This is supported by the fact that from the low concentration PLE spectrum of HBC-PhC12 the addition of *exo*-phenyl groups does not extend the conjugation length. The localised state may not have the same D_6h symmetry, thus allowing absorption and photo-luminescence from the S_1 state. The appeal of the latter case is that because the lowest electronic state of the localised system would be more symmetry allowed it does not require any breaking of Kasha's rule. To test the possibility that there might be an effective intramolecular delocalisation length (or area) of the exciton on HBC the molecular structure of HBC and coronene can be compared.

In conjugated polymers, the phase relationship between successive π -bonds will determine the electron coherence length in the molecule, i.e. the intramolecular delocalisation length. Likewise the coherence length of an electron in a PAH molecule will also be determined by the phase relationship between alternating π -bonds. Phase disruptions are more likely to be encountered along longer paths and at symmetrically different nodes. HBC is composed of a coronene core with an extra six *peri*-benzenes. Here the two resonant states of HBC are clearly shown and the relationship to the molecular structure of coronene is also shown. From the figure only paths that have an alternating single and double bond sequence allow electron transport. Thus for HBC there are two viable paths for electron transport, a) around the perimeter of the HBC molecule and b) a inner pathway that closely resembles one of the possible electron pathway of coronene.

Coronene is an unusually chemically stable molecule when compared to PAH molecules with a similar number of aromatic sextets¹. The symmetry of coronene enables the migration of sextets throughout the whole molecule and gives rise to a chemically stabilising sextet ring-current. This is evident in the lower heat of formation of coronene 284 kJ mol^{-1} compared to benzo(ghi)perylene 295 kJ mol^{-1} (with the same number aromatic sextets). Therefore it is possible that although HBC has six more fused benzene rings, the stable sextet ring current persists in HBC.

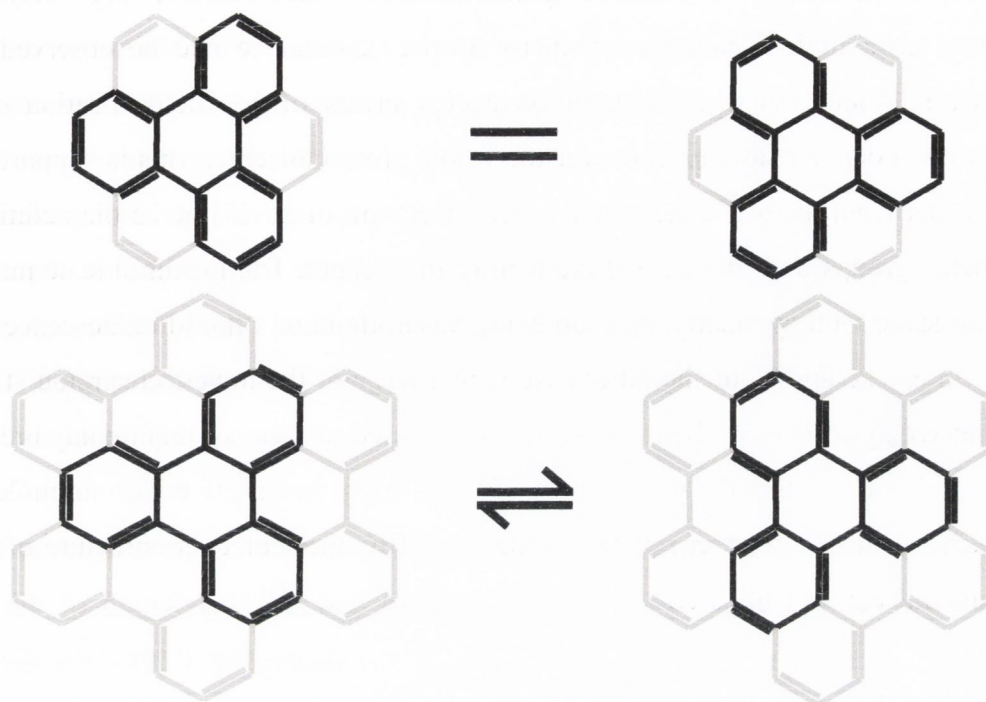


Figure A1: a) Coronene molecule with conjugated electronic paths illustrated (dark lines). b) Illustration of Resonant electronic states of HBC which have identical conjugated electronic paths as those found for coronene (Sextet Ring Current). Notice that HBC also has a conjugated pathway around the periphery of the molecule, this is termed the disrupted SRC.

The calculated and experimental values of coronene, listed in Table A1, are a much closer match than for HBC. For coronene, the PFEO S_1 transition energy 3.16 eV is very close to the experimental value of 3.0 eV. On the other hand, the 2D QB calculation overestimates both transition energies by around 0.4 –0.5 eV. Therefore, although PFEO theory correctly estimates the transition energy, the 2D QB calculation more accurately predicts the difference in energy between the experimental S_1 and S_2 transition energies.

Evidence for this can be found in the similarity between the absorption spectra of HBC and coronene. This is further supported by the underestimation of the S_1 transition energy of a quantum box of the true dimensions of HBC and the underestimation of the PFEO calculated S_1 transition energy for a molecule with the circumference of HBC. The evidence points towards the optical properties of HBC being determined by the sextet ring current of the coronene core of HBC and not by the physical dimension of the HBC molecule (see Figure A1). In order for a larger circumference sextet ring

current to exist, HBC would require an additional six fused benzene rings around the periphery of the molecule. Further evidence for the existence of a stabilised sextet ring-current can be found by comparing the absorption spectra of the different derivatives of HBC. For instance, the addition of *exo*-phenyl groups to the aromatic core, HBC-PhC12, does not significantly perturb the PLE spectrum. If the strong electronic transition observed in the PLE spectrum were to originate from electronic states fully delocalised over the molecule the change from benzenoid to quinoid of the *exo*-phenyl groups in the excited state should decrease the energy of the optical transition. This is not observed.

In studies of larger PAH molecules similar to HBC, a linear relationship was found between the number of π electrons in the system and the wavelength of the peak maximum². This arises from the relationship of the energy of a 2D delocalised π -electron system to the area of the system $E \propto 1/A$, where A is the area of the molecule. If the density of π electrons is uniform then the number of π electrons is proportional to the area, $n \propto A$. Since the wavelength λ is inversely proportional to the energy E the overall relationship is therefore linear i.e. $\lambda \propto n$. However, despite the correct linear relationship, the absolute value of the energy is too high given the size of the molecule. Therefore, the conclusion is that there is an effective conjugation area for 2D molecules that is analogous to the effective conjugation length of 1D conjugated polymers.

Examination of high concentration spectra reveals that there are in fact low energy features far below 3.1 eV. The question is why aren't these peaks observed for the low concentration species? The emission energy of the isolated PL (2.7 eV), corroborates the finding that for the low concentration species observed the lowest available state to the exciton is not below 2.7 eV. There are therefore two possibilities: a) the isolated HBC molecules emit from the S_2 state or b) the π -electron system of the isolated molecules are not fully in phase throughout the molecule resulting in a photo-exciton that has the imprint of the SRC associated with coronene.

As the lowest energy transition of the isolated species is readily observed at 10^{-15} M it is highly unlikely that it is a symmetry forbidden state. Therefore the conclusion must be that the lowest state observed for the isolated molecule is not the symmetry forbidden S_1 transition as would be expected for a D_{6h} symmetry molecule.

The ratio of the intensities of the S_1 to S_2 transitions are 0.01 and 1 for coronene and isolated HBC respectively. This suggest that the S_1 transition for isolated HBC has a similar energy as that of coronene but it is much more intense (hence HBC is observed at very low concentrations).

The D_{6h} symmetry of HBC should give rise to a symmetry forbidden S_0 to S_1 transition. This is not observed for isolated molecules of HBC. As will be shown in Chapter 4, if it were the case the PL of HBC would be symmetry-forbidden and isolated molecules at 10^{-13} M would not be observed.

The question is why are isolated HBC molecules not behaving as expected from the 2D QB and PFEO treatment and instead behaving more like coronene? How is it possible for a HBC molecule to behave like coronene and under what circumstances? The answer may lie in the common features between the molecular structure of coronene and that of HBC.

TBDC is the sodium salt of 1,1'-diethyl-3,3'-bis(4-sulfobutyl)-5,5',6,6'-tetrachloro-benzimidazolo carbocyanine.

Appendix B: OPTICAL SPECTRA AND FER DECOHERENCE

Frenkel Exciton Resonance (FER) has tended to be ignored when interpreting molecular optical absorption and photo-luminescence (PL) spectra. Instead, it has generally been assumed that the isolated molecule photo-absorption-luminescence (p-a-l) cycle can be applied. This makes little sense when one considers that the existence of polymer aggregates in solution is generally accepted.

If one examines the absorption or PL of polymers (for instance mLPPP in Fig.6.2) or small molecules there are generally 2 dominant peaks accompanied by several peaks of lower intensity. Variations of the relative intensities of the two dominant peaks are common when comparing isomers, or sometimes as a function of polymer concentration (aside from obvious changes due to self-absorption).

In the framework of an isolated molecule p-a-l cycle, all the peaks visible in the spectra belong to a vibrational progression of one electronic transition (or at least the 2 dominant peaks). Therefore, to explain the changes to the ratio of the intensities of the 2 lowest energy absorption peaks (2 highest energy peaks in the PL) a substantial variation in the electron-phonon (e-p) coupling ($S=g^2$) must be responsible. There are several problems with this. The e-p coupling is an intra-molecular property that, as explained in the text, can increase with FER. In the framework of the isolated molecule there is no FER, therefore it is hard to explain changes to the e-p coupling without aggregation (accompanied by some charge sharing and strong intermolecular vibronic coupling) or FER. A second problem with this interpretation is that if the Stokes shift is measured as for an isolated molecule, generally it is very small (specially for non-polar molecules). For example, with mLPPP the apparent “Stokes shift”, in the framework of the isolated molecule, is $E_{SI} \sim 0.1\text{eV}$. However, as we will show, this value is still much smaller than the calculated E_{SI} . Approximating the absorption or PL to a Poisson vibrational distribution (low temperature), $S_1 \sim 1$ if the ratio of the intensities of the 2 dominant peaks is ~ 1 (higher temperatures increases the oscillator strength of higher vibrational transitions). Using $E_{SI} = 2S_1\hbar\omega_{pl}$ and the vibrational transition energy $\hbar\omega_{pl} =$

0.15 eV, gives $E_{SI(\text{calc.})} \sim 0.3$ eV. This is much larger the apparent “Stokes shift”, indicating that the isolated molecule p-a-l cycle cannot be applied to mLPPP.

With the model presented in this paper, mLPPP is considered as a system of disordered aggregates. The disorder of the mLPPP aggregates is such that on average it limits the FER range to 2 molecules. The superposition of the v-e peaks of the symmetric and anti-symmetric transitions give rise to the spectral envelope observed for the absorption and PL. Considering the fact that to obtain this envelop the 0-0_J peak intensity > 0-0_H peak intensity (with an equivalent ratio for higher vibrational transitions), mLPPP aggregates could be classified as approximately 2:1 J to H aggregate dimer. This is in terms of their optical properties. The actual aggregate size can be order of magnitudes larger e.g. a solid film.

From the model, a rough guide of the degree of order of a given molecule’s aggregate can be established from the v-e transition energy. For carbon systems with a dominant C = C stretch vibration $\hbar\omega_{pI} > 0.1$ eV, the general trend is that polymers aggregates have $\hbar\omega_{pA} > 0.1$ eV and are therefore highly disordered, MSAs have $0.01 < \hbar\omega_{pA} < 0.1$ eV thus are more ordered and molecular crystals have $\hbar\omega_{pA} < 0.01$ eV and hence are highly ordered.

The Huang-Rhys parameter, S , remains unaltered as N increases due to charge screening beyond nearest-neighbour and weak charge sharing (hence S only changes from monomer to dimer and not dimer to trimer). Therefore, the observed S in the spectra is an average of S for each molecule in resonance not the sum over $2N$. Otherwise, S would increase unrealistically with $2N$. A significant result of the normalised p-a-l cycle superposition is that each of the $2N$ molecules v-e relax by the same amount $(RS_A\hbar\omega_{pI})/2kN$ (see Fig. 6.1). This ensures that all the molecules have the same electronic transition energy in the relaxed state, allowing FER during PL. If all molecules v-e relax differently, then a large variance in $\hbar\omega_{00LI}$ would result in negligible FER during luminescence. The consequent reduction in $2N$ would reduce the exchange-narrowing as well as increasing $\hbar\omega_{pA}$, resulting in a broader PL than absorption spectrum. Characteristically, this is not observed.

Broadening of optical spectra of aggregate ensembles in solution or solid state usually makes v-e features hard to observe. The main contributors to broadening arise from the natural variation of the aggregate morphologies in an ensemble varying $\hbar\omega_{00Abs}$, $\hbar\omega_{00L}$ and β (the former two are often termed diagonal and the latter off-diagonal disorder). The resulting large distribution of FER ranges broadens the distribution of $\hbar\omega_{pA}$ and the variance in the degree of exchange narrowing. This leads to many overlapping and broad v-e peaks in the spectra. Generally, most v-e peaks in optical spectra, higher in energy than the lowest energy absorption peak (and lower in energy than the highest energy PL peak), are broader than the 0-0 v-e transitions. A simple reason, according to our model, is that the v-e peaks of the symmetric and anti-symmetric electronic transitions overlap (see Fig. (p-a-l cycle)). Good examples of this are the spectra of mLPPP and HBC aggregates. HBC-C8,2 molecules self-assemble to form nanowires which further assemble into nanowire bundles. Because of the high symmetry of the molecules and the unfavourable side-chain molecular-core interaction, the available orientations and positions are limited and therefore closely related. In an analogous way to molecular crystals, this ensures that although a large number of molecules are present the molecular self-assembly is very ordered. For the more disordered liquid-crystalline HBC-PhC12, the v-e peaks are broader³ making the PL spectrum resemble the PL from PIC. Generally, for non-polar molecules at high concentrations, the solvent interaction is negligible as a majority of molecules do not lie at surface of large aggregate. This decreases the broadening arising from solvent – molecule interactions - for instance HBC-C8,2, at high concentration has very well defined v-e features.

For HBC-C8,2 $\hbar\omega_{pAbsA}$ was determined by superimposing the mirror image of the PL onto the PLE spectra. The energy axis of the PL was then expanded until the main peak positions coincided, thus helping to determine the exact position of the v-e shoulders in the PLE spectrum. For PIC analog, $\hbar\omega_{pA}$ was estimated the reasonable estimate that $S_A \sim 0.5$ where the overall FWHM of the absorption or PL peak is roughly equal to $\hbar\omega_{pA}$.

The physical reasons why a decrease of $\hbar\omega_{pA}$ is observed may be related to the fact that only the more efficient processes are observed. In terms of FER this means all states where the transition dipoles are in phase (bright state). The time dependence of the phase of the transition dipoles of a molecule is likely to be influenced by the nuclear

motion (in fact it is the relative phase of the excited state and ground state v-e wavefunctions that gives rise to the vibrational-electronic structure in the optical spectra). The electronic phase of the transition dipoles is therefore modulated by the nuclear vibrations. FER involves the creation of a standing wave of excitation that is composed of two waves travelling in opposite directions within the confines of $2N$. The exciton has equal probability of being in a wave travelling in either direction. If the exciton “hopping” up and down and aggregate is modulated by the nuclear frequency, the dominating frequency will likely be the higher frequencies as this will give the exciton a higher hopping attempt frequency. The time taken by an exciton hopping over $2N$ molecules *back and forth* for one cycle is given by $4Nt_{\text{hop}}$ where t_{hop} is the time between hops. If $2N$ is large the total cycle time of the exciton will be longer. Thus the nuclear motion of an atom at high frequencies will become decoherent very quickly with the phase of the exciton during the total cycle time of the exciton. For instance, if the molecule hops at a frequency f_h then by the time a molecule has hopped to the neighbour molecule the f_h vibration of transition dipole of the first molecule it started on will be 180° out of phase with its neighbour's transition dipole at f_h . The result will be a dark state. For larger $2N$ the high frequencies quickly become de-phased with the exciton, leading to FER states that will have very little oscillator strength. In fact as $2N$ increases only the low vibrational frequencies of the atoms (and hence the electronic transition dipole via the electron – phonon coupling) will be in phase with the exciton during a full cycle up and down $2N$ molecules. In fact, the FER states modulated at high frequency will tend to be more out of phase than lower frequencies, the result is that the only FER states for which the high frequencies are still in phase are those with a small $2N$. As described previously states with small number of molecules in resonance will tend to be swamped in intensity by larger $2N$ FER states. Thus it seems as though for large $2N$ only the low energy v-e transitions will be observed (i.e. with higher probability). However, this does not prevent from the molecule relaxing via high frequency modes (all the intramolecular vibrational modes are still accessible to the electron), but it does mean that large $2N$ with low v-e frequencies are more likely to be observed optically because they are in phase and many more molecules are involved. The example given above describes how by hopping to a next nearest neighbour the transition dipoles of both molecules will likely be 180° out of phase. This could explain why the R/k tends to 2. Perhaps the minimum requirement for an FER delocalisation $2N$

= 2 is that both transition dipoles must be in phase, this would necessitate that v-e relaxation occur simultaneously on both molecules. This will double the Stokes shift of an aggregate relative to the isolated molecule.

There is another entropic argument for an exciton favouring a high probability - low vibrational energy relaxation pathway. The multiplicity function for a any energy vibrational level of one molecule is unity. However for $2N$ molecules the multiplicity function will tend to increase rapidly the more oscillators and roughly with the more vibrational quanta involved. The multiplicity function of $2N$ oscillators is given⁴ by $g(2N, n) = (N+n-1)!/n!(N-1)!$, where n is the number of vibrational quanta to be distributed over $2N$ molecules. The entropy of a system is given by $S \sim \ln g$. The larger the change in entropy the greater the likelihood that the process will happen, when comparing processes with identical enthalpy changes. This is exactly the case for a resonant exciton. The total energy change is determined by the real Stokes shift. If the real Stokes shift is not a function of $2N$ then it will remain constant (as is observed). Two FER states with different $2N$ will have the same energy change, therefore the difference in entropic change will determine which is more likely (which process will have the largest change in Gibbs Free energy). Since the energy is set (the Stokes shift is constant) the number of phonons emitted in relaxing from the ϕ_f^* to the ϕ_f state, for instance, will be greater the smaller the quantum of each phonon emitted. Since for an isolated molecule all the vibrational levels of high and low frequency modes have $g(1, n) = 1$ no vibrational mode is preferred and the usual isolated molecule v-e structure is observed. However, as $2N$ increases so does the number of ways n quanta can be distributed. Especially so, the lower the vibrational mode energy. For an exciton delocalised over $2N \gg 2$ molecules the relaxation pathway that involves the lower energy phonon modes will have a larger multiplicity. The result is that the Free energy decrease for the exciton relaxing via a low energy vibrational modes will be larger than that of the high energy vibrational modes even though the change in enthalpy is the same!

Thus it could be that the favourable phase relationship and higher multiplicity of low energy v-e modes makes them more observable in systems with large $2N$ as predicted by the conservation of energy model.

¹ N. Nijegorodov, R. Mabbs, W.S.Downey, *Spectrochimica Acta Part A* **57**, (2001)

² M.D. Watson, A. Fechtenkoetter, K. Muellen, *Chem. Rev.* **101**, 2001.

³ A. J. Fleming, J. N. Coleman, A. B. Dalton, A. Fechtenkötter, M. D. Watson, K. Müllen, H. J. Byrne, W. J. Blau, *J. Phys. Chem. B*, **107** 37 (2003)

⁴ C. Kittel, H. Kroemer, *Thermal Physics*, 2nd Ed. Freeman p24